

Graduate Texts in Physics

Sandro Wimberger

Nonlinear Dynamics and Quantum Chaos

An Introduction



Graduate Texts in Physics

For further volumes:
<http://www.springer.com/series/8431>

Graduate Texts in Physics

Graduate Texts in Physics publishes core learning/teaching material for graduate- and advanced-level undergraduate courses on topics of current and emerging fields within physics, both pure and applied. These textbooks serve students at the MS- or PhD-level and their instructors as comprehensive sources of principles, definitions, derivations, experiments and applications (as relevant) for their mastery and teaching, respectively. International in scope and relevance, the textbooks correspond to course syllabi sufficiently to serve as required reading. Their didactic style, comprehensiveness and coverage of fundamental material also make them suitable as introductions or references for scientists entering, or requiring timely knowledge of, a research field.

Series editors

Professor William T. Rhodes

Department of Computer and Electrical Engineering and Computer
Science, Imaging Science and Technology Center

Florida Atlantic University

777 Glades Road SE, Room 456

Boca Raton, FL 33431

USA

wrhodes@fau.edu

Professor H. Eugene Stanley

Center for Polymer Studies Department of Physics

Boston University

590 Commonwealth Avenue, Room 204B

Boston, MA 02215

USA

hes@bu.edu

Professor Richard Needs

Cavendish Laboratory

JJ Thomson Avenue

Cambridge CB3 0HE

UK

rn11@cam.ac.uk

Professor Martin Stutzmann

Technische Universität München

Am Coulombwall

85748 Garching, Germany

stutz@wsi.tu-muenchen.de

Professor Susan Scott

Department of Quantum Science

Australian National University, Acton

ACT 0200, Australia

susan.scott@anu.edu.au

Sandro Wimberger

Nonlinear Dynamics and Quantum Chaos

An Introduction



Springer

Sandro Wimberger
Dipartimento di Fisica e Science della Terra
Università di Parma
Parma
Italy

ISSN 1868-4513 ISSN 1868-4521 (electronic)
ISBN 978-3-319-06342-3 ISBN 978-3-319-06343-0 (eBook)
DOI 10.1007/978-3-319-06343-0
Springer Cham Heidelberg New York Dordrecht London

Library of Congress Control Number: 2014936974

Every effort has been made to contact the copyright holders of the figures which have been reproduced from other sources. Anyone with a copyright claim who has not been properly credited is requested to contact the publishers, so that due acknowledgements may be made in subsequent editions.

© Springer International Publishing Switzerland 2014

This work is subject to copyright. All rights are reserved by the Publisher, whether the whole or part of the material is concerned, specifically the rights of translation, reprinting, reuse of illustrations, recitation, broadcasting, reproduction on microfilms or in any other physical way, and transmission or information storage and retrieval, electronic adaptation, computer software, or by similar or dissimilar methodology now known or hereafter developed. Exempted from this legal reservation are brief excerpts in connection with reviews or scholarly analysis or material supplied specifically for the purpose of being entered and executed on a computer system, for exclusive use by the purchaser of the work. Duplication of this publication or parts thereof is permitted only under the provisions of the Copyright Law of the Publisher's location, in its current version, and permission for use must always be obtained from Springer. Permissions for use may be obtained through RightsLink at the Copyright Clearance Center. Violations are liable to prosecution under the respective Copyright Law. The use of general descriptive names, registered names, trademarks, service marks, etc. in this publication does not imply, even in the absence of a specific statement, that such names are exempt from the relevant protective laws and regulations and therefore free for general use.

While the advice and information in this book are believed to be true and accurate at the date of publication, neither the authors nor the editors nor the publisher can accept any legal responsibility for any errors or omissions that may be made. The publisher makes no warranty, express or implied, with respect to the material contained herein.

Printed on acid-free paper

Springer is part of Springer Science+Business Media (www.springer.com)

*I dedicate this book to
Atena, Andreana, and Ilse,
and
to the scientific curiosity*

Foreword

The field of nonlinear dynamics and chaos has grown very much over the last few decades and is becoming more and more relevant in different disciplines. Nonlinear dynamics is no longer a field of interest to specialists. A basic knowledge of the main properties of nonlinear systems is required today in a wide range of disciplines from chemistry to economy, from medicine to social sciences. The point is that more than 300 years after that Newton equations had been formulated and after more than 100 years of quantum mechanics, a general understanding of the qualitative properties of the solutions of classical and quantum equations should be a common knowledge. This book is intended for such a purpose. It presents a clear and concise introduction to the field of nonlinear dynamics and chaos, suitable for graduate students in mathematics, physics, chemistry, engineering, and in natural sciences in general. Also students interested in quantum technologies and quantum information will find this book particularly stimulating. This volume covers a wide range of topics usually not found in similar books. Indeed dissipative and conservative systems are discussed, with more emphasis on the latter ones since, in a sense, they are more fundamental. The problem of the emergence of chaos in the classical world is discussed in detail. The second part of this volume is devoted to the quantum world, which is introduced via a semi-classical approach. Both the stationary aspects of quantum mechanics as well as the time-dependent quantum properties are discussed. This book is, therefore, a valuable and useful guide for undergraduate and graduate students in natural sciences. It is also very useful as a reference for researchers in the field of classical and quantum chaos.

Como, December 2013

Giulio Casati

Preface

This book developed from the urgent need of a text for students in their undergraduate and graduate career. While many excellent books on classical chaos as well as on quantum chaos are on the market, only a joint collection of some of them could be proposed to the students from my experience. Here, I try to give a coherent but concise introduction to the subject of classical Nonlinear Dynamics and Quantum Chaos on an equal footing, and adapted to a four hour semester course.

The stage is set by a brief introduction into the terminology of the physical description of nonintegrable problems. [Chapter 2](#) may as well be seen as part of the introduction. It presents the definition of dynamical systems in general, and useful concepts which are introduced while discussing simple examples of one-dimensional mappings. The core of the book is divided into the two main [Chaps. 3](#) and [4](#), which discuss classical and quantum aspects, respectively. Both chapters are linked wherever possible to stress the connections between classical mechanics, semiclassics, and a pure quantum approach. All the chapters contain problems which help the reader to consolidate the knowledge (hopefully!) gained from this book.

Readers will optimally profit from the book if they are familiar with the basic concepts of classical and quantum mechanics. The best preparation would be a theory course on classical mechanics, including the Lagrange and Hamiltonian formalism, and any introductory course on quantum theory, may it be theoretical or experimental.

This book could never have been prepared without the precious guidance of Tobias Schwaibold, Aldo Rampioni, and Christian Caron from Springer. I am very grateful for their support and patience. I acknowledge also the help of my students in preparing this text, in particular Andreas Deuchert, Stephan Burkhardt, Benedikt Probst, and Felix Ziegler. Many important comments on the manuscript came from my colleagues in Heidelberg, Heinz Rothe and Michael Schmidt, as well as from Giulio Casati, Oliver Morsch, and Vyacheslav Shatokhin, to all of whom I am very grateful. Finally, I thank my teachers in the very subject of the book, Andreas Buchleitner, Detlef Dürr, Italo Guarneri, Shmuel Fishman, and Peter Schlagheck, for their continuous support.

Heidelberg, December 2013

Sandro Wimberger

Contents

1	Introduction	1
1.1	Fundamental Terminology	1
1.2	Complexity	3
1.3	Classical Versus Quantum Dynamics	5
Problems		6
References		7
2	Dynamical Systems	9
2.1	Evolution Law	9
2.2	One-Dimensional Maps	11
2.2.1	The Logistic Map	11
2.2.2	The Dyadic Map	15
2.2.3	Deterministic Random Number Generators	17
Problems		18
References		18
3	Nonlinear Hamiltonian Systems	21
3.1	Integrable Examples	21
3.2	Hamiltonian Formalism	25
3.3	Important Techniques in the Hamiltonian Formalism	27
3.3.1	Conserved Quantity H	27
3.3.2	Canonical Transformations	28
3.3.3	Liouville's Theorem	31
3.3.4	Hamilton-Jacobi Theory and Action-Angle Variables	33
3.4	Integrable Systems	36
3.4.1	Examples	38
3.4.2	Poisson Brackets and Constants of Motion	39
3.5	Non-integrable Systems	40
3.6	Perturbation of Low-Dimensional Systems	40
3.6.1	Adiabatic Invariants	40
3.6.2	Principle of Averaging	43
3.7	Canonical Perturbation Theory	47
3.7.1	Statement of the Problem	47
3.7.2	One-Dimensional Case	48

3.7.3	Problem of Small Divisors	51
3.7.4	KAM Theorem	52
3.7.5	Example: Two Degrees of Freedom	55
3.7.6	Secular Perturbation Theory	56
3.8	Transition to Chaos in Hamiltonian Systems	60
3.8.1	Surface of Sections	60
3.8.2	Poincaré–Cartan Theorem	62
3.8.3	Area Preserving Maps	65
3.8.4	Fixed Points	67
3.8.5	Poincaré–Birkhoff Theorem	71
3.8.6	Dynamics Near Unstable Fixed Points	73
3.8.7	Mixed Regular-Chaotic Phase Space	78
3.9	Criteria for Local and Global Chaos	81
3.9.1	Ergodicity and Mixing	84
3.9.2	The Maximal Lyapunov Exponent	87
3.9.3	Numerical Computation of the Maximal Lyapunov Exponent	90
3.9.4	The Lyapunov Spectrum	92
3.9.5	Kolmogorov–Sinai Entropy	94
3.9.6	Resonance Overlap Criterion	95
Appendix	98
Problems	98
References	100
4	Aspects of Quantum Chaos	103
4.1	Introductory Remarks on Quantum Mechanics	103
4.2	Semiclassical Quantization of Integrable Systems	105
4.2.1	Bohr–Sommerfeld Quantization	105
4.2.2	Wentzel–Kramer–Brillouin–Jeffreys Approximation	106
4.2.3	Einstein–Keller–Brillouin Quantization	119
4.2.4	Semiclassical Wave Function for Higher Dimensional Integrable Systems	122
4.3	Semiclassical Description of Non-integrable Systems	126
4.3.1	Green’s Functions	126
4.3.2	Feynman Path Integral	128
4.3.3	Method of Stationary Phase	130
4.3.4	Van-Vleck Propagator	132
4.3.5	Semiclassical Green’s Function	134
4.3.6	Gutzwiller’s Trace Formula	136
4.3.7	Applications of Semiclassical Theory	141
4.4	Wave Functions in Phase Space	149
4.4.1	Phase Space Densities	149
4.4.2	Weyl Transform and Wigner Function	150
4.4.3	Localization Around Classical Phase Space Structures	155

Contents	xiii
4.5 Anderson and Dynamical Localization	159
4.5.1 Anderson Localization	160
4.5.2 Dynamical Localization in Periodically Driven Quantum Systems	163
4.5.3 Experiments	167
4.6 Universal Level Statistics	168
4.6.1 Level Repulsion: Avoided Crossings	169
4.6.2 Level Statistics	170
4.6.3 Symmetries and Constants of Motion	171
4.6.4 Density of States and Unfolding of Spectra	173
4.6.5 Nearest Neighbor Statistics for Integrable Systems	174
4.6.6 Nearest Neighbor Statistics for Chaotic Systems	176
4.6.7 Gaussian Ensembles of Random Matrices	179
4.6.8 More Sophisticated Methods	184
4.7 Concluding Remarks	188
Appendix	189
Problems	190
References	199
Index	203

Chapter 1

Introduction

Abstract We set the stage for our discussion of classical and quantum dynamical systems. Important notions are introduced, and similarities and differences of classical and quantum descriptions are sketched.

1.1 Fundamental Terminology

The notion *dynamics* derives from the Greek word $\eta \delta\upsilon\nu\alpha\mu\zeta$, which has the meaning of force or power. From a physical point of view we mean a change of velocity following Newton's second law

$$F = \frac{dp}{dt}, \quad (1.1.1)$$

where the momentum p is mass times velocity. If there is no external force and the motion occurs at constant velocity one speaks of "kinematics", whereas if there is a static equilibrium, in the simplest case of zero velocity, one speaks of "statics".

Chaos roots in the Greek word $\tau\ddot{o} \chi\acute{a}\sigma\zeta$ and means chaos in a sense of beginning or primary matter (unformed, empty). In this sense it is used in Greek mythology, where it designates the state of the world before all arranged order. This meaning is close to the colloquial use of the word today.

Here we will focus on *deterministic chaos*.¹ When saying deterministic we mean that each initial condition (x_0, v_0) at some given time $t = t_0$ of a differential equation is mapped in a unique way onto some final state at time $t > t_0$:

$$(x_0, v_0) \longmapsto (x(t), v(t)). \quad (1.1.2)$$

¹ From the Latin word *determinare* meaning to determine.

Since the initial condition determines the dynamics at all times such systems are predictable. Unfortunately, this is true only in a mathematical sense but problematic in practice. One may show that a solution of Newton's equations of motion (1.1.1) exists and that it is unique. But things change if one has to compute a solution when either (a) the initial condition is known only with a certain accuracy or (b) a computer (which always uses a reduced number system) is needed for the calculation. It turns out that there are differential equations (in fact most of them) whose solutions strongly depend on the initial conditions. When the computation is started with just slightly varied initial data the trajectories may differ substantially (from a point of view of shape and relative distance) already after a short time. Hence in all practical applications these systems turn out to be unpredictable. The weather forecast, for instance, usually breaks down after a few days (chaotic dynamics), whereas the earth has been traveling around the sun in 365.25 days for quite a long time now (quasi-regular dynamics).

When one is describing the reality with physical theories the notion of universality plays a crucial role:

Ein historisches Kriterium für die Eigenart der Prinzipien kann auch darin bestehen, dass immer wieder in der Geschichte des philosophischen und naturwissenschaftlichen Erkennens der Versuch hervortritt, ihnen die höchste Form der “Universalität” zuzusprechen, d.h. sie in irgendeiner Form mit dem allgemeinen Kausalsatz selbst zu identifizieren oder aus ihm unmittelbar abzuleiten. Es zeigt sich hierbei stets von neuem, dass und warum eine solche Ableitung nicht gelingen kann—aber die Tendenz zu ihr bleibt nichtsdestoweniger fortbestehen.

[Ernst Cassirer: Determinismus und Indeterminismus in der modernen Physik. Historische und systematische Studien zum Kausalproblem. Gesammelte Werke Bd. 19, Herausgegeben von Birgit Reckl, Meiner, 2004, S. 69f]

Translation:

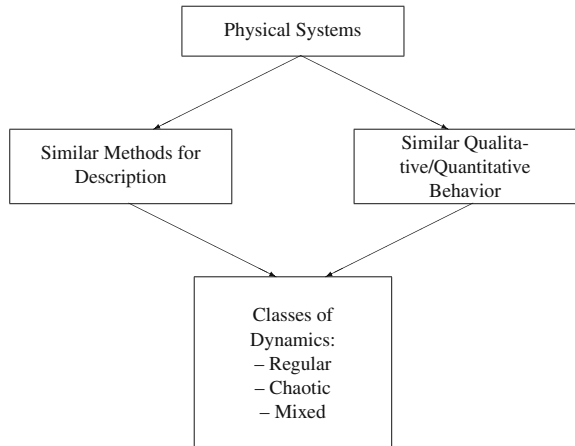
A historical criterion for the specific character of principles may also be found in the fact that in the development of philosophical and scientific knowledge the attempt is made repeatedly to ascribe to them the highest form of “universality”—that is, to identify them in some way with the general causal principle or to derive them immediately from it. In these attempts it becomes evident again and again why such derivation cannot succeed—but the tendency to attempt it nevertheless continues unabated.

[Ernst Cassirer: Determinism and indeterminism in modern physics: historical and systematic studies of the problem of causality. Yale University Press, 1956, p. 55]

Universality in physics describes the phenomenon that certain properties in mechanical systems are independent of the details of the system. Based on this similar qualitative or quantitative behaviour, it is possible to group these systems into universality classes. These contain different systems that show the same universal behaviour (described by the so-called universal quantities). Universality may show up in physics in many ways. Figure 1.1 summarises what we mean by it in the present context of dynamical systems. For classical Hamiltonian problems, the various classes of dynamics will be introduced and discussed in Chap. 3.

The number of *degrees of freedom* n and the number of conserved quantities s determine the possible dynamics of a physical system. As space dimension d one

Fig. 1.1 Ways of categorising dynamical systems



usually has $d = 1, 2, 3$. In the Hamiltonian description, see Sect. 3.2, this leads to a phase space of dimension $d_P = 2 \times d = 2, 4, 6$ per particle. Hence, the phase space of N particles moving in three space dimensions has the dimension

$$d_P = 2 \times 3N = 6N. \quad (1.1.3)$$

Thereby $n = 3N$ is the number of degrees of freedom and the factor of two in the formula arises because each point particle is described by a position and a generalized momentum. In Sect. 3.4 we will see that for $s = n$ the motion is always regular. We give two examples:

- One particle in one space dimension: If the system is conservative (no explicit time-dependence) the energy is conserved. Since there is only one degree of freedom the motion will always be regular, see Sect. 3.4.
- One particle in two space dimensions: If the energy is conserved, we have one constant of motion. For the motion to be integrable we would need yet another conserved quantity such as, for example, the momentum in one direction, or the angular momentum. An example where this is not the case is a particle moving on a billiard table with defocusing boundaries (accordingly the motion of typical orbits is chaotic). On the other hand, if the table has the shape of a circle the dynamics will be regular again (rotational symmetry then leads to angular momentum conservation).

1.2 Complexity

Many physical systems are *complex systems*. As their name already says, complex systems consist of a large number of coupled degrees of freedom. They appear in every day life, e.g. as traffic jams, and in many disciplines besides physics such as biology and chemistry [1]. Being more than just the sum of their parts, complex

systems may show emergent phenomena, see for instance the wonderful article by Anderson [2]. In this book we use the notion of complexity in a restricted sense of physical phenomena which are described by *finite* systems of coupled differential equations. For classical systems, these equations are typically nonlinear ordinary differential equations that are hard to solve by hand. In quantum theory one has to deal with the even harder problem of partial differential equations in general.

Two simple examples of classical mechanics, for which the corresponding nonlinear equations of motions can be solved analytically, are

- A pendulum in the gravity field: Let the angle ϕ describe the deflection; the equation of motion reads:

$$\ddot{\phi}(t) + \frac{g}{l} \sin(\phi(t)) = 0, \quad (1.2.1)$$

where g is the gravitational acceleration and l is the length of the pendulum.

- The Kepler problem (for two particles): The relative coordinate \mathbf{r} follows Newton's equation of motion

$$\ddot{\mathbf{r}} + \frac{\gamma M}{r^3} \mathbf{r} = 0. \quad (1.2.2)$$

Here γ is the gravitational constant and $M = m_1 + m_2$ denotes the sum of the particle masses [3–5].

Of course, these systems are not examples of complex systems. Over the last 150 years there has been a huge interest and progress in the area of nonlinear dynamics of strongly coupled systems. As an important example we mention the study of our solar system, that means of a classical many-body problem with gravitational interaction. Involved and extensive computations have been carried out in order to find fixed points of the highly nontrivial dynamics (e.g. Lagrangian points [6]). Questions of predictability and stability of the motion of asteroids or other objects which might hit the earth are of such importance that many research programs exist just for this purpose, see e.g. [7].

After the solvable two-body case the three-body Kepler problem is the next model in order of increasing complexity. Already in the nineteenth century Henri Poincaré investigated its dynamics in great detail, but nevertheless, until today it remains unsolved. Being one of the first examples of highly complicated dynamics which has been investigated so extensively, its study marked the beginning of the field of nonlinear and chaotic dynamics. General N -body Kepler problems in classical or in quantum mechanics can only be treated with perturbative methods, whose application range is typically restricted. Numerical techniques may be applied too. Computer simulations are indeed a standard tool nowadays. They are heavily used also in this book, in particular in Chaps. 2 and 3, as well as for the examples in Chap. 4. Numerical simulations are very well suited, for example,

- for “Experimental mathematics”,
- for computing solutions in a certain (possibly large) parameter range (over finite times),

- in order to find qualitative results which sometimes lead to a better understanding or even new theoretical methods.

The reliability of computational techniques (with unavoidable round-off errors) for chaotic systems is mathematically guaranteed by the so-called shadowing theorem for hyperbolic systems, discussed, for instance, in [8, 9].

1.3 Classical Versus Quantum Dynamics

Complex systems are equally important in the microscopic world where the laws of quantum mechanics are needed. Here a strong coupling between the degrees of freedom leads to the breakdown of approximations that use separable wave functions.² Results for strongly coupled or strongly distorted systems have been achieved, for instance, in

- Atomic physics: Rydberg atoms in time-dependent strong electromagnetic fields [10],
- Solid state physics: strongly interacting many-particle systems [11],
- Complex atomic nuclei (consisting of many nucleons which are heavily interacting): For them a universal description was introduced based on ensembles of random matrices [12, 13].

In this book we treat classical and quantum mechanical systems on an equal footing. So let us outline here already some relations between the two fields of physics:

- The *semiclassical limit*: $\hbar \rightarrow 0$.
 - The correspondence between classical and quantum dynamics is good if the dimensionless quantity (Action of the classical path)/($2\pi\hbar$) is a large number. This implies a large number of quantum levels per unit Planck cell, i.e. a high density of levels (or states) in the semiclassical picture, c.f. Sect. 4.2.2. The short-hand notation $\hbar \rightarrow 0$ implies exactly this approximation.
 - The approximation just discussed introduces a natural time scale (which depends on the effective \hbar). Hence, one has to be careful when treating time-dependent systems because the two limits $\hbar \rightarrow 0$ and $t \rightarrow \infty$ do not commute. A simultaneous limit procedure may be nevertheless possible under certain circumstances, see e.g. [14].
- *Decoherence*: The destruction of superpositions.
 - Describes the crossover from quantum to classical mechanics.
 - Attention: The semiclassical limit and the phenomenon of decoherence are not equivalent. An important open question: What happens if decoherence and semiclassics apply simultaneously? We will, however, not treat decohering systems

² A wave function $\Psi(x_1, x_2)$ is called separable if it is of the form $\Psi(x_1, x_2) = \Phi_1(x_1)\Phi_2(x_2)$. Formally this is true only if either the particles denoted by 1 and 2 are non-interacting or the potential is separable in the two degrees of freedom x_1 and x_2 of a single-particle problem.

but restrict ourselves to classical Hamiltonian problems and their quantum counterparts (see e.g. [15] for the treatment of dissipative problems).

- *Statistical comparison:* In classical mechanics the motion of particles is described by phase space trajectories and the description of a statistical ensemble uses probability distributions on phase space, which may mimic the evolution of a quantum mechanical wave packet of comparable size to some extent. In quantum mechanics one can also define a quasi-probability distribution on the phase space by, e.g., Wigner functions, see Sect. 4.4.2. It is then possible to compare the effects of classical and quantum mechanics by comparing these two functions. It turns out, for example, that non-classical states can be characterized by the fact that the Wigner function takes negative values (which is not possible for a probability distribution in the strict mathematical sense).

Chaos is a phenomenon that is present in many fields of classical physics (e.g., in dynamics of stars and fluids and in biophysical models [8, 9, 16, 17]). Since quantum mechanics is the more fundamental theory we can ask ourselves if there is chaotic motion in quantum systems as well. A key ingredient of the chaotic phenomenology is the sensitive dependence of the time evolution upon the initial conditions. The Schrödinger equation is a linear wave equation, implying also a linear time evolution. The consequence of linearity is that a small distortion of the initial conditions leads only to a small and constant change in the wave function at *all* times (see Sect. 4.1). Certainly, this is not what we mean when talking about “quantum chaos”. But how is then chaos created in the classical limit and is there another notion of quantum chaos? In general, a rigorous definition of quantum chaos, or “quantum chaology” (Berry [18, 19]) is more difficult than for classical systems. Usually, one computes corresponding properties of a classical and a quantum mechanical system and identifies connections. When treating billiard systems for example (particles moving on a billiard table) one finds a more pronounced amplitude of the wave function (and therefore a more pronounced density) in regions where the classical system has a periodic orbit, c.f. Sect. 4.4.3.3. This is the semiclassical approach presented in the first part of Chap. 4. It is also possible to characterize quantum mechanical systems by the analysis of their eigenspectra. This approach uses a statistical description based on ensembles of random matrices whose properties are compared with the ones of real quantum systems. Both approaches may be reconciled, as shown in Sect. 4.6, where we discuss the quantum spectra for regular and chaotic systems in some detail.

Problems

1.1. Try to think about possible ways to quantify the properties of a complex system. Think, in particular, about the dynamics of simple physical problems, such as a billiard ball moving in a plane and confined by hard reflecting walls. What is the origin of complicated dynamical behavior?

References

1. Mallamace, F., Stanley H.E. (eds.): The physics of complex systems. In: Proceedings of the International School of Physics ‘E. Fermi’, vol. Course XIX. IOS Press, Amsterdam (1996)
2. Anderson, P.W.: Science **177**(4047), 393 (1972)
3. Scheck, F.: Mechanics: From Newton’s Laws to Deterministic Chaos. Springer, Heidelberg (2007)
4. Rebhan, E.: Theoretische Physik: Mechanik. Spektrum Akademischer Verlag, Heidelberg (2006)
5. Arnold, V.I.: Mathematical Methods of Classical Mechanics. Springer, New York (1989)
6. Finn, J.M.: Classical Mechanics. Jones and Burtlett, Boston (2010)
7. Near-Earth Object Program—NASA. <http://neo.jpl.nasa.gov>
8. Lichtenberg, A.J., Lieberman, M.A.: Regular and Chaotic Dynamics. Springer, Berlin (1992)
9. Ott, E.: Chaos in Dynamical Systems. Cambridge University Press, Cambridge (2002)
10. Buchleitner, A., Delande, D., Zakrzewski, J.: Phys. Rep. **368**(5), 409 (2002)
11. Mahan, G.D.: Many Particle Physics (Physics of Solids and Liquids). Kluwer Academic/Plenum Publishers, New York (2000)
12. Guhr, T., Müller-Gröling, A., Weidenmüller, H.A.: Phys. Rep. **299**(4–6), 189 (1998)
13. Bohigas, O., Giannoni, M.J., Schmit, C.: Phys. Rev. Lett. **52**, 1 (1984)
14. Abb, M., Guarneri, I., Wimberger, S.: Phys. Rev. E **80**, 035206 (2009)
15. Haake, F.: Quantum Signatures of Chaos (Springer Series in Synergetics). Springer, Berlin (2010)
16. Strogatz, S.H.: Nonlinear Dynamics and Chaos. Westview Press, Boston (1994)
17. Thompson, J.M.T., Stewart, H.B.: Nonlinear Dynamics and Chaos. John Wiley & Sons, Chichester (2002)
18. Berry, M.V.: Phys. Scr. **40**(3), 335 (1989)
19. Berry, M.V.: Proc. R. Soc. Lond. A: Math. Phys. Sci. **413**(1844), 183 (1987)

Chapter 2

Dynamical Systems

Abstract Dynamical systems are formally defined—may they be classical or quantum. We introduce important concepts for the analysis of classical nonlinear systems. In order to focus on the essential questions, this chapter restricts to one-dimensional discrete maps as relatively simple examples of dynamical systems.

2.1 Evolution Law

A dynamical system is given by a set of states Ω and an evolution law telling us how to propagate these states in (discrete or continuous) time. Let us assume that the propagation law is homogeneous in time. That means it depends on the initial state but not on the initial time. Mathematically speaking a dynamical system is given by a one-parameter flow or map

$$T : G \times \Omega \rightarrow \Omega, \quad (2.1.1)$$
$$(g \in G, \omega \in \Omega) \mapsto T^g(\omega) \in \Omega,$$

such that the composition is given by

$$T^g \circ T^h = T^{g+h}. \quad (2.1.2)$$

For a *discrete dynamical system* we have $G = \mathbb{N}$ or $G = \mathbb{Z}$ (discrete time steps) and for a *continuous dynamical system* $G = \mathbb{R}^+$ or $G = \mathbb{R}$ (continuous time). The set Ω contains all possible states. It describes the physical reality one wants to model and is called the phase space. From an algebraic point of view the above defined maps form a semi-group that operates on Ω . If the map T is invertible for all $t \in G$ this structure extends to a group¹ and we say that the dynamical system is invertible.

¹ Translational invariance of the flow with respect to the time parameter g is only given if the generator of the dynamics is itself time-independent. Any classical problem can formally be made

The sets $\{T^t(\omega)\}_{t \in G}$ define *orbits* or *trajectories* of the map. They can be discrete or continuous, finite or infinite.

The above definitions are quite abstract and therefore we give a few examples.

1. The simplest example is a discrete dynamical system defined by an iterated map. Let f be a map of the interval Ω onto itself. We define

$$T^n = \underbrace{f \circ f \circ \dots \circ f}_{n \text{ times}}, \quad G = \mathbb{N}. \quad (2.1.3)$$

If the map f is invertible so is the dynamical system, and we can extend time to $G = \mathbb{Z}$. Two concrete examples of such discrete maps will be given in Sect. 2.2.

2. An example from classical physics is the motion of N particles in three space dimensions. The dynamics are governed by Newton's equations of motion for the vector of positions $\mathbf{x}(t)$

$$m\ddot{\mathbf{x}}(t) = F(\mathbf{x}(t)). \quad (2.1.4)$$

Defining the composite vector $\mathbf{y}(t) = (\mathbf{y}_1(t) \equiv \mathbf{x}(t), \dot{\mathbf{x}}(t))$ and $f(\mathbf{y}(t)) = (\mathbf{y}_1(t), F(\mathbf{y}_1(t))/m)$, we obtain

$$\dot{\mathbf{y}}(t) = f(\mathbf{y}(t)). \quad (2.1.5)$$

To make the connection between this formulation and the definition of dynamical systems we write the solution as $T^t(\mathbf{y}(0)) = \mathbf{y}(t)$. We obtain the solution in one step but also in two steps if we insert the end of the first trajectory as an initial condition into the second trajectory,² i.e. $T^{s+t}(\mathbf{y}(0)) = T^t(T^s(\mathbf{y}(0))) = (T^t \circ T^s)(\mathbf{y}(0))$. Note that $\mathbf{x}(t)$ is an element of the configuration space \mathbb{R}^{3N} while $\mathbf{y}(t)$ is an element of the phase space $\Omega = \mathbb{R}^{6N}$. Equation (2.1.5) is equivalent to the Hamiltonian formulation of the problem. Motivated by our general definition (2.1.1) and (2.1.2) we see that this is actually the natural way to treat classical dynamics. We will therefore use the formalism of Hamiltonian mechanics (Sect. 3.2), operating in phase space rather than configuration space, throughout the Chap. 3.

3. The time evolution of a quantum mechanical spinless particle in three space dimensions with time-independent hermitian Hamiltonian. Here $\Psi_0 \in \mathcal{L}^2(\mathbb{R}^3) = \Omega$ and

$$T^t(\Psi_0) = \hat{U}(t)\Psi_0 = e^{-i\hat{H}t/\hbar}\Psi_0. \quad (2.1.6)$$

The so-defined dynamical system is obviously invertible, with $T^{-t} = \hat{U}^\dagger(t)$.

(Footnote 1 continued)

time-independent, see Sect. 3.3.1; hence the property of a translationally invariant group is always obeyed in this generalized sense. The quantum evolution for periodically time-dependent systems can also be cast in a similar way using a theorem of Floquet [1]. For generally time-dependent quantum systems, time ordering [2] must be used to formally write down the evolution law.

² A formal proof is found in [3] based on the fact that every point in phase space has a unique time evolution.

4. Non-invertible quantum dynamics: A reduced quantum mechanical system (a subsystem of a larger one) can—under certain conditions—be described by a master equation for the density operator of the system

$$\dot{\hat{\rho}}(t) = -\frac{i}{\hbar} \left[\hat{H}, \hat{\rho}(t) \right] + \hat{\mathcal{L}}(\hat{\rho}(t)). \quad (2.1.7)$$

In this case the time evolution has only the property of a semi-group. With the above equation it is possible to model dissipation and decoherence by the Lindblad operator $\hat{\mathcal{L}}$, whilst the coherent evolution is induced by the first term on the right hand side of the equation. For more information see, e.g., [4, 5]. Replacing the density operator by a classical density distribution in phase space one may model the corresponding quantum evolution to some extent. On the classical level one then has to deal with a Fokker-Planck equation for phase space densities describing irreversible motion [6].

2.2 One-Dimensional Maps

In the following we discuss two seemingly simple discrete dynamical systems. Those are not Hamiltonian systems but one-dimensional mappings, i.e., the phase space is just one-dimensional. Yet, it will turn out that some general concepts can be easily introduced with the help of such maps, e.g. fixed points and their stability or periodic orbits. They have also the great advantage that much can be shown rigorously for them [7, 8]. Therefore, one-dimensional discrete maps form one of the bases for the mathematical theory of dynamical systems, see for instance [9].

2.2.1 The Logistic Map

The logistic map is a versatile and well understood example of a discrete dynamical map which was introduced in 1838 by Pierre Francois Verhulst as a mathematical model for demographic evolution [10]. Its nonlinear iteration equation is given by the formula

$$y_{n+1} = R y_n (M - y_n), \quad (2.2.1)$$

where y_n is a population at time n , $R \geq 0$ is a growth rate and M is an upper bound for the population. The population at the next time step is proportional to the growth rate times the population (which alone would lead to exponential growth for $R > 1/M$) and to the available resources assumed to be given by $M - y_n$. The system's evolution is relatively simple for $R < 1/M$ having the asymptotic solution $\lim_{n \rightarrow \infty} y_n = 0$ (extinct population) for all initial values. For general values of the growth rate, the system shows a surprisingly complicated dynamical behavior. Most

interestingly, in some parameter regimes the motion becomes chaotic, which means that the population y_n strongly depends on the initial condition y_0 . Additionally, the system might not converge to an asymptotic value or show non-periodic behavior.

Let us now analyse the logistic map in more detail. In order to get the standard form of the logistic map we rescale the variable describing the population $x_n = y_n/M$ and write the time step as the application of the evolution law T leading to

$$T(x) = rx(1-x), \text{ for } x \in \Omega = [0, 1]. \quad (2.2.2)$$

Here $r = MR$. If we want T to map the interval Ω onto itself we have to choose $r \in [0, 4]$. First, we look for fixed points of the map T , that means points for which

$$T(x^*) = x^* \Leftrightarrow x^* = rx^*(1-x^*). \quad (2.2.3)$$

holds. The above equation has two solutions:

$$x_{1,1}^* = 0 \text{ is } \begin{cases} \text{an attractive fixed point for } & r < 1 \\ \text{an indifferent fixed point for } & r = 1 \\ \text{a repulsive fixed point for } & r > 1, \end{cases} \quad (2.2.4)$$

and

$$x_{1,2}^* = 1 - \frac{1}{r} \text{ is } \begin{cases} \text{an attractive fixed point for } & 1 < r < 3 \\ \text{an indifferent fixed point for } & r \in \{1, 3\} \\ \text{a repulsive fixed point for } & |r - 2| > 1. \end{cases} \quad (2.2.5)$$

Thereby we have used the notion that a fixed point x^* is called *attractive/repulsive* if the derivative with respect to x $|T'(x^*)| \leq 1$, and *indifferent* if $|T'(x^*)| = 1$. Attractive fixed points are important quantities because they lead to asymptotically converging dynamics. For all initial conditions which lie in the subset of Ω around the fixed point where the map T is contracting (modulus of the derivative smaller than one), the evolution converges towards the fixed point for large times. How the system reaches the fixed point $x_{1,2}^*$ by iteration is shown schematically in Fig. 2.1.

Besides the two fixed points $x_{1,1}^*$ and $x_{1,2}^*$, the logistic map has fixed points of higher order, too. That means fixed points of the p -times iterated map T^p . A fixed point of order p is defined by

$$T^p(x^*) = x^*. \quad (2.2.6)$$

This includes the possibility that for all $n \leq p$ one has $T^n(x^*) = x^*$, as, for example, a fixed point of first order is also a fixed point of all higher orders. Usually, one assumes that p is the prime period of x^* , that is, we have $T^n(x^*) \neq x^*$ for all $n < p$. Fixed points lead to *periodic orbits* (PO), that means orbits $\{T^n(x^*)\}_{n \in \mathbb{N}}$ which consist only of finitely many points. If one starts the dynamics with a fixed

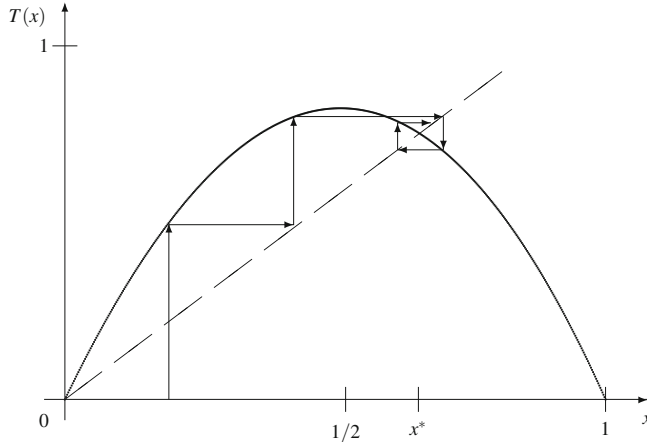


Fig. 2.1 Schematic iteration shown by the arrows which converges to the fixed point of the logistic map for $r = 2.5$

point of order p , the initial value is recovered after p time steps. The logistic map has, for example, two fixed points of order two

$$x_{2,(1,2)}^* = \frac{1}{2r} \left(r + 1 \pm \sqrt{(r+1)(r-3)} \right), \quad (2.2.7)$$

which are attractive for $3 < r < 1 + \sqrt{6} \approx 3.45$. As r is increased, attractive fixed points of higher order (4, 8, 16, ...) emerge. The fixed points are, however, determined by the solutions of high-order polynomials and analytical values are difficult to obtain, see, for example, [11] for more details.

We note that there is a natural relation between all fixed points of a given order $p > 1$. Assume, for instance, the two second-order fixed points $x_{2,1}^*$ and $x_{2,2}^*$. When we apply T^2 on $x_{2,1}^*$ we find $T(T(x_{2,1}^*)) = T(x_{2,2}^*) = x_{2,1}^*$. This behavior is found for all fixed points of order $p > 1$. Let $x_{p,i}^*$, $i = 1, \dots, p$, be the p fixed points of order p (the number of fixed points always equals the order). One finds

$$T^p(x_{p,1}^*) = \underbrace{T(T(\dots(x_{p,1}^*)\dots))}_{p \text{ times}} = \underbrace{T(T(\dots(x_{p,2}^*)\dots))}_{p-1 \text{ times}} = \dots = T(x_{p,p}^*) = x_{p,1}^*. \quad (2.2.8)$$

Hence, if one fixed point of order p is given, the $p - 1$ other fixed points of that order can be computed by applying T repeatedly. We illustrate the described phenomenon in (2.2.8) for $p = 2$. The two fixed-points of second order are mapped onto each other by T (Fig. 2.2).

The dynamical behavior of the logistic map is summarized in its bifurcation diagram, see Fig. 2.3. For each value of r on the abscissa, the value of x is plotted after 400 iterations for random initial data. It turns out that outside the chaotic regime

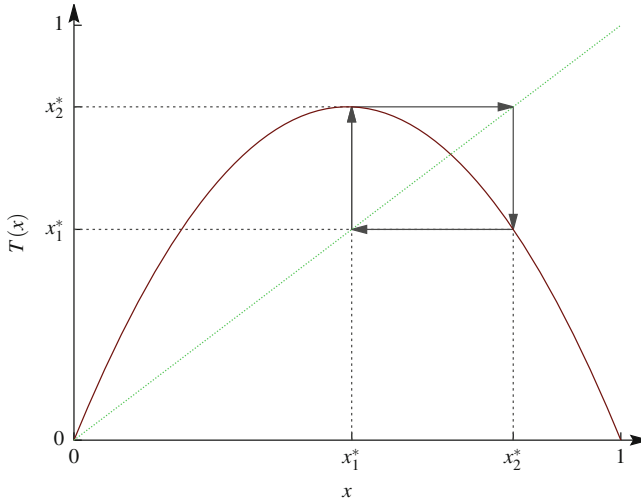


Fig. 2.2 T maps x_1^* onto x_2^* and vice versa. Accordingly, both x_1^* and x_2^* are fixed points of $T^2 = T \circ T$. The plot was made for the parameter $r = 3.214$, giving $x_1^* \approx 0.5078$ and $x_2^* \approx 0.8033$

the asymptotic evolution does not depend on the initial conditions. For $r < 1$, the motion converges towards the fixed point $x_{1,1}^* = 0$. For $1 < r < 3$, it goes to $x_{1,2}^* = 1 - \frac{1}{r}$ for almost every x_0 . At $r = 3$ is a *bifurcation* point. For larger values of the growth rate, the asymptotic dynamics converge towards the two fixed points of second order, $x_{2,1}^*$ and $x_{2,2}^*$ (defining a periodic orbit). This phenomenon is known as *period doubling*. In Fig. 2.3 we see both solutions, because x_{400} is plotted for many initial points. Note that, in the limit of many iterations, the dynamics do not converge to one of the fixed points, but the evolution jumps between them for all times.³ The two fixed points of order two split again into two new ones at $r = 1 + \sqrt{6}$. This scheme repeats itself infinitely often while the distance between the bifurcation points decreases rapidly. It can be shown [7, 12] that the ratios of the lengths between two subsequent bifurcation points approach a limiting value

$$\lim_{k \rightarrow \infty} \delta_k = \frac{r_k - r_{k-1}}{r_{k+1} - r_k} = 4.669201 \dots \in \mathbb{R} \setminus \mathbb{Q}, \quad (2.2.9)$$

known as the Feigenbaum constant. For most r beyond the critical value $r_\infty = 3.569945\dots$ (known as accumulation point) the system becomes chaotic, which means

³ When we say that the dynamics (for the initial condition x_0) converge towards a periodic orbit with p elements (or towards the fixed point x^* of order p , which is an element of the periodic orbit) we mean that $\lim_{n \rightarrow \infty} T^{np}(x_0) = x^*$.

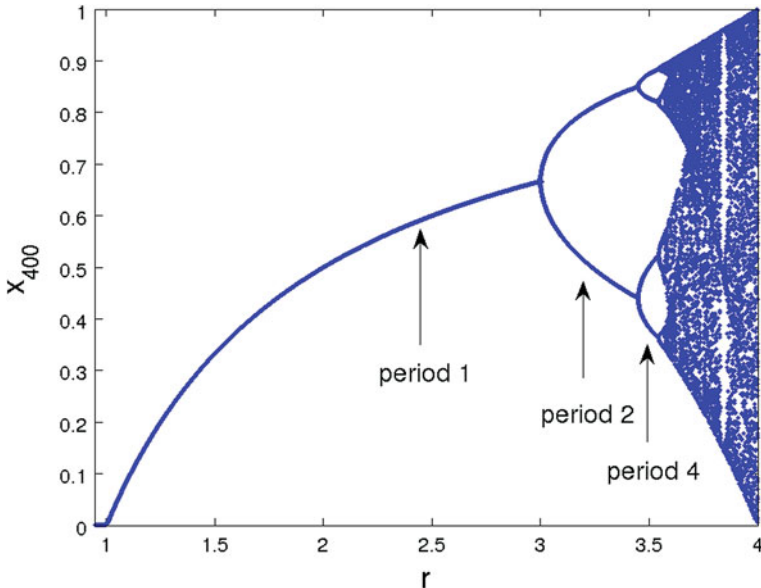


Fig. 2.3 Bifurcation diagram of the logistic map. For each value on the abscissa, the value $x_{n=400} \approx x_\infty$, i.e. after 400 iterations of the map, for random initial data is represented on the ordinate. The path into chaos goes along a cascade of accumulating bifurcation points. Up to $r < 3.5$ stable fixed points of order 1, 2 and 4 are shown. Above $r_\infty \approx 3.57$ chaos develops as motivated in the text

that the asymptotic evolution will not converge towards periodic orbits any more.⁴ Here the values x_{400} (for many random initial conditions) cover quasi-uniformly the whole phase space $\Omega = [0, 1]$. Note that in this regime the motion strongly depends on the initial value x_0 . Nevertheless there exist values $r > r_\infty$ for which new attractive fixed points (of order 3, 5, 6, 7 ...) appear, see [8]. The route into chaos via a cascade of accumulating bifurcation points (period doublings) is a general phenomenon and not limited to the here reported example of the logistic map. Examples of so-called mixed Hamiltonian systems showing bifurcations of initially stable resonance islands with increasing perturbation are discussed in Sect. 3.8.7.

2.2.2 The Dyadic Map

Another important example of a discrete dynamical map showing chaotic behavior is the dyadic map, also known as Bernoulli shift. It is defined by

⁴ Also in the chaotic regime there exist fixed points but they are not attractive. Since at each point of a period doubling the fixed point does not vanish but only loses the property of attraction, the fixed points in the chaotic regime form a dense set (yet of Lebesgue measure zero in the interval $[0, 1]$).

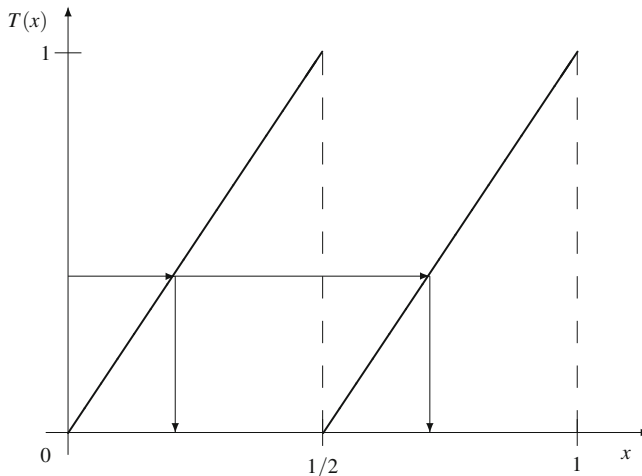


Fig. 2.4 The dyadic map. As indicated by the arrows, the map is not one-to-one

$$T(x) = \begin{cases} 2x & \text{for } 0 \leq x < \frac{1}{2} \\ 2x - 1 & \text{for } \frac{1}{2} \leq x \leq 1 \end{cases}. \quad (2.2.10)$$

Its phase space is the unit interval $\Omega = [0, 1]$. When we represent the numbers $x \in \Omega$ in the binary representation $x = \sum_{i=1}^{\infty} x_i 2^{-i}$, $x_i \in \{0, 1\}$, the map can be interpreted as a shift of decimals:

$$x = 0.x_1 x_2 x_3 x_4 \dots \rightarrow T(x) = 0.x_2 x_3 x_4 \dots \quad (2.2.11)$$

This explains also the name (Bernoulli) shift map. The dyadic map is displayed in Fig. 2.4.

It can be shown that it is topologically conjugate⁵ to the logistic map with $r = 4$ (which is chaotic for this parameter), see [13–15].⁶

The dynamics of the dyadic map can be summarized as follows. If the initial condition is irrational, the motion will be non-periodic. Note that this is true for

⁵ Two functions f and g are said to be topologically conjugate if there exists a homeomorphism h (continuous and invertible) that conjugates one into the other, in formulas $g = h^{-1} \circ f \circ h$. This is important in the theory of dynamical systems because the same must hold for the iterated system $g_n = h^{-1} \circ f_n \circ h$. Hence if one can solve one system, the solution of the other one follows immediately.

⁶ In the literature one often finds that the logistic map for $r = 4$ is topologically conjugate to the tent map [14], but the tent map is topologically equivalent to the dyadic map [15], which together gives the wanted equivalence.

almost all⁷ initial values. For $x_0 \in \mathbb{Q}$, the evolved value converges towards zero if the binary representation of x_0 is non-periodic and hence finite, or towards a periodic orbit if the representation shows periodicity. Hence, as for the logistic map, the fixed points in the chaotic regime form a set of Lebesgue measure zero. Being such a simple system the dyadic map can be solved exactly. Exploiting the connection to the logistic maps, the solution can be used to compute an analytical solution of the dynamics of the logistic map for $r = 4$ as well. It reads

$$x_{n+1} = \sin^2(2^n \Theta \pi), \quad (2.2.12)$$

with $\Theta = \frac{1}{\pi} \sin^{-1}(\sqrt{x_0})$ for the initial condition x_0 , see [17, 18].

Analyzing the dyadic map, it is particularly simple to see why the forecast of chaotic systems is so difficult. If one starts with a number that is only precisely known up to m digits, in the binary representation all information and therewith the predictability of the model is lost after m iterations. As a consequence, we can easily compute the rate of spreading of initially close points. This rate is known as *Lyapunov exponent* and defined by

$$\sigma = \lim_{n \rightarrow \infty} \lim_{m \rightarrow \infty} \frac{1}{n} \ln \left| \frac{x_n(x_0) - x_n(x'_0)}{2^{-m}} \right| = \lim_{n \rightarrow \infty} \lim_{m \rightarrow \infty} \frac{1}{n} \ln \left| \frac{2^{-m+n}}{2^{-m}} \right| = \ln 2. \quad (2.2.13)$$

Here the initial conditions x_0 and x'_0 differ only in the m -th digit in Eq. (2.2.11). σ is called exponent since it characterizes the speed of exponential spreading as time evolves. For Hamiltonian systems, we will discuss Lyapunov exponents in detail in Sect. 3.9.

2.2.3 Deterministic Random Number Generators

A somewhat surprising application of chaotic maps is the deterministic generation of so-called pseudo-random numbers. Since the motion of a chaotic map depends sensitively on the initial conditions, a different series of numbers is generated for different initial values. If one does not start the dynamics at one of the fixed points (which form a set of measure zero anyhow), these series will neither be periodic nor be converging to a single point. Unfortunately, this scenario does not work on a computer, which needs to rely on a finite set of numbers,⁸ and therefore necessarily produces periodic orbits at some stage. Nevertheless, so-called linear congruential generators, as generalizations of the dyadic map, can be used as low-quality random number generators:

⁷The measure theoretical notion “for almost all” means for all but a set of Lebesgue measure zero [16].

⁸This set is normally composed exclusively of rational numbers, leading e.g. to non-chaotic behavior for the dyadic map.

$$a_{n+1} = N_1 a_n \bmod N_2, \quad (2.2.14)$$

$$b_{n+1} = \frac{a_{n+1}}{N_2}, \quad (2.2.15)$$

where $N_1, N_2, a_n \in \mathbb{N}$ [19]. This procedure generates “uncorrelated” and uniformly distributed numbers b_i in the unit interval, but the constants N_1 and N_2 should be chosen very carefully in order to maximize the periodicity as well as to minimize correlations between subsequent numbers [20]. While this algorithm is very fast and easy to implement, it has many problems (see chapter 7.1 of [20]) and today other methods like the Mersenne Twister [21] have widely replaced it due to their high period ($2^{19937} - 1$, not a mistake!) and efficient implementations [22]. It should be stressed that the performance of these random number generators needs to be analyzed using number theoretical tools, not the ones presented in this chapter.

Therewith, we conclude the examination of one-dimensional discrete maps which have been introduced as toy models to exemplify chaotic behavior. In the next Chapter we come to “real” physical applications of classical mechanics. Since even systems with one degree of freedom have a two-dimensional phase space and a continuous time evolution a priori, we expect a more complicated dynamical behavior for them. In what follows in this book, we will restrict ourselves exclusively now to so-called Hamiltonian systems without friction or dissipation, whose time evolution is invertible.

Problems

2.1. Prove the following theorem:

Let T be a dynamical map, as introduced in Sect. 2.1, with a fixed point x^* , and continuously differentiable with respect to x close to the fixed point. If its derivative with respect to x is $|T'(x)|_{x=x^*} < 1$, then x^* is attractive.

2.2. Find the fixed points of order two of the logistic map from Eq. (2.2.2) with r as a free parameter. Check also the stability of the fixed points found.

2.3. Find all 1st and 2nd order fixed points of the dyadic shift map from Eq. (2.2.10).

References

1. Shirley, J.H.: Phys. Rev. **138**, B979 (1965)
2. Sakurai, J.J.: Modern Quantum Mechanics. Addison-Wesley Publishing Company, Reading (1994)
3. Teschl, G.: Ordinary differential equations and dynamical systems (Graduate Studies in Mathematics, Amer. Math. Soc., Providence, (to appear), <http://www.mat.univie.ac.at/~gerald/ftp/book-ode/index.html>, 2011)
4. Breuer, P., Petruccione, F.: The Theory of Open Quantum Systems. Oxford University Press, Oxford (2007)
5. Walls, D.F., Milburn, G.J.: Quantum Optics. Springer, Berlin (2008)

6. Risken, H.: The Fokker-Planck Equation: Methods of Solutions and Applications. Springer Series in Synergetics. Springer, Heidelberg (1996)
7. Schuster, H.G.: Deterministic Chaos. VCH, Weinheim (1988)
8. Ott, E.: Chaos in Dynamical Systems. Cambridge University Press, Cambridge (2002)
9. Metzler, W.: Nichtlineare Dynamik und Chaos. Teubner, Stuttgart (1998)
10. Verhulst, P.F.: Corr. Math. Phys. **10**, 113 (1838)
11. Weisstein, E.W.: Logistic map. MathWorld—a wolfram web resource. <http://mathworld.wolfram.com/LogisticMap.html>
12. Feigenbaum, M.J.: J. Stat. Phys. **21**, 669 (1979)
13. Driebe, D.J.: Fully Chaotic Maps and Broken Time Symmetry. Kluwer Academic Publishers, Dordrecht (1999)
14. Berglund, N.: Preprint. [arXiv:math/0111177v1](https://arxiv.org/abs/math/0111177v1) (2001)
15. Yoshioka, D., Tsuneda, A., Inoue, T.: Ieice Trans. Fundam. **E88-A**(10), 2745–2761 (2005)
16. Walter, W.: Analysis 2. Springer, Berlin (2002)
17. Little, M., Heesch, D.: J. Differ. Equ. Appl. **10**(11), 949 (2004)
18. Schröder, E.: Math. Ann. **3**, 296 (1870)
19. Castiglione, P., Falconi, M., Lesne, A., Vulpiani, A.: Chaos and Coarse Graining in Statistical Mechanics. Cambridge University Press, Cambridge (2008)
20. Press, W.H., Teukolsky, S.A., Vetterling, W.T., Flannery, B.P.: Numerical Recipes 3rd Edition: The Art of Scientific Computing, 3rd edn. Cambridge University Press, New York (2007)
21. Matsumoto, M., Nishimura, T.: ACM Trans. Model. Comput. Simul. **8**(1), 3 (1998)
22. Saito, M., Matsumoto, M.: SIMD-oriented fast Mersenne Twister. In: Keller, A., Heinrich, S., Niederreiter, H. (eds.) Monte Carlo and Quasi-Monte Carlo Methods 2006, pp. 607–622. Springer, Berlin Heidelberg (2008)

Chapter 3

Nonlinear Hamiltonian Systems

Abstract In this chapter we investigate the dynamics of classical nonlinear Hamiltonian systems, which—a priori—are examples of continuous dynamical systems. As in the discrete case (see examples in Chap. 2), we are interested in the classification of their dynamics. After a short review of the basic concepts of Hamiltonian mechanics, we define integrability (and therewith regular motion) in Sect. 3.4. The non-integrability property is then discussed in Sect. 3.5. The addition of small non-integrable parts to the Hamiltonian function (Sects. 3.6.1 and 3.7) leads us to the formal theory of canonical perturbations, which turns out to be a highly valuable technique for the treatment of systems with one degree of freedom and shows profound difficulties when applied to realistic systems with more degrees of freedom. We will interpret these problems as the seeds of chaotic motion in general. A key result for the understanding of the transition from regular to chaotic motion is the KAM theorem (Sect. 3.7.4), which assures the stability in nonlinear systems that are not integrable but behave approximately like them. Within the framework of the surface of section technique, chaotic motion is discussed from a phenomenological point of view in Sect. 3.8. More quantitative measures of local and global chaos are finally presented in Sect. 3.9.

3.1 Integrable Examples

The equations of motion in classical mechanics are ordinary differential equations. In this section we give examples where these equations can be solved with the help of constants of motion. The systems discussed here are all one-dimensional and hence one conserved quantity (as for example the energy) suffices to integrate the equations of motion for one particle and to obtain explicit solutions. For simplicity we set the particle mass $m = 1$.

As a first example, we analyze the harmonic oscillator. Its defining equation is linear and reads

$$\ddot{x} + \omega^2 x = 0. \quad (3.1.1)$$

The solution is found with the help of the ansatz $x(t) = Ae^{\lambda t} + Be^{-\lambda t}$, with constant coefficients A and B and an imaginary λ . However, there is a more systematic way of solving the problem. Therefore we transform to a system of two first-order differential equations:

$$\dot{x} = y, \quad (3.1.2)$$

$$\dot{y} = -\omega^2 x, \quad (3.1.3)$$

which implies that

$$y\dot{y} = -\omega^2 x\dot{x} \quad (3.1.4)$$

$$\Leftrightarrow 0 = \frac{d}{dt} \left(\frac{y^2}{2} + \frac{\omega^2 x^2}{2} \right). \quad (3.1.5)$$

We have found a constant of motion which is nothing but the total energy. It can be used to solve one of the two equations

$$E = \frac{y^2}{2} + \frac{\omega^2 x^2}{2} \quad (3.1.6)$$

$$\Rightarrow y = \dot{x} = \sqrt{2E - \omega^2 x^2}. \quad (3.1.7)$$

In the next step we use the relation $\frac{dt(x)}{dx} = \frac{1}{\dot{x}(t)}$:

$$\int dt = \int \frac{dx}{\sqrt{2E - \omega^2 x^2}} \quad (3.1.8)$$

$$\Leftrightarrow t = \frac{1}{\omega} \arcsin \left(\frac{x\omega}{\sqrt{2E}} \right) + t_0. \quad (3.1.9)$$

The solution of the original problem thus reads

$$x(t) = \frac{\sqrt{2E}}{\omega} \sin(\omega(t - t_0)). \quad (3.1.10)$$

Furthermore, we can compute the period of the motion by solving

$$\dot{x} = 0 \Rightarrow x = \pm \frac{\sqrt{2E}}{\omega} \Rightarrow T = \frac{2\pi}{\omega}. \quad (3.1.11)$$

Linear systems of differential equations can often be solved by a simple ansatz. One example are atoms located at the sites of a one-dimensional lattice which couple via a linear force to their nearest neighbors (as if there were harmonic springs between them). The system is used as a model for phononic degrees of freedom in a crystal [1]. Here we are specifically interested in nonlinear systems, e.g., with a force which is a nonlinear function of position. Nonlinearity leads to complex coupled Hamilton's equations of motion, and is hence a seed for realising chaotic motion. We give now three examples of integrable systems with a nonlinear force.

- (a) First we investigate a system with a more general force that includes the case of the harmonic oscillator

$$\ddot{x} = F(x), \quad F(x) = a + bx + cx^2 + dx^3 \quad (3.1.12)$$

(possible higher orders are rarely needed). We solve the problem in analogy to the linear system above:

$$\dot{x} = y, \quad (3.1.13)$$

$$\dot{y} = F(x). \quad (3.1.14)$$

Again we find a constant of motion (that we will denote by E because it is again the total energy)

$$y\dot{y} = F(x)\dot{x} \Leftrightarrow \frac{d}{dt} \left(\frac{y^2}{2} - \left(ax + \frac{1}{2}bx^2 + \frac{1}{3}cx^3 + \frac{1}{4}dx^4 \right) \right) = 0. \quad (3.1.15)$$

This can be integrated

$$\int dt = \int \frac{dx}{\sqrt{2(ax + \frac{1}{2}bx^2 + \frac{1}{3}cx^3 + \frac{1}{4}dx^4 + E)}} \quad (3.1.16)$$

and we obtain the so-called *elliptic integrals* as solutions (see [2, 3]).

- (b) The force is given by a power law:

$$F(x) = -an|x|^{n-1} \quad (3.1.17)$$

and derives from the potential $V(x) = a|x|^n$. We chose $a > 0$ and $n > 1$. Following the same derivation we arrive at the integral

$$\int dt = \int \frac{dx}{\sqrt{2(E - a|x|^n)}}. \quad (3.1.18)$$

The integral can be solved with a few mathematical tricks to compute the oscillation period

$$T = \int_0^T dt = \frac{2}{n} \sqrt{\frac{2\pi}{E}} \left(\frac{E}{a}\right)^{\frac{1}{n}} \frac{\Gamma(\frac{1}{n})}{\Gamma(\frac{1}{2} + \frac{1}{n})}, \quad (3.1.19)$$

using the Γ function [2, 3].

- (c) The classical pendulum obeys the equation

$$\ddot{\Theta} = -\frac{g \sin(\Theta)}{L}. \quad (3.1.20)$$

For small angles, the sine function can be approximated by the angle itself and one recovers the harmonic oscillator. For the general pendulum one finds

$$E = \frac{1}{2} \dot{\Theta}^2 - \frac{g \cos(\Theta)}{L}, \quad (3.1.21)$$

which leads to

$$\int dt = \int \frac{d\Theta}{\sqrt{2(E + g/L \cos(\Theta))}}. \quad (3.1.22)$$

The period can be computed as for the harmonic oscillator:

$$\dot{\Theta} = 0 \Rightarrow \Theta_{max} \text{ where } E = -g/L \cos(\Theta_{max}). \quad (3.1.23)$$

It reads

$$T = \int_0^T dt = 4 \sqrt{\frac{L}{2g}} \int_0^{\Theta_{max}} \frac{d\Theta}{\sqrt{\cos(\Theta) - \cos(\Theta_{max})}}. \quad (3.1.24)$$

We apply the transformation $\cos(\Theta) = 1 - 2k^2 \sin^2(\varphi)$ with

$$k = \sin(\Theta_{max}/2) = \sin\left[\frac{1}{2} \arccos(-\frac{EL}{g})\right] = \sqrt{\frac{1}{2} \left(1 + \frac{EL}{g}\right)} \quad (3.1.25)$$

and use $\cos(\Theta_{min}) = 1 - 2k^2$ to obtain

$$T = 4 \sqrt{\frac{L}{g}} \int_0^{\pi/2} \frac{d\varphi}{\sqrt{1 - k^2 \sin^2(\varphi)}} = 4 \sqrt{\frac{L}{g}} K(k). \quad (3.1.26)$$

The function $K(k)$ is the complete elliptic integral of the first kind [2]. When we approximate $\cos(x) = 1 - x^2/2$ the period for small k is given by

$$T(k \approx 0) = 2\pi \sqrt{\frac{L}{g}} \left(1 + \frac{\Theta_{max}^2}{16} + \dots \right). \quad (3.1.27)$$

The first term is just the period of the harmonic oscillator. The second term gives a correction, which already depends on the energy. Hence, T will in general be a function of E , a property typical of nonlinear systems. This implies that resonant driving at constant ω is not possible over long times. Additionally, the period at the crossover from libration to rotation where $\Theta = \pi$ and $E = g/L \Leftrightarrow k = 1$ diverges, $T(k = 1) = \infty$. Physically speaking it takes infinitely long to go through this separatrix.¹

3.2 Hamiltonian Formalism

The Lagrangian formalism in configuration space is well-suited for solving practical problems (in particular with constraints). It uses the Lagrangian function $\mathcal{L}(q, \dot{q}, t)$ where the dimension of the coordinate vector q equals the numbers of degrees of freedom n [4, 5]. For some problems, it is more useful to turn to a phase space description via a Legendre transform introducing the Hamiltonian $H(q, p, t) = p \cdot q - \mathcal{L}$. Here $p_i = \partial \mathcal{L} / \partial \dot{q}_i$ are the generalized momenta. When we introduce the notation $z^T = (q, p)$, the Hamiltonian equations of motion read²

$$\dot{z}(t) = J \cdot \nabla H(z, t), \quad J = \begin{pmatrix} 0 & I \\ -I & 0 \end{pmatrix}, \quad (3.2.1)$$

with I being the n -dimensional identity matrix. They form a set of $2n$ first order ordinary differential equations. The antisymmetric matrix J is also called symplectic. The symplectic property distinguishes the Hamiltonian formalism, see Ref. [6] for more details. For us, it suffices to note that both variable sets q and p are independent and equally important. The Hamiltonian formalism is well suited for

- the description of non-integrable systems,
- perturbation theory,
- the comparison to optics and to quantum mechanics in the framework of semiclassical methods (for the latter see Sects. 4.2 and 4.3).

Since the Hamiltonian is the total energy of the system, it can easily be given in explicit form. Here are some simple examples:

1. Mass point in an external potential:

¹ A separatrix is a boundary in phase space separating two regions of qualitatively different motions, see Fig. 3.1 below for the pendulum.

² To simplify the notation, vector quantities are not always specified in boldface. From the local context it should be clear that the corresponding symbols represent n -dimensional vectors.

$$H = \frac{p^2}{2m} + V(q). \quad (3.2.2)$$

The equations of motion are equivalent to Newton's second law $m\ddot{q} = -\partial V/\partial q$ and read

$$\dot{q} = \frac{\partial H}{\partial p} = \frac{p}{m}, \quad \dot{p} = -\frac{\partial H}{\partial q} = -\frac{\partial V}{\partial q}. \quad (3.2.3)$$

2. The one-dimensional harmonic oscillator, see Eq. (3.1.1),

$$H = \frac{p^2}{2m} + \frac{1}{2}m\omega^2q^2. \quad (3.2.4)$$

The equations of motion are

$$\dot{q} = \frac{p}{m}, \quad \dot{p} = -m\omega q^2, \quad (3.2.5)$$

with solution

$$q(t) = q_0 \sin(\omega t + \varphi_0), \quad p(t) = m\omega q_0 \cos(\omega t + \varphi_0). \quad (3.2.6)$$

The solution obeys the defining equation for an ellipse in the plane spanned by q and p for all times

$$\frac{q(t)^2}{q_0^2} + \frac{p(t)^2}{(q_0 m \omega)^2} = 1, \quad (3.2.7)$$

showing that there are only closed (oscillatory) orbits possible in phase space.

3. The pendulum in a gravity field, see Eq. (3.1.20),

$$H = \frac{p_\vartheta^2}{2mL^2} - mgL \cos(q). \quad (3.2.8)$$

The equations of motion are

$$\dot{q} = \frac{p_\vartheta}{mL^2} \quad \text{and} \quad \dot{p}_\vartheta = -mgL \sin(q). \quad (3.2.9)$$

The phase space trajectories for different total energies are shown in Fig. 3.1. Using the identification $\vartheta = q \bmod 2\pi$, the angle ϑ and the angular momentum p_ϑ form a canonical pair of variables, see Sect. 3.3.2.

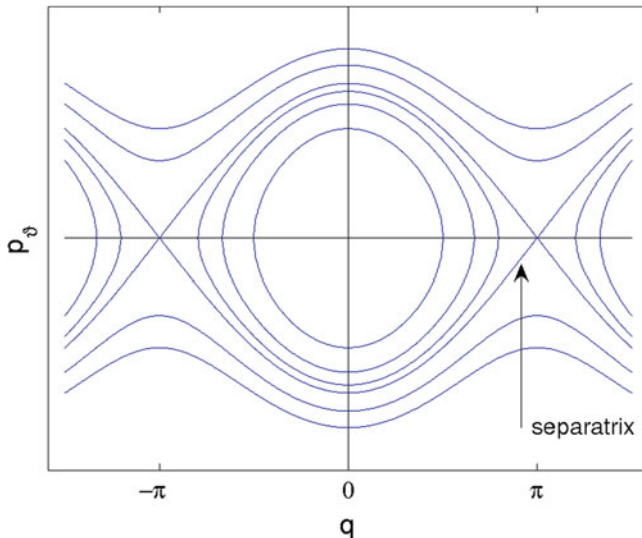


Fig. 3.1 Phase space trajectories of the pendulum. We see two different kinds of dynamical behavior. *Closed curves* around the origin represent oscillations, where the position variable is restricted to $-\pi < q < \pi$. In contrast, curves for which $p_\theta \neq 0$ holds for all times describe rotations of the pendulum. The points in phase space separating the two qualitatively different types of motion form the separatrix (marked by the arrow). In phase space we have two trajectories intersecting at $(q, p_\theta) = (\pm\pi, 0)$ moving along the separatrix

3.3 Important Techniques in the Hamiltonian Formalism

3.3.1 Conserved Quantity H

3.3.1.1 Autonomous Systems

A system that is not explicitly time-dependent is called *autonomous*. For such systems the form of the differential equations implies that every point in phase space (q, p) has a unique time evolution.³ The Hamiltonian $H(q, p) = E$ does not depend explicitly on time and is a constant of the motion.

3.3.1.2 Explicitly Time-Dependent Systems

The energy of the system $E(t) = H(q(t), p(t), t)$ is generally time-dependent. The reduction to a time-independent (autonomous) system is yet always possible. For this, we introduce the extended phase space spanned by the new variables

³ This is due to the fact that the velocity field of (q, p) , which is given by $J \cdot \nabla H(q, p)$ in Eq. (3.2.1) does not depend on time [7].

$$\mathcal{P} = (\mathcal{P}_0 \equiv -E, p) = \mathcal{P}(\tau), \quad \mathcal{Q} = (\mathcal{Q}_0 \equiv t, q) = \mathcal{Q}(\tau). \quad (3.3.1)$$

With the Hamiltonian $\mathcal{H}(\mathcal{P}, \mathcal{Q}) = H(q, p, t) - E(t)$ the generalized equations of motion read

$$\frac{\partial \mathcal{P}}{\partial \tau} = -\frac{\partial \mathcal{H}}{\partial \mathcal{Q}}, \quad \frac{\partial \mathcal{Q}}{\partial \tau} = \frac{\partial \mathcal{H}}{\partial \mathcal{P}}. \quad (3.3.2)$$

From

$$\frac{\partial \mathcal{Q}_0}{\partial \tau} = \frac{\partial \mathcal{H}}{\partial \mathcal{P}_0} \Leftrightarrow \frac{dt}{d\tau} = -\frac{\partial \mathcal{H}}{\partial E} = 1 \quad (3.3.3)$$

we can infer that $\tau = t + \text{const.}$ which leads to

$$\frac{\partial \mathcal{P}_0}{\partial \tau} = -\frac{\partial \mathcal{H}}{\partial \mathcal{Q}_0} \Leftrightarrow \frac{dE}{dt} = \frac{dE}{dt} = \frac{\partial H}{\partial t}. \quad (3.3.4)$$

The number of independent variables is thus raised by one. For this reason one-dimensional systems described by Hamiltonian as, e.g., $H = \frac{p^2}{2m} + V(x)[1 + \cos(\omega t)]$ are sometimes referred to as having “one-and-a-half degrees of freedom”. Going to the extended phase space defined by Eq. (3.3.1) formally reduces all time-dependent problems to time-independent ones. For this reason and almost exclusively, the following sections treat the time-independent case without loss of generality.

3.3.2 Canonical Transformations

The choice of the generalized coordinates q is not restricted. Physically speaking it is possible to use n arbitrary quantities which describe the system’s location in configuration space in a unique way. The structure of the Lagrangian equations does not depend on this choice. If the problem is given in a certain set of coordinates it can be useful to change to another set of coordinates, in which the formulation of the problem is simpler in some way. In general, new coordinates are of the form⁴ $Q_i = Q_i(q, t)$, for $i = 1, \dots, n$. Since in the Hamiltonian theory coordinates and momenta are treated as independent variables, one can enlarge the class of possible coordinate transformations and change the $2n$ coordinates (q, p) to $(Q(q, p, t), P(q, p, t))$. This enlargement is one of the main features of Hamiltonian mechanics. In order to preserve the symplectic structure of the equations of motion,

$$\dot{Q}_i = \frac{\partial H'}{\partial P_i}, \quad \dot{P}_i = -\frac{\partial H'}{\partial Q_i}, \quad (3.3.5)$$

⁴ From a mathematical point of view $Q(q, t)$ has to be a diffeomorphism (differentiable and invertible) for all t .

with a new Hamiltonian H' , the coordinate transformations have to fulfill certain conditions. Such transformations are then called *canonical transformations*.

Usually, one arrives at Hamilton's equations of motion via the principle of extremal action. This principle is then valid for both, the Hamiltonian H in the old coordinates and H' in the new ones. This gives [4–6]

$$0 = \delta \mathcal{L} = \delta \int [(p\dot{q} - H) - (P\dot{Q} - H')] dt = \delta \int \frac{d\mathcal{F}}{dt} dt, \quad (3.3.6)$$

where δ denotes the variation of the corresponding function. This relation directly implies that

$$\frac{d\mathcal{F}}{dt}(q, Q, t) = p\dot{q} - P\dot{Q} + (H' - H) = \frac{\partial \mathcal{F}}{\partial q}\dot{q} + \frac{\partial \mathcal{F}}{\partial Q}\dot{Q} + \frac{\partial \mathcal{F}}{\partial t}. \quad (3.3.7)$$

The function \mathcal{F} generates the canonical transformation and its Legendre transforms with respect to the coordinates (q, Q) immediately give the three other possible *generating functions* which connect the old and new coordinates [5, 6].

In the following, we implicitly use the extended phase space picture of the last section and drop all explicit time dependencies. Eq. (3.3.6) can then be cast in the form of total differentials

$$\delta \int (pdq - PdQ) = 0, \quad (3.3.8)$$

which implies

$$dF = pdq - PdQ. \quad (3.3.9)$$

Here dF denotes the total differential of the generating function $F(q, Q)$. Total differentials have the property that their contribution to a closed curve integral in phase space vanishes. Any canonical transformation is induced by such a generating function. From Eq. (3.3.9) we obtain in the same way as above in Eq. (3.3.7)

$$p_i = \frac{\partial F}{\partial q_i}, \quad P_i = -\frac{\partial F}{\partial Q_i}. \quad (3.3.10)$$

For a given function F these equations connect the old and the new variables. For some applications it can be more convenient to express the generator as a function of q and P . This can be done by a Legendre transform

$$d(F + PQ) = pdq + QdP. \quad (3.3.11)$$

The expression in brackets on the left hand side is a function of q and P which we denote by S . Using the new generator, the equations connecting the old and the new coordinates read

$$p_i = \frac{\partial S}{\partial q_i}, \quad Q_i = \frac{\partial S}{\partial P_i}. \quad (3.3.12)$$

When doing practical computations, the first part of Eq. (3.3.12) is used to calculate the new P_i by inverting the function, the second one to determine the new coordinates Q_i . Because the notion of a canonical transformation is quite general, the original sense of coordinates and momenta may get lost (just think of the transformation which interchanges momenta and coordinates, see below). Therefore the variables q and p are often simply referred to as *canonically conjugate variables*.

For a given set of new conjugate variables (Q, P) , the transformation $(q, p) \rightarrow (Q, P)$ is canonical if (and only if) the following three conditions are fulfilled with respect to the derivative in the old and the new variables⁵

$$\{Q_i, Q_k\} = 0, \quad \{P_i, P_k\} = 0, \quad \{Q_i, P_k\} = \delta_{i,k}. \quad (3.3.13)$$

The expression $\{f, g\} = \{f, g\}_{q, p} = \sum_k \left(\frac{\partial f}{\partial q_k} \frac{\partial g}{\partial p_k} - \frac{\partial f}{\partial p_k} \frac{\partial g}{\partial q_k} \right)$ denotes the *Poisson bracket*. These formal conditions are discussed in many textbooks on classical mechanics, see for example [4–6, 8].

Two examples for canonical transformations are:

1. The function $S(q, P) = qP$ leads to the new coordinates

$$Q_i = \frac{\partial S}{\partial P_i} = q_i, \quad p_i = \frac{\partial S}{\partial q_i} = P_i \quad (3.3.14)$$

and therefore generates the identity.

2. When defining $F(q, Q) = qQ$, we find

$$p_i = \frac{\partial F}{\partial q_i} = Q_i, \quad P_i = -\frac{\partial F}{\partial Q_i} = -q_i. \quad (3.3.15)$$

The so-defined canonical transformation interchanges coordinates and momenta.

We note that a canonical transformation can be interpreted in two ways (see Fig. 3.2). To visualize the two possibilities we show how a closed curve γ in a two-dimensional phase space changes. The area encircled by γ is proportional to the action of the curve. In the active picture, the new coordinates are viewed as functions of the old coordinates (in other words we still use the old coordinate system) and γ transforms to the new curve $A(\gamma)$ ($A(q, p) = (Q, P)$ defines the canonical transformation) encircling a deformed area of the same size. In the passive picture instead the coordinate system is changed while γ preserves its form. This latter view motivates the following theorem.

⁵ As for the coordinates, the transformation from the old to the new variables has to be a diffeomorphism, see previous footnote.

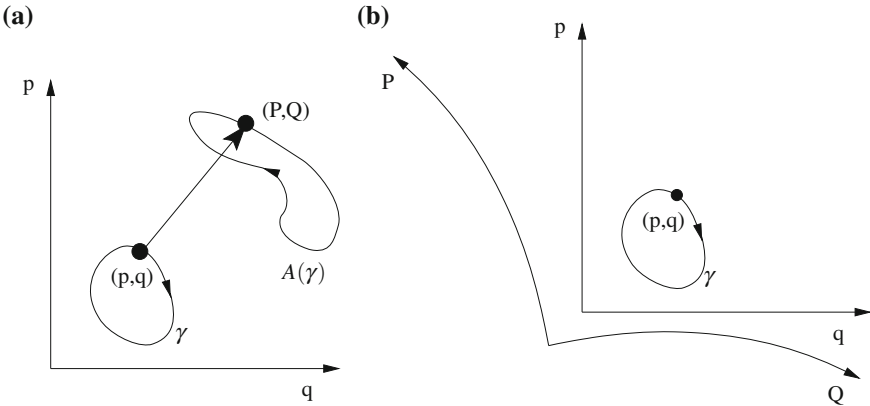


Fig. 3.2 A canonical transformation can be interpreted in two ways. In the active interpretation a *closed curve* is transformed leaving the action (given by the *encircled area*) invariant (a), whereas in the passive interpretation the coordinates (the axes) change (b)

3.3.3 Liouville's Theorem

Liouville's theorem states that the time evolution of a Hamiltonian system conserves the phase space volume. A simple way to see this is to show that canonical transformations are phase space volume preserving. Since every time evolution can be expressed as a canonical transformation the same has to be true for the time evolution. Another proof is based on the fact that the Hamiltonian flow is divergence free. We will come back to this idea in Sect. 3.4. Another, more formal proof is given in the appendix at the end of this chapter.

Let Ω be an arbitrary phase space volume, (q, p) the set of old coordinates, and A the transformation from the old coordinates to the new coordinates (Q, P) . We want to show that

$$\int_{\Omega} dq dp \stackrel{!}{=} \int_{A(\Omega)} dQ dP = \int_{\Omega} D(q, p) dq dp, \quad (3.3.16)$$

where D denotes the functional determinant of the coordinate transformation. In order to have equality we need $D = 1$. Doing a few straight forward transformations we obtain

$$D = \frac{\partial(Q_1, \dots, Q_N, P_1, \dots, P_N)}{\partial(q_1, \dots, q_N, p_1, \dots, p_N)} \quad (3.3.17)$$

$$= \left\{ \frac{\partial(Q_1, \dots, Q_N, P_1, \dots, P_N)}{\partial(q_1, \dots, q_N, P_1, \dots, P_N)} \right\}_{\substack{\\ \partial(q_1, \dots, q_N, P_1, \dots, P_N)}} \quad (3.3.18)$$

$$= \frac{\left\{ \frac{\partial(Q_1, \dots, Q_N)}{\partial(q_1, \dots, q_N)} \right\}_{P=const.}}{\left\{ \frac{\partial(p_1, \dots, p_N)}{\partial(P_1, \dots, P_N)} \right\}_{q=const.}}. \quad (3.3.19)$$

Now we express the canonical transformation with the generating function $S(q, P)$, see Sect. 3.3.2. Inserting the relations of Eq. (3.3.12) into the above formulas we find

$$\frac{\partial Q_i}{\partial q_k} = \frac{\partial^2 S}{\partial q_k \partial P_i}, \quad \frac{\partial p_i}{\partial P_k} = \frac{\partial^2 S}{\partial q_i \partial P_k}. \quad (3.3.20)$$

We note that the determinants in the numerator and in the denominator of Eq. (3.3.19) equal each other because they can be brought into the same form by interchanging rows and columns.

After having shown that canonical transformations preserve the phase space volume we demonstrate that the temporal evolution itself is generated by canonical transformations. Let us assume we are given the solution of the Hamiltonian equations of motion. We define the old and the new coordinates by $q_0 = q$, $p_0 = p$ and $Q(q, t) = q(t)$, $P(p, t) = p(t)$. To show that the transformation defined in this way is canonical we explicitly give a generating function that fulfills Eq. (3.3.7). It reads

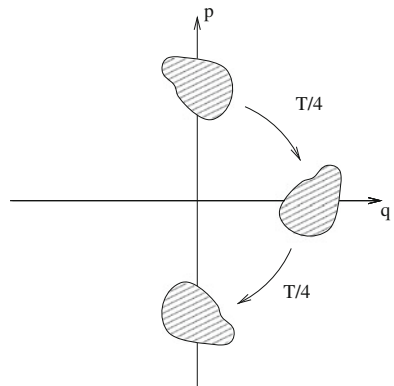
$$\mathcal{F}(q, Q, t) = - \int_q^Q p dq', \quad (3.3.21)$$

where the integral goes along the trajectory that solves the Hamiltonian equations of motion for the initial condition (q, p) . For the sake of clarity we have explicitly mentioned the time dependence of the generator \mathcal{F} . The momentum is assumed to be a function of the trajectory $q(t')$, $0 \leq t' \leq t$. We note that from a physical point of view the generating function is (apart from the minus sign in Eq. (3.3.21)) the action as a function of the starting point and the endpoint of the given trajectory. To check whether we get the right initial and final momentum p and P we calculate

$$\frac{\partial \mathcal{F}}{\partial q_i} = p_i, \quad \frac{\partial \mathcal{F}}{\partial Q_i} = -P_i. \quad (3.3.22)$$

For the computation of p we have to differentiate the integral of Eq. (3.3.21) with respect to its starting point and find $\frac{\partial \mathcal{F}}{\partial q_i} = p_i(q) = p_i(q_0) = p_i(t=0)$. Differentiation with respect to the endpoint results in $\frac{\partial \mathcal{F}}{\partial Q_i} = -P_i(Q) = -P_i(q(t)) = -p_i(t)$. Hence \mathcal{F} gives the right relations which concludes our proof. Figure 3.3 gives an example of how a phase space volume is transformed in time.

Fig. 3.3 For the harmonic oscillator the phase space evolution of an ensemble of initial conditions (shaded area) is a rotation with constant period T



3.3.4 Hamilton–Jacobi Theory and Action-Angle Variables

In Sect. 3.3.2, we have briefly reviewed canonical transformations which are an important tool. Now we are going to use them to solve the equations of motion by trying to find new variables in such a way that the Hamiltonian becomes trivial. Assume the Hamiltonian does not depend on the spatial coordinates any more, i.e. $H' = H'(P)$. In this case the equations of motion are of the form

$$\dot{P}_i = -\frac{\partial H'}{\partial Q_i} = 0, \quad \dot{Q}_i = \frac{\partial H'}{\partial P_i}. \quad (3.3.23)$$

From the first equation, we conclude that the P_i are constants of motion. Therefore, the right hand side of the second equation is constant in time. The solution for the coordinates therefore reads

$$Q_i(t) = Q_i(0) + t \frac{\partial H'}{\partial P_i}. \quad (3.3.24)$$

To reach this goal we work with an ansatz for the transformation based on the generator $S(q, P)$. Inserting $p_i = \frac{\partial S}{\partial q_i}$ into the original Hamiltonian and assuming that it equals a Hamiltonian of the above form, we arrive at the Hamilton–Jacobi equation for the generating function S

$$H\left(q_1, \dots, q_N, \frac{\partial S}{\partial q_1}, \dots, \frac{\partial S}{\partial q_N}\right) = H'(P) = E = \text{const.} \quad (3.3.25)$$

Without loss of generality we assumed energy conservation, see Sect. 3.3.1.2.

To understand the meaning of the generating function its total differential is computed:

$$dS = \sum_i \frac{\partial S}{\partial q_i} dq_i + \frac{\partial S}{\partial P_i} dP_i = \sum_i p_i dq_i. \quad (3.3.26)$$

Since the new momenta P are constants of motion ($dP = 0$), S can be obtained by integration along the classical trajectory $q(t)$. We find

$$S(q, P, E) = \int_{q_0}^q \sum_i p_i(q') dq'_i = \int_{q_0}^q \mathbf{p}(\mathbf{q}') d\mathbf{q}', \quad (3.3.27)$$

where q_0 is the coordinate at $t = 0$ and by $q = q(t)$ we denote the endpoint of the trajectory. Therefore the generator S is the action function of the trajectory that solves the equations of motion.

The Hamilton–Jacobi equation generally gives a nonlinear partial differential equation which determines S as a function of its $2n$ arguments. In contrast, the original Hamilton's equations of motion are $2n$ ordinary differential equations of first order. While the number of equations is reduced, the Hamilton–Jacobi equation is difficult to solve in general. However, the Hamilton–Jacobi theory is very important in the classification of the dynamics (see below) and for the understanding of the correspondences between classical and quantum mechanics (see Sect. 4.2.2).

3.3.4.1 Special Case: One-Dimensional Systems

As an example, we discuss the motion of a particle in a one-dimensional and time-independent potential. The corresponding Hamiltonian is conservative and of the form

$$H(p, x) = \frac{p^2}{2m} + V(x). \quad (3.3.28)$$

If we denote the new coordinates and the generating function by (θ, I) and $S(x, I)$, the Hamilton–Jacobi equation reads

$$H\left(\frac{\partial S}{\partial x}, x\right) = \frac{1}{2m} \left(\frac{\partial S}{\partial x}\right)^2 + V(x) = H'(I). \quad (3.3.29)$$

Note that $H'(I) = E(I)$ is a constant of motion. Solving for $p = \frac{\partial S}{\partial x}$, see Eq. (3.3.12), allows us to integrate the equation. The result is the following expression

$$\frac{\partial S(x, I)}{\partial x} = \pm \sqrt{2m(E(I) - V(x))} \quad (3.3.30)$$

$$\Rightarrow S(x, I) = \int_{x_1}^x \sqrt{2m(E(I) - V(x'))} dx', \quad (3.3.31)$$

where x_1 is the left turning point of the motion, see Fig. 3.4 below.

Using the formal solution, the new coordinate can be computed

$$\theta = \frac{\partial S}{\partial I} = \int_{x_1}^x \frac{dx'}{\sqrt{\frac{2}{m} (H'(I) - V(x'))}} \frac{\partial H'}{\partial I}. \quad (3.3.32)$$

A confined system shows periodic behavior which means that θ is periodic. Therefore we define $\theta(x_2, I) = \pi$, where we assume x_2 to be a turning point of the motion. The relation between H' and I is calculated in the following way:

$$\frac{\partial I}{\partial H'} = \left(\frac{\partial H'}{\partial I} \right)^{-1} = \frac{1}{\pi} \int_{x_1}^{x_2} \frac{dx}{\sqrt{\frac{2}{m} (H'(I) - V(x))}}. \quad (3.3.33)$$

Integrating (3.3.33) over $E = H'$, one obtains a relation for $I(E)$,

$$I(E) = \frac{1}{\pi} \int_{x_1}^{x_2} \sqrt{2m (E(I) - V(x))} dx = \frac{1}{2\pi} \oint p dx, \quad (3.3.34)$$

where we have denoted $H' = E$ to stress its physical meaning. The contour integral is over one period T . Hence I is the action of a trajectory with energy E . This is also the reason why (I, θ) are called *action-angle variables*. As the action I is fixed, the time evolution of the angle θ is given by periodic oscillations

$$\theta = \frac{2\pi}{T} t + \text{const} \quad (3.3.35)$$

The period can be computed from the equation

$$\omega(I) = \frac{2\pi}{T} = \frac{\partial H'}{\partial I}. \quad (3.3.36)$$

Hence the solution of the 1D problem is given up to the integral (3.3.34). For an illustration of the action-angle variables see Fig. 3.4.

But solving the Hamilton–Jacobi equation is simple only in two cases:

- In one-dimensional systems as presented above.
- In separable systems. A classical system we call separable if the action can be written as

$$S = \sum_{i=1}^n S_i(q_i, P, E), \quad (3.3.37)$$

which effectively reduces the problem to the one-dimensional case for each index $i = 1, \dots, n$ separately. In all other cases the calculation of the action is a difficult task,

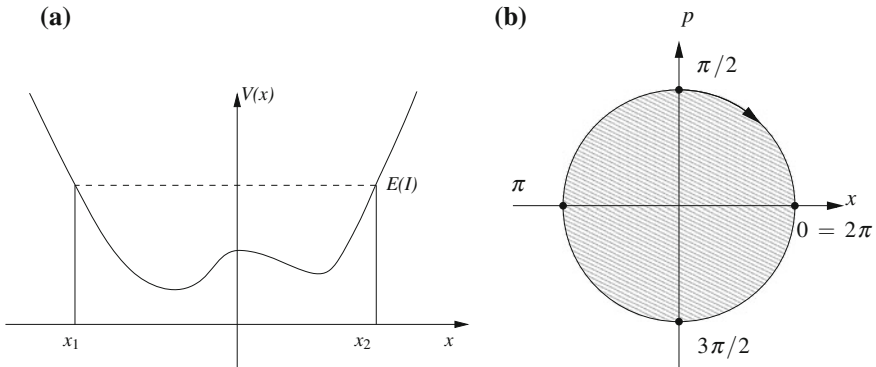


Fig. 3.4 Motion of a particle in a one-dimensional potential. **a** shows the potential and the energy-dependent turning points x_1 and x_2 . **b** represents the motion schematically in phase space. The radius of the circle is determined by the action variable I ($2\pi I$ is the area within the circle, see Eq. (3.3.34)) while the position on the circle is given by the angle variable θ . The turning points correspond to $\theta = 0$ and $\theta = \pi$

since one must solve an implicit partial differential equation for the unknown new momenta. Apart from that, the Hamilton–Jacobi theory is used as the starting point for canonical perturbation theory. It is also one of the bridges to quantum mechanics: The path integral formulation uses the action as a functional of the trajectory. In the classical limit it is possible to make a stationary phase approximation which then essentially yields the Hamilton–Jacobi equation for the action, see Sect. 4.2.2.

3.4 Integrable Systems

The definition of integrability is the following: Let n be the number of degrees of freedom and let s be the number of constants of motion. If $s = n$ the system is called *integrable*. Thereby the constants of motion $c_i(q, p)$ have to be *in involution* and *independent*. Here *in involution* means that they fulfill the relations $\{c_i, c_j\} = 0$ for all i, j , with the Poisson bracket defined in Sect. 3.3.2. The second condition states that the differential 1-forms $dc_i(q, p)$ are linearly independent at each point of the set $M_C = \{(q, p) : c_i(q, p) = C_i \text{ for } i = 1 \dots n\}$. The independence of the constants of motion ensures that they actually characterize the dynamics in the entire accessible phase space. If a Hamiltonian system is integrable, its equations of motion can be solved by quadratures,⁶ just in the spirit of the previous section.

If n constants of motion exist, the canonical transformation defined by

⁶ The notion quadrature means the application of basic operations such as addition, multiplication, the computation of inverse functions and the calculation of integrals along a path.

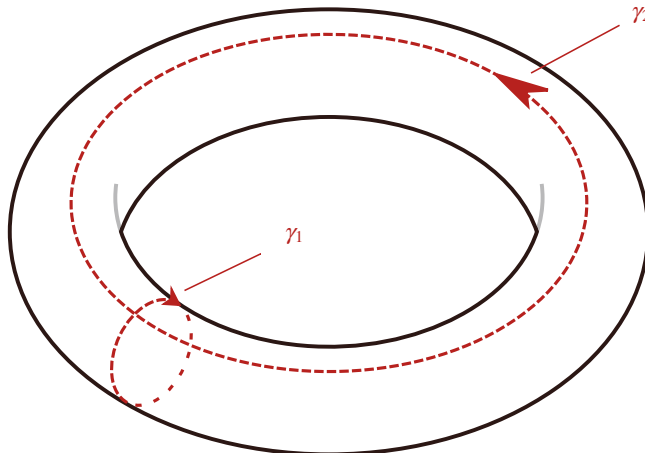


Fig. 3.5 Example for a basis of cycles on a two-dimensional torus (having a *doughnut-like shape*). While γ_2 encloses the “hole” of the torus, γ_1 encircles the tube forming it. Both curves γ_1 and γ_2 cannot be contracted to a point, they are so-called irreducible curves

$$(q, p) \mapsto (\theta, I) \text{ with } I_i = C_i, \quad (3.4.1)$$

gives a solution of the Hamilton–Jacobi equation. Therefore another equivalent definition of integrability is that a solution of the Hamilton–Jacobi equation can be found with the action-angle variables (θ, I) .

In the last section we have introduced action-angle variables for an integrable one-dimensional system. It turns out that this concept can indeed be extended to higher dimensional integrable systems. Mathematically speaking one can show that the set M_C is diffeomorphic to the n -dimensional torus (if it is compact and connected).⁷ The action-angle variables can then be introduced as follows. Let θ_i , $i = 1, \dots, n$ be the angle variables. We assume they are scaled such that $\theta_i \in [0, 2\pi]$. Taking a basis of cycles on the torus γ_i , $i = 1, \dots, n$ one can define action variables by

$$I_i = \frac{1}{2\pi} \oint_{\gamma_i} p(I, \theta_i) dq(I, \theta_i). \quad (3.4.2)$$

A basis of cycles is given if the increase of the coordinate θ_i on the cycle γ_j is equal to 2π if $i = j$ and 0 if $i \neq j$. For the two dimensional torus (see Fig. 3.5), such a basis is given by a cycle encircling the tube of the torus and another one going around it. Generally speaking, the tori are defined as the following sets of phase space points

⁷ The set M_C is not compact if the motion is not restricted to a finite area in phase space. Examples for such unbounded motion are the free particle or a particle in a linear potential (Wannier-Stark problem).

$$\mathcal{T} \equiv \{(p, q) \in \text{phase space} : p = p(I, \theta), q = q(I, \theta) \text{ for fixed action } I \text{ and } \theta_i \in [0, 2\pi]\}, \quad (3.4.3)$$

with periodic variables in the angles: $q(I; \dots, \theta_i + 2\pi, \dots) = q(I; \dots, \theta_i, \dots)$ and $p(I; \dots, \theta_i + 2\pi, \dots) = p(I; \dots, \theta_i, \dots)$.

The generating function connects the old and the new variables by $\theta_i = \partial S / \partial I_i$. The action integrals are related to the generating function, see Eq. (3.3.27), by computing the integrals along a closed circle

$$\Delta_i S(q, I) \equiv \int_0^{2\pi} p(I, \theta_i) dq(I, \theta_i) = 2\pi I_i. \quad (3.4.4)$$

The solution of the equations of motion for an integrable system, see Eq. (3.3.24), is then given in the possibly high-dimensional phase space parametrized by the action-angle variables (I, θ) :

$$\theta(t) = \theta_0 + \omega(I)t, \quad \omega(I) = \frac{\partial H'}{\partial I} = \text{const} \quad (3.4.5)$$

By construction, the action variables I_i are the constants of motion. The fact that the components of θ are angle-like, and called therefore cyclic variables in the Lagrange formalism, does not necessarily mean that the actual *motion* in phase space is periodic. This is only true in a system with one spatial dimension where the motion is along a simple circle. On a doughnut (a two-dimensional torus) this may no longer be the case since the periodicities in the motion of the two angles may differ. A general (non-periodic) motion on a torus is called *conditionally periodic*.

The following table summarizes the dimensionality of the important objects in phase space for integrable systems where a torus structure exists:

Phase space	2 n
Energy surface	2 n - 1
Torus	n

The reduction of $2n$ first-order differential equations to only n constants of the motion is remarkable. The origin of this reduction is the symplectic structure in the phase space variables. For a careful derivation of what we have shortly summarized please see [6].

3.4.1 Examples

In conservative systems the energy is a constant of motion. Therefore, conservative systems of one particle in one space dimension are always integrable. Another class

of integrable systems are separable systems, see Eq. (3.3.37). The simplest example of a separable system is a Hamiltonian that can be written as a sum over n independent Hamiltonians (non-interacting degrees of freedom). Conserved quantities are then simply the independent energies. Another example is the two-body Kepler problem (the motion of two point particles in free space that interact via gravity). Here the conserved quantities are six: the energy, the three components of the momentum and two quantities coming from angular momentum conservation (usually the square \mathbf{L}^2 and one of its projections, e.g., L_z). This can be best seen by using the conservation of the centre-of-mass momentum to reduce the system to an effective one-body problem [6]. Then the conserved quantities mentioned above are three independent constants of motion for this one-body problem.

3.4.2 Poisson Brackets and Constants of Motion

The Poisson brackets we used to define the notion of two constants of motion being in involution can also be applied to compute the time evolution of a function $f(q, p, t)$ in phase space

$$\frac{df}{dt} = \{f, H\} + \frac{\partial f}{\partial t}. \quad (3.4.6)$$

Assume f is not explicitly time-dependent, then in order to be a constant of motion it has to fulfill $\{H, f\} = 0$. If we take for f a given density in phase space, i.e. $f = \rho(q, p, t)$, we immediately find the following continuity equation

$$\frac{\partial \rho(q, p, t)}{\partial t} + \left(\frac{\dot{q}}{\dot{p}} \right) \cdot \nabla_{q,p} \rho(q, p, t) = 0. \quad (3.4.7)$$

We used Hamilton's equations and Liouville's theorem stating that the total time derivative of any phase space density is zero. Consequently, the Hamiltonian flow in phase space corresponds to the one of an incompressible fluid. This idea is applied, e.g., in [6, 9] to proof Liouville's theorem based on the fact that Hamilton's flow is free of any divergence in phase space. To see this we write Hamilton's equations of motion as $\dot{z}(t) = J \cdot \nabla H(z)$ (see Sect. 3.2) and compute

$$\begin{aligned} \operatorname{div} \dot{z}(t) &= (\nabla_q, \nabla_p) \begin{pmatrix} 0 & I \\ -I & 0 \end{pmatrix} \begin{pmatrix} \nabla_q \\ \nabla_p \end{pmatrix} H(q, p) \\ &= (\nabla_q \cdot \nabla_p - \nabla_p \cdot \nabla_q) H(q, p) = 0. \end{aligned} \quad (3.4.8)$$

Inserting q and p into Eq. (3.4.6) one also arrives at a compact formulation of Hamilton's equations of motion:

$$\{q_i, H\} = \dot{q}_i, \quad \{p_i, H\} = \dot{p}_i. \quad (3.4.9)$$

We note that Eq. (3.4.6) is formally similar to the Heisenberg equations in quantum mechanics, see for instance [10].

3.5 Non-integrable Systems

A system is non-integrable if there are less independent constants of motion than degrees of freedom. The most famous example is the three-body Kepler problem whose Hamiltonian is given by (we assume equal masses m for simplicity)

$$H = \frac{1}{2m} (\mathbf{p}_1^2 + \mathbf{p}_2^2 + \mathbf{p}_3^2) - \frac{\gamma m^2}{|\mathbf{r}_1 - \mathbf{r}_2|} - \frac{\gamma m^2}{|\mathbf{r}_2 - \mathbf{r}_3|} - \frac{\gamma m^2}{|\mathbf{r}_3 - \mathbf{r}_1|}. \quad (3.5.1)$$

As in Eq. (1.2.2) γ is the gravitational constant. The system has three coordinates each of them with three components. Therefore we have nine degrees of freedom. The number of independent conserved quantities is, as for the two-particle Kepler problem, just six.

In 1899 Poincaré showed that it is impossible to even compute approximate long time solutions for the N -body Kepler problem if $N \geq 3$ [11]. Small errors grow very fast during the temporal evolution for most initial conditions. At this stage, it seems that there are only a few integrable systems, for which computations can be done, and that long time predictions in all other cases are nearly a hopeless task. Fortunately, it turns out that this is not the whole story.

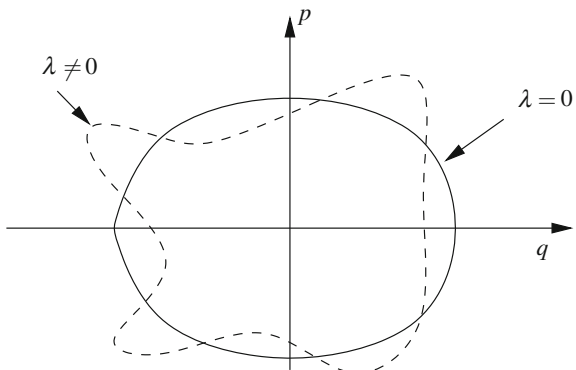
In 1954 Kolmogorov [12] and in 1963 Arnold [13, 14] and Moser [15, 16] were able to show that there are systems which are not integrable, but nevertheless remain predictable in some sense. Assume a Hamiltonian describing an integrable system that (in a sense that needs to be clarified) is distorted just weakly by a perturbation which makes the system non-integrable. Then the solution of the distorted system is very close to the solution of the integrable system. This statement, which we will treat in more detail in Sect. 3.7.4, is known as KAM Theorem and justifies the application of perturbation theory. Prior to that, as an additional motivation, we treat special cases of perturbed systems in the following section.

3.6 Perturbation of Low-Dimensional Systems

3.6.1 Adiabatic Invariants

We consider a system whose Hamiltonian depends continuously on a parameter λ . As an example one may think of a pendulum with length λ or of two particles whose interaction is varied with λ . Suppose that the parameter changes slowly with time. Then (if we think of the pendulum) the amplitude of the oscillation will be a function

Fig. 3.6 In one-dimensional systems the action is an adiabatic invariant. Therefore the area that is enclosed by a phase space trajectory is changing only weakly when the parameter λ is varied



of the length of the pendulum. If we very slowly increase its length and then very slowly decrease it to the original value, the amplitude will be the same again at the end of the process. Furthermore, we will observe that the ratio between the energy and the frequency changes very little although the energy and the frequency themselves may change a lot. It turns out that this is a general phenomenon. Quantities which change just a bit under slow variations of a parameter are called *adiabatic invariants*. A strict mathematical definition of an adiabatic invariant can be found in [6].

In the following, we want to show that in one-dimensional systems the action $I(E, \lambda) = \frac{1}{2\pi} \oint pdq$ is an adiabatic invariant under a slow change of the parameter⁸ λ . A consequence of this statement is that the area enclosed by a phase space trajectory changes only slightly when the parameter is varied, see Fig. 3.6. The proof follows the one given in [5].

When λ is varying slowly with time the system is no longer autonomous. By slowly we mean that the change of λ is small during one period of the motion, i.e. $T \frac{d\lambda}{dt} \ll \lambda$. The energy and therewith the period $T(E)$ of the motion change (the trajectories in phase space are not strictly closed any more). Since the variation of λ is small, the variation of the energy $\dot{E} \equiv \frac{dE}{dt}$ will be small as well. If \dot{E} is averaged over one period of the motion, possible short time oscillations are “smeared out” and one finds a good measure for the temporal evolution of the system’s energy by computing

$$\langle \dot{E} \rangle_T = \frac{1}{T} \int_0^T \left(\frac{\partial H(t)}{\partial t} \right) dt \approx \frac{1}{T} \dot{\lambda} \int_0^T \frac{\partial H}{\partial \lambda}(t) dt. \quad (3.6.1)$$

The period T is the one obtained by assuming that λ is constant. Since the change of λ is nearly constant we take $\dot{\lambda}$ out of the time integration and obtain an integral over a closed trajectory. Using this fact, it can be expressed as a closed line integral over the coordinate. We use $\dot{q} = \frac{\partial H}{\partial p}$ and find

⁸ There can be more than one such parameter but for simplicity we assume only one. This result is strictly true only if the angular frequency $\omega(I, \lambda)$ never equals zero, see [6] and Sect. 3.7.2.

$$\frac{dq}{dt} = \frac{\partial H}{\partial p} \Rightarrow dt = \frac{dq}{\frac{\partial H}{\partial p}}. \quad (3.6.2)$$

Applying this expression, the period is written as

$$T = \int_0^T dt = \oint \frac{dq}{\frac{\partial H}{\partial p}} \quad (3.6.3)$$

and we obtain from Eq. (3.6.1) the following formula for the average energy change

$$\langle \dot{E} \rangle_T \approx \dot{\lambda} \frac{\oint \frac{\partial H}{\partial \lambda} \left(\frac{\partial H}{\partial p} \right)^{-1} dq}{\oint \left(\frac{\partial H}{\partial p} \right)^{-1} dq}. \quad (3.6.4)$$

As already mentioned, the integration has to be done along a closed trajectory and hence for constant λ . Therefore the energy is also constant along that trajectory. The momentum $p = p(q, E, \lambda)$ is a function of the coordinate, the energy and the parameter λ . At this point, it is sufficient to let p (and not as well q) depend on λ . This is because we assume that the closed curve $p(q)$ has a sufficiently regular structure such that when cutting it into two (or more) pieces it can be expressed as a graph $p(q)$. The assumption is justified because the trajectory is distorted only slightly switching on the perturbation λ . Since we know that the energy must be constant on a closed trajectory, differentiating the equation $H(p, q, \lambda) = E$ with respect to λ results in

$$\frac{\partial H}{\partial \lambda} + \frac{\partial H}{\partial p} \frac{\partial p}{\partial \lambda} = 0 \Leftrightarrow \frac{\partial H}{\partial \lambda} = -\frac{\partial p}{\partial \lambda} \left(\frac{\partial H}{\partial p} \right). \quad (3.6.5)$$

Inserting the expression into Eq. (3.6.4) we find

$$\langle \dot{E} \rangle_T \approx -\dot{\lambda} \frac{\oint \frac{\partial p}{\partial \lambda} dq}{\oint \frac{\partial p}{\partial E} dq}, \quad (3.6.6)$$

or

$$0 \approx \oint \left(\frac{\partial p}{\partial E} \left(\frac{dq}{dt} \right)_T + \frac{\partial p}{\partial \lambda} \frac{d\lambda}{dt} \right) dq. \quad (3.6.7)$$

But this implies

$$\left\langle \frac{d}{dt} \oint p dq \right\rangle_T = 2\pi \left\langle \frac{dI}{dt} \right\rangle_T \approx 0. \quad (3.6.8)$$

The result shows that, in the range of validity of the approximations used, the action remains invariant when the parameter λ is adiabatically varied.

3.6.2 Principle of Averaging

We want to present two examples in which the idea of averaging over one period of a periodic drive is used (see previous subsection). We therefore treat systems that have two different time scales. The Hamiltonians shall be of the form

$$H(p, x, t) = H_0(p, x) + V(x) \sin(\omega t), \quad (3.6.9)$$

where the time scale of the unperturbed (and integrable) system H_0 is assumed to be much larger than $2\pi/\omega$. A valuable description will be obtained by averaging over the short time behavior. The idea to average over the fast time scale is also known as *principle of averaging*, which turns out to be very useful for practical applications.

3.6.2.1 Free Particle with Dipole Coupling

Let us start with the simple and exactly solvable example of a free particle driven by a time-dependent linear force. The system's Hamiltonian reads

$$H(p, x, t) = \frac{p^2}{2} + Fx \sin(\omega t), \quad (3.6.10)$$

which results in the following equations of motion:

$$\dot{x}(t) = p(t), \quad \dot{p}(t) = -F \sin(\omega t). \quad (3.6.11)$$

Since the force is linear the equations can easily be solved. Solutions are of the form

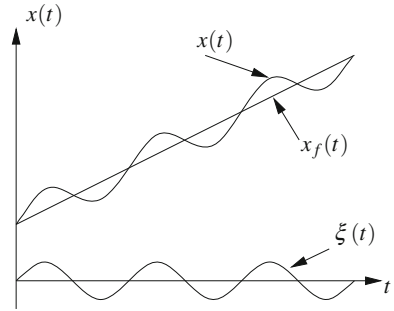
$$x(t) = x_f(t) + \xi(t), \quad p(t) = p_0 + \eta(t), \quad (3.6.12)$$

with $x_f(t) = x_0 + p_0 t$, $\xi(t) = \frac{F}{\omega^2} \sin(\omega t)$, and $\eta(t) = \frac{F}{\omega} \cos(\omega t)$. They consist of two parts, one for the free motion and another one describing the short time oscillations due to the dipole coupling, see Fig. 3.7. In the limit of very fast driving ($\omega \rightarrow \infty$) the system behaves like a free particle because it cannot follow the force. A reasonable effective description in the regime of fast driving is obtained by averaging the solution over one period of the perturbation which will lead to an effective static Hamiltonian [see Eq. (3.6.21)]. Finally we note that the amplitude of the momentum correction η is by one order of magnitude in the perturbation parameter ω^{-1} larger than that of the amplitude of the spatial correction ξ .

3.6.2.2 General Case

In the general case we have $H(p, x, t) = H_0(p, x) + V(x) \sin(\omega t)$. As above, we make the following ansatz to separate the slowly varying part and the fast part of the solution [17]

Fig. 3.7 Fast driving leads to small oscillations $\xi(t)$ around the free motion $x_f(t)$



$$x(t) = \bar{x}(t) + \xi(t), \quad p(t) = \bar{p}(t) + \eta(t). \quad (3.6.13)$$

The bared quantities describe the slow varying parts and the Greek variables are the fast oscillating part. They are assumed to satisfy $\langle \xi \rangle_T = \langle \eta \rangle_T = 0$ for $T = 2\pi/\omega$ (ω is the angular frequency of the time-dependent part of the Hamiltonian). We now derive effective equations of motion by expanding the Hamiltonian in η and ξ , thereby assuming $|\eta^n| \sim |\xi^{n-1}|$ as motivated in the previous subsection.⁹ Starting from $\dot{x} = \frac{\partial H}{\partial p} = \frac{\partial H_0}{\partial p}$ we find (by Taylor expansion)

$$\dot{\bar{x}} + \dot{\xi} \approx \frac{\partial H_0}{\partial \bar{p}} + \eta \frac{\partial^2 H_0}{\partial \bar{p}^2} + \frac{\eta^2}{2} \frac{\partial^3 H_0}{\partial \bar{p}^3}. \quad (3.6.14)$$

The same can be done with the momentum. Application of $\dot{p} = -\frac{\partial H}{\partial x} = -\frac{\partial H_0}{\partial x}$ results in

$$\begin{aligned} \dot{\bar{p}} + \dot{\eta} &\approx -\frac{\partial H_0}{\partial \bar{x}} - \eta \frac{\partial^2 H_0}{\partial \bar{x} \partial \bar{p}} \\ &\quad - \frac{\partial V}{\partial \bar{x}} \sin(\omega t) - \frac{\partial^2 V}{\partial \bar{x}^2} \xi \sin(\omega t) - \frac{\eta^2}{2} \frac{\partial^3 H_0}{\partial \bar{x} \partial \bar{p}^2}. \end{aligned} \quad (3.6.15)$$

These equations are averaged over one period. Using $\langle \xi \rangle_T = \langle \eta \rangle_T = 0$ we arrive at

$$\begin{aligned} \dot{\bar{x}} &= \frac{\partial H_0}{\partial \bar{p}} + \frac{1}{2} \frac{\partial^3 H_0}{\partial \bar{p}^3} \langle \eta^2 \rangle_T \\ \dot{\bar{p}} &= -\frac{\partial H_0}{\partial \bar{x}} - \frac{\partial^2 V}{\partial \bar{x}^2} \langle \xi \sin(\omega t) \rangle_T - \frac{1}{2} \frac{\partial^3 H_0}{\partial \bar{x} \partial \bar{p}^2} \langle \eta^2 \rangle_T. \end{aligned} \quad (3.6.16)$$

Substituting the latter equations back into Eqs. (3.6.14) and (3.6.15) we obtain the equations of motion for the fast oscillating variables

⁹ This ansatz implicitly takes account of the symplectic structure of the variables η and ξ , i.e. of the area preservation conserved also by the perturbation. The orderly way of doing perturbation theory is formally introduced in the next section.

$$\dot{\xi} \approx \eta \frac{\partial^2 H_0}{\partial \bar{p}^2}, \quad (3.6.17)$$

$$\dot{\eta} \approx -\frac{\partial V}{\partial \bar{x}} \sin(\omega t), \quad (3.6.18)$$

in first order and zeroth order in $|\eta|$ for $\dot{\xi}$ and $\dot{\eta}$, respectively. The solutions are then readily found and read

$$\begin{aligned} \dot{\xi} &\approx \frac{1}{\omega^2} \frac{\partial V}{\partial \bar{x}} \frac{\partial^2 H_0}{\partial \bar{p}^2} \sin(\omega t), \\ \eta &\approx \frac{1}{\omega} \frac{\partial V}{\partial \bar{x}} \cos(\omega t). \end{aligned} \quad (3.6.19)$$

As expected they describe small and quick oscillations around $(\bar{x}(t), \bar{p}(t))$. Using Eqs. (3.6.16) and (3.6.19), it is possible to derive an averaged system such that the equations of motion for the slowly varying parts read

$$\dot{\bar{x}} = \frac{\partial \bar{H}}{\partial \bar{p}}, \quad \dot{\bar{p}} = -\frac{\partial \bar{H}}{\partial \bar{x}}. \quad (3.6.20)$$

In order to satisfy Eq. (3.6.20), the averaged Hamiltonian \bar{H} needs to take the form

$$\begin{aligned} \bar{H}(\bar{p}, \bar{x}) &= H_0(\bar{p}, \bar{x}) + \frac{1}{4\omega^2} \left(\frac{\partial V}{\partial \bar{x}} \right)^2 \frac{\partial^2 H_0}{\partial \bar{p}^2}, \\ &= \underbrace{\frac{\bar{p}^2}{2} + V_0(\bar{x})}_{\equiv V_{\text{eff}}(\bar{x})} + \frac{1}{4\omega^2} \left(\frac{\partial V}{\partial \bar{x}} \right)^2. \end{aligned} \quad (3.6.21)$$

In the final step we assumed the special form $H_0(p, x) = p^2/2 + V_0(x)$ for the unperturbed Hamiltonian. We note that the effective potential may be trapping even if the original potential is not. Assume for example $V(x) = x^3$. The potential is—strictly speaking—not trapping because it has no minimum, the effective potential has, however, a shape proportional to \bar{x}^4 . From a physical point of view the time-dependent term proportional to x^3 changes its sign so quickly that the particle effectively feels a static confining potential. An important application of this behavior is the trapping of charged particles like ions in time-dependent electric fields [18, 19].

3.6.2.3 Gauß Averaging

In what follows, we express—in the spirit of Sect. 3.6.1—the above principle of averaging as a statement for the change of action arising from perturbations. We assume a one-dimensional conservative system and choose action-angle variables

(θ, I) . The Hamiltonian function is of the form $H_0(I)$ and the equations of motion read

$$\dot{I} = 0, \quad \dot{\theta} = \omega(I), \quad \omega(I) = \frac{\partial H_0}{\partial I}. \quad (3.6.22)$$

Next we add a small perturbation to the Hamiltonian ($\varepsilon \ll 1$)

$$H = H_0(I) + \varepsilon H_1(I, \theta). \quad (3.6.23)$$

Since H_0 is independent of θ , the new equations of motion read

$$\dot{I} = -\varepsilon \frac{\partial H_1}{\partial \theta} \equiv \varepsilon f(I, \theta), \quad \dot{\theta} = \omega(I) + \varepsilon \frac{\partial H_1}{\partial I} \equiv \omega(I) + \varepsilon g(I, \theta). \quad (3.6.24)$$

The *averaging principle* (which has already been used by Gauß for estimating how planets perturb each other's motion) states that the given system can be approximated by an averaged one [6]. By J we denote a new (averaged) action variable and define it via the equation

$$J = \varepsilon \bar{f}(I) \quad \text{with} \quad \bar{f}(I) \equiv \frac{1}{2\pi} \int_0^{2\pi} f(I, \theta) d\theta. \quad (3.6.25)$$

We note that this equation is simpler because it does (by construction) not depend on the angle any more. The time evolution of the new action variable reads $J(t) = J(0) + \varepsilon t \bar{f}(I) = I(0) + \varepsilon t \bar{f}(I)$. Let us estimate the difference between the full and the approximate solution in first order¹⁰ in ε :

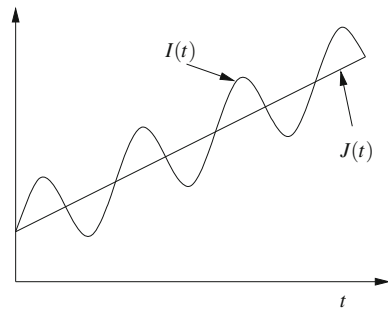
$$\begin{aligned} J(t) - I(t) &\approx \varepsilon t \bar{f} - \varepsilon \int_0^t f(I, \theta(t) = \theta_0 + \omega t) dt \\ &= -\varepsilon \int_0^t [f(I, \theta_0 + \omega t) - \bar{f}(I)] dt \\ &= -\frac{\varepsilon}{\omega} \int_{\theta_0}^{\theta_0 + \omega t} [f(I, \theta) - \bar{f}(I)] d\theta. \end{aligned} \quad (3.6.26)$$

The function $[f(I, \theta) - \bar{f}(I)]$ is trivially 2π -periodic in θ . Hence the integral over it gives a finite number which we call C . Then the following estimate holds

$$|J(t) - I(t)| \leq \frac{\varepsilon}{\omega} C. \quad (3.6.27)$$

¹⁰ Note that we can assume in Eq. (3.6.26) $\dot{\theta} \approx \omega$ within this approximation.

Fig. 3.8 The figure shows the full solution $I(t)$ and the approximate (averaged) solution $J(t)$, c.f. the previous Fig. 3.7



Equation (3.6.27) tells us that there is a continuous connection between the perturbed and the unperturbed system. Accordingly, for small perturbations the two systems behave similarly, and for $\varepsilon \rightarrow 0$ they give the same solution.¹¹ For an illustration of the full and the approximate solution see Fig. 3.8. The averaging principle expressed by Eq. (3.6.27) gives the essential idea for the more formal and more general theory introduced in the next section.

3.7 Canonical Perturbation Theory

Perturbation theory is an important concept in many areas of physics. If a system differs from a solvable one only by a small perturbation we can hope to describe the full system by the solvable one plus a small change. The computation of this small change often has to be done carefully, and it is a common phenomenon that the perturbative expansion obtained suffers from difficulties (e.g. a divergence, see Sect. 3.7.6). Nevertheless also in these cases the first few terms often give a hint on what happens. In classical mechanics there is an elegant concept of how to perform perturbative calculations in a systematic manner, known as *canonical perturbation theory*. The concept is exemplified in Sect. 3.7.2 for conservative systems of one degree of freedom only. For systems of two or more degrees of freedom profound difficulties arise, which, in a sense, can be understood as the seeds of chaotic motion (Sect. 3.7.3).

3.7.1 Statement of the Problem

As in the previous section, we assume a Hamiltonian function H_0 describing an integrable system that is altered by a small perturbation εH_1 , with $\varepsilon \ll 1$. We further assume that action-angle variables (I, θ) can be used to solve the unperturbed system. The Hamiltonian of the full system thus reads

¹¹ C.f. footnote in Sect. 3.6.1.

$$H(\theta, I) = H_0(I) + \varepsilon H_1(\theta, I). \quad (3.7.1)$$

A solution of the problem would be obtained if one finds a new set of action-angle variables (φ, J) such that the Hamiltonian in the new coordinates has the form $H = K(J)$. Using perturbation theory one could expand the new variables in terms of the old ones. Usually, this is not done because one must be careful to preserve the symplectic structure in the variables φ and J . This is also the reason why we have used an expansion linear in ξ and quadratic in η in Sect. 3.6.2.2. A convenient way to take care of this is to expand the generating function. Therefore, we write

$$S(\theta, J) = J \cdot \theta + S_1(\theta, J). \quad (3.7.2)$$

The first term generates the identity while the second term is meant to describe the perturbation and needs to be calculated.

3.7.2 One-Dimensional Case

We start with the case of one-dimensional motion and follow the analysis from Tabor [20], where more details can be found. The canonical transformation $(\theta, I) \mapsto (\varphi, J)$ defined by the generating function $S(\theta, J)$ can be written as

$$I = \frac{\partial S}{\partial \theta} = J + \frac{\partial S_1}{\partial \theta}, \quad \varphi = \frac{\partial S}{\partial J} = \theta + \frac{\partial S_1}{\partial J}. \quad (3.7.3)$$

In order to preserve the periodicity of φ , the perturbative part of the generating function needs to be periodic too, i.e. $S_1(\theta, J) = S_1(\theta + 2\pi, J)$. In canonical perturbation theory, S_1 is expanded in orders of ε

$$S_1(\theta, J) = \varepsilon S_1^{(1)}(\theta, J) + \varepsilon^2 S_1^{(2)}(\theta, J) + O(\varepsilon^3) \quad (3.7.4)$$

Next we insert the expansion into the Hamiltonian function and obtain the Hamilton–Jacobi equation, see Eq. (3.3.25),

$$\begin{aligned} K(J) &= H_0 \left(J + \varepsilon \frac{\partial S_1^{(1)}}{\partial \theta} + \varepsilon^2 \frac{\partial S_1^{(2)}}{\partial \theta} + O(\varepsilon^3) \right) \\ &\quad + \varepsilon H_1 \left(\theta, J + \varepsilon \frac{\partial S_1^{(1)}}{\partial \theta} + \varepsilon^2 \frac{\partial S_1^{(2)}}{\partial \theta} + O(\varepsilon^3) \right), \end{aligned} \quad (3.7.5)$$

where, for the sake of clarity, we have labeled the new Hamiltonian by K . In order to get an expansion in ε also the Hamiltonian functions H_0 and H_1 are expanded in a Taylor series.

$$\begin{aligned}
K(J) = H_0(J) &+ \frac{\partial H_0}{\partial J} \left\{ \varepsilon \frac{\partial S_1^{(1)}}{\partial \theta} + \varepsilon^2 \frac{\partial S_1^{(2)}}{\partial \theta} + O(\varepsilon^3) \right\} \\
&+ \frac{1}{2} \frac{\partial^2 H_0}{\partial J^2} \left\{ \varepsilon \frac{\partial S_1^{(1)}}{\partial \theta} + \varepsilon^2 \frac{\partial S_1^{(2)}}{\partial \theta} + O(\varepsilon^3) \right\}^2 \\
&+ \varepsilon H_1(J, \theta) + \varepsilon \frac{\partial H_1}{\partial J} \left\{ \varepsilon \frac{\partial S_1^{(1)}}{\partial \theta} + \varepsilon^2 \frac{\partial S_1^{(2)}}{\partial \theta} + O(\varepsilon^3) \right\} + O(\varepsilon^4). \quad (3.7.6)
\end{aligned}$$

Sorting the different powers of ε we find

$$\begin{aligned}
K(J) = H_0(J) &+ \varepsilon \left\{ \omega_0(J) \frac{\partial S_1^{(1)}}{\partial \theta} + H_1(\theta, J) \right\} \\
&+ \varepsilon^2 \left\{ \omega_0(J) \frac{\partial S_1^{(2)}}{\partial \theta} + \frac{1}{2} \frac{\partial \omega_0(J)}{\partial J} \left(\frac{\partial S_1^{(1)}}{\partial \theta} \right)^2 + \frac{\partial H_1}{\partial J} \frac{\partial S_1^{(1)}}{\partial \theta} \right\} + O(\varepsilon^3), \quad (3.7.7)
\end{aligned}$$

where we have introduced the angular frequency $\omega_0(J) = \frac{\partial H_0(J)}{\partial J}$. We expand also the left-hand side of Eq. (3.7.5)

$$K(J) = K_0(J) + \varepsilon K_1(J) + \varepsilon^2 K_2(J) + O(\varepsilon^3), \quad (3.7.8)$$

such that we can equate the same powers of ε . Thus we find

$$O(\varepsilon^0) : H_0(J) = K_0(J), \quad (3.7.9)$$

$$O(\varepsilon^1) : \omega_0(J) \frac{\partial S_1^{(1)}}{\partial \theta} + H_1(\theta, J) = K_1(J), \quad (3.7.10)$$

$$O(\varepsilon^2) : \omega_0(J) \frac{\partial S_1^{(2)}}{\partial \theta} + \frac{1}{2} \frac{\partial \omega_0(J)}{\partial J} \left(\frac{\partial S_1^{(1)}}{\partial \theta} \right)^2 + \frac{\partial H_1}{\partial J} \frac{\partial S_1^{(1)}}{\partial \theta} = K_2(J). \quad (3.7.11)$$

As it should be the new Hamiltonian equals H_0 in zeroth-order. To compute the next correction to the energy we exploit the periodicity of the motion in the old angle variable θ and average Eq. (3.7.10) over it. Since S_1 is periodic in θ , the average value of $\partial S_1 / \partial \theta$ over one period has to vanish. For the first-order energy correction we then find

$$K_1(J) = \bar{H}_1(J) \equiv \frac{1}{2\pi} \int_0^{2\pi} H_1(J, \theta) d\theta. \quad (3.7.12)$$

The result for K_1 is used to compute S_1

$$\frac{\partial S_1^{(1)}}{\partial \theta} = \frac{1}{\omega_0(J)} [K_1(J) - H_1(J, \theta)]. \quad (3.7.13)$$

We note that the right-hand side of Eq.(3.7.13) is just the difference between the perturbation $H_1(J, \theta)$ and its average $K_1(J)$. The latter is subtracted to render the first order correction periodic in θ , as initially required for $S_1(\theta, J)$. The generating function can be used to compute the new action-angle variables in first order in ε :

$$\varphi = \theta + \varepsilon \frac{\partial S_1(\theta, J)}{\partial J}, \quad J = I - \varepsilon \frac{\partial S_1(\theta, J)}{\partial \theta}. \quad (3.7.14)$$

Using Eq. (3.7.8) we obtain for the frequency corrected to first order

$$\omega(J) = \omega_0(J) + \varepsilon \frac{\partial K_1(J)}{\partial J}. \quad (3.7.15)$$

The fact that the perturbation induces a shift of the unperturbed frequency is sometimes called “frequency pulling”. The perturbed motion consists of the unperturbed motion plus an $O(\varepsilon)$ oscillatory correction. A potential source of difficulties is the frequency $\omega_0(J)$ which may be close or equal to zero. This can occur for a motion near a separatrix (remember the pendulum problem from Sect. 3.1, where the frequency goes to zero when approaching the separatrix), and in higher dimensions generally at nonlinear resonances (see next subsection).

The computation of the second order correction goes along the same line. First we average Eq. (3.7.11) over θ and obtain

$$K_2(J) = \frac{1}{2} \frac{\partial \omega_0(J)}{\partial J} \overline{\left(\frac{\partial S_1^{(1)}(\theta, J)}{\partial \theta} \right)^2} + \overline{\frac{\partial H_1(\theta, J)}{\partial J} \frac{\partial S_1^{(1)}(\theta, J)}{\partial \theta}}. \quad (3.7.16)$$

The solution for the energy correction is used to compute the next correction to the generating function

$$\frac{\partial S_1^{(2)}(\theta, J)}{\partial \theta} = \frac{1}{\omega_0(J)} \left[K_2(J) - \frac{1}{2} \frac{\partial \omega_0(J)}{\partial J} \left(\frac{\partial S_1^{(1)}}{\partial \theta} \right)^2 - \frac{\partial H_1}{\partial J} \frac{\partial S_1^{(1)}}{\partial \theta} \right]. \quad (3.7.17)$$

The corresponding terms for the action-angle variables and the frequency can be calculated as above.

We have seen that computations become simpler when we average over the original variable θ . Nevertheless, the non-averaged part of the Hamiltonian function enters the computation again when we calculate the correction to the generating function. Here terms like $K_1 - H_1$ appear, which is nothing else than the average of H_1 minus the function itself. That also means that, when doing canonical perturbation theory, it is helpful to separate the mean motion from a small oscillatory motion. This is a more formal justification of the method of Gauß averaging introduced in Sect. 3.6.2.3.

3.7.3 Problem of Small Divisors

When applying canonical perturbation theory to systems with more than one degree of freedom, the derivation is a bit less transparent than in the previous subsection. The generalization of Eq. (3.7.7) reads

$$\begin{aligned} K(J) &= H_0(J) + \varepsilon \left\{ \omega_0(J) \cdot \nabla_\theta S_1^{(1)} + H_1(\theta, J) \right\} \\ &\quad + \varepsilon^2 \left\{ \omega_0(J) \cdot \nabla_\theta S_1^{(2)} + \frac{1}{2} \sum_{i,j} \frac{\partial \omega_{0i}(J)}{\partial J_j} \frac{\partial S_1^{(1)}}{\partial \theta_i} \frac{\partial S_1^{(1)}}{\partial \theta_j} + \nabla_J H_1 \cdot \nabla_\theta S_1^{(1)} \right\} \\ &\quad + O(\varepsilon^3), \end{aligned} \quad (3.7.18)$$

with frequencies $\omega_0(J) = \nabla_J H_0(J)$. Difficulties occur when we want to calculate the first-order correction to the generating function. The first two equations for the energy correction read

$$O(\varepsilon^0) : H_0(J) = K_0(J), \quad (3.7.19)$$

$$O(\varepsilon^1) : \omega_0(J) \cdot \nabla_\theta S_1^{(1)}(\theta, J) + H_1(\theta, J) = K_1(J). \quad (3.7.20)$$

To compute the first-order energy correction we average Eq. (3.7.20) over the angles $\theta_i, i = 1, \dots, n$:

$$K_1(J) = \overline{H}_1(J) = \int_0^{2\pi} d\theta_1 \cdots \int_0^{2\pi} d\theta_n H_1(\theta, J). \quad (3.7.21)$$

Using the expression for K_1 we solve for the first-order correction of the generating function which reads

$$\omega_0(J) \cdot \nabla_\theta S_1^{(1)}(\theta, J) = K_1(J) - H_1(\theta, J). \quad (3.7.22)$$

Since $\omega_0(J)$ is a vector we cannot just devide by it. To derive a formal solution we exploit the periodicity of S_1 and H_1 and expand both into Fourier series:

$$S_1^{(1)}(\theta, J) = \sum_{k \neq 0} S_{1,k}^{(1)} e^{ik \cdot \theta}, \quad H_1(\theta, J) = \sum_k H_{1,k} e^{ik \cdot \theta}. \quad (3.7.23)$$

Inserting the ansatz into Eq. (3.7.22) we solve for $S_1^{(1)}$ and find

$$S_1^{(1)}(\theta, J) = i \sum_{k \neq 0} \frac{H_{1,k} e^{ik \cdot \theta}}{k \cdot \omega_0(J)}. \quad (3.7.24)$$

While in the one-dimensional case the only source of problems was the single frequency $\omega_0(J)$, we now have a term of the form $k \cdot \omega_0(J)$ in the denominator where $\omega_0(J)$ is a vector with n components each depending on J , and k is summed over \mathbb{Z}^n . But if $k \cdot \omega_0(J) = 0$ (resonance condition) the sum will obviously diverge. This is always the case if there exist ω_{0i} and ω_{0j} such that $\frac{\omega_{0i}}{\omega_{0j}} \in \mathbb{Q}$ for all $i \neq j$. Hence, the set of frequencies for which the perturbative expansion diverges lies dense in the set of all possible frequencies. Furthermore, even if this does not occur it is always possible to find a $k \in \mathbb{Z}^n$ such that $k \cdot \omega_0(J)$ is arbitrarily small. This phenomenon is known as the *problem of small divisors* [11, 12, 14, 15]. Despite these difficulties, results which are valid for finite times can be computed by brute force truncations of the perturbation series.

3.7.4 KAM Theorem

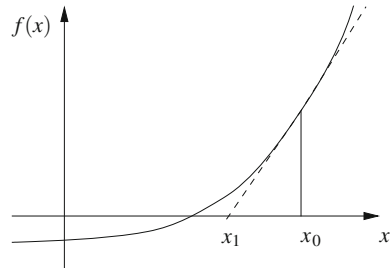
We have just seen that the addition of even smallest non-integrable perturbations can lead to difficult analytic problems. For a long time it was an open question whether such perturbations would immediately render an integrable system chaotic. One can reformulate this question and ask whether there is a smooth or an immediate transition (in the strength of the perturbation) from regular to chaotic motion when a non-integrable perturbation is added to an integrable system. This problem was resolved in the early 1960s when Arnold and Moser proved a theorem that had previously been suggested by Kolmogorov. This theorem (today known as KAM theorem) assures the existence of regular structures under small perturbations.

For their proof Arnold and Moser used a technique known as superconvergent perturbation theory. The basic idea of this method is to compute the change of the coordinates successively in first order perturbation theory. That means a correction is computed in first order and the result is used to do again first order perturbation theory. If this procedure is applied infinitely often one obtains a perturbation series of the form $\sum_\alpha c_\alpha \varepsilon^{(2^\alpha)}$ that is quadratically convergent. Although the very quick convergence in some way outstrips the divergences found in traditional perturbation theory, it produces very complicated expressions. However, for mathematical proofs such series are a very useful tool.

The idea of superconvergent perturbation theory is explained with the help of Newton's algorithm for finding the root of an equation, which is based on a similar iterative construction. Given a function f we are interested in the solution of the equation $f(x) = 0$. Using Newton's technique we start with an initial value x_0 . The next value x_1 is found by taking the intersection of the tangent of f at x_0 with the abscissa, see Fig. 3.9. When successively iterating this procedure one may find the root. Newton's algorithm leads to the following iterative equation

$$x_{n+1} = x_n - \frac{f(x_n)}{f'(x_n)}. \quad (3.7.25)$$

Fig. 3.9 The Newton procedure uses an initial guess x_0 and the tangent of $f(x_0)$ to obtain an estimate x_1 for the root. Iterating this procedure results in a very fast convergence rate



The change of the approximate result in the n -th step is given by

$$\varepsilon_n = x_n - x_{n-1} = -\frac{f(x_{n-1})}{f'(x_{n-1})}. \quad (3.7.26)$$

In order to compute the convergence rate, we estimate ε_{n+1} in terms of ε_n . Therefore f is expressed as

$$\begin{aligned} f(x_n) &\approx f(x_{n-1}) + (x_n - x_{n-1})f'(x_{n-1}) + \frac{1}{2}(x_n - x_{n-1})^2 f''(x_{n-1}) + \dots \\ &= f(x_{n-1}) + \varepsilon_n f'(x_{n-1}) + \frac{1}{2}\varepsilon_n^2 f''(x_{n-1}) + \dots \end{aligned} \quad (3.7.27)$$

The same can be done with the derivative of f

$$f'(x_n) \approx f'(x_{n-1}) + \varepsilon_n f''(x_{n-1}) + \frac{1}{2}\varepsilon_n^2 f'''(x_{n-1}) + \dots \quad (3.7.28)$$

The wanted relation is computed in the following way

$$\begin{aligned} \varepsilon_{n+1} &= -\frac{f(x_n)}{f'(x_n)} \approx -\frac{f(x_{n-1}) + \varepsilon_n f'(x_{n-1}) + \frac{1}{2}\varepsilon_n^2 f''(x_{n-1}) + \dots}{f'(x_{n-1}) + \varepsilon_n f''(x_{n-1}) + \dots} \\ &\approx -\frac{f(x_{n-1})}{f'(x_{n-1})} - \varepsilon_n - \frac{\varepsilon_n^2}{2} \frac{f''(x_{n-1})}{f'(x_{n-1})} = \varepsilon_n - \varepsilon_n - \frac{\varepsilon_n^2}{2} \frac{f''(x_{n-1})}{f'(x_{n-1})}. \end{aligned} \quad (3.7.29)$$

Hence $O(\varepsilon_{n+1}) = O(\varepsilon_n^2)$. This means that the iteration is quadratically convergent and we can write

$$x = x_0 + \sum_{n=1}^{\infty} c_n \varepsilon_n = \sum_{n=0}^{\infty} c_n \varepsilon_0^{2^n}. \quad (3.7.30)$$

The last equation highlights both, the quick convergence and the importance of a good initial guess in order for the method to converge (i.e. ε_0 must be sufficiently small).

3.7.4.1 Statement of the KAM Theorem

KAM theorem: Let $H = H_0 + \varepsilon H_1$ be a Hamiltonian function where H_0 describes an integrable system. In the action-angle variables (I, θ) of H_0 the motion lies on tori, see the set \mathcal{T} in Sect. 3.4. We assume that the given torus (fixed by the chosen energy of the system) is non-resonant, i.e.

$$\forall k \in \mathbb{Z} : k \cdot \omega(I) \neq 0, \quad (3.7.31)$$

where the frequencies are defined by $\omega_i = \frac{\partial H_0(I)}{\partial I_i}$. Then for sufficiently small ε there exists a torus for the whole system and new action-angle variables (φ, J) which read

$$\varphi = \theta + \varepsilon g(\varepsilon, \theta), \quad J = I + \varepsilon f(\varepsilon, \theta). \quad (3.7.32)$$

This means that the new torus parametrized by φ is “near” the old one and that the old and the new torus transform smoothly into each other. The frequencies on the new torus are again given by $\omega(J)$.

For the proof several conditions are required [21–23]:

- **Sufficient nonlinearity or nondegeneracy condition:** The nonlinearity has to be strong enough to make the frequencies linearly independent over some domain in J (please keep in mind that J and ω are vectors in general).

$$\det \left(\frac{\partial \omega(J)}{\partial J} \right) \Big|_{J \approx I} \neq 0. \quad (3.7.33)$$

A system for which Eq. (3.7.33) is fulfilled is called non-degenerate.

- **Sufficient regularity:** A smoothness condition for the perturbation (sufficient number of continuous derivatives of H_1) has to hold. This condition guarantees that the Fourier coefficients of expansions as in Eq. (3.7.23) decrease sufficiently fast. For more details consult [22, 24].
- **Diophantine condition:** The frequency vector ω is “badly” approximated by rationals, which is quantified by

$$\forall k \in \mathbb{Z}^n : |k \cdot \omega(I)| \geq \frac{\gamma}{|k|^\tau}, \quad (3.7.34)$$

where γ is a constant that depends only on ε , on the magnitude of the perturbation H_1 and on some measure of the nonlinearity of the unperturbed Hamiltonian H_0 . The exponent τ depends on the number of degrees of freedom and the regularity properties of H_1 .

Let us discuss the range of application of the theorem. For a more detailed discussion consult the appendix on Kolmogorov’s theorem in [6]. The tori of an integrable system are defined by the action variables I_i , $i = 1, \dots, n$. Another way to distinguish them is by their frequencies (every torus has its own frequency vector $\omega(I)$).

Assume we are given a frequency vector that fulfills the resonant condition, which means that $\exists k \in \mathbb{Z} : k \cdot \omega(I) = 0$. This relation can only be fulfilled if the frequencies are rationally related. But since the irrational numbers lie dense in \mathbb{R} we can find a new frequency vector ω' with only rationally unrelated components in the neighborhood of $\omega(I)$. Hence the set of non-resonant tori lies dense in the set of all tori. The same holds for the set of resonant tori. More important, it can be shown that the Lebesgue measure of the union of all resonant tori of the unperturbed non-degenerate system is equal to zero. Hence, the non-resonant condition and the non-degeneracy condition restrict the tori for which the KAM theorem can be applied to a set of Lebesgue measure one. However, there is still the Diophantine condition which is a stronger assumption. It restricts the set of tori for which the KAM theorem can be applied to a set of Lebesgue measure nearly one in the sense that the measure of the complement of their union is small when the perturbation is small.

In the next section we will illustrate the Diophantine condition for systems with two degrees of freedom.

3.7.5 Example: Two Degrees of Freedom

For two degrees of freedom the non-resonant condition for $\omega_{1,2} \neq 0$ reads

$$\omega_1 k_1 + \omega_2 k_2 \neq 0 \Leftrightarrow \frac{\omega_1}{\omega_2} \neq -\frac{k_2}{k_1}. \quad (3.7.35)$$

Hence the frequencies are not allowed to be rationally related. A stronger restriction whose meaning is not so easily accessible is the Diophantine condition. In our case it reads

$$\forall k \in \mathbb{Z}^2 : |k \cdot \omega(I)| \geq \frac{\gamma}{|k|^\tau}. \quad (3.7.36)$$

The condition refers to the question how good irrational numbers can be approximated by rational numbers. The better $-\frac{k_2}{k_1}$ approximates $\frac{\omega_1}{\omega_2}$, the smaller is the left hand side of Eq. (3.7.36). On one hand every irrational number can be approximated by rational numbers in arbitrary precision (the rational numbers lie dense in the real numbers). On the other hand one may need large k_1 and k_2 , which make the right hand side of Eq. (3.7.36) smaller as both k_1 and k_2 have to increase. Hence, we are confronted with an interplay of these two effects.

The KAM theorem states the existence of a function $\gamma(\varepsilon)$, which goes to zero as $\varepsilon \rightarrow 0$, and gives the following condition for the stability of a torus of a two-dimensional system:

$$\left| \frac{\omega_1}{\omega_2} - \frac{k_2}{k_1} \right| > \frac{\gamma(\varepsilon)}{k_1^{2.5}}, \quad \forall k_1, k_2 \in \mathbb{Z}, \quad (3.7.37)$$

see Ott [25]. In general very little is known about γ . To fulfill Eq. (3.7.37) one needs fractions of frequencies which are difficult to approximate by rational numbers. The question how good an irrational number can be approximated by rational numbers can be answered with the help of the theory of continued fractions, see Ott [25] and references therein. For rational numbers, the continued fraction expansion¹² is finite. For non-rational numbers it is infinite. π , for instance, is well approximated already by

$$\pi = 3 + \frac{1}{7 + \frac{1}{15 + \frac{1}{\dots}}} \approx \frac{355}{15} = 3.141592. \quad (3.7.38)$$

The reason is that the numbers 7 and 15 appearing in the expansion are rather large making the convergence to the true value fast. For the same reasoning, it turns out that the worst approximated number is the golden mean μ which is defined by

$$\mu = \frac{1}{1 + \frac{1}{1 + \frac{1}{\dots}}} = \frac{\sqrt{5} - 1}{2}. \quad (3.7.39)$$

Here the continued fraction expansion consists just of 1's, hence the convergence of finite approximations of the series is worst. As an aside, we mention that $\mu^{-1} = \frac{\sqrt{5}+1}{2}$. Hence, the tori whose frequencies fulfill $\frac{\omega_1}{\omega_2} = \mu^{\pm 1}$ are most stable with respect to perturbations.

3.7.6 Secular Perturbation Theory

We have now learnt that the KAM theorem does not apply for resonances occurring in the unperturbed system. In this case one may use instead secular or resonant perturbation theory. We introduce the method for the special and most transparent case of an unperturbed system with one degree of freedom and a time-periodic perturbation. For a more general discussion the reader may consult [21]. We assume that the unperturbed Hamiltonian function H_0 can be solved with action-angle variables and write the full Hamiltonian as

$$H(I, \theta, t) = H_0(I) + \varepsilon H_1(I, \theta, \Omega t), \quad (3.7.40)$$

where H_1 is assumed to be periodic in time, $H_1(I, \theta, \Omega t + 2\pi) = H_1(I, \theta, \Omega t)$. As long as ε is small the system has two different time scales. The internal time scale of H_0 given by the rotational frequency along a given torus of the unperturbed problem with frequency $\omega_0 = \frac{\partial H_0}{\partial I}$. The second one is defined by the driving frequency Ω . The goal of this section is to make an approximate calculation near to resonance conditions on the two frequencies, that means for

¹² Number theory shows that the continued fraction representation is unique [26].

$$r\omega_0 = s\Omega, \quad r, s \in \mathbb{Z}. \quad (3.7.41)$$

In the following, we use a time-independent Hamiltonian \mathcal{H} in the extended phase space (Sect. 3.3) which equivalently describes the same system. It is given by $\mathcal{H} = H - E$ and can be written as

$$\mathcal{H} = H_0(I) + \Omega J + \varepsilon H_1(I, \theta, \varphi), \quad (3.7.42)$$

where we have introduced the variables $\varphi = \Omega t$ and $J = -\frac{E}{\Omega}$. Obviously, we have to solve the new system for $\dot{\mathcal{H}} = 0$.

In the next step we transform into the coordinate system that is rotating with $\bar{\theta}(t) = \theta + \omega_0 t$. The generating function of this transformation reads $S(\bar{I}, \theta, \bar{J}, \varphi) = \theta \bar{I} + \varphi \bar{J} - \frac{s}{r} \varphi \bar{I}$, where \bar{I} , $\bar{\theta}$, \bar{J} and $\bar{\varphi}$ denote the new coordinates. The relation between the old and the new coordinates is given by

$$I = \frac{\partial S}{\partial \theta} = \bar{I}, \quad \bar{\theta} = \frac{\partial S}{\partial \bar{I}} = \theta - \frac{s}{r} \varphi \quad (3.7.43)$$

and

$$J = \frac{\partial S}{\partial \varphi} = \bar{J} - \frac{s}{r} \bar{I}, \quad \bar{\varphi} = \frac{\partial S}{\partial \bar{J}} = \varphi. \quad (3.7.44)$$

We note that on the resonance $\dot{\bar{\theta}}(t)$ is a constant, since $\dot{\bar{\theta}} = \omega_0 - \frac{s}{r} \Omega = 0$ due to Eq.(3.7.41). When we express the Hamiltonian function in the new coordinates it reads

$$\mathcal{H} = H_0(\bar{I}) + \Omega \left(\bar{J} - \frac{s}{r} \bar{I} \right) + \varepsilon H_1(\bar{I}, \bar{\theta} + \frac{s}{r} \bar{\varphi}, \bar{\varphi}). \quad (3.7.45)$$

In order to compute an approximate solution of the full system we make two approximations, one concerning H_0 and one concerning H_1 . The first one is a second order approximation of $H_0(\bar{I})$ in the vicinity of the resonance which reads

$$H_0(\bar{I}) \approx H_0(\bar{I}_0) + \omega_0(\bar{I}_0)(\bar{I} - \bar{I}_0) + \frac{1}{2m_0(\bar{I}_0)} (\bar{I} - \bar{I}_0)^2, \quad (3.7.46)$$

where $\frac{1}{m_0}(\bar{I}) = \frac{\partial^2 H_0}{\partial \bar{I}^2}(\bar{I})$. Using the resonance condition $\Omega \frac{s}{r} = \omega_0$, we write

$$H_0(\bar{I}) - \Omega \frac{s}{r} \bar{I} \approx H_0(\bar{I}_0) - \omega_0 \bar{I}_0 + \frac{1}{2m_0} (\bar{I} - \bar{I}_0)^2 \quad (3.7.47)$$

and find that in zeroth order of ε

$$\frac{d\bar{\theta}}{dt} = \frac{\partial \mathcal{H}}{\partial \bar{I}} \approx \frac{\bar{I} - \bar{I}_0}{m_0}, \quad \frac{d\bar{\varphi}}{dt} = \frac{\partial \mathcal{H}}{\partial \bar{J}} = \Omega. \quad (3.7.48)$$

The second approximation is an average of H_1 over r periods of the variable $\bar{\varphi}$ which is known under the name *adiabatic perturbation theory* (c.f. also Sect. 3.6) and leads to an effective Hamiltonian

$$\overline{\mathcal{H}}(\bar{I}, \bar{\theta}, \bar{J}) = H_0(\bar{I}) - \omega_0 \bar{I} + \Omega \bar{J} + \varepsilon \overline{H}_1(\bar{I}, \bar{\theta}), \quad (3.7.49)$$

$$\overline{H}_1(\bar{I}, \bar{\theta}) = \frac{1}{2\pi r} \int_0^{2\pi r} H_1(\bar{I}, \bar{\theta} + \frac{s}{r}\bar{\varphi}, \bar{\varphi}) d\bar{\varphi}. \quad (3.7.50)$$

According to our initial assumptions, H_1 is 2π -periodic in φ as well as θ . Hence, it can be written as $H_1(I, \theta, \varphi) = \sum_{m,n=-\infty}^{\infty} H_{nm}(I) e^{i(m\theta+n\varphi)}$. Expressed in the new variables this reads

$$H_1(\bar{I}, \bar{\theta} + \frac{s}{r}\bar{\varphi}, \bar{\varphi}) = \sum_{m,n=-\infty}^{\infty} H_{nm}(\bar{I}) e^{im\bar{\theta}} e^{i(\frac{s}{r}m+n)\bar{\varphi}}. \quad (3.7.51)$$

Averaging Eq. (3.7.51) over $\bar{\varphi}$ leads to

$$\begin{aligned} \bar{H}_1(\bar{I}, \bar{\theta}) &= \sum_{m,n=-\infty}^{\infty} H_{nm}(\bar{I}) e^{im\bar{\theta}} \delta_{sm, -rn} \\ &= H_{00}(\bar{I}) + \sum_{l=1}^{\infty} \left[H_{sl, -rl} e^{-irl\bar{\theta}} + H_{-sl, rl} e^{irl\bar{\theta}} \right] \\ &= H_{00}(\bar{I}) + 2 \sum_{l=1}^{\infty} H_{sl, -rl} \cos(rl\bar{\theta}), \end{aligned} \quad (3.7.52)$$

where for simplicity we assumed that $H_{n,m} = H_{-n,-m}$. If this equality did not hold, we would have to deal with an additional (l -dependent) phase factor in the cosine.

Now we transform back to the old coordinate system. The energy is given by $E = -\Omega \bar{J}$ and the old Hamiltonian \overline{H} is therefore given by $\overline{H} = \overline{\mathcal{H}} + \Omega \bar{J}$. Additionally, we make a relatively crude approximation and neglect all but the constant and the first term ($l = 1$) of the Fourier expansion of \overline{H}_1 . The result is an effective Hamiltonian function near the resonance:

$$\overline{H}(\bar{I}, \bar{\theta}) = H_0(\bar{I}) - \omega_0 \bar{I} + \varepsilon \overline{H}_1(\bar{I}, \bar{\theta}). \quad (3.7.53)$$

Since $\bar{I} = \bar{I}_0 + O(\varepsilon)$, we can write $\overline{H}_1(\bar{I}, \bar{\theta}) = \overline{H}_1(\bar{I}_0, \bar{\theta}) + O(\varepsilon)$. Ignoring all terms of $O(\varepsilon^2)$ and higher results in

$$\begin{aligned} \overline{H}(\bar{I}, \bar{\theta}) &\approx H_0(\bar{I}_0) - \omega_0 \bar{I}_0 + \varepsilon H_{00}(\bar{I}) \\ &\quad + \frac{1}{2m_0} (\bar{I} - I_0)^2 + 2\varepsilon H_{r, -s}(\bar{I}) \cos(r\bar{\theta}) + \text{higher orders.} \end{aligned} \quad (3.7.54)$$

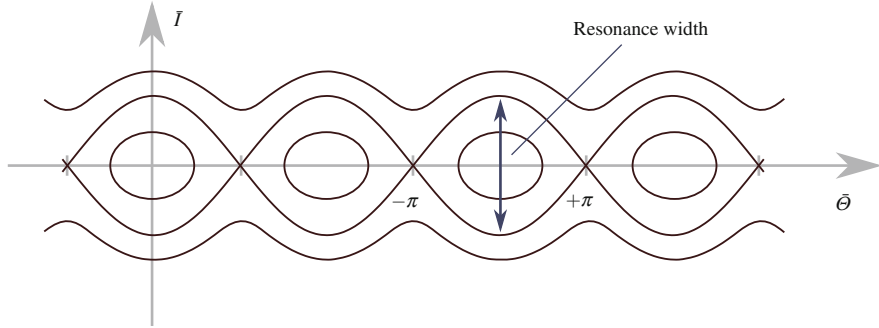


Fig. 3.10 The *resonance width* W is the width of the separatrix in the I -direction and according to (3.7.56) $W \approx 4\sqrt{2m_0\varepsilon H_{r,-s}} \propto \sqrt{\varepsilon}$

$$\approx \frac{1}{2m_0} (\bar{I} - I_0)^2 + 2\varepsilon H_{r,-s}(\bar{I}_0) \cos(r\bar{\theta}) + \text{const.}(\bar{I}_0). \quad (3.7.55)$$

When we introduce $p = \bar{I} - I_0$ and $c = 2\varepsilon H_{r,-s}(I_0)$, the effective Hamiltonian \bar{H} in Eq. (3.7.55) has the form $H = \frac{p^2}{2m_0} + c \cos(r\bar{\theta})$. This is the same Hamiltonian as the one of a pendulum in a gravitational field. The central result of this section is thus that the dynamics created by small resonant perturbations can be effectively described by a pendulum approximation:

$$\bar{I}(\bar{\theta}) = 2\sqrt{2m_0\varepsilon H_{r,-s}} \cos\left(\frac{\bar{\theta}}{2}\right) \quad (3.7.56)$$

This directly gives an estimate for the resonance width W assuming it equals the width of the separatrix of the pendulum, see Figs. 3.1 and 3.10:

$$W \approx 4\sqrt{2m_0\varepsilon H_{r,-s}}. \quad (3.7.57)$$

We highlight that W is proportional to the square root of the perturbation $W \propto \sqrt{\varepsilon}$.

As a possible application we give an example much studied in the literature. We take the Hamiltonian of the hydrogen atom and assume an additional time-dependent driving force pointing in the x -direction (originating, for example, from a time-dependent electric field).

$$H(\mathbf{r}, \mathbf{p}, t) = \frac{\mathbf{p}^2}{2} - \frac{1}{|\mathbf{r}|} + Fx \cos(\omega t). \quad (3.7.58)$$

At time $t = 0$ the quantum spectrum reads $E_n(t = 0) = -\frac{1}{2n^2}$. If we choose $n \geq 10$ this Hamiltonian can be used to describe a Rydberg atom which starts to behave similar as its classical counterpart. In the classical system resonance islands

appear if the orbital period is resonant with the driving period, e.g. for $\omega_{\text{Kepler}} \approx \omega$. Also stable quantum wave packets exist corresponding to quantized states on the resonance island in classical phase space, see [27] for details and more references. We will come back to this example in Sect. 4.4.3.3.

3.8 Transition to Chaos in Hamiltonian Systems

In the previous sections we have focused on near integrable systems. The equations of motion of integrable systems can be solved by quadratures (see Sect. 3.4), the phase space trajectory is confined to an n -dimensional torus and action-angle variables can be used. In one space dimension this leads always to a periodic motion, while in higher dimensions there are more possible kinds of dynamics. Since the motion is periodic in each single coordinate (in action-angle variables) the structure of the overall dynamics of higher dimensional systems is determined by the coordinate's frequencies. In case of all frequencies being rationally related, i.e. $k \cdot \omega(I) = 0$ for a tuple of integers k , the motion is periodic. If in contrast this is not true for all frequencies the phase space trajectory explores the whole torus and the systems motion is ergodic on the torus, see Sect. 3.9.1.

The characterization of chaotic dynamics instead turns out to be much more involved. From the KAM theorem, we know that there exist systems which are “near” to integrable ones and therefore behave (at least for some time) approximately like them. In this section we will be concerned with systems and their phenomenology for which this is no longer true. When analyzing chaotic dynamics (especially by means of numerical simulations) it is important to be able to visualize the results. Therefore we start this section by introducing the *surface of section*, which is a highly valuable method to visualize and to analyze chaotic systems of low dimensionality.

3.8.1 Surface of Sections

The phase space of a system with n degrees of freedom is $2n$ -dimensional. This makes a visualization of the dynamics of Hamiltonian systems in nearly all cases impossible. Already for a conservative system with two degrees of freedom the energy surface is a three dimensional hyperplane and hence a plot of the trajectory is sometimes possible, but difficulties arise in many circumstances. To this end, a valuable technique called the *surface of section* (or Poincaré surface of section) has been introduced by Poincaré (1892) and Birkhoff (1932). In principle, the technique is applicable to systems with an arbitrary phase space dimension but its most important application is to conservative systems with two degrees of freedom, for which we introduce the method now. As already mentioned their energy surface is three-dimensional. In order to find a two-dimensional object that can easily be plotted on a sheet of paper (or on a computer screen), we choose a plane in phase space and visualize each point

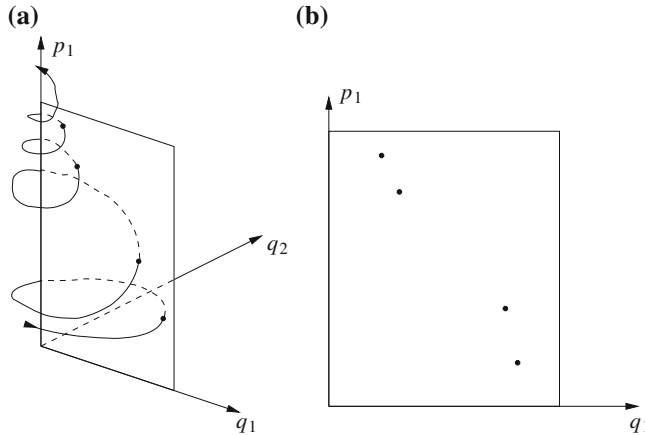


Fig. 3.11 The surface of section is a method to visualize the dynamics. **a** shows a phase space trajectory reduced to the energy surface with $E = \text{const}$. In **(b)** we see the corresponding points on the surface of section reduced by one dimension with respect to the original phase space shown in **(a)**

where the trajectory passes through the plane, see Fig. 3.11. A possible and often used example for such a plane is the one defined by setting $q_2 = 0$. The surface of section (SOS) is then filled up by the points from the following set

$$\text{SOS} = \left\{ (q, p) \in \mathbb{R}^4 \mid q_2 = 0, H(q, p) = E \right\}. \quad (3.8.1)$$

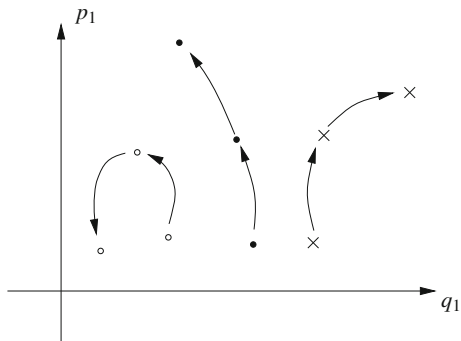
Since the momenta typically appear quadratically in the Hamiltonian ($H = \frac{p_1^2}{2m_1} + \frac{p_2^2}{2m_2} + V(q_1, q_2)$) there is an ambiguity in sign. For fixed energy E , solving for p_2 gives at $q_2 = 0$:

$$p_2 = \pm \sqrt{2m_2 \left(E - \frac{p_1^2}{2m_1} - V(q_1, 0) \right)}. \quad (3.8.2)$$

For consistency, the SOS must be constructed by only considering trajectories with one fixed sign, e.g. by taking only trajectories which cross the section in Fig. 3.11 a from one side (from $q_2 < 0$ towards $q_2 = 0$).

Using the SOS we can define the so-called *Poincaré map* that maps a phase space point on the SOS to the next point on the SOS, see Fig. 3.12. Since the time evolution in Hamiltonian systems is unique the same is true for the Poincaré map. Since it is a discretization of a continuous dynamical system, it has the mathematical structure of a discrete dynamical system (see Sect. 2.1). We note that many properties of the system's dynamics are encoded in the Poincaré map. Assume, for example, that the system has a periodic orbit for the initial condition $(q_0, p_0) \in \text{SOS}$. Then the

Fig. 3.12 Every point (q_0, p_0) on the SOS is mapped by the Poincaré map \mathcal{P} to the next point where the trajectory (starting at (q_0, p_0)) passes through the SOS. This way the surface of section allows one to reduce the three-dimensional continuous time evolution to a two-dimensional and discrete time evolution



corresponding Poincaré map \mathcal{P} has a fixed point of some order n for that initial condition, i.e. $\mathcal{P}_n(q_0, p_0) = (q_0, p_0)$.

A simpler construction of the SOS is possible when the system's Hamiltonian is periodic in one variable. The natural way to define the SOS in these models is by taking snapshots at multiple integers of the period (with fixed energy). Assume q_2 is the periodic variable with period Q then the snapshots are taken for $q_2 = 0, Q, 2Q, \dots$ and $H(q_1, q_2, p_1, p_2) = E$. Since time-dependent Hamiltonian systems can be understood as time-independent systems on an extended phase space the periodic variable can also be the time. Assume a Hamiltonian (with one-and-a-half degrees of freedom) that is periodic in the time variable $H(q, p, t) = H(q, p, t + T)$. In this case, the Poincaré map is a *stroboscopic map* which is obtained by simply plotting the point of the trajectory at all multiples of the period:

$$\text{SOS} = \left\{ (q, p, t) \in \mathbb{R}^3 \mid t = nT, n \in \mathbb{N}; H(q, p) = E \right\}, \quad (3.8.3)$$

which is illustrated in Fig. 3.13.

It is possible to introduce a surface of section also in higher-dimensional systems. For a conservative system with n degrees of freedom the energy surface is $(2n - 1)$ -dimensional and hence the SOS is $(2n - 2)$ -dimensional. Therefore for $n > 2$ the technique is often not useful anymore to visualize the dynamics. On the other hand if one still uses a two-dimensional, i.e. further reduced SOS, the result is not necessarily meaningful because the trajectory does not necessarily pass through the chosen plane.

3.8.2 Poincaré–Cartan Theorem

Liouville's theorem states that the phase space volume is preserved under time evolution. We want to show that the same is true for the Poincaré map of a two-degrees-of-freedom conservative system, or also for a system with one-and-a-half degrees of freedom whose Hamiltonian function is time dependent. The area preservation

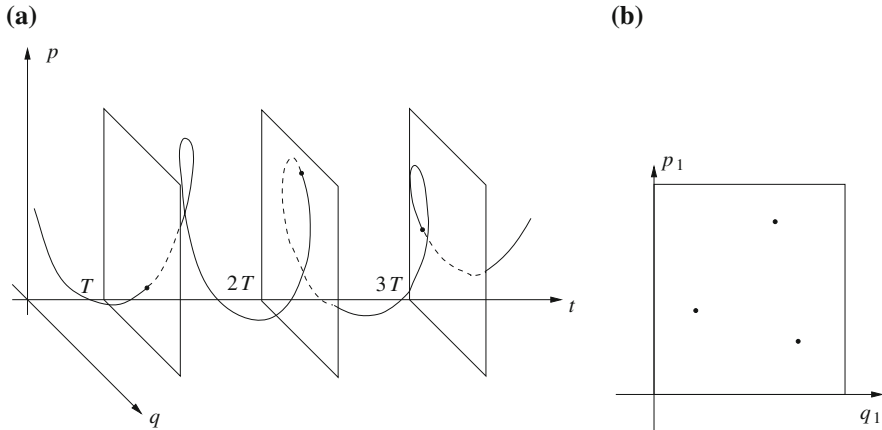


Fig. 3.13 A stroboscopic map exploits the periodicity of the Hamiltonian in time. The points on the SOS are shown in (b) and originate from the trajectory shown in (a)

of the Poincaré map is known as Poincaré–Cartan theorem. Exactly this property of area conservation makes the Poincaré map such a valuable tool. To derive the result we make use of the Poincaré–Cartan integral invariant, which we introduce because it is of importance by itself. Its natural formulation is in the language of differential forms which can be found in [6].

As reviewed in Sect. 3.3.2, Hamilton’s principle of extremal action directly leads to the result that the differential forms

$$pdq - Hdt \quad (3.8.4)$$

are invariant under canonical transformations. Since the Hamiltonian flow can itself be seen as a continuous canonical transformation we obtain

$$\oint_{\gamma_1} (pdq - Hdt) = \oint_{\gamma_2} (pdq - Hdt). \quad (3.8.5)$$

Here the two closed curves γ_1 and γ_2 encircle the flow, i.e. the trajectories as they evolve in time in the extended phase space. In the present context the integral above is called *Poincaré–Cartan integral invariant*.

Having the Poincaré–Cartan integral invariant at hand we come back to our original intention, namely the proof of the Poincaré–Cartan theorem which states that the Poincaré map is area preserving [25]. First we treat the case of a Hamiltonian system with one-and-a-half degrees of freedom. This includes the special case of $H(q, p, t + T) = H(q, p, t)$. By $h_t(q_0, p_0) = (q(t), p(t))$ we denote the time evolution of the Hamiltonian system. Let $\sigma_0 \subset SOS$ be an area in the (q, p) -plane at $t = 0$ and let $\sigma_i = \mathcal{P}_i(\sigma_0) = h_{iT}(\sigma_0) \subset SOS$ be the same area propagated i -times

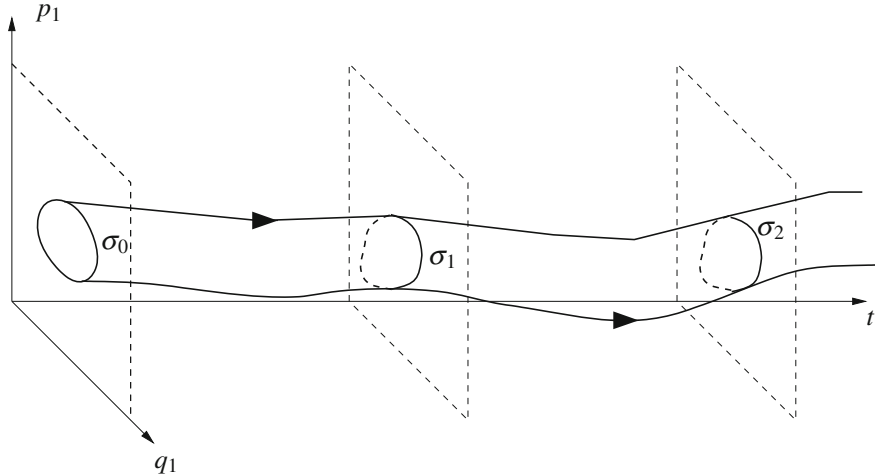


Fig. 3.14 All three areas, σ_0 , $\sigma_1 = \mathcal{P}(\sigma_0)$ and $\sigma_2 = \mathcal{P}(\mathcal{P}(\sigma_0))$, have the same size because the Poincaré map is area preserving

with the Poincaré map, see Fig. 3.14. We have to show that $|\sigma_0| = |\sigma_i|$ for all $i \in \mathbb{N}$. Since the σ_i lie in planes of constant time we apply Eq. (3.8.5) for $dt = 0$ and find immediately

$$\oint_{\partial\sigma_0} p_1 dq_1 = \oint_{\partial\sigma_1} p_1 dq_1, \quad (3.8.6)$$

with $\partial\sigma_0$ and $\partial\sigma_1$ denoting the closed curves encircling the areas σ_0 and σ_1 .

The situation is a little more complicated for conservative systems with two degrees of freedom because constructing the SOS is slightly more complicated (see the previous subsection). Assume we start the time evolution with an area $\sigma_0 \subset SOS$ at time zero. When the area is propagated in time it forms a tube just as one can see in Fig. 3.14. Now the SOS is not a plane at a certain point in time, but a hyperplane in phase space. Therefore, it is possible that the points of the propagated area σ_0 do not pass the SOS at the same time. Mathematically speaking it is not always possible to find a t such that $\sigma_1 = \mathcal{P}(\sigma_0) = h_t(\sigma_0)$. That means we have to start the analysis with Eq. (3.8.5) for $dt \neq 0$. The SOS is defined by the two conditions $q_2 = 0$ and $H(q, p) = E$. Exploiting this we have

$$\oint_{\partial\sigma_0} H dt = \oint_{\partial\sigma_1} H dt = 0, \quad (3.8.7)$$

giving again

$$\oint_{\partial\sigma_0} p_1 dq_1 = \oint_{\partial\sigma_1} p_1 dq_1, \quad (3.8.8)$$

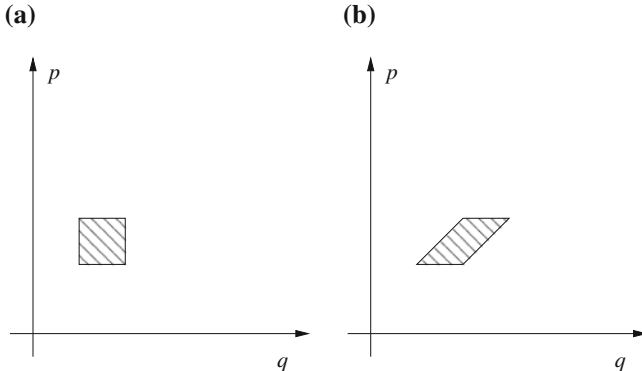


Fig. 3.15 Shearing as an example of an area preserving map: at $t = 0$ (a) and after an iteration of the map (b). Here p is kept constant while q is shifted by an amount linear in p and independent of q

where the two closed curves do *not* have to be at constant time. Formally one may apply Stokes' theorem now, relating the closed line integral with the area enclosed by the line. The result is the invariance of the areas, i.e. $|\sigma_0| = |\sigma_i|$ valid for all sections $i \in \mathbb{N}$, what we wanted to show. In the next section we give some examples of area preserving maps, which can be seen as Poincaré maps of real or fictitious continuous time dynamics.

3.8.3 Area Preserving Maps

One of the simplest examples of an area preserving map is *shearing*. It keeps p constant and shifts q by an amount linear in p and independent of q , see Fig. 3.15.

An important class of area preserving maps that are connected with Hamiltonian systems are *twist maps*. Assume the dynamics of an integrable system with two degrees of freedom that can be solved with action-angle variables (θ, I) . The motion is confined to a two-dimensional torus parametrized by the two angle variables. In general the Hamiltonian flow on the torus reads

$$\theta_1(t) = \omega_1 t + \theta_1(0), \quad (3.8.9)$$

$$\theta_2(t) = \omega_2 t + \theta_2(0), \quad (3.8.10)$$

where $\omega_i = \frac{\partial H(I)}{\partial I_i}$. By $t_2 = \frac{2\pi}{\omega_2}$ we denote the time for $\theta_2(t)$ to complete a circle. Since the SOS is defined by $\theta_2 = q_2 = 0$ this is also the time after which the curve passes through the SOS again. Hence the Poincaré map is given by $\mathcal{P}(\theta_1, I_1) = (\theta_1 + \omega_1 t_2, I_1) = (\theta_1 + 2\pi\alpha, I_1)$, where we have introduced the winding number $\alpha = \frac{\omega_1}{\omega_2}$, see Fig. 3.16.

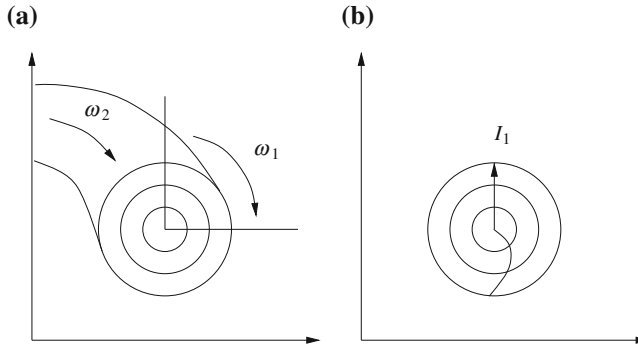


Fig. 3.16 The twist map twists a point on the *circle* (parametrized by θ_1) with radius I_1 . In (a) both directions of the torus are indicated whereas in (b) the Poincaré map of the initially *straight line* (with the *arrow*) is shown as a *curved line* since the winding number depends on the actions in general

Poincaré maps derived from perturbed integrable Hamiltonian systems generally have the form of so-called *twist maps* [21]

$$I_{n+1} = I_n + f(I_{n+1}, \theta_n), \quad (3.8.11)$$

$$\theta_{n+1} = \theta_n + 2\pi\alpha(I_{n+1}) + g(I_{n+1}, \theta_n), \quad (3.8.12)$$

where f and g are smooth functions and α denotes the winding number. An important non-trivial special case is the standard map, which is also called Chirikov–Taylor map. It describes the dynamics in the SOS of the kicked rotor whose Hamiltonian is formally given by Chirikov and Shepelyansky [28]

$$H(\theta, I, t) = \frac{I^2}{2} + K \cos(\theta) \sum_{n=-\infty}^{\infty} \delta(t - n). \quad (3.8.13)$$

It is called rotor because the motion is confined to a circle parametrized by the angle θ with angular momentum I . The iteration has the form

$$I_{n+1} = I_n + K \sin(\theta_n) \mod 2\pi, \quad (3.8.14)$$

$$\theta_{n+1} = \theta_n + I_{n+1} \mod 2\pi. \quad (3.8.15)$$

More details and motivation for the standard map may be found in [21, 25, 29].

The SOS dynamics of this map are shown in Fig. 3.17. For $K = 0$ we see a straight movement of the points on the SOS. In case of $K \neq 0$ the topology changes. At the upper and the lower edge the straight lines have transformed to wavy curves and in the middle circles have emerged. The structure in the middle of Fig. 3.17b is called a *nonlinear resonance island*, compare Sect. 3.7.6.

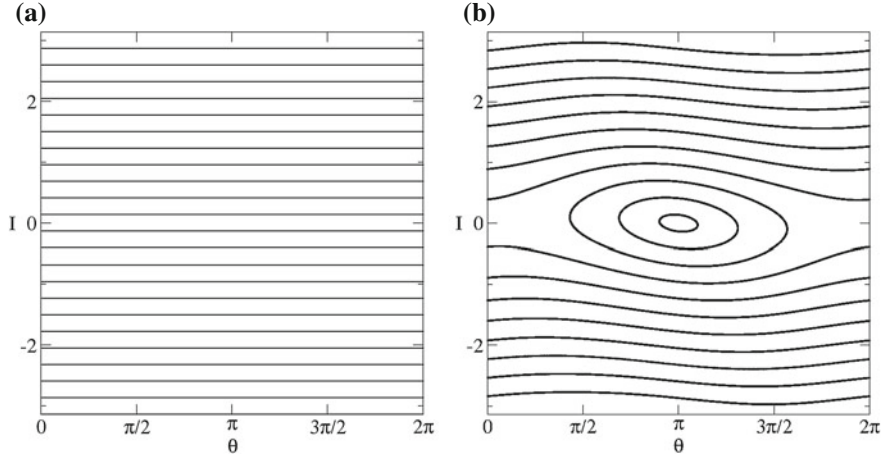


Fig. 3.17 **a** Dynamics of the standard map for $K = 0$. **b** For small $K = 0.2$ the topology changes. The island structure in the middle is called a nonlinear resonance, the straight lines going from $\theta = 0$ to $\theta = 2\pi$ are the stable KAM tori surviving the perturbation characterized by K . The center of the island is a stable/elliptic fixed point of the motion

3.8.4 Fixed Points

A fixed point of the Poincaré map \mathcal{P} is defined by

$$\mathcal{P}(z^*) = z^*, \quad (3.8.16)$$

for $z^* = (q^*, p^*) \in \text{SOS}$. As in the case of the logistic map (Sect. 2.2.1), the fixed point and therewith the dynamics near the fixed point can be characterized by the derivative of the map at the fixed point. This is due to the fact that in a small neighborhood of the fixed point the map can be linearly approximated by

$$\mathcal{P}(z^* + \delta z) = z^* + \underbrace{d\mathcal{P}(z^*) \cdot \delta z}_{\equiv \delta z'} + O(\delta z^2). \quad (3.8.17)$$

Usually $\mathcal{M}(z^*) = d\mathcal{P}(z^*)$ is called monodromy matrix or tangent map. It gives the linear relation between $\delta z'$ and δz

$$\begin{pmatrix} \delta q' \\ \delta p' \end{pmatrix} = \begin{pmatrix} \frac{\partial \mathcal{P}_1}{\partial q}(q^*, p^*) & \frac{\partial \mathcal{P}_1}{\partial p}(q^*, p^*) \\ \frac{\partial \mathcal{P}_2}{\partial q}(q^*, p^*) & \frac{\partial \mathcal{P}_2}{\partial p}(q^*, p^*) \end{pmatrix} \begin{pmatrix} \delta q \\ \delta p \end{pmatrix}. \quad (3.8.18)$$

As an example we compute the monodromy matrix of the standard map. Following the notation of Sect. 3.8.3 we write it as

$$I' = I + K \sin(\theta), \quad (3.8.19)$$

$$\theta' = \theta + I'. \quad (3.8.20)$$

It is convenient to split the map into two maps $\mathcal{P} = \mathcal{P}_2 \circ \mathcal{P}_1$. First we perform the iteration in I and keep θ fixed

$$I' = I + K \sin(\theta), \quad (3.8.21)$$

$$\theta' = \theta. \quad (3.8.22)$$

The resulting monodromy matrix is

$$\mathcal{M}_1 = \begin{pmatrix} \frac{\partial I'}{\partial I} & \frac{\partial I'}{\partial \theta} \\ \frac{\partial \theta'}{\partial I} & \frac{\partial \theta'}{\partial \theta} \end{pmatrix} = \begin{pmatrix} 1 & K \cos(\theta) \\ 0 & 1 \end{pmatrix}. \quad (3.8.23)$$

In the second step we change θ

$$I' = I, \quad (3.8.24)$$

$$\theta' = \theta + I. \quad (3.8.25)$$

The monodromy matrix of \mathcal{P}_2 reads

$$\mathcal{M}_2 = \begin{pmatrix} \frac{\partial I'}{\partial I} & \frac{\partial I'}{\partial \theta} \\ \frac{\partial \theta'}{\partial I} & \frac{\partial \theta'}{\partial \theta} \end{pmatrix} = \begin{pmatrix} 1 & 0 \\ 1 & 1 \end{pmatrix}, \quad (3.8.26)$$

which leads to the overall monodromy matrix

$$\mathcal{M} = \mathcal{M}_2 \circ \mathcal{M}_1 = \begin{pmatrix} 1 & K \cos(\theta) \\ 1 & 1 + K \cos(\theta) \end{pmatrix}. \quad (3.8.27)$$

Since \mathcal{P} is area preserving the determinant of \mathcal{M} equals ± 1 . In fact one can easily see that $\det(\mathcal{M}) = 1$. In Sect. 3.8.2 we have shown that the Poincaré map leaves the integral $\oint_{\partial\sigma_0} pdq$ invariant. This integral measures not only the surface area of σ_0 , but also its orientation, which is preserved as well. We check this property for our example by computing $\det(\mathcal{M}) = \det(\mathcal{M}_2)\det(\mathcal{M}_1) = 1 \cdot 1 = 1$.

After this example we come to the classification of fixed points. In the case of one-dimensional maps, see, e.g., Sect. 2.2.1, there was only one relevant quantity namely the absolute value of the derivative of the map at the fixed point. For two-dimensional maps we have two directions and hence the nature of the fixed point is determined by the eigenvalues of the monodromy matrix. The characteristic equation for the monodromy matrix reads

$$\det(\mathcal{M} - \lambda I) = 0, \quad (3.8.28)$$

which can be written as

$$\lambda^2 - \lambda \operatorname{tr}(\mathcal{M}) + \det(\mathcal{M}) = 0, \quad (3.8.29)$$

where by “tr” we have denoted the trace. Using $\det(\mathcal{M}) = 1$ we find the following simple formula for the eigenvalues of \mathcal{M}

$$\lambda_{1,2} = \frac{1}{2}\operatorname{tr}(\mathcal{M}) \pm \frac{1}{2}\sqrt{\operatorname{tr}(\mathcal{M})^2 - 4}. \quad (3.8.30)$$

Depending on the value of $\operatorname{tr}(\mathcal{M})$ we distinguish three cases:

1. $|\operatorname{tr}(\mathcal{M})| < 2$: The eigenvalues are two complex numbers that can be written as

$$\lambda_1 = e^{i\beta}, \quad \lambda_2 = e^{-i\beta}, \quad (3.8.31)$$

with $0 < \beta < \pi$.

2. $|\operatorname{tr}(\mathcal{M})| > 2$: The eigenvalues are two real numbers whose product equals one:

$$\lambda_1 = \lambda, \quad \lambda_2 = \frac{1}{\lambda}. \quad (3.8.32)$$

3. $|\operatorname{tr}(\mathcal{M})| = 2$: The eigenvalues are $\lambda_1 = \lambda_2 = \pm 1$.

Having the eigenvalues of the monodromy matrix at hand, it is easy to gain an intuition on the dynamics near the fixed point. Therefore, we perform a coordinate transformation to the eigenbasis of \mathcal{M} , which is also called principle axis representation. The linearized Poincaré map then reads

$$\begin{pmatrix} \xi' \\ \eta' \end{pmatrix} = \begin{pmatrix} \xi \\ \eta \end{pmatrix} + \begin{pmatrix} \lambda_1 & 0 \\ 0 & \lambda_2 \end{pmatrix} \begin{pmatrix} \xi \\ \eta \end{pmatrix} + O\left(\begin{pmatrix} \xi \\ \eta \end{pmatrix}^2\right). \quad (3.8.33)$$

In the first case (Eq. (3.8.31)), the special form of the eigenvalues tells us that there is a basis in which \mathcal{M} can be written as a rotation. Using the same β as introduced in Eq. (3.8.31) it is possible to write

$$\mathcal{M} = \begin{pmatrix} \cos(\beta) & -\sin(\beta) \\ \sin(\beta) & \cos(\beta) \end{pmatrix}. \quad (3.8.34)$$

Hence, in the direct neighborhood of z^* the Poincaré map \mathcal{P} behaves like a rotation around the fixed point, see Fig. 3.18a. The dynamics around such a fixed point are stable in the sense that the orbit $\{\mathcal{P}_n(z)\}_{n \in \mathbb{N}}$ remains in the neighborhood of the fixed point z^* for a long time if z lies next to it.

In the second case the monodromy matrix takes the form

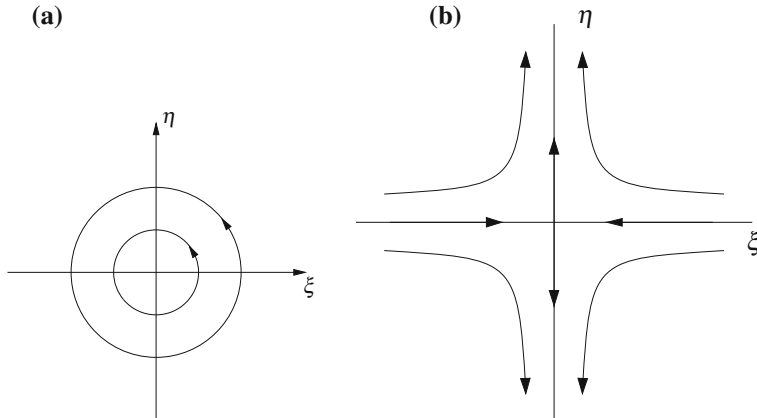


Fig. 3.18 Behavior of the dynamics near an elliptic (a) and an hyperbolic (b) fixed point in normal coordinates (ξ, η) , i.e. after transforming to an appropriate principle axis representation. In the first case, points on a small *concentric circle* around the fixed point are mapped onto points on the same *circle*. In the second case, the invariant geometrical object is a hyperbola

$$\mathcal{M} = \begin{pmatrix} \lambda & 0 \\ 0 & 1/\lambda \end{pmatrix}. \quad (3.8.35)$$

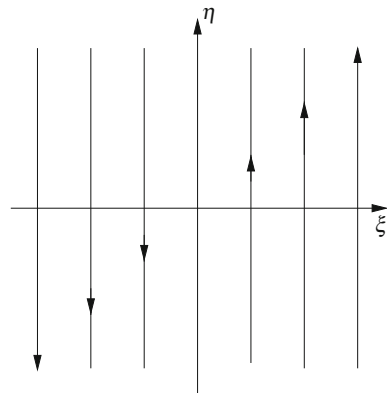
As for the elliptic fixed point there is a geometrical object that stays invariant when the linearized map is applied—a hyperbola, see Fig. 3.18b. If we start with a point on a hyperbola in the neighborhood of z^* and apply the linearized map, we end up on the hyperbola again. For $\lambda < 0$, we additionally jump between the two inversion symmetric branches of the hyperbola with every application of the Poincaré map. When moving along the principle axis, one direction leads to stable dynamics while the other direction leads to unstable dynamics. This is because the absolute value of one eigenvalue is always smaller than one (in this direction the fixed point is attractive) while the absolute value of the other eigenvalue is always larger than one (in this direction the fixed point is repulsive). In case of the elliptic fixed point the winding number, defined by $\alpha = \frac{\beta}{2\pi}$, is a measure how fast points on a circle around the fixed point rotate when \mathcal{M} acts on them. Analogously to the winding number one defines the Lyapunov exponent for the hyperbolic fixed point, see also Sect. 2.2.2, by

$$\sigma \equiv \ln \lambda. \quad (3.8.36)$$

The Lyapunov exponent and its connection to the stability of trajectories will be discussed in detail in Sect. 3.9.2.

The third case ($\lambda_1 = \lambda_2 = \pm 1$) is special in the sense that it marks the transition between the stable and the unstable case. Such a fixed point is called parabolic, and it is said to be marginally stable. The monodromy matrix can be written as ($\lambda_1 = 1$)

Fig. 3.19 A parabolic fixed point leads to shearing



$$\mathcal{M} = \begin{pmatrix} 1 & 0 \\ c & 1 \end{pmatrix} \quad (3.8.37)$$

with a real constant c . The invariant curves of this map describe a shearing along a straight line with constant q , see Fig. 3.19. In case of $q = 0$ the q -axis is a line of fixed points. If the eigenvalue equals -1 then the map additionally flips the sign of q .

3.8.5 Poincaré–Birkhoff Theorem

In Sect. 3.7.4 we have introduced the KAM theorem which assures the existence of invariant tori with irrational frequency ratios and therewith the stability of conditionally periodic phase space trajectories under small perturbations. Here we treat the tori and phase space curves for which the KAM theorem is not applicable. This section is about the fate of tori with rational frequency ratios, in other words curves with rational winding number, when a small perturbation is added to the Hamiltonian. The presentation qualitatively follows [20].

To keep things simple we assume a conservative Hamiltonian system with two degrees of freedom and apply the surface of section technique. The Hamiltonian function is given by an integrable part that is assumed to be solved by action-angle variables $(I_1, I_2, \theta_1, \theta_2)$ plus a small perturbation

$$H(I_1, I_2, \theta_1, \theta_2) = H_0(I_1, I_2) + \varepsilon H_1(I_1, I_2, \theta_1, \theta_2). \quad (3.8.38)$$

The unperturbed motion governed by H_0 is constrained to a two-dimensional torus in the four-dimensional phase space. The corresponding Poincaré map is a twist map (see Sect. 3.8.3) and reads

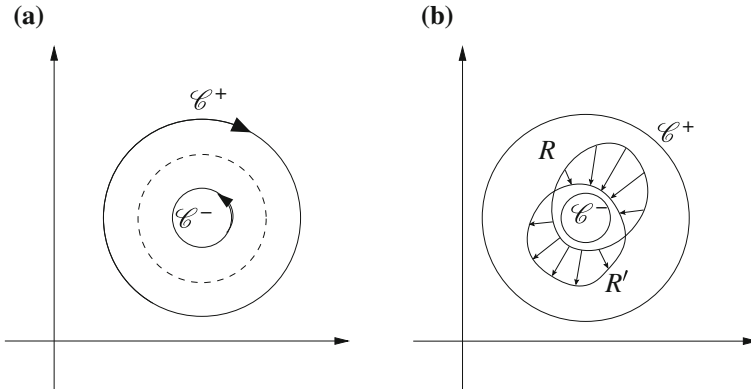


Fig. 3.20 **a** We see the dynamics of the unperturbed system. The curve \mathcal{C} (dashed line) has a rational winding number $\alpha = \frac{r}{n}$. The two neighboring curves \mathcal{C}^- and \mathcal{C}^+ have an irrational winding number and rotate anticlockwise and clockwise with respect to \mathcal{C} when \mathcal{P}_n is applied. **b** In the perturbed system \mathcal{C} is destroyed while the other two curves are distorted only a little. The curves R and $R' = \mathcal{P}_n^\varepsilon R$ can be used to analyze the fixed point structure of $\mathcal{P}_n^\varepsilon$

$$\theta'_1 = \theta_1 + 2\pi\alpha(I'_1), \quad (3.8.39)$$

$$I'_1 = I_1, \quad (3.8.40)$$

where the primes indicate the iterated variables and $\alpha = \frac{\omega_1}{\omega_2}$ is the winding number.¹³ The KAM theorem tells us that for a sufficiently small perturbation εH_1 the phase space curves with irrational winding number α are only slightly perturbed as long as the non-degeneracy condition from Eq. (3.7.33) is satisfied. We are now going to show how a phase space trajectory with a rational winding number behaves when the perturbation is switched on.

Let $\mathcal{C} \in \text{SOS}$ be a circle that is invariant under the application of the Poincaré map \mathcal{P} of the unperturbed system, i.e. $\mathcal{P}(\mathcal{C}) = \mathcal{C}$. In the following we are going to call such curves *invariant curves*. Additionally, we assume that the dynamics of the points on \mathcal{C} are described by a rational winding number

$$\alpha(I_1) = \frac{r}{n}, \quad r, n \text{ coprime integers.} \quad (3.8.41)$$

By construction all points on \mathcal{C} are fixed points of the n times iterated Poincaré map \mathcal{P}_n . Now let us assume that the winding number α depends smoothly on I_1 . Then there exist two curves \mathcal{C}^+ and \mathcal{C}^- with irrational winding numbers in a small neighborhood of \mathcal{C} which lie on either side of it, see Fig. 3.20a. When we also assume that $\alpha(I_1)$ is decreasing smoothly with I_1 then, relative to \mathcal{C} , \mathcal{C}^+ rotates clockwise and \mathcal{C}^- rotates anticlockwise when \mathcal{P}_n is applied.

¹³ The winding number α depends via the frequencies on both actions I_1 and I_2 but we skip the dependence on I_2 in the following since I_2 is fixed for the Poincaré map, c.f. Eq. (3.8.1).

Next we consider the perturbed system with Poincaré map \mathcal{P}^e . Since \mathcal{C} has a rational winding number it is already destroyed for weak perturbations, whereas the nearby curves \mathcal{C}^+ and \mathcal{C}^- are only slightly distorted since their winding number is irrational. By definition the distorted curves are invariant curves of \mathcal{P}^e . Additionally, for sufficiently small perturbations their relative twist is preserved under the application of \mathcal{P}_n^e . Because of this relative twist there must be one point between them for each radius whose angle is conserved when \mathcal{P}_n^e is applied. The union of these points also forms a curve which we denote by R . Because of the angle preservation property of the points of R , any fixed point z^* of \mathcal{P}_n^e will lie on R . Hence, if we define the curve $R' = \mathcal{P}_n^e R$ the set of fixed points of \mathcal{P}_n^e is given by $F(\mathcal{P}_n^e) = R \cap R'$, see Fig. 3.20b. Simple geometry tells us that if there are no tangent points of R and R' the fixed points always come in pairs (“what goes in has to come out”—a closed curve that enters another closed curve has to leave it at another point). This result is called the **Poincaré–Birkhoff theorem**: For any curve \mathcal{C} of an unperturbed system with rational winding number $\alpha = \frac{r}{n}$ and r, n coprime (whose points are all fixed points of \mathcal{P}_n), there will remain only an even number of fixed points $2kn$ ($k = 1, 2, 3, \dots$) under perturbation (that means fixed points of the map \mathcal{P}_n^e).

The exact number of $2kn$ fixed points can be explained as follows. We already mentioned that there are in general $2k$ intersections of the curves R and R' . Each of these intersections leads to a fixed point of order n . But as we have shown in Sect. 2.2.1 for one-dimensional maps (around Eq. 2.2.8) there are always n fixed points of order n and hence $2kn$ fixed points overall.

Following the flow lines (coming from the action of \mathcal{P}_n^e) near the fixed point it is easy to distinguish between an elliptic and a hyperbolic fixed point, see Fig. 3.21a. The property whether a fixed point is elliptic or hyperbolic alternates from fixed point to fixed point. Hence in the perturbed system we have kn stable and kn unstable fixed points. Around the stable ones there are again invariant curves (see, Fig. 3.21b) which we treat in the same way as the original curves. A successive application of the KAM theorem and the Poincaré–Birkhoff theorem therefore results in a self-similar fixed point structure which is becoming more and more complicated with increasing perturbation. After having understood the behavior of the dynamics in the neighborhood of a resonant trajectory we characterize the motion near unstable fixed points in more detail. We will see the theorem of Poincaré and Birkhoff at work in the following subsections when discussing the seeds of chaotic motion.

3.8.6 Dynamics Near Unstable Fixed Points

As we have seen in Sect. 3.8.4 stable (elliptic) fixed points locally lead to invariant curves in the SOS that have the shape of circles centered around the fixed point. This structure can be compared with the phase space of the pendulum, see Fig. 3.1, and hence the dynamics near such fixed points are small oscillations. The dynamical behavior near unstable (hyperbolic) fixed points is more complicated. In Sect. 3.8.4 we learned that the monodromy matrix \mathcal{M} at an unstable fixed point has two eigen-

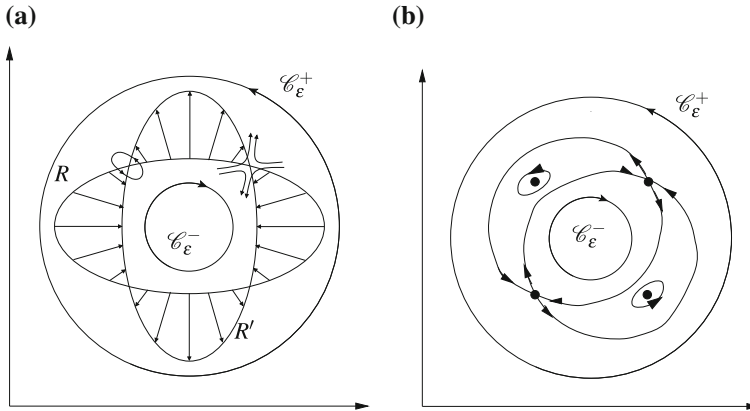


Fig. 3.21 **a** To distinguish between elliptic and hyperbolic fixed points the flow-lines (coming from the action of $\mathcal{P}_n^\varepsilon$) near the fixed point are analyzed. The fixed points are found to alternate between being elliptic and hyperbolic. **b** Around an elliptic (stable) fixed point the trajectories oscillate, whilst they diverge away from a hyperbolic (unstable) fixed point. Convergence is only obtained when the stable manifold is hit exactly, c.f. Sect. 3.8.6

values which read

$$\lambda_- = \lambda, \quad \lambda_+ = \frac{1}{\lambda}, \quad (3.8.42)$$

where without loss of generality we assume $|\lambda| > 1$. Therefore, the eigenvector v_+ belonging to λ_+ indicates the directions $(\pm v_+)$ for which the fixed point acts attractively while $\pm v_-$ gives the directions for which the fixed point acts repulsively. In general, a hyperbolic fixed point can be characterized by two invariant curves which are the stable (or ingoing) manifold V_+ and the unstable (or outgoing) manifold V_- defined by

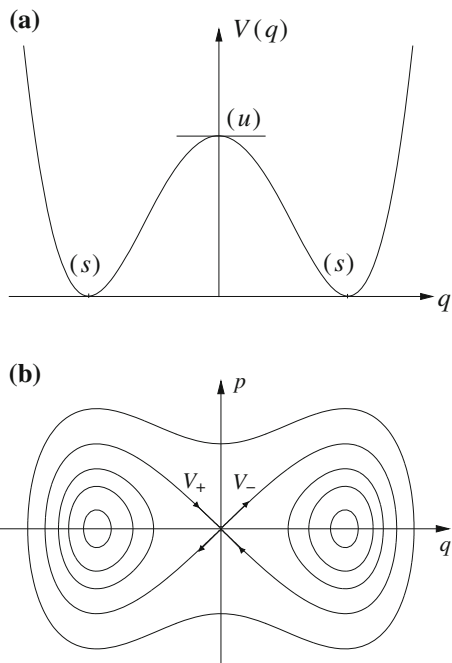
$$V_\pm \equiv \left\{ z \in \text{SOS} \mid \lim_{n \rightarrow \pm\infty} \mathcal{P}_n(z) = z^* \right\}. \quad (3.8.43)$$

Negative n means that we iterate backwards in time. As before, z^* denotes the fixed point. The same definition is used to examine the continuous dynamics $h_t(z)$ in the whole phase space Ω . One just has to replace $z \in \text{SOS}$ by $z \in \Omega$ and $\lim_{n \rightarrow \pm\infty} \mathcal{P}_n(z)$ by $\lim_{t \rightarrow \pm\infty} h_t(z)$. Of course, in this case there can be more than two directions (phase space dimensions). In order to illustrate the definition, two examples of integrable systems are discussed.

1. *Double Well:* The first example is the dynamics of a point particle with mass $m = 1$ in a double well potential given by the Hamiltonian function

$$H = \frac{p^2}{2} + (q^2 - 1)^2. \quad (3.8.44)$$

Fig. 3.22 **a** The double well potential with the two minima (s) and the unstable maximum (u). **b** The stable and the unstable manifold V_+ and V_- coincide and form the separatrix



The system has three fixed points from which two are stable and one is unstable, see Fig. 3.22. The two stable fixed points correspond to the two minima (s) of the potential in configuration space, while the unstable fixed point corresponds to the maximum (i). For all fixed points $p = 0$ holds. In our example, the stable and the unstable manifolds V_+ and V_- coincide and form a separatrix between the two types of motion.

2. *Pendulum:* As a second example we treat the pendulum in a (scaled) gravity field described by the Hamiltonian

$$H = \frac{p^2}{2} - \cos(q). \quad (3.8.45)$$

Due to the periodicity in q , the system has an infinite number of stable and unstable fixed points corresponding to the maxima and the minima of the potential, see Fig. 3.23. Here the unstable manifold of the fixed point located at point $q = \frac{(2n+1)\pi}{2}$ equals the stable manifold of the neighboring fixed point with $q' = \frac{(2(n\pm 1)+1)\pi}{2}$. The phenomenon that V_+ and V_- form a separatrix is not just present for the particle in the double well potential and for the pendulum, but it is a general phenomenon for integrable systems.

The two examples have special features because both are integrable systems. The separatrix is highly unstable with respect to non-integrable perturbations. Hence,

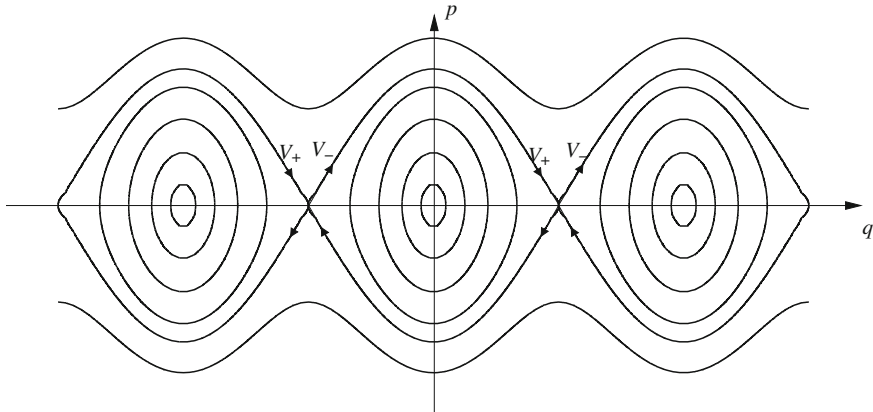


Fig. 3.23 Phase space of the pendulum including stable (V_+) and unstable (V_-) manifolds. The unstable manifold of each fixed point equals the stable manifolds of its two neighboring fixed points

for non-integrable systems the smooth joining or the equality of stable and unstable manifolds is not possible [20, 30]. Even though the generic situation is far more complicated, there are some rules that need to be obeyed. It is, for example not possible that V_+ or V_- intersect with themselves, yet V_\pm may intersect with V_\mp . When the stable and the unstable manifolds from the same fixed point or from fixed points of the same family¹⁴ intersect, we call them *homoclinic points*. If this is not the case and the intersecting manifolds originate from different fixed points, or fixed points of different families, the intersections are called *heteroclinic points*.

By definition V_\pm are invariant curves, that means $\mathcal{P}(V_\pm) = V_\pm$. Using this property, it is easy to show that if $z \in \text{SOS}$ is a homoclinic point then $\mathcal{P}_n(z)$, $n \in \mathbb{N}$ is a homoclinic point as well. Additionally, we have $z \in V_\pm$ which means that $\lim_{n \rightarrow \pm\infty} \mathcal{P}_n(z) = z^*$. From this we conclude that either $z = z^*$ or $\{\mathcal{P}_n(z)\}_{n \in \mathbb{N}}$ is a sequence of homoclinic points with accumulation point z^* . Let us assume the situation shown in Fig. 3.24a where $z \neq z^*$. We see a hyperbolic fixed point z^* and its stable and unstable manifold V_+ and V_- which intersect at the homoclinic point z . We also see two points $z' \in V_+$ and $z'' \in V_-$ slightly behind z (with respect to the direction indicated by the application of \mathcal{P}). Because \mathcal{P} is pushing every point on V_\pm in a well defined direction, it preserves the order of the points $\mathcal{P}(z)$, $\mathcal{P}(z')$ and $\mathcal{P}(z'')$. The only possible way to keep this order and to take care of $\mathcal{P}(z)$ being a homoclinic point is by constructing a loop, see Fig. 3.24b. Since the enclosed areas of the loops are mapped onto each other they must be the same because of area preservation. It is clear that the distance between the homoclinic points decreases as we come closer to z^* . Therefore, the curve has to extend much more in the direction perpendicular to V_+ in order to preserve the area. This behavior is shown in Fig. 3.24c.

¹⁴ If the map \mathcal{P}_n has a fixed point z^* there will always be $n - 1$ other fixed points of \mathcal{P}_n given by $\mathcal{P}_i(z^*)$ ($i = 1, \dots, n - 1$), see Sect. 2.2.1. We say these fixed points belong to the same family.

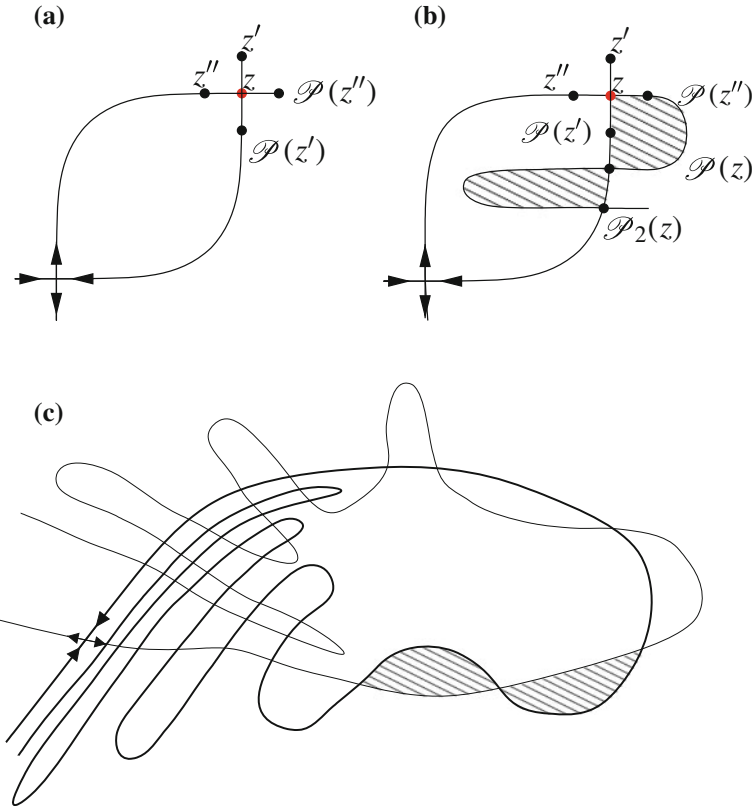
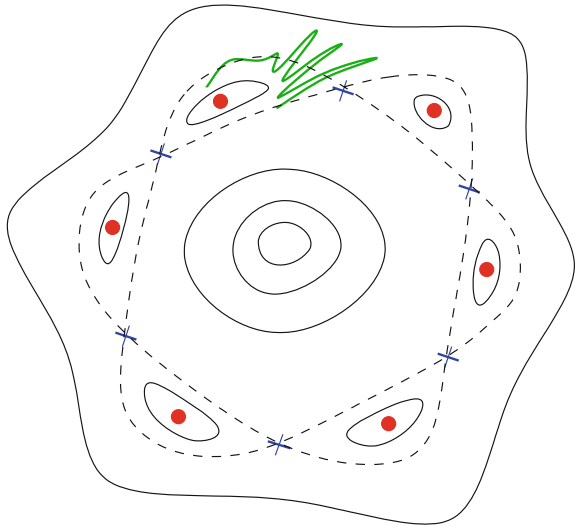


Fig. 3.24 If z is a homoclinic point then $\mathcal{P}(z)$ is a homoclinic point, too. **a** shows a homoclinic point z and nearby points z' and z'' on the stable and unstable manifold, respectively. The manifolds V_+ and V_- have to intersect again at $\mathcal{P}(z)$ and additionally, the order of the points $\mathcal{P}(z')$ and $\mathcal{P}(z'')$ relative to $\mathcal{P}(z)$ needs to be preserved. This can be achieved with a loop (**b**). Because the Poincaré map is area preserving the enclosed areas need to be the same. Iterating this procedure one obtains more complex pictures (**c**)

The result is a highly complicated structure of infinitely many homoclinic points and enclosed areas.

Another way to examine chaotic dynamics is the propagation of a whole line element. Here, each point of the line element corresponds to a single initial condition. In many cases this method is more appropriate because it is easier to compute the propagation of many initial conditions than to compute the stable and the unstable manifold of a fixed point. Starting with such a line element in the neighborhood of a fixed point one finds two different structures depending on whether the fixed point is stable (elliptic) or unstable (hyperbolic). Since in the first case the Poincaré map is a twist map (Sect. 3.8.4) the line element forms a tightly curling structure looking like a *whorl*. In the case of a hyperbolic fixed point, the line element stretches exponentially

Fig. 3.25 Phase space structure with elliptic (red dots) and hyperbolic (blue crosses) fixed points. Due to the Poincaré–Birkhoff theorem the fixed points always come in pairs. Additionally, we see a typical structure that arises when a line element is propagated close to a hyperbolic fixed point—a tendril (green thick structure)



fast and flails backwards and forwards. The resulting structures have been termed a *tendril*, see Fig. 3.25. More pictures of whorls and tendrils can be found in [20, 30].

The Poincaré–Birkhoff theorem assures the existence of a hierarchy of stable and unstable fixed points at all scales where all the unstable fixed points lead to chaotic structures of the just mentioned form. Therefore, chaotic motion is present in a self-similar manner on all scales of the system. This behavior and what happens for even larger perturbations is summarized in the next subsection.

3.8.7 Mixed Regular-Chaotic Phase Space

In the previous two subsections the formation of chaos in nearly integrable systems was discussed. We have shown that hierarchies of stable and unstable fixed points and therefore of chaotic structures arise near resonant unperturbed orbits. In the neighborhood of hyperbolic fixed points phase space trajectories show a strange behavior and form tendrils. When regular structures (invariant curves) gradually disappear, chaotic structures (stochastically distributed looking points in the SOS) appear, and in some parameter regime both structures coexist. In this subsection we give a brief account of the transition from regular to chaotic dynamics. Formal criteria and concepts for the classification of chaotic motion are then introduced in the next section.

We assume a physical system governed by the Hamiltonian function

$$H(q, p) = H_0(q, p) + \varepsilon H_1(q, p), \quad (3.8.46)$$

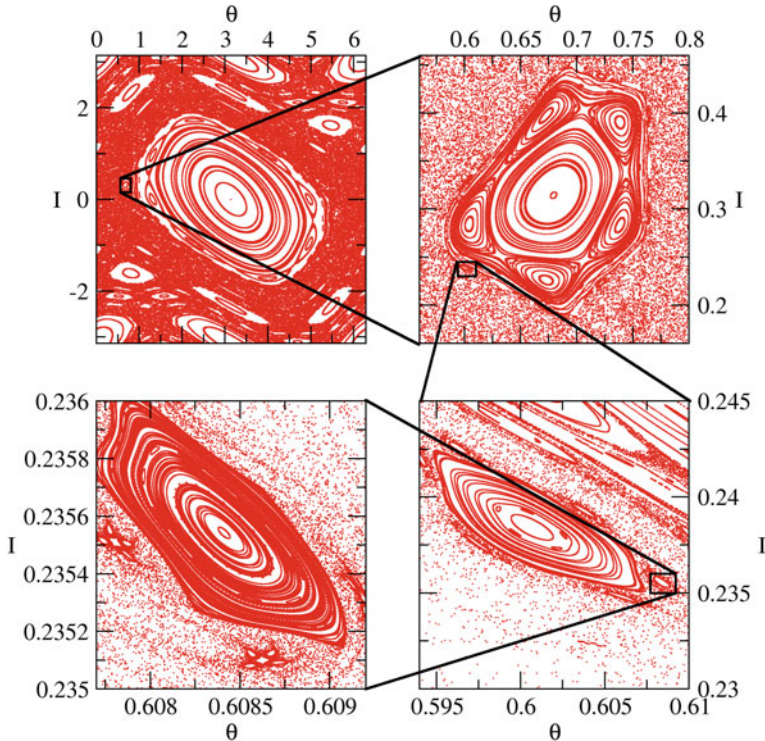


Fig. 3.26 SOS of the standard map (Sect. 3.8.4) for $K = 1$. Regular structures can be found even on very small scales

where H_0 is assumed to be integrable and H_1 is a non-integrable perturbation, whose strength is given by ε (in other words H_0 and H_1 have approximately the same magnitude). Depending on ε several regimes can be distinguished. We partly illustrate the corresponding change of phase space by the standard map.

1. $\varepsilon \rightarrow 0$: In this limit the KAM theorem (Sect. 3.7.4) is applicable and one finds quasi-regular dynamics which are similar to the one given by H_0 . The phase space mostly consists of invariant tori. The union of all destroyed tori has a measure of order ε .
2. ε small: We are in the regime that is described by the Poincaré-Birkhoff theorem (Sect. 3.8.5). Close to tori with rational winding number, chains of hyperbolic fixed points become visible. These fixed points lead to chaotic structures (Sect. 3.8.6).
3. ε intermediate: The chaotic layers grow, merge and macroscopic chaotic structures form. Curves with a highly irrational winding number (Sect. 3.7.4) encircle islands of regularity in the chaotic sea. The phase space is now dominated by self-similar structures, see Fig. 3.26.

4. ε large: In case of very strong perturbations even the islands of regular structures become smaller and smaller as the dynamics become more and more unstable there. A phenomenon that can be observed is the bifurcation of stable fixed points—a stable fixed point transforms into two stable and an unstable fixed point, see Fig. 3.27, just what happens at the period doubling transition of the logistic map (see Fig. 2.3).
5. $\varepsilon \rightarrow \infty$: In numerical calculations no regular structures are visible anymore. Nevertheless, there may be such structures on very small scales. In general there is no guarantee for global chaos in the sense that all (fixed) points have become unstable.

3.8.7.1 The Hénon and Heiles Problem

As a preparation for Sect. 3.9 and as an additional example for the discussed mechanisms, we introduce the Hénon and Heiles model. It was proposed by Hénon and Heiles as a simplified model for the motion of a star in a gravity field [31] and is defined by the Hamiltonian function

$$H = \frac{1}{2} (p_x^2 + p_y^2) + \frac{1}{2} (x^2 + y^2) + x^2 y - \frac{y^3}{3}. \quad (3.8.47)$$

The third term of the Hamiltonian couples the motion in the x and the y direction and the last term introduce a nonlinear force. The only conserved quantity is the energy E . Hence, the solutions lie on a three-dimensional energy surface in the four-dimensional phase space. We restrict ourselves to situations where $E < 1/6$, since in this case the motion remains bounded. In order to visualize the dynamics the surface of section technique (Sect. 3.8.2) is used.

Numerical results of the dynamics of the Hénon and Heiles System are shown in Fig. 3.28. For low energies (Fig. 3.28a, $E = 0.01$) the potential $U(x, y) = \frac{1}{2} (x^2 + y^2) + x^2 y - \frac{y^3}{3}$ is nearly rotationally symmetric, the angular momentum is approximately conserved and the system is therefore quasi-integrable. With increasing energy (Fig. 3.28b, $E = 0.045$) the phase space trajectories explore regions where the potential is no longer rotationally symmetric. Nevertheless, there are still mostly invariant curves. Even Fig. 3.28c ($E = 0.08$) still looks regular on a macroscopic scale, but when zooming in (Fig. 3.28f) we see how chaotic structures have developed in the neighborhood of the separatrix. For $E = 0.115$ (Fig. 3.28d) the phase space shows regular and macroscopic chaotic structures of similar size. If the energy is increased further ($E = 0.15$), the system becomes almost completely chaotic and we have the impression to see mostly stochastically distributed points, see Fig. 3.28e.

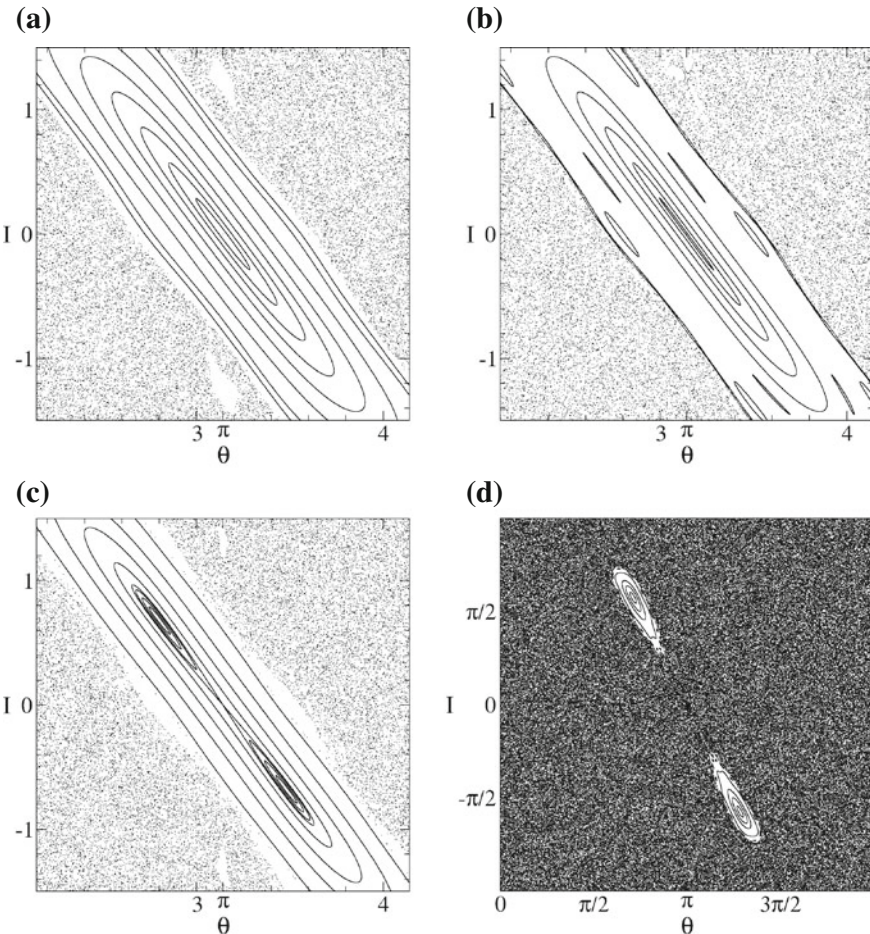


Fig. 3.27 Part of the SOS of the standard map (Sect. 3.8.4) for different kicking strengths K . When K is increased the main (stable) fixed point bifurcates (**a–d**). First it stretches (**a–b**), afterwards a double island structure is developed via a pitchfork bifurcation of the previously stable fixed point (**c–d**). For very strong kicking strengths the two islands (stable fixed points) drift apart (**d**) and finally disappear for $K \rightarrow \infty$

3.9 Criteria for Local and Global Chaos

In Sect. 3.4 we have defined integrable systems. For such systems the phase space consists of invariant tori. The phase space trajectories lie on the tori and the motion is conditionally periodic in most cases. Hence, we know how regular phase space structures look like and we have tools at hand, such as the criterion for integrability and the KAM theorem, to quantify regular structures. Additionally, the Poincaré-Birkhoff theorem tells us how these structures are destroyed when a non-integrable

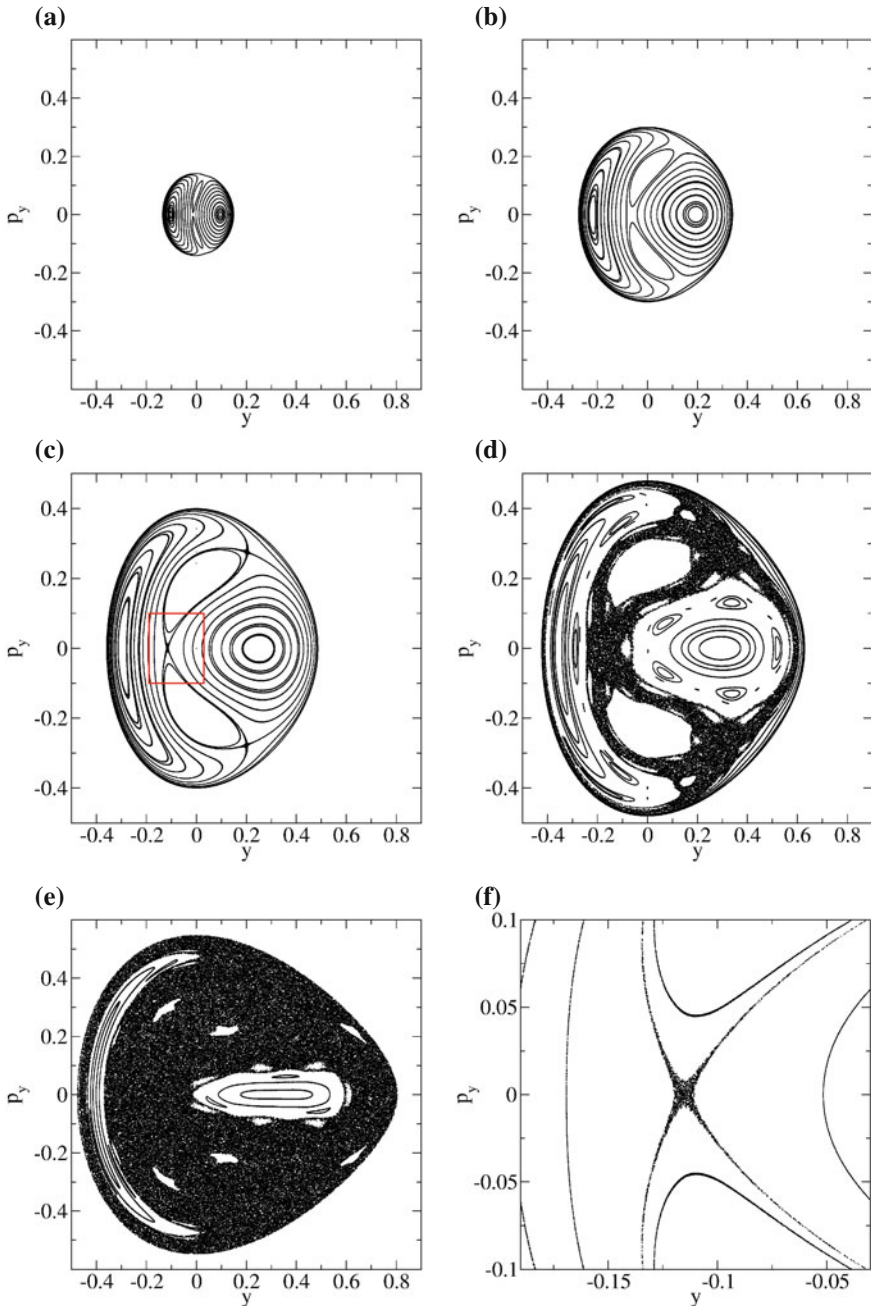


Fig. 3.28 Surfaces of sections for the Hénon and Heiles System for different energies E (a–e). f shows the details inside the *red square* of (c). We note that chaotic structures grow fast around unstable fixed points, whilst the surroundings of stable fixed points are largely preserved

perturbation is added to the Hamiltonian. What we do not have yet, are criteria for local or global chaos when the perturbation is not small any more. In this section, we close this gap and present a number of techniques that have been developed to characterize chaotic motion. Some of these methods are more stringent than others, and not all of them are easy to apply in practice. We note that there is a great interest in such criteria since widespread chaos enhances transport processes, and a knowledge of the stability properties can be used to engineer transport in phase space.

First we present two strong criteria:

- *Lyapunov exponents* > 0 : The idea behind this criterion is that in the chaotic regime the distance between two trajectories belonging to nearby initial conditions increases exponentially with time. We are going to treat Lyapunov exponents in detail in Sects. 3.9.2 and 3.9.3.
- *Kolmogorov–Sinai entropy* > 0 : The Kolmogorov–Sinai entropy is a concept that is defined via the deformation of sets in phase space under time evolution. Similar to the Lyapunov exponents it makes use of the fact that the distance of nearby trajectories increases exponentially in the chaotic regime. Therefore it is no great surprise that it can be expressed as a sum over averaged Lyapunov exponents, see Sect. 3.9.5. If the Kolmogorov–Sinai entropy is larger than zero, the system has the mixing property (Sect. 3.9.1), from which it then follows that it is ergodic.

The criteria mentioned above are strong but often difficult to prove or even to compute for a given system. Many more chaos criteria exist though. We mention just a small selection of weaker criteria which work in some cases and may not work so well in others. The following criteria are quite intuitive:

- *Resonance overlap criterion*: The resonance overlap criterion exploits the fact that when different resonances overlap there can be no KAM tori in between them anymore, see Sect. 3.9.6. The perturbation strength for which this happens is used as an approximate definition for the onset of global chaos. Lacking a strict justification and becoming computationally very demanding in its refined versions [21] the overlap criterion is mostly used to give rough estimates.
- *Decay of correlations*: The behavior of long-time correlations is a measure for the stability of a trajectory. One example for such a correlation is the autocorrelation function defined by

$$C(\tau) = \lim_{T \rightarrow \infty} \frac{1}{T} \int_{-T/2}^{T/2} f(t + \tau) f(t) dt \quad (3.9.1)$$

for any dynamical quantity f . Often C is averaged over the phase space to become a global instead of a local measure. Whether a system is chaotic or not manifests itself in the decay of the correlation with time [21]. Typically, chaotic systems show a fast correlation decay, while regular and mixed ones lead to a slower decay, possibly garnished by regular recurrences from orbits within a resonance

island. More information and rigorous statements for hyperbolic systems may be found in [32].

- *Power spectrum:* The power spectrum of a dynamical quantity f is defined by

$$S(\omega) = \left| \lim_{T \rightarrow \infty} \frac{1}{T} \int_{-T/2}^{T/2} f(t) e^{-i\omega t} dt \right|^2. \quad (3.9.2)$$

It is connected with the autocorrelation function via the Wiener-Khinchin theorem [32, 33]. As discussed in [20, 32, 33], the power spectrum consists of single lines for regular systems, whilst one expects a broad distribution of frequencies for chaotic ones.

- *Strong exchange of energy between the degrees of freedom:* A strong energy exchange between different degrees of freedom can be an indicator for chaotic motion. This happens, for instance, in the double pendulum moving in a plane, see e.g. [34, 35].

3.9.1 Ergodicity and Mixing

In this section we introduce two concepts to characterize the behavior of dynamical systems—ergodicity and mixing. Ergodicity is a concept that is of great importance in statistical physics, but should be well distinguished from chaotic motion. It is a necessary condition for chaos but even integrable systems can be ergodic. The property of mixing is stronger and a nearly sufficient condition for the existence of chaos. For further information on these topics consult [9, 23, 32].

We assume a dynamical system defined in Sect. 2.1 with phase space Ω and time evolution T . The dynamics may be discrete or continuous but we assume that T is invertible. Possible applications are the continuous dynamics of a Hamiltonian system ($T^t = h_t$) or the discrete dynamics in a SOS governed by the Poincaré map ($T^n = \mathcal{P}_n$). We also assume a measure¹⁵ ν for which $\nu(\Omega) = 1$ holds and that is invariant under the time evolution. This means that for all measurable sets $A \subseteq \Omega$ we have

$$\nu(T^t(A)) = \nu(A). \quad (3.9.3)$$

Using these definitions we introduce the notion of an ergodic system:

Definition (Ergodicity): A dynamical system is called ergodic if for all T^t invariant sets $A \subseteq \Omega$ one has either $\nu(A) = 0$ or $\nu(A) = 1$. The set A is called T^t invariant if $T^t(A) = A$.

From a physical point of view this tells us that in ergodic systems there are no other sets of non-zero measure that are invariant under time evolution than the whole

¹⁵ For a short introduction to measures theory consult, e.g., Lieb and Loss [36].

phase space Ω . If a dynamical system is ergodic it is possible to interchange time averages and ensemble averages. Let us express this with formulas. We assume a function $f \in \mathcal{L}^1(\Omega, \nu)$ with values in \mathbb{R} . Then for almost every (with respect to ν)¹⁶ $\omega \in \Omega$ the function $\bar{f}(\omega) = \lim_{t \rightarrow \infty} \frac{1}{t} \sum_{n=0}^{t-1} f(T^n(\omega))$ exists and the relation

$$\bar{f} = \int_{\Omega} f \, d\nu \quad (3.9.4)$$

holds. Since the right hand side of Eq. (3.9.4) does not depend on an initial condition the same has to be true for \bar{f} . Hence the time-average does not depend on the choice of ω . This is only possible if the (forward) orbit $\{T^t(\omega)\}_{t \geq 0}$ in some sense fills the whole phase space. We have defined \bar{f} for a discrete dynamical system. In the continuous case the sums are replaced by integrals. In case of a Hamiltonian system the definition reads $\bar{f} = \lim_{t \rightarrow \infty} \frac{1}{t} \int_0^t f(q(t'), p(t')) \, dt'$. As invariant measure one usually chooses the Lebesgue measure μ and hence the phase space average of f reads $\frac{1}{\mu(\Omega)} \int_{\Omega} f(q, p) \, d\mu(q, p) = \frac{1}{|\Omega|} \int_{\Omega} f(q, p) \, dqdp$, where $|\Omega| = \int_{\Omega} dqdp$. The property that the time average equals the ensemble average can also be used to define ergodicity.

Ergodicity obviously does not imply chaotic motion. Assume, for example, an integrable system that is solved by action-angle variables. If the frequencies ω_i are not rationally related the motion is conditionally periodic and explores the whole torus¹⁷ defined by the action variables I_i . Therefore, such a system with more than one degree of freedom is ergodic on the torus, which defines the allowed phase space (energy surface) (see Sect. 3.4). The concept of ergodicity is of great importance in statistical mechanics where the ergodic-hypothesis (hypothetical equality of time and ensemble average) is used to derive, e.g., the micro-canonical ensemble [37].

A first and important result of ergodic theory is the famous *recurrence theorem* by Poincaré [9]. It is valid for Hamiltonian flows in a finite phase space Ω , and says:

Poincaré recurrence theorem: Let $A \subseteq \Omega$ be a measurable subset. Then the set

$$S = \{a \in A \mid \exists t' : \forall t > t', T^t(a) \in A^c\} \quad (3.9.5)$$

has measure zero, i.e. $\nu(S) = 0$. By A^c we denote the complement of A .

The theorem tells us that every point $\omega \in \Omega$ (except for a set of points whose union has measure zero) will come arbitrarily close to itself again when it is propagated in time. This phenomenon is called *Poincaré recurrence*.

Let us come to the definition of mixing which is a stronger property than ergodicity. It can be shown that a mixing system is ergodic but ergodicity does not necessarily imply mixing. The idea for the definition comes from everyday life. Assume we have a cocktail shaker with initially 20 % rum and 80 % coke (the example is taken from Lichtenberg and Lieberman [21]). At $t = 0$ the two fluids are not well mixed because

¹⁶ For almost every $\omega \in \Omega$ means for all ω except a set of measure zero.

¹⁷ To be more precise the points of the trajectory $z(t)$ are dense on the torus [6].

we have just put them together. When stirring the shaker for some time the rum and the coke will be well mixed and every volume of the resulting fluid will contain approximately 20 % rum. More mathematically thinking, we could say that if we stir the shaker infinitely often, there is reasonable hope that in a dynamical system modeling the physical situation of the shaker this will be true for any arbitrarily small volume.

Definition (Mixing) A measure preserving dynamical system is said to be (strongly) mixing if for any two measurable sets $A, B \subseteq \Omega$ one has

$$\lim_{t \rightarrow \infty} \nu(A \cap T^t(B)) = \nu(A)\nu(B). \quad (3.9.6)$$

To understand the definition we come back to the example with the shaker. Let A be the region in phase space that is originally occupied by rum ($\nu(A) = 0.2$) and let B be the region originally occupied by coke ($\nu(B) = 0.8$). Then the fraction p_r of rum in the region initially filled with coke after an infinite time of stirring is given by

$$p_r = \frac{\lim_{t \rightarrow \infty} \nu(A \cap T^t(B))}{\nu(B)}. \quad (3.9.7)$$

If the system is mixed we have $p_r = 0.2$, and hence $p_r = \nu(A)$.

Bearing this physical picture in mind, it is reasonable that mixing implies ergodicity. Why the other direction does not hold can be seen for the example used above. Assume an integrable Hamiltonian system whose motion is confined to a two-dimensional torus with frequencies that are not rationally related. The motion on the torus is diffeomorphic to the motion on a square with periodic boundary conditions. Assume now the time evolution of two little squares inside the large square. Because of the simple structure of the time evolution the squares do not intersect or change their shape. This is because each point in the original square is propagated with a constant velocity vector. Hence, the system does not have the property of mixing although it is ergodic.

We mention that there is another possible way to define mixing that finds application in the mathematical theory of dynamical systems. Let $f(T^t(\omega))$ be a time-dependent and square-integrable observable of our system with $f \in \mathcal{L}^2(\Omega, \nu)$. One may define an operator \hat{U} (called Koopman operator) by $\hat{U}f(\omega) = f(T\omega)$. One can show that if the system is mixing the Koopman operator \hat{U} has a purely continuous spectrum [23, 32]. The Koopman operator (and its adjoint/inverse) can be seen as classical analogue of the quantum evolution operator (see also the Appendix of Chap. 4).

In contrast to ergodicity, mixing is a necessary and a nearly sufficient criterion for global chaos (complete hyperbolicity) [23] in the whole phase space or in a subset of it. As an example for a system that has the property of mixing we give Arnold's cat map [21]. Let Ω be the unit square. The time evolution is given by the map

$$\begin{pmatrix} x' \\ y' \end{pmatrix} = \underbrace{\begin{pmatrix} 1 & 1 \\ 1 & 2 \end{pmatrix}}_{\equiv T} \begin{pmatrix} x \\ y \end{pmatrix}, \quad \text{mod } 1. \quad (3.9.8)$$

The monodromy matrix of this map is given by T itself. It is straight forward to check that $\det(T) = 1$ and hence the cat map is area and orientation preserving. From the characteristic equation $\det(T - \lambda I) = 0$ we compute the eigenvalues of T which are given by

$$\lambda_{\pm} = \frac{-3 \pm \sqrt{5}}{2}. \quad (3.9.9)$$

In the direction of λ_- the map is contracting and in the direction of λ_+ it is expanding. Hence, all points in the phase space are hyperbolic points and therefore the system is called *completely hyperbolic*. This tells us, in particular, that also all the fixed points of the maps T^n ($n \in \mathbb{N}$) are hyperbolic. In Sect. 3.9.2 we will investigate Lyapunov exponents. The Lyapunov exponents of the cat map are particularly simple to compute and serve as a good example. Taking the definition from Sect. 3.8.4 ($\sigma = \ln(\lambda)$) we find $\sigma_{\pm} = \ln(\lambda_{\pm})$. The complete hyperbolicity is stronger than the mixing property and actually implies true chaoticity in the sense of exponential growth of deviations with time [21, 23, 32].

The cat map would result from a Poincaré map of a free particle where an harmonic potential $\propto \theta^2$ is kicked on periodically in time (with periodic boundary conditions for both variables (θ, p)). Standard examples of chaotic Hamiltonian systems with existing physical realizations are:

- *Standard map*: The system still shows tiny local regular structures even for large kicking strength K (for the definition of the standard map see Sect. 3.8.4.). Hence, it is not globally hyperbolic and its “chaoticity” is not strictly proven.
- *Sinai billiard*: It represents a particle moving in a quadratic box with a circular scatterer in the middle, see Fig. 3.29. It can be shown that its dynamics are globally chaotic in the sense of exponential instability [38, 39].

3.9.2 The Maximal Lyapunov Exponent

One of the most striking characteristics of chaotic dynamics is the exponential separation of nearby trajectories. In systems with a bounded phase space this certainly happens only until the borders are reached. From the Poincaré recurrence theorem we also know that two trajectories get close to each other again after some time. Nevertheless, the exponential growth of perturbations or errors in the initial condition (for some time) turns out to be a well applicable indicator for chaotic motion. Lyapunov exponents are used to quantify this process. We start considering the Lyapunov exponent for Poincaré maps.

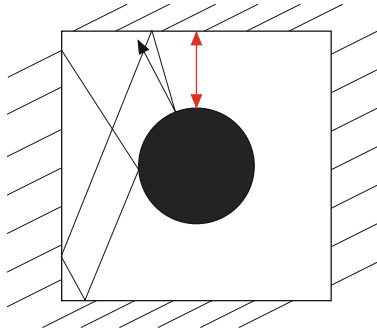


Fig. 3.29 The Sinai billiard is a particle moving in a *quadratic box* with a circular scatterer in the middle. Two trajectories are shown, one of them is periodic (red line with two arrows, corresponding to the simplest unstable periodic orbit), the other one is not and represents a chaotic trajectory (black line with only one arrow). An experimental realization in the semiclassical regime is shown in Fig. 4.16

We assume the dynamics of a Hamiltonian system on the SOS governed by the Poincaré map \mathcal{P} . By $z^* \in \text{SOS}$ we denote a hyperbolic fixed point. We start with the computation of the monodromy matrix $\mathcal{M}_n(z^*)$ of the n -fold iterated Poincaré map \mathcal{P}_n at the fixed point. Straight forward differentiation leads to $d\mathcal{P}_n(z^*) = \prod_{i=1}^n \mathcal{M}(\mathcal{P}_{n-i+1}(z^*))$, where $\mathcal{M}(z^*) = d\mathcal{P}(z^*)$ is the monodromy matrix of $\mathcal{P}(z^*)$. Using the fixed point property $\mathcal{P}(z^*) = z^*$ we find

$$\mathcal{M}_n(z^*) = \mathcal{M}^n(z^*). \quad (3.9.10)$$

Now let $\lambda > 1$ and $\frac{1}{\lambda} < 1$ be the eigenvalues of $\mathcal{M}(z^*)$. The eigenvalues of $\mathcal{M}^n(z^*)$ therefore read

$$\lambda_1 = \lambda^n, \quad \lambda_2 = \frac{1}{\lambda^n}. \quad (3.9.11)$$

The result can be used to illustrate the dynamics near unstable fixed points. Starting with the initial condition z^* the dynamics are trivial and we find $z_n = \mathcal{P}_n(z^*) = z^*$. Now we start the dynamics with a slightly distorted initial condition $\zeta = z^* + \delta z$. The perturbation δz is assumed to be small, and hence we linearize the dynamics around the orbit $z_n = z^*$. This allows us to compute an approximate solution of the dynamics which reads $\zeta_n = \mathcal{P}_n(\zeta) = z^* + \mathcal{M}_n(z^*) \cdot \delta z + O(\delta z^2)$. Inserting the eigenvalues of $\mathcal{M}_n(z^*)$ and changing to its eigenbasis we find

$$\zeta_n = z^* + e^{n \ln(\lambda)} \delta z_1 + e^{-n \ln(\lambda)} \delta z_2 + O(\delta z^2), \quad (3.9.12)$$

where δz_1 is the component of δz pointing in the direction of the first eigenvector of \mathcal{M} and δz_2 the component pointing in the direction of the second eigenvector. In the contracting direction the dynamics converge exponentially fast towards the fixed point while in the expanding direction the distance to the fixed point and therewith

to the original orbit increases exponentially. As we know from Sect. 3.8.4, the two quantities $\pm \ln(\lambda)$ are the Lyapunov exponents of \mathcal{P} at the point z^* .

In the example above, we have seen that the dynamics near an unstable fixed point can be described with the two Lyapunov exponents at the fixed point. After a few applications of the Poincaré map \mathcal{P} the distance of ζ_n to the orbit $z_n = z^*$ is approximately given by $e^{n \ln(\lambda)} \delta z_1$ (the other contribution is exponentially small). Hence, when characterizing the dynamics, there is a special interest in computing the largest Lyapunov exponent. Extending the example to a general situation one defines the maximal Lyapunov exponent by

$$\sigma(z) \equiv \lim_{n \rightarrow \infty} \lim_{\delta z \rightarrow 0} \frac{1}{n} \ln \left(\frac{\|\mathcal{P}_n(z + \delta z) - \mathcal{P}_n(z)\|}{\|\delta z\|} \right), \quad (3.9.13)$$

where $\|\cdot\|$ denotes the euclidean norm. Why does this definition make any sense? The term $\mathcal{P}_n(z + \delta z) - \mathcal{P}_n(z)$ can be written as $\mathcal{M}_n(z) \cdot \delta z + O(\delta z^2)$. Let us look at the matrix $\frac{1}{n} \mathcal{M}_n(z)$. By $\lambda_{\pm}(n)$ we denote its larger/smaller eigenvalue and by $v_{\pm}(n)$ the corresponding eigenvectors. Assume further that $\lambda_{\pm} = \lim_{n \rightarrow \infty} \lambda_{\pm}(n)$ and $v_{\pm} = \lim_{n \rightarrow \infty} v_{\pm}(n)$ exist [20]. Then for almost every δz the Lyapunov exponent is given by $\sigma = \ln(\lambda_+)$ (because of the limits the large eigenvalue eventually dominates). Only if one chooses the perturbation exactly in the direction of the stable direction, $\delta z \propto v_-$, the outcome will be $\sigma = \ln(\lambda_-)$. What we have just shown can be applied to the practical computation of the maximal Lyapunov exponent at a hyperbolic fixed point.

It turns out that in the chaotic regime the maximal Lyapunov exponent is (nearly) independent of the initial condition z . We motivate this by noting that the expression in the logarithm of Eq. (3.9.13) can be written as

$$\frac{\|\mathcal{P}_n(z + \delta z) - \mathcal{P}_n(z)\|}{\|\delta z\|} = \prod_{i=1}^n \frac{\|\mathcal{P}_i(z + \delta z) - \mathcal{P}_i(z)\|}{\|\mathcal{P}_{i-1}(z + \delta z) - \mathcal{P}_{i-1}(z)\|}, \quad (3.9.14)$$

where $\mathcal{P}_0(z) \equiv z$. As above we use the notation $z_n = \mathcal{P}_n(z)$. Since we are interested in the limit $\delta z \rightarrow 0$ we make a linear approximation and write $\mathcal{P}_i(z + \delta z) = \mathcal{P}_i(z) + \mathcal{M}_i(z) \cdot \delta z + O(\delta z^2)$. Additionally, we use $\mathcal{M}_i(z) = \mathcal{M} \circ \mathcal{M}_{i-1}(z)$. Then Eq. (3.9.14) can be written as

$$\begin{aligned} \prod_{i=1}^n \frac{\|\mathcal{M}_i(z) \cdot \delta z + O(\delta z^2)\|}{\|\mathcal{M}_{i-1}(z) \cdot \delta z + O(\delta z^2)\|} &= \prod_{i=1}^n \frac{\|\mathcal{M} \circ \mathcal{M}_{i-1}(z) \cdot \delta z + O(\delta z^2)\|}{\|\mathcal{M}_{i-1}(z) \cdot \delta z + O(\delta z^2)\|} \\ &\approx \prod_{i=1}^n \lambda(z_{i-1}), \end{aligned} \quad (3.9.15)$$

where $\lambda(z_{i-1})$ denotes the larger of the two eigenvalues of $\mathcal{M}(z_{i-1})$. With every iteration the orbit z_i follows the direction of the largest eigenvalue of \mathcal{M} a little farther (if the eigenvalues are of different magnitude), and hence the approximation

is good for small δz as long as i is not too small. The Lyapunov exponent therefore reads

$$\sigma(z) \approx \lim_{n \rightarrow \infty} \frac{1}{n} \sum_{i=0}^{n-1} \ln [\lambda(z_i)]. \quad (3.9.16)$$

We note that this formula has the structure of a time average. If we assume the system to be ergodic in some region in the SOS that we denote by Ω_e , we find

$$\sigma \approx \frac{1}{|\Omega_e|} \int_{\Omega_e} \ln [\lambda(z)] dz. \quad (3.9.17)$$

In this approximation the maximal Lyapunov exponent is given by an average over some phase space region of the maximal eigenvalue of $\mathcal{M}(z)$. If this approximation for σ is good, it can depend just weakly on the initial condition z .

For the continuous time evolution of an Hamiltonian system the maximal Lyapunov exponent is defined analogously:

$$\sigma(z) \equiv \lim_{t \rightarrow \infty} \lim_{\delta z \rightarrow 0} \frac{1}{t} \ln \left(\frac{\|h_t(z + \delta z) - h_t(z)\|}{\|\delta z\|} \right). \quad (3.9.18)$$

Assume we are given the Lyapunov exponent of the full dynamics. The theorem of Abramov tells us how to relate this exponent to the one computed for the dynamics in the SOS [21].

Theorem of Abramov: Let σ_c be the maximal Lyapunov exponent of the full dynamics and let τ be the mean return time onto the SOS. Then the maximal Lyapunov exponent σ_{SOS} of the dynamics in the SOS is given by $\sigma_{SOS} = \tau \sigma_c$.

This can be seen as follows. Let t_n denote the time in which the continuous trajectory propagates from $z_{n-1} \in \text{SOS}$ to $z_n \in \text{SOS}$. We write $\frac{1}{n} = \frac{1}{t_n} \frac{t_n}{n} \equiv \frac{1}{t_n} \tau_n$ and define the mean return time onto the SOS by $\tau = \lim_{n \rightarrow \infty} \tau_n$. Insertion into the definitions leads to

$$\frac{1}{n} \ln \left(\frac{\|\mathcal{P}_n(z + \delta z) - \mathcal{P}_n(z)\|}{\|\delta z\|} \right) = \frac{\tau_n}{t_n} \ln \left(\frac{\|h_{t_n}(z + \delta z) - h_{t_n}(z)\|}{\|\delta z\|} \right). \quad (3.9.19)$$

In the limit $n \rightarrow \infty$ and $\delta z \rightarrow 0$ this gives the above theorem.

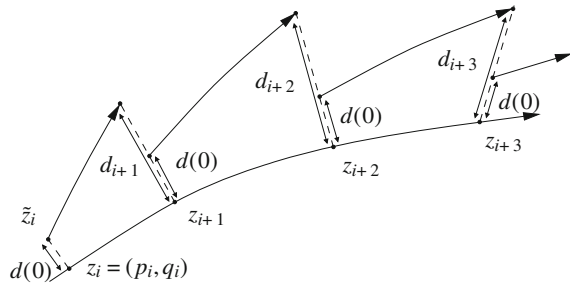
3.9.3 Numerical Computation of the Maximal Lyapunov Exponent

We present here a numerical method to compute the maximal Lyapunov exponent of a Hamiltonian system. The time evolution follows from

$$\dot{z}(t) = J \cdot \nabla H(z(t)) \equiv F(z(t)), \quad (3.9.20)$$

Fig. 3.30 Computation of the maximal Lyapunov exponent.

After each time step τ the distance d_i is renormalized to one



see Eq. (3.2.1). For the computation of the Lyapunov exponent we compare a trajectory $z(t)$ starting from the initial value z_0 and a nearby trajectory starting at $z_0 + h_0$ with time evolution $z(t) + h(t)$. The distance between the two trajectories is given by $d(t) = \|h(t)\|$. Using this notation the maximal Lyapunov exponent is given by

$$\sigma = \lim_{t \rightarrow \infty} \lim_{d(0) \rightarrow 0} \frac{1}{t} \ln \left(\frac{d(t)}{d(0)} \right). \quad (3.9.21)$$

If $d(t)$ increases exponentially we may reach the boundary of the phase space during the numerical computation. Additionally, there is the risk of computer overflow because of very large numbers. The method we present here tries to avoid these problems. We start with $d(0) = \|h_0\|$ which is assumed to be normalized to one. Then we propagate h_0 along a time interval τ and obtain $h(\tau) = h_1$ and therewith $d_1 = \|h_1\|$. The vector h_1 is normalized to one again and afterward propagated by τ . With the result h_2 we compute d_2 . Going on like this, the sequence d_i for $i = 1, \dots, k$ is calculated, see Fig. 3.30.

In analogy with Eq. (3.9.21) we define

$$\sigma_k = \frac{1}{k\tau} \sum_{i=1}^k \ln(d_i). \quad (3.9.22)$$

It can be shown that if τ is small enough the limit $\lim_{k \rightarrow \infty} \sigma_k$ exists and gives the maximal Lyapunov exponent σ [20]. What remains is the question how to propagate h_i in time. Since τ and $\|h_0\|$ will be small numbers we can linearize the dynamics. The linearized equations of motions read $\dot{z}(t) + \dot{h}(t) = F(z(t)) + dF(z(t)) \cdot h(t) + O(h(t)^2)$ and lead to the formula

$$\dot{h}(t) \approx dF(z(t)) \cdot h(t). \quad (3.9.23)$$

For the numerical calculation this is written as $\delta h_i \approx dF(z_i) \cdot h_i \tau$, where $z_i = z(i\tau)$ and $h_{i+1} = h_i + \delta h_i$. The trajectory $z(t)$ is practically computed with a stable and precise numerical method [40].

3.9.4 The Lyapunov Spectrum

In Sect. 3.9.2 and in our examples we have seen that it is reasonable to define not only one Lyapunov exponent but one for each phase space dimension. Such a full set of Lyapunov exponents is called the *Lyapunov spectrum*. Using the definition of the maximal Lyapunov exponent for the two-dimensional Poincaré map [Eq. (3.9.13)], the Lyapunov spectrum is defined by

$$\begin{aligned}\sigma_{\pm}(z) &\equiv \lim_{n \rightarrow \infty} \lim_{h \rightarrow 0} \frac{1}{n} \ln \left(\frac{\|\mathcal{P}_n(z + hv_{\pm}) - \mathcal{P}_n(z)\|}{|h|} \right) \\ &= \ln(\lambda_{\pm}).\end{aligned}\quad (3.9.24)$$

The quantities λ_{\pm} and v_{\pm} are defined in Sect. 3.9.2. $\sigma_+ = \sigma$ is the maximal Lyapunov exponent and σ_- is a measure for the rate of contraction of the Poincaré map in the direction perpendicular to v_+ (v_+ points in the direction in which \mathcal{P} is maximally expanding). In the neighborhood of a hyperbolic fixed point the Lyapunov spectrum contains the same information as the eigenvalues of the monodromy matrix, see Sects. 3.8.4 and 3.9.2.

In the case of the continuous dynamics of a Hamiltonian system the Lyapunov spectrum is defined in a similar way. As for the Poincaré map, there exist distinct directions v_i such that $2n$ (dimensionality of the phase space) Lyapunov exponents can be defined by

$$\sigma_i(z) \equiv \lim_{t \rightarrow \infty} \lim_{h \rightarrow 0} \frac{1}{t} \ln \left(\frac{\|h_t(z + hv_i) - h_t(z)\|}{|h|} \right). \quad (3.9.25)$$

Since the time evolution h_t is phase space volume preserving the exponents σ_i fulfill the relation $\sum_{i=1}^{2n} \sigma_i = 0$. In general the Lyapunov spectrum has the following structure

$$\sigma_1 \geq \sigma_2 \geq \dots \geq \sigma_n = 0 = -\sigma_n \geq \dots \geq -\sigma_2 \geq -\sigma_1. \quad (3.9.26)$$

This relation changes slightly if the energy is conserved. Because the energy-surface is $(2n-1)$ -dimensional there are only $2n-1$ Lyapunov exponents. Equation (3.9.26) then holds with one exponent less ($-\sigma_n$ has to be left away). The vector v_n corresponding to $\sigma_n = 0$ points in the direction of the Hamiltonian flow. This is because perturbations can only grow linearly in the direction of the flow. We note that there may be more than one (or two) exponents equal to zero. It can easily be shown, for example, that for integrable systems one has $\sigma_i = 0$ for all i .

The numerical computation of the full Lyapunov spectrum is more sophisticated than the computation of the maximal exponent, but in principle follows the same line of reasoning. More details on the presented method can be found in [41, 42]. To compute the maximal Lyapunov exponent we have to calculate the time evolution of the distance of two nearby initial conditions (which is given by the norm of a

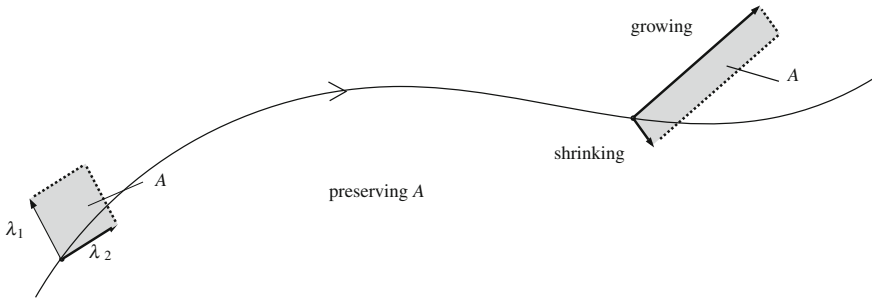


Fig. 3.31 In order to calculate the Lyapunov spectrum an m -dimensional volume is propagated in tangent space and its distortion is measured in every direction. This is shown in the figure in case of $n = 2$ and of energy conservation ($E = \text{const.}$). Consequently, there are $m = 2n - 1 = 3$ Lyapunov exponents

vector), see Sect. 3.9.3. The natural generalization of this method is to propagate an m -dimensional volume in the tangent space and to measure its distortion in all directions. This is illustrated in Fig. 3.31. If there are no conserved quantities $m = 2n$; in case of energy conservation we have $m = 2n - 1$.

For the propagation we choose a set of pairwise orthogonal vectors $\omega_i \in \mathbb{R}^m$, $i = 1, \dots, p$ with $1 \leq p \leq m$ that span a p -dimensional parallelepiped $\omega_1 \times \omega_2 \times \dots \times \omega_p$ (The edges of the parallelepiped are given by the vectors ω_i). By V_p we denote its volume

$$V_p = |\omega_1 \times \omega_2 \times \dots \times \omega_p|. \quad (3.9.27)$$

For the computation we need a quantity called the p -th order Lyapunov exponent which is defined by

$$\sigma_p(V_p) = \lim_{t \rightarrow \infty} \frac{1}{t} \ln \left(\frac{V_p(t)}{V_p(0)} \right), \quad (3.9.28)$$

where we have used the notation $V_p(t) = |h_t(\omega_1) \times h_t(\omega_2) \times \dots \times h_t(\omega_p)|$. It can be shown that σ_p in the chaotic regime is almost independent of V_p (like the Lyapunov exponents are nearly independent of the choice of z and δz , see Sect. 3.9.2). Its relation to the Lyapunov spectrum is given by

$$\sigma_p = \sum_{i=1}^p \sigma_i, \quad (3.9.29)$$

where $\sum_{i=1}^p \sigma_i$ denotes the sum over the p largest Lyapunov exponents. Hence, if we want to compute the full spectrum we have to successively compute σ_p for $p = 1, \dots, m - 1$ ($\sum_{i=1}^m \sigma_i = 0$).

We note that during the numerical computation the parallelepiped $\omega_1 \times \omega_2 \times \dots \times \omega_p$ will be stretched much more in some directions than in others. Therefore, numerical problems occur when very small angles cannot be resolved anymore. The solution of this problem is not only to renormalize successively the size of the volume (as we did in the computation of the maximal Lyapunov exponent), but also to orthogonalize the vectors ω_i after each time step. During this procedure, we have to take care that the orthogonalized vectors span the same p -dimensional subspace as the original ones.

3.9.5 Kolmogorov–Sinai Entropy

The Kolmogorov–Sinai (KS) entropy is a concept, which was originally developed within information theory and is applied to the theory of dynamical systems [25, 32, 43]. For the definition we need a measure preserving dynamical system as defined in Sect. 3.9.1. The time evolution is assumed to be discrete and invertible. By $\xi = \{C_1, \dots, C_k\}$ we denote a finite partition of the phase space Ω into k pairwise disjoint and measurable sets. We assume that such a partition exists for all $k \in \mathbb{N}$. To shorten the writing we define the function $\mathcal{E}(x) = x \ln(x)$ for $x \in \mathbb{R}_+$. The ξ -dependent function h is defined by

$$h(\xi) = \lim_{k \rightarrow \infty} \sum_{i_1, \dots, i_k} \mathcal{E} \left\{ \nu \left[T^{-1}(C_{i_1}) \cap \dots \cap T^{-k}(C_{i_k}) \right] \right\}. \quad (3.9.30)$$

To obtain the KS entropy we have to take the supremum of $h(\xi)$ over all possible partitions ξ

$$h = \sup_{\xi} [h(\xi)]. \quad (3.9.31)$$

Let us interpret this definition. When we propagate the partition ξ backwards in time we obtain a new partition $\xi(-1) = \{T^{-1}(C_1), \dots, T^{-1}(C_k)\}$. Now assume the refinement of the two partitions ξ and $\xi(-1)$ which is defined by $\xi \wedge \xi(-1) = \{C_i \cap T^{-1}(C_j) \mid i, j = 1, \dots, k; \nu(C_i \cap T^{-1}(C_j)) > 0\}$. Typically each set $B \in \xi \wedge \xi(-1)$ has a smaller measure than one of the C_i . In the next step one takes the refinement of ξ , $\xi(-1)$ and $\xi(-2)$ and so on. The Kolmogorov–Sinai entropy quantifies the decrease of the measure of sets belonging to the successive refinements. It is only positive if there is an exponential decay in the average measure of the elements of the refinements in each step. Therefore, it is no big surprise that h is related to the Lyapunov exponents of the system [21]. The relation reads

$$h = \int_{\Omega} \left[\sum_{\sigma_i(\omega) > 0} \sigma_i(\omega) \right] d\nu(\omega), \quad (3.9.32)$$

where the sum is taken over all positive Lyapunov exponents. For a chaotic system with just two degrees of freedom this simplifies to

$$h = \sigma_+. \quad (3.9.33)$$

Here σ_+ denotes the maximal Lyapunov exponent. Systems for which almost every connected phase space region has a positive KS entropy are called K-systems. All K-systems have the property of mixing and therefore they are ergodic as well. For Hamiltonian systems, a positive KS entropy is a strong criterion for chaotic dynamics. Nevertheless, the application of this criterion is generally difficult because it is hard to show that a given system is actually a K-system. Two examples of K-systems are the Sinai billiard (Sect. 3.9.1) and the related Lorentz gas model [32, 44, 45].

3.9.6 Resonance Overlap Criterion

One of the great challenges in the field of nonlinear dynamics and chaos is to find criteria for the onset of global chaos. In a two-dimensional system, global transport is possible only without KAM tori. A criterion that is used to give analytical (and numerical) predictions for the onset of global chaos has been developed by Chirikov and others. It is known as resonance overlap criterion or just overlap criterion. It is very intuitive but lacks a strict justification and accurate predictions since the method—when refined to give more accurate results—quickly becomes computationally very demanding. Nevertheless, it is used as a qualitative criterion to give rough estimates. For more information on the topic consult [21] and references therein.

During its development the resonance overlap criterion has been applied mostly to the standard map which is the Poincaré map of the kicked rotor (it works especially well for this system). We will also follow this path and introduce the method by applying it to the kicked rotor. The Hamiltonian of the kicked rotor is given by

$$H(I, \theta, t) = \frac{I^2}{2} + K \cos(\theta) \sum_{n=-\infty}^{\infty} \delta(t - n). \quad (3.9.34)$$

We recall the standard map which has been introduced in Sect. 3.8.3 and reads

$$I_{n+1} = I_n + K \sin(\theta_n) \bmod 2\pi, \quad (3.9.35)$$

$$\theta_{n+1} = \theta_n + I_{n+1} \bmod 2\pi. \quad (3.9.36)$$

It is a stroboscopic map evaluated at times $t_n = n \in \mathbb{Z}$ when the system is kicked [25]. In the vicinity of regions with regular structures (as for example near the first order fixed point of the standard map at $(I_1, \theta_1) = (0, 0)$) there are two frequencies in the system. One is given by the frequency of the time-dependent part of the Hamiltonian $\omega_1 = 2\pi$ and the other one (ω_2) by the dynamics in the

(q, p) -plane. The frequency ω_2 is difficult to compute but obviously exists, since there are invariant closed curves in the SOS (at least for not too large values of K , see Fig. 3.17). The resonance centered around (I_1, θ_1) in the SOS is called the 1:1 resonance. This is because (I_1, θ_1) is a first-order fixed point of the standard map and hence the condition $\omega_1 = \omega_2$ holds. The resonances centered around the two second-order fixed points are called 2:1 resonances because at these points one has $2\omega_1 = \omega_2$. Resonances should not be confused with KAM tori which in case of the standard map create continuous curves in the SOS extending from $\theta = 0$ to $\theta = 2\pi$, see Fig. 3.17 and [25] for more figures. This structure can easily be understood when we look at the unperturbed and therefore integrable system. For $K = 0$, the invariant curves in the SOS are straight lines describing the free motion (with constant velocity) of the rotor in configuration space, see Fig. 3.17.

Numerically, three different regimes can be identified:

- $K \rightarrow 0$: The system is nearly integrable.
- $K \gtrsim K_c \approx 0.972$: The last KAM torus, which divides the phase space into two non-connected regions, is destroyed.
- $K \gtrsim 4$: The linear stability of the 1:1 resonance is destroyed and bifurcations appear. This value is a good approximation for the onset of global chaos in the standard map.

The resonance overlap criterion estimates the critical kicking strength K_c at which the last KAM torus is destroyed. As explained above, KAM tori of the kicked rotor create invariant curves in the SOS going from $\theta = 0$ to $\theta = 2\pi$. These curves lie in between the resonances and therefore separate them. When K is increased, the resonances grow and successively new resonances are created. Assume now this happens until the borders of the different resonances touch each other. Obviously, there will be no more KAM curves between them anymore. The strategy of the overlap criterion is to estimate the width of the resonances and, with this information, the value of the kicking strength K for which they overlap. This result is then taken as an approximation to K_c .

- **Overlap of the 1:1 resonance with itself:** In the simplest approximation we estimate at which kicking strength the 1:1 resonance in the SOS overlaps with itself. This is possible because the phase space is 2π -periodic in both variables (I and θ). To estimate the width of the island we use lowest order secular perturbation theory (pendulum approximation, see Sect. 3.7.6) and find $\Delta I_1 \approx 4\sqrt{K}$. The resonance overlaps with itself when ΔI_1 equals the length of the SOS in the I -direction (2π). Equating these two values we find

$$K_c \approx \frac{\pi^2}{4} \approx 2.47. \quad (3.9.37)$$

As mentioned above the numerical result is $K_c \approx 0.972$, and hence we obviously need to improve the analytical estimate.

- **Overlap of the 1:1 and the 2:1 resonance:** To be more accurate we take into account also the two 2:1 resonances and compute the value of K for which they

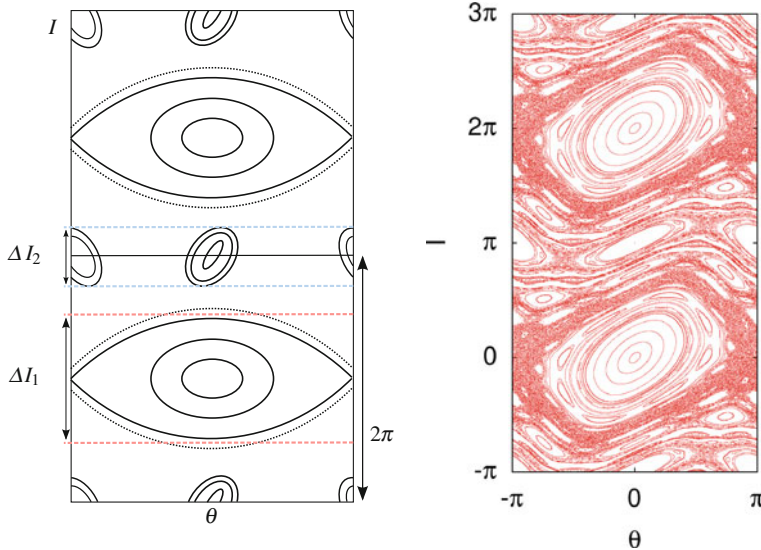


Fig. 3.32 The left figure shows a schematic illustration of the resonance overlap criterion: To find an approximation for the critical kicking parameter K_c at which the last KAM-torus vanishes the widths of the islands corresponding to the 1:1 and the 2:1 resonances are calculated. To improve the estimation of K_c the width of the separatrix has to be taken into account. The separatrix region is described by the dotted (black) lines. The figure on the right shows the phase space of the kicked rotor for $K = 1$ as a direct application of the criterion

start to overlap with the 1:1 resonance. For the calculation of the width of the 2:1 resonance we have to do second order secular perturbation theory and find $\Delta I_2 \approx K$. When we use the overlap condition $\Delta I_1 + \Delta I_2 = 2\pi$, the defining equation for K_c can be derived. It reads $2\sqrt{K_c} + \frac{K_c}{2} = \pi$ and has the solution

$$K_c \approx 1.46. \quad (3.9.38)$$

We have obtained a better result but still we need to improve.

- **Overlap of the 1:1 and the 2:1 resonance plus width of separatrix:** Refining the approximation in a third step we take into account also the width of the separatrix. This is done in [21] and results in

$$K_c \approx 1.2. \quad (3.9.39)$$

This result is again better than the previous one but still above the numerically obtained value. Further improvements become very complicated and computationally demanding. But at least for the standard map renormalization techniques accurately predict K_c [21]. The resonance overlap criterion and the described approximation method is illustrated in Fig. 3.32.

Appendix

Another Proof of Liouville's Theorem Using the notation from Eq. (3.2.1), we denote the time-evolution by $h_t(z) = z(t)$. Liouville's theorem then states that $|\Omega| = |h_t(\Omega)|$ for any set Ω in the phase space. By $|\Omega|$ we denote the volume of Ω . An explicit formula for the time-dependent phase space volume reads

$$|h_t(\Omega)| = \int_{h_t(\Omega)} dz = \int_{\Omega} \det \left(\frac{\partial h_t(z)}{\partial z} \right) dz. \quad (3.9.40)$$

To prove Liouville's theorem we will show that $\frac{d|h_t(\Omega)|}{dt} = 0$. Since the derivative of a function is its unique linear approximation we expand the determinant in the integral of Eq. (3.9.40) in first order in t . When we write the time evolution as $h_t(z) = z + \dot{h}_t(z)t + O(t^2)$ the integrand reads

$$\det \left(I + \frac{\partial \dot{h}_t(z)}{\partial z} + O(t^2) \right)$$

(I is the identity matrix). To expand also the determinant we make use of the relation $\det(I + At) = 1 + \text{tr}(A)t + O(t^2)$ which holds for any matrix A and any real number t . In our case the trace reads

$$\text{tr} \left(\frac{\partial \dot{h}_t(z)}{\partial z} \right) = \text{div } \dot{h}_t(z)$$

which leads to

$$|h_t(\Omega)| = \int_{\Omega} \left(1 + \text{div } \dot{h}_t(z) \cdot t + O(t^2) \right) dz. \quad (3.9.41)$$

The derivate of this expression with respect to time is given by

$$\frac{d |h_t(\Omega)|}{dt} = \int_{\Omega} \text{div } \dot{h}_t(z) dz = 0, \quad (3.9.42)$$

which concludes our proof, c.f. Sect. 3.4.2.

Problems

- 3.1.** Given the Hamiltonian $H(x, p) = p^2/2 + V(x)$, with $V(x) = a|x|^n$ from Eq. (3.1.17), for a particle of unit mass, determine the period of oscillations as a function of a and of the energy E .

3.2. Nonlinear oscillator. A particle of unit mass moves in one-dimension in the potential $V(x) = \omega^2 x^2/2 - ax^3/3$, with $a > 0$.

- (a) Prove that the Hamiltonian is a constant of the motion.
- (b) Sketch the potential $V(x)$ as a function of x .
- (c) Sketch the flow of trajectories in phase space (p, x) . Locate any hyperbolic (unstable) and elliptic (stable) fixed point. Draw any separatrix of the motion.

3.3. Pendulum. Show that the area enclosed by the separatrix of the pendulum, with $H = p^2/2 - k \cos(\theta)$, equals $16\sqrt{k}$. Deduce from this result the maximal action for librating motion.

3.4. Symplectic matrices. A real $2n \times 2n$ matrix is called symplectic if:

$$M^T JM = J \text{ with } J = \begin{pmatrix} 0 & -1 \\ 1 & 0 \end{pmatrix}, \quad (3.9.43)$$

with the identity $n \times n$ matrix 1.

Prove now the following statements:

- (a) If M_1 and M_2 are symplectic then $M_1 M_2$ is symplectic.
- (b) If λ is an eigenvalue of a symplectic matrix then also $1/\lambda$.
- (c) M is symplectic if and only if M is invertible with $M^{-1} = -JM^T J$.
- (d) 2×2 matrices have the property: M symplectic $\Leftrightarrow \det M = 1$.

3.5. Separable Motion. Find the solution of the Hamilton–Jacobi equation for the motion of a particle of unit mass in three dimensions governed by the Stark Hamiltonian:

$$H(|\mathbf{r}| = r, \mathbf{p}) = \frac{p^2}{2} - \frac{1}{r} + Fz.$$

You can solve this problem step by step.

- (a) Using parabolic coordinates (ξ, η, ϕ) obtained from the cylindrical coordinates (ρ, ϕ, z) via $\xi = r + z$ and $\eta = r - z$, with $r = \sqrt{\rho^2 + z^2}$ and $\rho = \sqrt{\xi\eta} = \sqrt{x^2 + y^2}$, show first that

$$p_\phi = \xi\eta\dot{\phi}, \quad p_\eta = \frac{1}{4\eta}(\xi + \eta)\dot{\eta}, \quad p_\xi = \frac{1}{4\xi}(\xi + \eta)\dot{\xi}.$$

- (b) Now show that

$$H(\eta, \xi, \phi; p_\eta, p_\xi, p_\phi) = 2\frac{\xi p_\xi^2 + \eta p_\eta^2}{\xi + \eta} + \frac{p_\phi^2}{2\eta\xi} - \frac{2}{\xi + \eta} + \frac{F}{2}(\xi - \eta).$$

- (c) Finally, write down the time-independent Hamilton–Jacobi equation

$$\tilde{H}\left(\frac{\partial S}{\partial \xi}, \frac{\partial S}{\partial \eta}, \frac{\partial S}{\partial \phi}; \xi, \eta, \phi\right) = E,$$

and solve it with the separation ansatz for $S = S_1(\phi) + S_2(\xi) + S_3(\eta)$.

3.6. Canonical perturbation theory. Find the generating function and the new Hamiltonian in second order perturbation theory for the Hamiltonian of Problem 3.1 with $a \equiv -3\varepsilon$, i.e., for

$$H = H_0(x, p) + \varepsilon H_1(x) = \frac{p^2 + \omega^2 x^2}{2} + \varepsilon x^3.$$

3.7. Kicked Rotor I. Given the time-dependent Hamiltonian

$$H(p, q, t) = H_0(p) + V(q)T \sum_{n=-\infty}^{\infty} \delta(t - nT),$$

how must one choose $H_0(p)$, $V(q)$ and T such that the following mapping corresponds to the standard map of Eq. (3.8.15):

$$\begin{pmatrix} p_n \\ q_n \end{pmatrix} \mapsto \begin{pmatrix} p_{n+1} \\ q_{n+1} \end{pmatrix} \text{ with } \begin{pmatrix} p_n \\ q_n \end{pmatrix} = \lim_{\delta \rightarrow 0^+} \begin{pmatrix} p(t = nT - \delta) \\ q(t = nT - \delta) \end{pmatrix}.$$

3.8. Kicked rotor II—chaos and stochasticity. Let us use the following form of the standard map

$$\begin{aligned} p &\mapsto p' = p + K \sin(q) \\ q &\mapsto q' = q + p'. \end{aligned} \tag{3.9.44}$$

In this problem we do not take the modulus operation in the evolution of momenta p (in the evolution of q it might as well be taken, why?).

- (a) For $K = 10$, compute numerically how the average energy $p^2/2$ increases with the number of iterations of the map. To do so define ca. 1000 initial points at $p = 0$, with equidistant values $q \in [1.0001, 1.0002, \dots, 1.1]$, and average the energy over these initial conditions. What kind of stochastic-like motion do you observe?
- (b) Calculate analytically how, for large $K \gg 1$, the energy $p^2/2$ increases on average with the number of iterations of the map. You should express p_n as a function of p_0 and q_0, q_1, \dots, q_{n-1} . Use the fact that the iterated values of $\sin(q)$ are in good approximation uncorrelated for large $|p|$.

References

1. Kittel, C.: Introduction to Solid State Physics. Wiley, New York (2005)
2. Abramowitz, M., Stegun, I.A.: Handbook of Mathematical Functions. Dover, New York (1972)

3. Gradshteyn, I., Ryzhik, I.: Table of Integrals, Series and Products. Academic Press, New York (1980)
4. Rebhan, E.: Theoretische Physik: Mechanik. Spektrum Akademischer Verlag, Heidelberg (2006)
5. Landau, L.D., Lifschitz, E.M.: Course in Theoretical Physics I, Mechanics. Pergamon Press, Oxford (1960)
6. Arnold, V.I.: Mathematical Methods of Classical Mechanics. Springer, New York (1989)
7. Arnold, V.I.: Geometrical Methods in the Theory of Ordinary Differential Equations. Springer, New York (1988)
8. Scheck, F.: Mechanics: from Newton's Laws to Deterministic Chaos. Springer, Heidelberg (2007)
9. Dürr, D.: Bohmsche Mechanik als Grundlage der Quantenmechanik. Springer, Berlin (2001)
10. Schwabl, F.: Quantum Mechanics. Springer, Berlin (2005)
11. Poincaré, H.: Les Méthodes nouvelles de la mécanique céleste. Gauthier-Villars (1899)
12. Kolmogorov, A.N.: Dokl. Akad. Nauk. SSSR **98**, 527 (1954)
13. Arnold, V.I.: Russ. Math. Surv. **18**, 13 (1963)
14. Arnold, V.I.: Dokl. Akad. Nauk SSSR **156**, 9 (1964)
15. Moser, J.K.: Nach. Akad. Wiss. Göttingen, Math. Phys. Kl. **II**(1), 1 (1962)
16. Moser, J.K.: Math. Ann. **169**, 136 (1967)
17. Percival, I.C., Richards, D.: Introduction to Dynamics. Cambridge University Press, Cambridge (1982)
18. Dehmelt, H.G.: Adv. At. Mol. Phys. **3**, 53 (1967)
19. Paul, W.: Rev. Mod. Phys. **62**, 531 (1990)
20. Tabor, M.: Chaos and Integrability in Nonlinear Dynamics. Wiley, New York (1989)
21. Lichtenberg, A.J., Lieberman, M.A.: Regular and Chaotic Dynamics. Springer, Berlin (1992)
22. Moser, J.K.: Stable and Random Motion in Dynamical Systems. Princeton University Press, Princeton (2001)
23. Arnold, V.I., Avez, A.: Ergodic Problems of Classical Mechanics. W. A. Benjamin, New York (1968)
24. Chierchia, L., Mather, J.N.: Scholarpedia **5**(9), 2123 (2010)
25. Ott, E.: Chaos in Dynamical Systems. Cambridge University Press, Cambridge (2002)
26. Hardy, G., Wright, E.: An Introduction to the Theory of Numbers. Oxford University Press, Oxford (2008)
27. Buchleitner, A., Delande, D., Zakrzewski, J.: Physics Reports **368**(5), 409 (2002)
28. Chirikov, B., Shepelyansky, D.: Scholarpedia **3**(3), 3550 (2008)
29. Chirikov, B.V.: Physics Reports **52**(5), 263 (1979)
30. Berry, M.V.: In Topics in nonlinear mechanics. In: Jorna, S. (ed.) American Institute of Physics Conference Proceedings, vol. 46, pp. 16–120 (1978)
31. Hénon, M., Heiles, C.: Astron. J. **69**, 73 (1964)
32. Gaspard, P.: Chaos, Scattering and Statistical Mechanics. Cambridge University Press, Cambridge (1998)
33. Schuster, H.G.: Deterministic Chaos. VCH, Weinheim (1988)
34. Weisstein, E.W.: Double Pendulum. MathWorld—A Wolfram Web Resource. <http://mathworld.wolfram.com/DoublePendulum.html>
35. Korsch, H.J., Jodl, H.J., Hartmann, T.: Chaos—A Program Collection for the PC. Springer, Berlin (2008)
36. Lieb, E.H., Loss, M.: Analysis. American Mathematical Society, Providence (2001)
37. Landau, L.D., Lifschitz, E.M.: Course in Theoretical Physics V, Statistical Physics. Butterworth-Heinemann, Oxford (1990)
38. Sinai, Y.G.: Uspekhi Mat. Nauk **25**(2), 141 (1970)
39. Chernov, N., Marhavian, R.: Chaotic Billiards. American Mathematical Society, Providence (2006)
40. Press, W.H., Teukolsky, S.A., Vetterling, W.T., Flannery, B.P.: Numerical Recipes 3rd Edition: The Art of Scientific Computing, 3rd edn. Cambridge University Press, New York (2007)

41. Benettin, G., Froeschle, C., Schneidecker, J.P.: Phys. Rev. A **19**, 2454 (1979)
42. Benettin, G., Galgani, L., Giorgilli, A., Strelcyn, J.M.: Meccanica **15**, 9 (1980)
43. Sinai, Y.: Scholarpedia **4**(3), 2034 (2009)
44. van Beijeren, H., Latz, A., Dorfman, J.R.: Phys. Rev. E **57**, 4077 (1998)
45. Bunimovich, L., Burago, D., Chernov, N., Cohen, E., Dettmann, C., Dorfman, J., Ferleger, S., Hirsch, R., Kononenko, A., Lebowitz, J., Liverani, C., Murphy, T., Piasecki, J., Posch, H., Simanyi, N., Sinai, Y., Szasz, D., Tel, T., van Beijeren, H., van Zon, R., Vollmer, J., Young, L.: Hard Ball Systems and the Lorentz Gas. Springer, Berlin (2001)

Chapter 4

Aspects of Quantum Chaos

Abstract This chapter discusses two important ways of defining quantum chaoticity. One access to characterize dynamical quantum systems is offered by the powerful approach of semiclassics. Here we compare the properties of the quantum system with its classical analogue, and we combine classical intuition with quantum evolution. The second approach starts from the very heart of quantum mechanics, from the quantum spectrum and its properties. Classical and quantum localization mechanisms are presented, again originating either from the classical dynamics of the corresponding problem and semiclassical explanations, or from the quantum spectra and the superposition principle. The essential ideas of the theory of random matrices are introduced. This second way of characterizing a quantum system by its spectrum is reconciled with the first approach by the conjectures of Berry and Tabor and Bohigas, Giannoni, and Schmit, respectively.

4.1 Introductory Remarks on Quantum Mechanics

The origins of quantum mechanics lie in the attempt to explain the behavior and the dynamics of systems at atomic scales. One important motivation to search for a new theory in the 1920s was the stability of the hydrogen atom. While classical electrodynamics predicts that an electron encircling the nucleus loses energy emitting electro-magnetic radiation and quickly falls into the nucleus, experiments tell us that the hydrogen atom has certainly a stable ground state. In analogy to the wave nature of light, it was assumed that atomic and elementary particles exhibit a wave behavior. Famous experiments that support this theory are the diffraction of electrons on crystalline lattices (Davisson–Germer experiment [1]) as well as Young’s double slit experiment conducted with electrons [1]. On the other hand it was already clear from the onset of the twenties century that light not only exhibits the characters of a wave, but it acts as if it was composed of particles. This is for example illustrated by Einstein’s photo-electric effect. Starting from this wave-particle duality, Louis

de Broglie postulated the wave nature of particles. One fundamental mathematical description of the quantum theory lies in Schrödinger's wave mechanics. The wave equation of a particle in an external field is given by the Schrödinger equation:

$$i\hbar \frac{d\psi(\mathbf{r}, t)}{dt} = \hat{H}\psi(\mathbf{r}, t) \quad (4.1.1)$$

Equation (4.1.1) is a partial differential equation which describes the time evolution of the given physical system. Moreover, it contains information about the energy spectrum. The function $\psi(\mathbf{r}, t)$ is called wave function and completely determines the state of a physical system of N particles for $\mathbf{r} \in \mathbb{R}^{3N}$ at all times (as far as this is possible within the statistical interpretation of quantum mechanics). Schrödinger's wave mechanics is hence a fully deterministic theory. From $\psi(\mathbf{r}, t)$, which is also interpreted as a probability amplitude, we can draw information about distributions in momentum and position space as well as the expectation value of quantities such as the energy [1–3].

The Hamiltonian \hat{H} is a linear operator acting on the wave function $\psi(\mathbf{r}, t)$. Its linearity is the origin of the superposition principle in quantum mechanics. It is responsible for the wave-like character of the solutions of Schrödinger's equation. Consequently, it may be difficult to define chaos in quantum mechanics. As we have seen in Chap. 3, chaos in classical systems relies on the nonlinear nature of the corresponding evolution equations. Therefore, the quantum evolution cannot be chaotic in the sense of the Lyapunov instability discussed in Sect. 3.9 and Fig. 3.30. We even have that the overlap between two different wave functions remains identical for all times

$$\langle \psi(\mathbf{r} + \delta\mathbf{r}, t) | \psi(\mathbf{r}, t) \rangle = \langle \psi(\mathbf{r} + \delta\mathbf{r}, 0) | \underbrace{\hat{U}^\dagger \hat{U}}_{=I} | \psi(\mathbf{r}, 0) \rangle = \langle \psi(\mathbf{r} + \delta\mathbf{r}, 0) | \psi(\mathbf{r}, 0) \rangle, \quad (4.1.2)$$

with the quantum mechanical evolution operator¹ $\hat{U} = e^{-i\hat{H}t/\hbar}$.

Instead of the initial conditions, a parameter of the system may be varied. This idea goes back to Peres [5] who introduced the so-called fidelity as a measure of stability in quantum mechanics. It is defined by the overlap of two initially identical wave functions which have a slightly different time evolution. Let us assume a small perturbation $\delta\lambda$ of some parameter λ of the Hamiltonian operator. Then the following overlap is time dependent and its evolution may teach something about the stability of the quantum system with respect to the corresponding change of the parameter λ :

$$|\langle \psi(\mathbf{r}, t; \lambda) | \psi(\mathbf{r}, t; \lambda + \delta\lambda) \rangle|^2 \equiv \underbrace{F(t, \delta\lambda)}_{\text{"fidelity"}}. \quad (4.1.3)$$

¹ This relation between the hermitian operator \hat{H} and the unitary \hat{U} is due to a theorem of Stone [4]. We assume \hat{H} was time-independent, otherwise time-ordering must be used.

Since there are many, partly contradicting results established for the fidelity, we will not elaborate on it here. We rather refer the interested reader to the specialized literature [6, 7].

We may thus ask ourselves: What is quantum chaos? The original idea is to study the relations between a quantum system and its corresponding classical analogue. Starting from this idea, we present some methods of the phenomenology of quantum chaos in this chapter. On the one hand, we focus on semiclassical quantization techniques of integrable systems (Sect. 4.2). On the other hand, we describe semiclassical tools for fully chaotic systems in Sect. 4.3. Having these tools at hand, we study the evolution of quantum mechanical wave packets projected into phase space, see Sect. 4.4, and classical as well as quantum mechanical localization of the wave packet evolution, see Sects. 4.4.3.3 and 4.5.1, respectively. Doing so we can characterize also generic systems whose classical analogues show a mixed regular-chaotic phase space, c.f. Sect. 3.8.7. Quantum chaology, a term tossed by Berry [8, 9], can arguably be put onto firm grounds by analyzing the spectral properties of quantum systems. These properties can be compared with predictions from the theory of random matrices. In this way, all quantum systems can be formally analyzed without referring to a classical analogue. The introduction to this vast field of research, presented in Sect. 4.6, should help to appreciate the concepts and allow the reader its practical application.

4.2 Semiclassical Quantization of Integrable Systems

4.2.1 Bohr–Sommerfeld Quantization

In 1885 Balmer investigated the spectral properties of light emitted by a hydrogen lamp and discovered the following empirical law describing the energy levels of the hydrogen atom. The frequency derived from the wave length of the corresponding Balmer line is given by

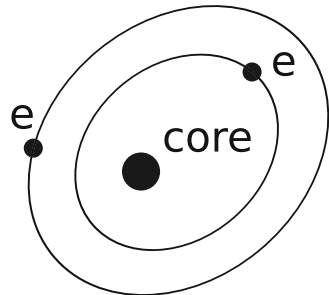
$$\nu = R \left(\frac{1}{n^2} - \frac{1}{k^2} \right), \quad (4.2.1)$$

with positive integers n and k . Here, R denotes the Rydberg constant and $k = 2$ holds in case of the Balmer lines. For the energy we have the relation:

$$hv = \hbar\omega = E_k - E_n, \quad (4.2.2)$$

where $E_n = -\frac{me^4}{2\hbar^2 n^2} = -\frac{1}{2n^2} mc^2 \alpha^2$ for the hydrogen atom. m is the atomic mass and $\alpha \equiv \frac{e^2}{\hbar c}$ denotes Sommerfeld's fine-structure constant, with the speed of light c , electron charge e and Planck constant \hbar . This experimental law can also be derived from the action integral along a closed trajectory $q(t)$, i.e. along a quantized torus, see Sect. 3.4, which is described by the atomic model after Bohr and Sommerfeld

Fig. 4.1 Simple model of the helium atom as an example for a non-integrable three-body problem with core and two electrons denoted by e. For generic initial conditions the classical dynamics can be chaotic [11]



$$S(E) = \oint pdq = hn = 2\pi\hbar n, \quad n \in \mathbb{N}. \quad (4.2.3)$$

It is also possible to derive the Bohr-Sommerfeld quantization from the WKB approximation which is considered in detail in Sect. 4.2.2.

The mentioned quantization condition was postulated in 1915 and belongs to the so-called “old quantum theory”. This old quantum theory does not really constitute a consistent theory but is instead a collection of heuristic results from the early twentieth century. These results, achieved before the advent of a full quantum theory, which were able to describe the phenomenon of discrete energy levels for systems as simple as the hydrogen atom. Today, the old quantum theory can be interpreted as giving low order quantum corrections to classical mechanics and is thus known as the simplest version of a semiclassical theory.

Already from a look at the quantization condition (4.2.3), one can see that the formulation relies on assumptions that will necessarily break down in more complex (in the sense of more degrees of freedom) systems:

- This approach does not work for non-integrable systems. The formulation relies on the existence of closed trajectories that fulfill the quantization condition. Einstein noticed this already in his pioneering paper from 1917 [10].
- This means that many-body problems, e.g. the three-body helium atom (c.f. Fig. 4.1), cannot be analyzed with this method, see also our discussion in Sect. 1.2. Separable many-body systems may be quantized using a proper extension of WKB presented in Sect. 4.2.3.

4.2.2 Wentzel–Kramer–Brillouin–Jeffreys Approximation

In this section we present a famous and powerful semiclassical approximation method which was formulated by Wentzel, Kramers, and Brillouin in 1926. Jeffreys had already found a general method for the approximation of linear differential equations of second order in 1923. It treats the solution of the Schrödinger equation in the semiclassical limit, i.e. for particles with large momenta and consequently short

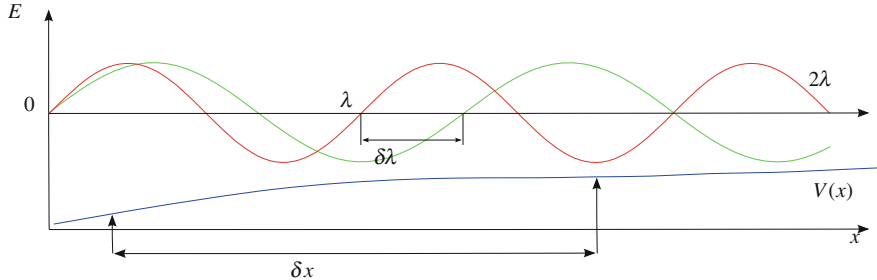


Fig. 4.2 The WKB approximation is valid in the range of short wavelengths, i.e. the potential varies slowly with respect to the particle wavelength, i.e. $\delta x \gg \delta\lambda$

de Broglie wave lengths. In other words, the action of the particle must be large compared to \hbar . As mentioned in Sect. 1.3, the semiclassical limit $\hbar \rightarrow 0$ intends exactly this. It stands in analogy to the transition from wave-optical to geometric optics which results from $\lambda \ll L$ (in short “ $\lambda \rightarrow 0$ ”), where λ denotes the wave length of the light and L is the characteristic length of the optic system. The development of the method roots also in the work of Liouville, Green, Stokes, and Rayleigh in connection with geometric and wave optics. Further historical information may be found in Appendix 11 of [12].

In case of one-dimensional problems, the approximation is valid if the de Broglie wave length varies slowly over distances of its order. In other words the change of the potential is small against the particle wave length: $\delta\lambda \ll \lambda \ll \delta x$. δx is the characteristic distance for which there is no significant change of the potential. This is illustrated in Fig. 4.2.

The most important applications of the WKB method are the calculation of semiclassical approximations of eigenenergies of bound states and of tunneling rates through potential barriers. Examples will be shown below.

4.2.2.1 Derivation of WKB Wave Functions

We start with the *stationary* Schrödinger equation describing the one-dimensional motion of a particle in an external potential

$$\underbrace{\left[-\frac{\hbar^2}{2m} \frac{d^2}{dx^2} + V(x) \right]}_{=\hat{H}} \psi(x) = E\psi(x) \quad (4.2.4)$$

The WKB ansatz leads to an analytical solution for the approximation in the limit “ $\hbar \rightarrow 0$ ”, i.e. $\hbar \ll S$ for typically classical actions S of the system. In order to find an approximate solution of Eq. (4.2.4), we start with the following ansatz for the wave function

$$\psi(x) = \exp\left(\frac{i}{\hbar}g(x)\right) \quad (4.2.5)$$

$$\Rightarrow \frac{d^2\psi(x)}{dx^2} = \left[\frac{i}{\hbar} \frac{d^2g(x)}{dx^2} - \frac{1}{\hbar^2} \left(\frac{dg(x)}{dx} \right)^2 \right] e^{\frac{i}{\hbar}g(x)} \quad (4.2.6)$$

$$\Rightarrow -\frac{i\hbar}{2m} \frac{d^2g(x)}{dx^2} + \frac{1}{2m} \left(\frac{dg(x)}{dx} \right)^2 + V(x) = E. \quad (4.2.7)$$

Here $g(x)$ is assumed to be a complex valued function for $x \in \mathbb{R}$. The first term in Eq. (4.2.7) is a correction term proportional to \hbar , whilst the \hbar -independent part of the equation can be compared to the classical Hamilton-Jacobi equation (3.3.25) from Sect. 3.3.4. From Eq. (4.2.7) we may write

$$\frac{dg(x)}{dx} = \pm \sqrt{p^2(x) + i\hbar \frac{d^2g(x)}{dx^2}}, \quad (4.2.8)$$

where $p(x) \equiv \sqrt{2m(E - V(x))}$ denotes the classical momentum. The solution in lowest order of \hbar is given by

$$\frac{dg(x)}{dx} = \pm p(x) + O(\hbar) \quad (4.2.9)$$

$$\Rightarrow \frac{d^2g(x)}{dx^2} = \pm \frac{dp(x)}{dx} + O(\hbar) = \mp \frac{m}{\sqrt{p(x)}} \frac{dV(x)}{dx} + O(\hbar). \quad (4.2.10)$$

An improved solution can be derived by putting (4.2.10) into (4.2.8) to obtain

$$\frac{dg(x)}{dx} = \pm \sqrt{p^2(x) + i\hbar \frac{d^2g(x)}{dx^2}} \approx \pm p(x) + i\hbar \frac{1}{2p^2(x)} \frac{dp(x)}{dx} + O(\hbar^2). \quad (4.2.11)$$

Here, we expanded the square root in the approximation

$$\left| \frac{1}{p^2} \frac{dp(x)}{dx} \right| \ll \frac{1}{\hbar}. \quad (4.2.12)$$

The latter condition is equivalent to

$$\left| \frac{d\bar{\lambda}}{dx} \right| \ll 1, \quad (4.2.13)$$

with the de Broglie wave length of the particle

$$\bar{\lambda} \equiv \frac{\hbar}{p}. \quad (4.2.14)$$

The latter condition is the semiclassical condition, and it gives the range when our approximation is valid. It can be rewritten as follows, with

$$\frac{dp}{dx} = -\frac{m}{p} \frac{dV}{dx}, \quad (4.2.15)$$

$$\left| \frac{d\bar{\lambda}}{dx} \right| \ll 1 \Rightarrow \frac{m\hbar}{p^3} \left| \frac{dV}{dx} \right| \ll 1. \quad (4.2.16)$$

This summarizes what we said earlier. Consequently, the semiclassical approximation will not be applicable when the momentum is too small. Particularly, it is not directly applicable at the turning points of the classical dynamics.

Going on with our solution, it follows that

$$g(x) = \pm \int_{x_0}^x p(x') dx' + \frac{i\hbar}{2} \ln(p(x)) + C + O(\hbar^2) \quad (4.2.17)$$

$$\Rightarrow \psi(x) = \frac{A}{\sqrt{p(x)}} \exp \left[\pm \frac{i}{\hbar} \int_{x_0}^x p(x') dx' \right]. \quad (4.2.18)$$

The following relation corresponds to the *classically allowed* region, see Fig. 4.3a: $p(x') > 0 \forall x' \in [x_0, x] \Leftrightarrow V(x') < E \forall x' \in [x_0, x]$. Consequently, the general WKB solution in this region is given by

$$\psi(x) = \frac{1}{\sqrt{p(x)}} \left(A \exp \left[\frac{i}{\hbar} \int_{x_0}^x p(x') dx' \right] + B \exp \left[-\frac{i}{\hbar} \int_{x_0}^x p(x') dx' \right] \right). \quad (4.2.19)$$

The general WKB solution in the *classically forbidden* region, where $E < V(x') \forall x' \in [x_0, x]$ yields

$$\psi(x) = \frac{1}{\sqrt{\tilde{p}(x)}} \left(C \exp \left[-\frac{1}{\hbar} \int_{x_0}^x \tilde{p}(x') dx' \right] + D \exp \left[\frac{1}{\hbar} \int_{x_0}^x \tilde{p}(x') dx' \right] \right). \quad (4.2.20)$$

Here, we define $\tilde{p}(x) \equiv \sqrt{2m(V(x) - E)}$. The wave function in this region is of purely quantum mechanical origin and can be used to describe, e.g., tunneling processes.

An obvious problem occurs near the classical turning points, c.f. Fig. 4.3a. In the limit $E \rightarrow V(x)$, the momentum vanishes, that means that the de Broglie wave length diverges. As $p, \tilde{p} \rightarrow 0$, the wavefunction from our ansatz becomes singular. The probability $|\psi(x)|^2 dx$ that the particle is located at $x' \in [x, x + dx]$ is proportional to the absolute value of $p(x)^{-1}$, meaning that the particle rests only a short time at

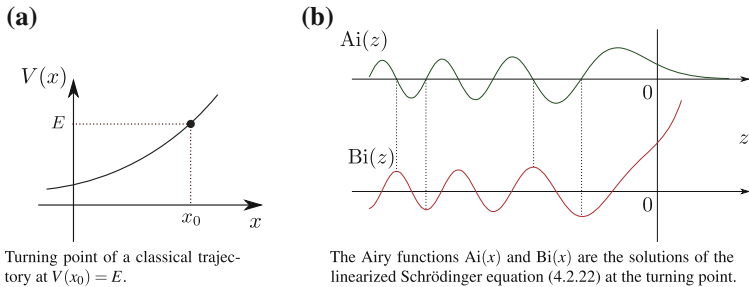


Fig. 4.3 The naive WKB approximation diverges close to the turning points of the classical trajectory as seen in (a). This problem can be solved by approximating the solution close to these turning points by the Airy functions sketched in (b)

a certain place where $p(x)$ is large, i.e. where it moves fast. On the other hand, in accordance with the classical intuition, the particle can most likely be found close to the turning points where it is the slowest and spends most of the time.

There are several ways to solve the turning point problem. An excellent way is presented in [2], where the singularity is encircled in the complex plane. Here, we follow the simpler and more standard approach and consider a linear approximation of the potential close to the turning points. Naturally, this approximation will produce good results only for smooth potentials. We expand

$$x \approx x_0 : \quad V(x) \approx \underbrace{V(x_0)}_{=E} + \underbrace{\alpha}_{=\frac{dV(x_0)}{dx}} (x - x_0) + O\left[(x - x_0)^2\right] \quad (4.2.21)$$

The Schrödinger equation for the linearized problem reads

$$-\frac{\hbar^2}{2m} \frac{d^2\psi(x)}{dx^2} + \alpha(x - x_0)\psi(x) = 0. \quad (4.2.22)$$

With a change of variables,

$$z^3 = \frac{2m\alpha}{\hbar^2}(x - x_0), \quad (4.2.23)$$

the equation can be rewritten in the following form

$$\frac{d^2\psi(z)}{dz^2} = z\psi(z). \quad (4.2.24)$$

The last equation is known as the Airy equation, its solutions are the Airy functions $\text{Ai}(z)$ and $\text{Bi}(z)$ [13]. This yields

$$\psi(x) = a \text{Ai}\left[\sqrt[3]{\frac{2m\alpha}{\hbar^2}}(x - x_0)\right] + b \text{Bi}\left[\sqrt[3]{\frac{2m\alpha}{\hbar^2}}(x - x_0)\right], \quad (4.2.25)$$

with real and constant coefficients a and b .

In the following, we discuss the asymptotic behavior of the Airy functions $\text{Ai}(z)$ and $\text{Bi}(z)$:

$$\begin{aligned}\text{Ai}(z) &= \frac{1}{\sqrt{\pi} \sqrt{|z|}} \begin{cases} \frac{1}{2} e^{-\frac{2}{3} z^{\frac{3}{2}}}, & z \rightarrow +\infty \\ \cos \left(\frac{2}{3} |z|^{\frac{3}{2}} - \frac{\pi}{4} \right), & z \rightarrow -\infty \end{cases} \\ \text{Bi}(z) &= \frac{1}{\sqrt{\pi} \sqrt{|z|}} \begin{cases} e^{\frac{2}{3} z^{\frac{3}{2}}}, & z \rightarrow +\infty \\ -\sin \left(\frac{2}{3} |z|^{\frac{3}{2}} - \frac{\pi}{4} \right), & z \rightarrow -\infty. \end{cases} \quad (4.2.26)\end{aligned}$$

Let us now consider what this means for the wave function $\psi(x)$ close to a classical turning point. We want to look at the limit $\hbar \rightarrow 0$, where the argument z of the Airy functions will tend to $\pm\infty$. We can thus replace the Airy functions in (4.2.25) by their asymptotic form given in (4.2.26). The wave function $\psi(x)$ close to the turning point thus has to have the form

$$\psi(x) \xrightarrow{\hbar \rightarrow 0} \frac{1}{\sqrt{\pi} \sqrt{k_0|x-x_0|}} \begin{cases} \frac{a}{2} e^{-\frac{2}{3}(k_0(x-x_0))^{\frac{3}{2}}} + b e^{\frac{2}{3}(k_0(x-x_0))^{\frac{3}{2}}}, & x > x_0 \\ a \cos \left(\frac{2}{3}(k_0(x_0-x))^{\frac{3}{2}} - \frac{\pi}{4} \right) - b \sin \left(\frac{2}{3}(k_0(x_0-x))^{\frac{3}{2}} - \frac{\pi}{4} \right), & x < x_0, \end{cases} \quad (4.2.27)$$

where the new constant $k_0 \equiv \sqrt[3]{\frac{2m\alpha}{\hbar^2}}$ denotes the wave number. We see already that we obtain oscillating, wave-like solutions in the classically allowed region, and exponential behavior inside the classically forbidden region. We can now compare this wave function to the results of the WKB ansatz in the classically allowed, Eq. (4.2.19), as well as classically forbidden region, Eq. (4.2.20). Close to the turning point, the value of $\int p(x)dx$ takes the form:

Case $x < x_0$:

$$p(x) = \sqrt{2m(E - V(x))} \xrightarrow{x \approx x_0} \sqrt{2m\alpha(x_0 - x)} \quad (4.2.28)$$

$$\Rightarrow \int_x^{x_0} p(x')dx' \approx \frac{2}{3} \sqrt{2m\alpha(x_0 - x)^3} \quad (4.2.29)$$

Case $x > x_0$:

$$\tilde{p}(x) = \sqrt{2m(V(x) - E)} \xrightarrow{x \approx x_0} \sqrt{2m\alpha(x - x_0)} \quad (4.2.30)$$

$$\Rightarrow \int_{x_0}^x \tilde{p}(x')dx' \approx \frac{2}{3} \sqrt{2m\alpha(x - x_0)^3}. \quad (4.2.31)$$

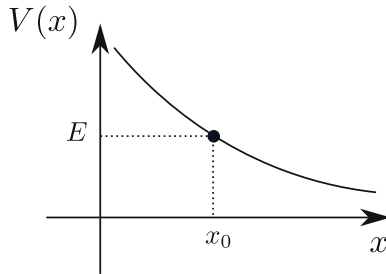


Fig. 4.4 Left turning point of a classical trajectory at $V(x_0) = E$ in analogy to Fig. 4.3a

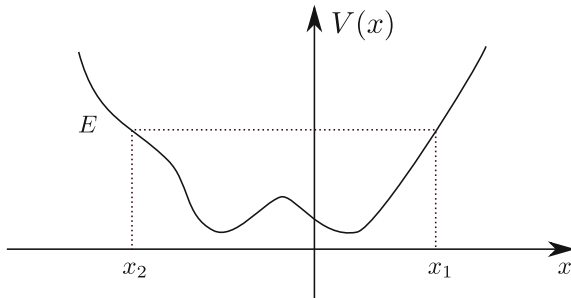


Fig. 4.5 A one-dimensional bound potential with two turning points for an energy E

This leads to an improved WKB ansatz that replaces the equations (4.2.19) and (4.2.20)

$$\psi(x) = \begin{cases} \frac{1}{\sqrt{p(x)}} \left(A \cos \left[\frac{1}{\hbar} \int_x^{x_0} p(x') dx' - \frac{\pi}{4} \right] + B \sin \left[\frac{1}{\hbar} \int_x^{x_0} p(x') dx' - \frac{\pi}{4} \right] \right), & x < x_0 \\ \frac{1}{\sqrt{\tilde{p}(x)}} \left(C \exp \left[-\frac{1}{\hbar} \int_{x_0}^x \tilde{p}(x') dx' \right] + D \exp \left[\frac{1}{\hbar} \int_{x_0}^x \tilde{p}(x') dx' \right] \right), & x > x_0. \end{cases} \quad (4.2.32)$$

By comparison with the solution (4.2.27) at the right turning point, it follows immediately that $C = \frac{A}{2}$ and $D = -B$. Analogously, one derives the solutions at the left turning point, see Fig. 4.4, from the matching conditions there by just replacing

$$\int_x^{x_0} p dx \rightarrow \int_{x_0}^x p dx \quad (4.2.33)$$

in the discussion above. To better illustrate the procedure we now look at some explicit examples.

4.2.2.2 Example 1: Bound States in a Potential $V(x)$

A bound particle in one-dimensional must have two classical turning points. According to the WKB method from above one has to consider a left turning point x_1 as well as a right turning point x_2 , see Fig. 4.5. We already know the form of the WKB ansatz, Eq. (4.2.32), for one turning point that our ansatz for the system with two turning points takes the following form (at fixed energy E):

$$\psi(x) = \begin{cases} \frac{1}{\sqrt{\tilde{p}(x)}} \left(C_1 e^{-\tilde{\sigma}_1(x)/\hbar} + D_1 e^{\tilde{\sigma}_1(x)/\hbar} \right), & x < x_1 \\ \frac{1}{\sqrt{p(x)}} \left(A_1 \cos \left[\sigma_1(x)/\hbar - \frac{\pi}{4} \right] + B_1 \sin \left[\sigma_1(x)/\hbar - \frac{\pi}{4} \right] \right) \\ \stackrel{!}{=} \frac{1}{\sqrt{p(x)}} \left(A_2 \cos \left[\sigma_2(x)/\hbar - \frac{\pi}{4} \right] + B_2 \sin \left[\sigma_2(x)/\hbar - \frac{\pi}{4} \right] \right), & x_1 < x < x_2 \\ \frac{1}{\sqrt{\tilde{p}(x)}} \left(C_2 e^{-\tilde{\sigma}_2(x)/\hbar} + D_2 e^{\tilde{\sigma}_2(x)/\hbar} \right), & x > x_2, \end{cases} \quad (4.2.34)$$

where the σ 's are defined as

$$\tilde{\sigma}_1(x) \equiv \int_x^{x_1} \tilde{p}(x') dx' \quad \sigma_1(x) \equiv \int_{x_1}^x p(x') dx' \quad (4.2.35)$$

$$\tilde{\sigma}_2(x) \equiv \int_{x_2}^x \tilde{p}(x') dx' \quad \sigma_2(x) \equiv \int_{x_2}^x p(x') dx'. \quad (4.2.36)$$

From Eq. (4.2.34) we learn the following:

- Matching the coefficients at each individual turning point (in accordance with Eq. (4.2.27)) results in

$$C_1 = \frac{A_1}{2}, \quad D_1 = -B_1 \quad (4.2.37)$$

$$C_2 = \frac{A_2}{2}, \quad D_2 = -B_2. \quad (4.2.38)$$

- Since the wave function has to be normalizable, the exponentially growing parts in the left and right forbidden regions must be zero, hence

$$D_1 = D_2 = 0, \quad B_1 = B_2 = 0. \quad (4.2.39)$$

- For the region $x_1 < x < x_2$, inside the classical zone the two wave functions must coincide:

$$A_1 \cos \left(\frac{\sigma_1(x)}{\hbar} - \frac{\pi}{4} \right) \stackrel{!}{=} A_2 \cos \left(\frac{\sigma_2(x)}{\hbar} - \frac{\pi}{4} \right). \quad (4.2.40)$$

The latter relation can now be used to derive a quantization conditions, similar to the Bohr-Sommerfeld ansatz from Eq. (4.2.3). For this we split up the momentum integral in the following way

$$\int_{x_1}^x p(x') dx' = \underbrace{\int_{x_1}^{x_2} p(x') dx'}_{\equiv \frac{S}{2}} - \int_x^{x_2} p(x') dx' \quad (4.2.41)$$

$$\Leftrightarrow \sigma_1(x) = \frac{S}{2} - \sigma_2(x). \quad (4.2.42)$$

This yields

$$A_1 \cos \left[\frac{\sigma_1}{\hbar} - \frac{\pi}{4} \right] = A_1 \cos \left[\left(\frac{S}{2\hbar} - \frac{\pi}{2} \right) - \left(\frac{\sigma_2}{\hbar} - \frac{\pi}{4} \right) \right] \quad (4.2.43)$$

$$= A_1 \cos \left(\frac{S}{2\hbar} - \frac{\pi}{2} \right) \cos \left(\frac{\sigma_2}{\hbar} - \frac{\pi}{4} \right) + A_1 \sin \left(\frac{S}{2\hbar} - \frac{\pi}{2} \right) \sin \left(\frac{\sigma_2}{\hbar} - \frac{\pi}{4} \right). \quad (4.2.44)$$

Using Eq. (4.6.6), we know that the right hand part of Eq. (4.2.43) has to be equal to $A_2 \cos \left(\frac{\sigma_2}{\hbar} - \frac{\pi}{4} \right)$ for all values of x . This can only non-trivially be fulfilled if $A_1 = A_2$ and

$$\begin{cases} \sin \left(\frac{S}{2\hbar} - \frac{\pi}{2} \right) = 0 \\ \cos \left(\frac{S}{2\hbar} - \frac{\pi}{2} \right) = 1 \end{cases} \Leftrightarrow \frac{S}{2\hbar} - \frac{\pi}{2} = n\pi \quad (n \in \mathbb{N}_0) \quad (4.2.45)$$

$$\Leftrightarrow \int_{x_1}^{x_2} p(x) dx = \pi\hbar \left(n + \frac{1}{2} \right). \quad (4.2.46)$$

The latter can also be written in the following form

$$S \equiv \oint p dx = 2\pi\hbar \left(n + \frac{1}{2} \right) \quad (n \in \mathbb{N}_0), \quad (4.2.47)$$

which justifies the quantization condition in Eq. (4.2.3). Equation (4.2.47) also includes an additional term with respect to the previous Bohr-Sommerfeld condition, allowing only a minimal action value of $\hbar/2$. To motivate this constant minimal contribution, we note that the new expression in Eq. (4.2.47) contains an implicit equation for the eigenenergies of the system. As an example we mention the harmonic oscillator with the well-known potential $V(x) = \frac{1}{2}m\omega^2x^2$. The classical

turning points are obtained from conservation of energy

$$E = V(x_{1,2}) \Rightarrow x_{1,2} = \pm \sqrt{\frac{2E}{m\omega^2}}. \quad (4.2.48)$$

The positive sign corresponds to the first and the negative sign to the second turning point. For the action integral from one turning point to the other we find

$$\int_{x_1}^{x_2} p(x) dx = \int_{x_1}^{x_2} \sqrt{2m(E - \frac{1}{2}m\omega^2 x^2)} dx = \pi \frac{E}{\omega} \quad (4.2.49)$$

$$\Rightarrow E_{\text{HO}}(n) = \hbar\omega \left(n + \frac{1}{2} \right) \quad (n \in \mathbb{N}_0). \quad (4.2.50)$$

Here our approximation not only gives the exact quantum mechanical eigenvalues but also the zero point energy, the energy of the quantum mechanical ground state $E_{\text{HO}}^{\text{q.m.}}(0) = \frac{1}{2}\hbar\omega$. Within our WKB approach, the minimal energy is a consequence of the phase matching condition leading to a phase $\frac{\pi}{4}$, which comes from the Airy functions in Eq. (4.2.26).

4.2.2.3 Example 2: Tunneling Decay

Another important application of the WKB method is the computation of tunneling rates of particles in an excited, or metastable state. An example is a simple model for the radioactive alpha decay, which occurs due to quantum tunneling. The particle couples from one classically allowed region to another one in which it is then asymptotically free. This situation is sketched in Fig. 4.6. For the action we find in this case:

$$\hbar\sigma = \int_{r_1}^{r_2} \sqrt{2m \left(\frac{e^2}{r} - E \right)} dr = \sqrt{2mE} \int_{r_1}^{r_2} \sqrt{\left(\frac{r_2}{r} - 1 \right)} dr \quad (4.2.51)$$

$$= \sqrt{2mE} \left[r_2 \arccos \left(\sqrt{\frac{r_1}{r_2}} \right) - \sqrt{r_1(r_2 - r_1)} \right]. \quad (4.2.52)$$

Here, we used $E = V(r_2) = \frac{e^2}{r_2}$. The tunneling probability at each hit at $r = r_1$ is

$$T \approx e^{-2\sigma}. \quad (4.2.53)$$

Giving a mean oscillation frequency (or “knocking” frequency) of the particle in the left potential well of $v/2r_1$ ($v = \sqrt{E/2}$ is its classical speed), we obtain for the tunneling rate:

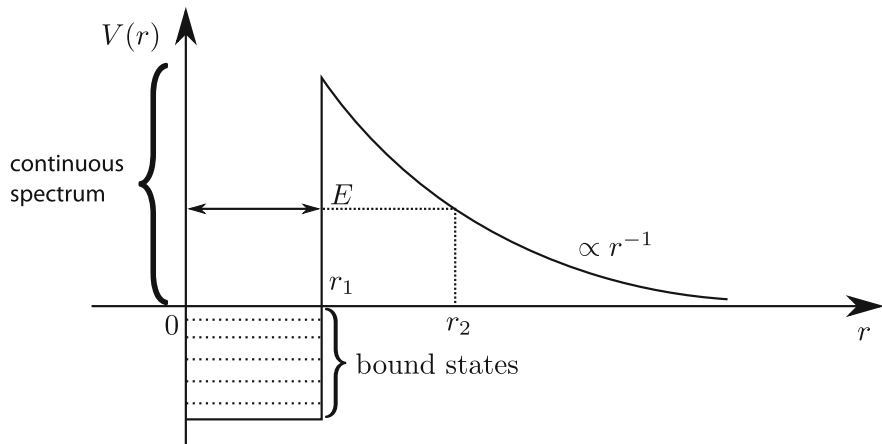


Fig. 4.6 Model for a quantum particle with energy $E > 0$ which can decay via a tunneling process from the energy well

$$\Gamma \approx \frac{v}{2r_1} e^{-2\sigma}. \quad (4.2.54)$$

Then we can define the lifetime of the exponential decay $\propto e^{-t/\tau}$ as the inverse decay rate

$$\tau \approx \Gamma^{-1}. \quad (4.2.55)$$

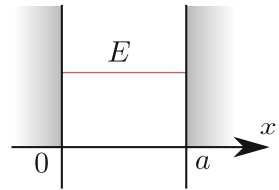
4.2.2.4 Example 3: Particle in a Box

We study a particle with energy $E > V_0$ in the potential, see Fig. 4.7,

$$V(x) = \begin{cases} V_0 & 0 < x < a \\ \infty & \text{otherwise.} \end{cases} \quad (4.2.56)$$

At the turning point the momentum changes sign. Consequently, we obtain an additional phase factor with respect to the argument of Eq. (4.6.6), giving a total phase of $\pi/2$ for the reflection. In this example, a linearisation of the potential around the turning point is not necessary since the wave function and therefore the probability density at the turning point is exactly zero, i.e. $\psi(0) = \psi(a) \equiv 0$, due to the hard wall boundary conditions. This only allows sin function solutions and is directly related to the phase change just mentioned: $\cos\left(\frac{\sigma_2}{2} - \frac{\pi}{2}\right) \stackrel{!}{=} \sin\left(\frac{\sigma_2}{\hbar}\right)$. The action as a function of the energy is computed from

Fig. 4.7 A quantum particle in a box with constant potential V_0 in the box and infinitely high walls at the boundaries. Solutions obviously exist only for energies $E > V_0$



$$S(E) = \oint p(x)dx \stackrel{!}{=} h(n+1) \quad (n \in \mathbb{N}_0). \quad (4.2.57)$$

From this it follows using that $p = \sqrt{2mE} = \text{const.}$ and $V_0 = 0$

$$p \cdot a \cdot 2 = h(n+1) = 2\pi\hbar(n+1) \quad (4.2.58)$$

$$E(n) = \frac{p^2}{2m} = \frac{1}{2m} \left(\frac{\pi\hbar}{a} \right)^2 (n+1)^2. \quad (4.2.59)$$

The value

$$E(n=0) = \frac{1}{2m} \left(\frac{\pi\hbar}{a} \right)^2 \quad (4.2.60)$$

is the zero-point energy of the system. We note that here, the WKB method again yields the exact quantum mechanical spectrum, as in the case of the harmonic oscillator. Though almost obvious for this simple problem, there is also a simple argument to understand why we find the exact result. The eigenfunction of this system are exactly sin functions: $\psi_n(x) = \sqrt{\frac{2}{a}} \sin \frac{n\pi x}{a}$. The probability to find the particle in the interval $A = [x - \frac{dx}{2}, x + \frac{dx}{2}] \subseteq [0, a]$ is given by

$$P_{\text{qm}}^{(n)}(A) = |\psi_n(x)|^2 dx. \quad (4.2.61)$$

For large quantum numbers

$$\lim_{n \rightarrow \infty} P_{\text{qm}}^{(n)} \equiv P_{\text{qm}}(A), \quad (4.2.62)$$

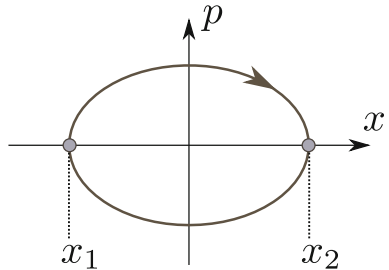
the classical P_{cl} and quantum probabilities P_{qm} are indeed identical

$$P_{\text{qm}}(A) = \frac{dx}{L} = P_{\text{cl}}(A). \quad (4.2.63)$$

4.2.2.5 Summary of the One Dimensional WKB Quantization

From the examples just introduced we can deduce the following general rule

Fig. 4.8 Trajectory of a classical integrable system in one dimension. The closed curves lead to ambiguities in the projections onto the x -axis at the turning points



$$\oint p(x)dx = 2\pi\hbar(n + \beta_1 + \beta_2) \quad (n \in \mathbb{N}_0). \quad (4.2.64)$$

Here, the β_i with $i = 1, 2$ denote the *Morse index* which is a special case of the Maslov index for manifolds [14]. For the β_i we have, see the above examples,

$$\beta_i = \begin{cases} \frac{1}{4} & \text{for } \left| \frac{dV(x)}{dx} \right|_{x=x_i} < \infty, \text{ soft reflection} \\ \frac{1}{2} & \text{for } \left| \frac{dV(x)}{dx} \right|_{x=x_i} = \infty, \text{ hard reflection.} \end{cases} \quad (4.2.65)$$

The physical origin of the Morse indices lies in the problem of the turning points. There, the naive WKB ansatz diverges, which has to be dealt with somehow. The problem essentially comes from the fact that the semiclassical quantization has to project a classical object from phase space into position space to arrive at a reasonable wavefunction. Projections of the phase space trajectory onto configuration space or the x -axis become singular exactly at the turning points where

$$\frac{\partial x}{\partial p} = 0 \quad \text{or} \quad \frac{\partial p}{\partial x} = " \pm \infty ", \quad (4.2.66)$$

as is seen also in Fig. 4.8. In higher dimensional systems, the turning points generalize to focus points or caustics where bundles of trajectories meet in the projected space. For further details consult Appendix 11 in [12]. We will come back to this problem in Sect. 4.2.4 when discussing similar singularities arising from a stationary phase approximation.

As we have seen, the WKB approximation provides many advantages. It yields the exact spectra of the harmonic oscillator and box potentials with perfectly reflecting walls. The comparison between the obtained eigenenergies E_n^{WKB} and the true quantum values $E_n^{\text{q.m.}}$ generally becomes the better the higher the energy quantum number n due to Bohr's correspondence principle. However, the WKB method cannot be directly applied for higher dimensional problems. Considering separable higher dimensional systems, the trajectories in phase space are not necessarily closed. This

makes it necessary to well define a generalized version of the quantization conditions including the various dimensions which we will do in the following.

4.2.3 Einstein–Keller–Brillouin Quantization

The following quantization principle EKB (in honor of Einstein, Brillouin and Keller) is applicable to higher dimensional integrable systems. By a canonical transformation we solve the Hamilton-Jacobi equation and write the Hamiltonian in action-angle variables, c.f. Sect. 3.3.4, for a classical Hamiltonian

$$H(\mathbf{q}, \mathbf{p}) \rightarrow \tilde{H}(\mathbf{I}, \phi) = \tilde{H}(\mathbf{I}). \quad (4.2.67)$$

In d dimensions the actions corresponding to each dimension are given by

$$I_i = \frac{1}{2\pi} \oint_{C_i} \mathbf{p} d\mathbf{q} = \hbar \left(n_i + \frac{\mu_i}{4} \right) \quad i = 1, \dots, d. \quad (4.2.68)$$

The C_i denote *elementary* loops that span the d -torus. Neither are they null-homotopic, i.e. they cannot be transformed continuously into a point (a constant function), nor two loops C_1 and C_2 are homotopic. This means, that they cannot be converted continuously into each other. A graphical representation of tori in one and two dimensions is shown in Fig. 4.9a, b, c.f. also our discussion of integrable systems in Sect. 3.4. For the Morse index μ_i it holds, as above in Eq. (4.2.65), that

$$\mu_i = \text{number of “soft” reflexions} + 2 \cdot \text{number of “hard” reflexions}, \quad (4.2.69)$$

within each closed loop C_i . As in the WKB case, Eq. (4.2.68) leads to an implicit quantization condition for the energy levels $E_{n_1, \dots, n_d}^{\text{EKB}}$, with d quantum numbers $\{n_i\}_{i=1, \dots, d}$.

4.2.3.1 Examples for EKB Quantization

As an application of the EKB quantization we study a rectangular billiard in two dimensions (c.f. Fig. 4.10). Its length is denoted by a and its width by b . The potential is given by

$$V(x, y) = \begin{cases} 0, & (x, y) \in (0, a) \times (0, b) \\ \infty, & \text{otherwise.} \end{cases} \quad (4.2.70)$$

The conserved quantities of this system are the absolute values of the momenta in x - and y -direction $|p_x|$ and $|p_y|$. At each reflexion the momentum components change as follows

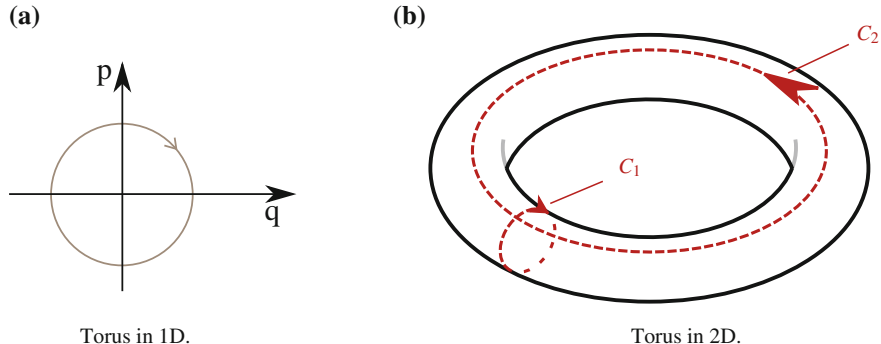
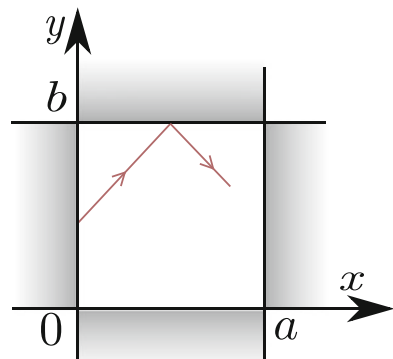


Fig. 4.9 Representation of a torus in one dimension (a) and in two dimension where the two elementary loops C_1 and C_2 are not homotopic to each other (b)

Fig. 4.10 A rectangular billiard is a standard example for the EKB-quantization and homeomorphic to a 2D torus. It represents a completely separable box potential and the EKB-method yields its exact quantum mechanical energy spectrum



$$p_x \mapsto -p_x \quad (4.2.71)$$

$$p_y \mapsto -p_y, \quad (4.2.72)$$

implying that the product of the two momentum changes is always positive:

$$p_x dq_x > 0 \quad (4.2.73)$$

$$p_y dq_y > 0. \quad (4.2.74)$$

One can see that the motion is actually topologically equivalent to the one on a two dimensional torus as shown in Fig. 4.9b.

For the corresponding action variables we find using Eq. (4.2.68)

$$I_{x,y} = \frac{1}{2\pi} \oint_{C_{x,y}} p_{x,y} dq_{x,y} = \begin{cases} \frac{a}{\pi} |p_x| \\ \frac{b}{\pi} |p_y|. \end{cases} \quad (4.2.75)$$

Following Eq. (4.2.67) we get for the Hamiltonian

$$H = \frac{1}{2m}(p_x^2 + p_y^2) = E \quad (4.2.76)$$

$$\Rightarrow \tilde{H} = \frac{\pi^2}{2m} \left(\frac{I_x^2}{a^2} + \frac{I_y^2}{b^2} \right). \quad (4.2.77)$$

Due to axial symmetry and the two hard reflexion for each of the two elementary loops the Morse index and, consequently, the quantization condition reads

$$\mu_{x,y} = 4 \Rightarrow I_{x,y} = \hbar(n_{x,y} + 1). \quad (4.2.78)$$

From this and Eq. (4.2.76) we can calculate the semiclassical energy spectrum

$$E_{n_x,n_y}^{\text{EKB}} = \frac{\pi^2 \hbar^2}{2m} \left(\frac{(n_x + 1)^2}{a^2} + \frac{(n_y + 1)^2}{b^2} \right), \quad n_{x,y} \in \mathbb{N}. \quad (4.2.79)$$

We conclude that the rectangular billiard constitutes a separable box potential and the EKB quantization reproduces indeed the exact quantum mechanical energy spectrum.

A further example for the EKB method in three dimensions is offered by the Kepler problem whose radial potential reads

$$V(r \equiv |\mathbf{r}|) = -\frac{\alpha}{r}, \quad \alpha \in \mathbb{R}_+. \quad (4.2.80)$$

This problem is classically solved by a separation ansatz for the actions corresponding to the independent constants of motion [15], see Sects. 3.3.4 and 3.4 and the problem 3.5. Then the corresponding action integrals are straightforwardly quantized following Eq. (4.2.68) to determine the eigenspectrum of bound states. We leave it to the reader as problem 4.3.

We finish with an important consequence of the EKB-quantization. From the quantization condition (4.2.68) we obtain

$$\oint_{C_j} I_j d\theta_j = 2\pi I_j = 2\pi \hbar \left(n_j + \frac{\mu_j}{4} \right). \quad (4.2.81)$$

The quantization is done with respect to cuts in the I_j - θ_j -planes of the multidimensional volumes $\oint \mathbf{Id}\theta = \oint \mathbf{pdq}$. This allows one to compare the volume of phase space which the quantized states occupy. It is obviously related to the total volume $N(2\pi\hbar)^d$, which N semiclassical states have according to (4.2.81). This is equivalent to one quantum state per Planck cell $(2\pi\hbar)^d$. This reflects Heisenberg's uncertainty principle that two conjugated variables cannot be simultaneously determined with a precision better than $2\pi\hbar$ [2, 3].

4.2.4 Semiclassical Wave Function for Higher Dimensional Integrable Systems

Next to the EBK condition for the energy spectra, we can also compute corresponding semiclassical wavefunctions. The approach used in Sect. 4.2.2 only works for one-dimensional systems but breaks down for higher dimensions. Here a similar but generalized approach will be presented.

We start, again, with the stationary Schrödinger equation:

$$\left(\frac{-\hbar^2}{2m} \nabla^2 + V(\mathbf{r}) \right) \psi(\mathbf{r}) = E \psi(\mathbf{r}) \quad (4.2.82)$$

and use the following ansatz for the wave function:

$$\psi(\mathbf{r}) = A(\mathbf{r}) e^{\frac{i}{\hbar} R(\mathbf{r})}. \quad (4.2.83)$$

In this case, the amplitude A and the phase R are both real-valued functions of \mathbf{r} (unlike the complex function $g(x)$ from Sect. 4.2.2). Expressing the second derivative of $\psi(\mathbf{r})$ in terms of these real-valued functions we obtain

$$\nabla \psi = (\nabla A) e^{\frac{i}{\hbar} R} + \left(\frac{i}{\hbar} \nabla R \right) A e^{\frac{i}{\hbar} R} \quad (4.2.84)$$

$$\begin{aligned} \nabla^2 \psi &= \left(\nabla^2 A + 2 \underbrace{\frac{i}{\hbar} \nabla R \cdot \nabla A + \frac{i}{\hbar} \left(\nabla^2 R \right) A}_{= \frac{i}{\hbar} A \nabla (A^2 \nabla R)} - \frac{1}{\hbar^2} (\nabla R)^2 A \right) e^{\frac{i}{\hbar} R}. \end{aligned} \quad (4.2.85)$$

Inserting this into the stationary Schrödinger equation (4.2.82) and separating the imaginary and the real-valued part yields two equations (one for the real, one for the imaginary part). Let us first look at the real-valued part of the Schrödinger equation:

$$\frac{-\hbar^2}{2m} \nabla^2 A + \frac{1}{2m} (\nabla R)^2 A + V(\mathbf{r}) A = E A \quad (4.2.86)$$

$$\Leftrightarrow \underbrace{\frac{[\nabla R(\mathbf{r})]^2}{2m} + V(\mathbf{r})}_{\text{Hamilton-Jacobi-Equation}} = E + \underbrace{\frac{\hbar^2}{2m} \frac{\nabla^2 A(\mathbf{r})}{A(\mathbf{r})}}_{\text{QM. corrections } O(\hbar^2)}. \quad (4.2.87)$$

The structure of the last equation is again reminiscent of the Hamilton-Jacobi equation $H(\mathbf{r}, \partial S/\partial \mathbf{r}) = E = \text{const.}$, with $R(\mathbf{r})$ in place of the generating function S (see Sect. 3.3.4). This analogy is only correct in first order of \hbar , but for the further analysis, we will assume that the $O(\hbar^2)$ term in (4.2.86) can be neglected.²

² The validity of this approximation is similar to the conditions discussed at the beginning of Sect. 4.2.2.

In the limit $\hbar \rightarrow 0$, the real-valued part of the Schrödinger equation is the Hamilton-Jacobi equation. In this case, we are, however, not interested in the dynamics themselves, but instead in the classical action S which is (up to $O(\hbar^2)$) identical to the phase of the wave function. The value of the action $R = S$ can be calculated as

$$R(\mathbf{r}) \underset{\mathcal{O}(\hbar)}{\approx} S(\mathbf{r}, \mathbf{I}) = \int_{\mathbf{r}_0}^{\mathbf{r}} \mathbf{p}(\mathbf{r}', \mathbf{I}) d\mathbf{r}', \quad (4.2.88)$$

where \mathbf{I} denotes the new momentum variables.

Let us now analyze the imaginary part of the Schrödinger Eq. (4.2.84)

$$\nabla \left(A^2(\mathbf{r}) \nabla R(\mathbf{r}) \right) = 0. \quad (4.2.89)$$

With the help of the divergence theorem (or Gauß theorem), we then obtain

$$\oint_{\delta V} A^2 \nabla R \cdot d\mathbf{n} = 0. \quad (4.2.90)$$

In order to better understand the meaning of this statement, let us look at a trajectory in a three-dimensional system as shown in Fig. 4.11. This volume is generated by choosing a small area δF_0 around the trajectory at the point \mathbf{r}_0 and propagating it from time t_0 to t_1 . At the latter time, it forms the area δF_1 around \mathbf{r}_1 . The volume thus forms a tube around the trajectory $\mathbf{r}(t)$, and both areas δF_0 and δF_1 are oriented perpendicular to the trajectory. Let us now evaluate the integral in Eq. (4.2.90) for the surface of this volume. Since the direction of the trajectory is given by the momentum $\mathbf{p} = \nabla R$, the product $\nabla R \cdot d\mathbf{n}$ vanishes for the walls of the tube that are shown as lightly shaded in Fig. 4.11. The only parts of the surface that contribute to the integral are δF_0 and δF_1 . We can thus write with Eq. (4.2.88)

$$0 = A^2(\mathbf{r}_1) \delta F_1 \mathbf{n}_1 \cdot \nabla R(\mathbf{r}_1) + A^2(\mathbf{r}_0) \delta F_0 \mathbf{n}_0 \cdot \underbrace{\nabla R(\mathbf{r}_0)}_{\mathbf{p} = \frac{\delta \mathbf{r}}{\delta t} m}, \quad (4.2.91)$$

from which it follows, for a small enough δt , see Fig. 4.11, that

$$A^2(\mathbf{r}_1) \underbrace{\delta F_1 \mathbf{n}_1 \cdot \delta \mathbf{r}_1}_{\delta V_1} = -A^2(\mathbf{r}_0) \underbrace{\delta F_0 \mathbf{n}_0 \cdot \delta \mathbf{r}_0}_{=-\delta V_0 < 0} \quad (4.2.92)$$

$$A^2(\mathbf{r}_1) = A^2(\mathbf{r}_0) \left(\frac{\delta V_1}{\delta V_0} \right)^{-1} \quad (4.2.93)$$

$$= A^2(\mathbf{r}_0) \left| \det \left(\frac{\partial \mathbf{r}(t_1)}{\partial \mathbf{r}(t_0)} \right)^{-1} \right|. \quad (4.2.94)$$

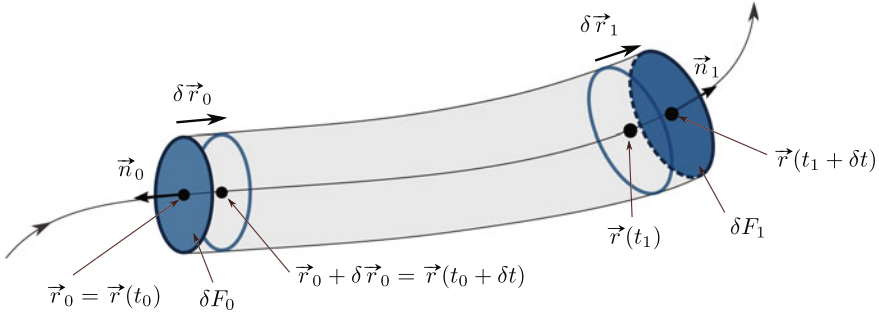


Fig. 4.11 Trajectory $\mathbf{r}(t)$ in 3D space with a “tube” generated by nearby trajectories. The tube is generated by all trajectories that start in the area δF_0 and end in the area δF_1

In order to understand the relation between the volumes δV and the Jacobi determinant of the time evolution $\mathbf{r}(t_0) \rightarrow \mathbf{r}(t_1)$ in Eq. (4.2.94), it is helpful to remember that both volumes encompass the same trajectories. The relation between them is thus given by the “spreading out” of these trajectories.

For an integrable system, the time evolution can be described by using the action-angle variables $(\mathbf{I}, \boldsymbol{\theta})$:

$$\mathbf{r}(t) \equiv \mathbf{r}(\boldsymbol{\theta}(t)) \quad \boldsymbol{\theta}(t) = \boldsymbol{\theta}(t_0) + (t - t_0)\boldsymbol{\omega}, \quad (4.2.95)$$

with $\boldsymbol{\omega} = \partial H / \partial \mathbf{I}$. Using this, we can rewrite the Jacobi matrix of the time evolution as:

$$\frac{\partial \mathbf{r}(t)}{\partial \mathbf{r}(t_0)} = \underbrace{\frac{\partial \mathbf{r}(t)}{\partial \boldsymbol{\theta}(t)}}_{\text{Jacobi matrix}} \cdot \underbrace{\frac{\partial \boldsymbol{\theta}(t)}{\partial \boldsymbol{\theta}(t_0)}}_{\text{time evolution}} \cdot \underbrace{\frac{\partial \boldsymbol{\theta}(t_0)}{\partial \mathbf{r}(t_0)}}_{\text{action-angle variables}} \quad (4.2.96)$$

$$= \left(\frac{\partial \boldsymbol{\theta}}{\partial \mathbf{r}}(\mathbf{r}_1) \right)^{-1} \cdot I_{d \times d} \cdot \frac{\partial \boldsymbol{\theta}}{\partial \mathbf{r}}(\mathbf{r}_0). \quad (4.2.97)$$

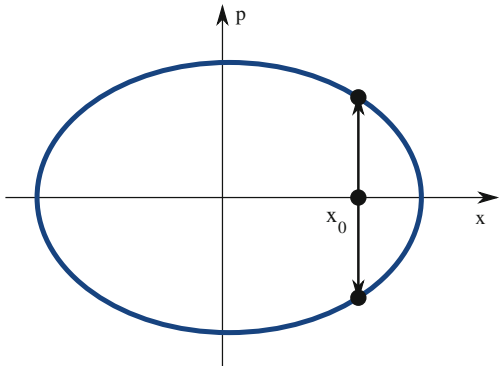
Since we know that $R = S(\mathbf{r}, \mathbf{I})$ is the generating function of the transformation to action-angle variables with $\frac{\partial S}{\partial \mathbf{r}} = \mathbf{p}$ and $\frac{\partial S}{\partial \mathbf{I}} = \boldsymbol{\theta}$, it follows from Eqs. (4.2.94) and (4.2.97) that, for fixed \mathbf{r}_0 and $A(\mathbf{r}_0)$,

$$\mathbf{A}^2(\mathbf{r}_1) \propto \left| \det \left(\frac{\partial \boldsymbol{\theta}}{\partial \mathbf{r}}(\mathbf{r}_1) \right) \right| = \left| \det \left(\frac{\partial^2 S}{\partial \mathbf{r} \partial \mathbf{I}}(\mathbf{r}_1, \mathbf{I}) \right) \right|. \quad (4.2.98)$$

According to our ansatz (4.2.83), the wave function is thus given as

$$\psi(\mathbf{r}) = \text{const.} \sqrt{\left| \det \left(\frac{\partial^2 S}{\partial \mathbf{r} \partial \mathbf{I}}(\mathbf{r}, \mathbf{I}) \right) \right|} \exp \left(\frac{i}{\hbar} S(\mathbf{r}, \mathbf{I}) \right), \quad (4.2.99)$$

Fig. 4.12 Example for a function with multiple branches in one dimension. At a fixed position x_0 , the momentum of a harmonic oscillator can assume two different values: $p_{1,2} = \pm\sqrt{2m(E - V)}$



where the constant factor is defined by the normalization condition.

A problem that already arises in one dimension is that the function $S(\mathbf{r}, \mathbf{I})$ in Eq. (4.2.99) is not uniquely defined for a fixed value of \mathbf{r} . In Fig. 4.12, the phase space trajectory of the one-dimensional harmonic oscillator is visualized and we can see that for one value of $x = x_0$, two branches of S exist (the forward and the backward trajectory). For an ansatz that at least replicates the results of the WKB approximation, we thus need to sum $\psi(\mathbf{r})$ over all possible branches:

$$\psi(\mathbf{r}) = \text{const.} \sum_v \sqrt{\left| \det \left(\frac{\partial^2 S_v(\mathbf{r}, \mathbf{I})}{\partial \mathbf{r} \partial \mathbf{I}} \right) \right|} \exp \left[\frac{i}{\hbar} S_v(\mathbf{r}, \mathbf{I}) + i\mu_v \right], \quad (4.2.100)$$

where μ is the so-called Maslov index. The Maslov indices are a result of the behavior of the system at the turning points.³ The Maslov indices can be determined by treating the system consistently at the turning points. Following Maslov and Gutzwiller, one way to achieve this is by locally changing the description of the wave function from $\psi_x(\mathbf{r})$ to $\hat{\psi}_p(\mathbf{p})$. The two resulting wave functions then have to be “stitched together” such that the wave function is consistent along the whole torus [16, 17]. A more detailed description of the multidimensional semiclassical approach is given in [14].

The approach presented in this chapter can even be generalized to non-integrable systems. For these we cannot any more describe the action function as a function of the fixed action \mathbf{I} , but we may use instead a more general form of the action function for any kind of orbit:

$$S_v(\mathbf{r}, \mathbf{I}, E) \rightarrow R_v(\mathbf{r}', \mathbf{r}, t), \quad (4.2.101)$$

R then describes the action of an orbit that needs the time t for the transition $\mathbf{r}' \rightarrow \mathbf{r}$. This idea goes back to early work by Vleck [18]. We elaborate now on the semiclassical description of nonintegrable systems in the following section.

³They had to be treated separately in the WKB approximation. There, this was achieved by using the Airy functions close to the turning point.

4.3 Semiclassical Description of Non-integrable Systems

4.3.1 Green's Functions

We start now from the time-dependent Schrödinger equation

$$i\hbar \frac{d\psi(t)}{dt} = \hat{H}\psi(t), \quad (4.3.1)$$

where we set the initial condition $\psi(t=0) = \psi_0$. We are not specifying yet the representation of ψ , it can be, e.g., in coordinate as well as in momentum representation.

In order to compute physical observables of the dynamical system we need an expression of the time evolution operator;

$$\psi(t) = \hat{U}(t)\psi_0 \quad (4.3.2)$$

$$= \exp\left(-\frac{i}{\hbar}\hat{H}t\right)\psi_0 \quad (4.3.3)$$

which is only correct for a time-independent Hamiltonian \hat{H} , otherwise time-ordering has to be taken into account. For the latter case, we refer to the literature on quantum field theory as presented for example in [19].

Since we are interested in the energy spectrum of the system, we consider the Laplace-Fourier transform of $\hat{U}(t)$

$$\hat{G}^+(E) = -\frac{i}{\hbar} \int_0^\infty \underbrace{e^{-\frac{i}{\hbar}\hat{H}t}}_{\hat{U}(t)} e^{\frac{i}{\hbar}(E+i\varepsilon)t} dt \quad (4.3.4)$$

$$= (E - \hat{H} + i\varepsilon)^{-1}. \quad (4.3.5)$$

This yields an expression for the (*retarded*) *Green function* or the *propagator* in energy space. $\varepsilon > 0$ is introduced in order to ensure convergence of the integral.

The wave function in Laplace-Fourier space

$$\tilde{\psi}(E) \equiv -\frac{i}{\hbar} \int_0^\infty \psi(t) e^{\frac{i}{\hbar}(E+i\varepsilon)t} dt, \quad (4.3.6)$$

can be obtained by acting upon the initial state ψ_0 with $\hat{G}^+(E)$

$$\tilde{\psi}(E) = \hat{G}^+(E)\psi_0. \quad (4.3.7)$$

The back transform is given by

$$\psi(t) = \frac{i}{2\pi} \int_{\mathbb{R}} \tilde{\psi}(E) e^{-\frac{i}{\hbar}(E+i\varepsilon)t} dE, \quad (4.3.8)$$

which can be computed remembering the identity

$$\int_{\mathbb{R}} e^{-\frac{i}{\hbar}(E+i\varepsilon)(t-t')} dE = 2\pi \delta(t - t'). \quad (4.3.9)$$

The Green function propagates any initial state forward in time. From the Green function we can compute observables. An example is the quantum mechanical level density, also known as *density of states*, which relates to $\hat{G}^+(E)$ as follows

$$\rho(E) = \sum_n \delta(E - E_n) = -\frac{1}{\pi} \text{tr} [\text{Im} \hat{G}^+(E)]. \quad (4.3.10)$$

Here, the $\{E_n\}_n$ denote a discrete set of eigenvalues of \hat{H} . The relation (4.3.10) can be proven straightforwardly, expanding into the eigenbasis of \hat{H} :

$$\hat{H} = \sum_n E_n |n\rangle \langle n| \Rightarrow \hat{U}(t) = \sum_n e^{-\frac{i}{\hbar} E_n t} |n\rangle \langle n|. \quad (4.3.11)$$

Using Eq. (4.3.5) we obtain

$$\hat{G}^+(E) = \sum_n \frac{1}{E - E_n + i\varepsilon} |n\rangle \langle n|, \quad (4.3.12)$$

and with the help of the following identity, we arrive at

$$\text{Im} \left[\frac{1}{x \pm i\varepsilon} \right] = \text{Im} \left[\frac{x \mp i\varepsilon}{x^2 + \varepsilon^2} \right] = \mp \frac{\varepsilon}{x^2 + \varepsilon^2} \underset{\varepsilon \rightarrow 0^+}{\underset{\curvearrowright}{\sim}} \mp \pi \delta(x) \quad (4.3.13)$$

$$\Rightarrow -\frac{1}{\pi} \text{Im} \hat{G}^+(E) = \sum_n \delta(E - E_n) |n\rangle \langle n|. \quad (4.3.14)$$

In general, the Green function allows us to calculate expectation values of operators with respect to the basis of eigenenergies:

$$\text{tr} \left[\left(-\frac{1}{\pi} \text{Im} \hat{G}^+(E) \right) \hat{A} \right] = \sum_n \langle n | \left(\sum_{n'} \delta(E - E_{n'}) |n'\rangle \langle n'| \right) \hat{A} |n\rangle \quad (4.3.15)$$

$$= \sum_n \delta(E - E_n) \langle n | \hat{A} |n\rangle. \quad (4.3.16)$$

Our aim in the following is to find semiclassical expressions for the time-evolution operator $\hat{U}(t)$, the propagator in energy space $\hat{G}^+(E)$, and the density of states $\rho(E)$ with the help of purely classical quantities.

4.3.2 Feynman Path Integral

In order to compute transition amplitudes in quantum mechanics we need an appropriate expression for the spatial representation of the time evolution operator. For the latter it holds

$$\psi(\mathbf{r}, t) = \hat{U}(t)\psi_0(\mathbf{r}) = \int d\mathbf{r}' K(\mathbf{r}, \mathbf{r}', t)\psi_0(\mathbf{r}'), \quad (4.3.17)$$

where

$$K(\mathbf{r}, \mathbf{r}', t) \equiv \langle \mathbf{r} | \hat{U}(t) | \mathbf{r}' \rangle. \quad (4.3.18)$$

For the sake of simplicity we take a Hamiltonian of the special form

$$\hat{H} = \hat{T} + \hat{V} \equiv \frac{\hat{\mathbf{p}}^2}{2m} + V(\hat{\mathbf{r}}). \quad (4.3.19)$$

The operators \hat{T} and \hat{V} are generally non-commuting. But if we replace t by δt and consider the limit $\delta t \rightarrow 0$ the Trotter product formula [4] states that

$$\begin{aligned} \hat{U}(\delta t) &= \exp\left(-\frac{i}{\hbar}\delta t [\hat{T} + \hat{V}]\right) \\ &= \exp\left(-\frac{i}{\hbar}\delta t \hat{T}\right) \exp\left(-\frac{i}{\hbar}[\delta t \hat{V}]\right) + O(\delta t^2). \end{aligned} \quad (4.3.20)$$

This follows also from the maybe better known Baker Campbell Hausdorff formula [3]. Writing the time evolution operator in the form of Eq. (4.3.17) yields

$$\langle \mathbf{r} | \hat{U}(t) | \mathbf{r}' \rangle = \langle \mathbf{r} | e^{-\frac{i}{\hbar}\delta t \hat{T}} | \mathbf{r}' \rangle \exp\left(-\frac{i}{\hbar}[\delta t V(\mathbf{r}')]\right) + O(\delta t^2), \quad (4.3.21)$$

where \hat{V} is of course diagonal in the position representation. Inserting now into the first factor in Eq. (4.3.21) the identity operator (which is given by $\int d\mathbf{p} |\mathbf{p}\rangle \langle \mathbf{p}| = I_d$) yields the following expression:

$$\langle \mathbf{r} | e^{-\frac{i}{\hbar}\delta t \hat{T}} | \mathbf{r}' \rangle = \int d\mathbf{p} \exp\left[-\frac{i\delta t}{2\hbar m} p^2\right] \langle \mathbf{r} | \mathbf{p} \rangle \langle \mathbf{p} | \mathbf{r}' \rangle \quad (4.3.22)$$

$$= \int \frac{d\mathbf{p}}{(2\pi)^d} \exp\left[-\frac{i\delta t}{2\hbar m} p^2\right] \exp\left(\frac{i}{\hbar} \mathbf{p}(\mathbf{r} - \mathbf{r}')\right) \quad (4.3.23)$$

$$= \prod_{j=1}^d \left\{ \frac{1}{2\pi\hbar} \int_{\mathbb{R}} dp_j \exp \left[-\frac{i}{\hbar} \left(\frac{\delta t}{2m} p_j^2 - p_j(r_j - r'_j) \right) \right] \right\}. \quad (4.3.24)$$

In order to evaluate the integral in Eq.(4.3.24), we recall the complex Gaussian integral which is also known as *Fresnel-integral* [13]

$$\int_{\mathbb{R}} e^{i\alpha x^2} dx = \lim_{\varepsilon \rightarrow 0^+} \int_{\mathbb{R}} e^{-(\varepsilon - i\alpha)x^2} dx = \lim_{\varepsilon \rightarrow 0^+} \sqrt{\frac{\pi}{\varepsilon - i\alpha}} = \sqrt{\frac{\pi}{|\alpha|}} e^{i\frac{\pi}{4}\text{sgn}(\alpha)}. \quad (4.3.25)$$

We note that generally $\frac{1}{\sqrt{i}} = \sqrt{-i} = e^{\pm i\frac{\pi}{4}}$. For definiteness, we use in the sequel the convention⁴ that the minus sign is taken in the latter exponential, i.e. $\sqrt{-i}$ is always intended as $e^{-i\frac{\pi}{4}}$.

Using the relation (4.3.25) and plugging in the result from (Eq. 4.3.24), we obtain

$$\langle \mathbf{r} | e^{-\frac{i}{\hbar} \delta t \hat{T}} | \mathbf{r}' \rangle = \prod_{j=1}^d \sqrt{\frac{m}{2\pi i \hbar \delta t}} \exp \left[\frac{i}{\hbar} \frac{m}{2\delta t} (r_j - r'_j)^2 \right] = \left(\frac{m}{2\pi i \hbar \delta t} \right)^{\frac{d}{2}} \exp \left[\frac{i}{\hbar} \frac{m}{2\delta t} (\mathbf{r} - \mathbf{r}')^2 \right]. \quad (4.3.26)$$

Consequently, the following holds for the sandwiched time-evolution operator up to order δt

$$K(\mathbf{r}, \mathbf{r}', \delta t) \approx \left(\frac{m}{2\pi i \hbar \delta t} \right)^{\frac{d}{2}} \exp \left[\frac{i \delta t}{\hbar} \left(\frac{1}{2} m \left(\frac{\mathbf{r} - \mathbf{r}'}{\delta t} \right)^2 - V(\mathbf{r}') \right) \right]. \quad (4.3.27)$$

Here

$$\left(\frac{1}{2} m \left(\frac{\mathbf{r} - \mathbf{r}'}{\delta t} \right)^2 - V(\mathbf{r}') \right) \equiv \mathcal{L} \left(\mathbf{r}', \frac{\mathbf{r} - \mathbf{r}'}{\delta t} \right) \quad (4.3.28)$$

denotes the classical Lagrangian function [12, 15, 21]. In the first argument we chose \mathbf{r}' . The following choices for \mathcal{L} are equally possible:

- exchange \mathbf{r}' and \mathbf{r} : $\mathcal{L} \left(\mathbf{r}, \frac{\mathbf{r} - \mathbf{r}'}{\delta t} \right)$
- symmetrized version: $\frac{1}{2} \left[\mathcal{L}(\mathbf{r}, \frac{\mathbf{r} - \mathbf{r}'}{\delta t}) + \mathcal{L}(\mathbf{r}', \frac{\mathbf{r} - \mathbf{r}'}{\delta t}) \right]$.

Furthermore using the composition property of the time-evolution law $U(t_1 + t_2) = U(t_1) \circ U(t_2)$, we obtain

$$K(\mathbf{r}, \mathbf{r}', t_1 + t_2) = \langle \mathbf{r} | \hat{U}(t_1 + t_2) | \mathbf{r}' \rangle = \langle \mathbf{r} | \hat{U}(t_1) \circ \hat{U}(t_2) | \mathbf{r}' \rangle \quad (4.3.29)$$

⁴Following [20].

$$= \int d\mathbf{r}'' \langle \mathbf{r} | \hat{U}(t_1) | \mathbf{r}'' \rangle \langle \mathbf{r}'' | \hat{U}(t_2) | \mathbf{r}' \rangle \quad (4.3.30)$$

$$= \int d\mathbf{r}'' K(\mathbf{r}, \mathbf{r}'', t_1) K(\mathbf{r}'', \mathbf{r}', t_2). \quad (4.3.31)$$

Consequently, we can now build up the full evolution by applying Eq. (4.3.20) for each single small step. In Eq. (4.3.30) we used the identity $\int d\mathbf{r}'' |\mathbf{r}''\rangle \langle \mathbf{r}''| = I_d$ on our Hilbert space. Now the idea is, to divide $K(\mathbf{r}, \mathbf{r}', t)$ into N parts in the above manner and considering the limit $N \rightarrow \infty$. Hence, we find

$$K(\mathbf{r}, \mathbf{r}', t) = \int d\mathbf{r}_1 \dots \int d\mathbf{r}_{N-1} K(\mathbf{r} = \mathbf{r}_N, \mathbf{r}_{N-1}, \delta t) \dots K(\mathbf{r}_2, \mathbf{r}_1, \delta t) K(\mathbf{r}_1, \mathbf{r}_0 \equiv \mathbf{r}', \delta t) \quad (4.3.32)$$

$$\rightarrow \int d\mathbf{r}_1 \dots \int d\mathbf{r}_{N-1} \prod_{j=1}^N \left(\frac{m}{2\pi i \hbar \delta t} \right)^{\frac{d}{2}} \exp \left[\frac{i}{\hbar} \delta t \mathcal{L} \left(\mathbf{r}_{j-1}, \frac{\mathbf{r}_j - \mathbf{r}_{j-1}}{\delta t} \right) \right] \quad (4.3.33)$$

$$= \left(\frac{m}{2\pi i \hbar \delta t} \right)^{N \frac{d}{2}} \int d\mathbf{r}_1 \dots \int d\mathbf{r}_{N-1} \exp \left[\frac{i}{\hbar} \delta t \sum_{j=1}^N \mathcal{L} \left(\mathbf{r}_{j-1}, \frac{\mathbf{r}_j - \mathbf{r}_{j-1}}{\delta t} \right) \right]. \quad (4.3.34)$$

The propagator can finally be rewritten in a compact way which denotes the integral over all *classical* and *non-classical* paths $\mathbf{q} : [0, t] \rightarrow \mathbb{R}^d$ with $\mathbf{q}_0 = \mathbf{r}'$ and $\mathbf{q}(t) = \mathbf{r}$, see also the sketch in Fig. 4.13:

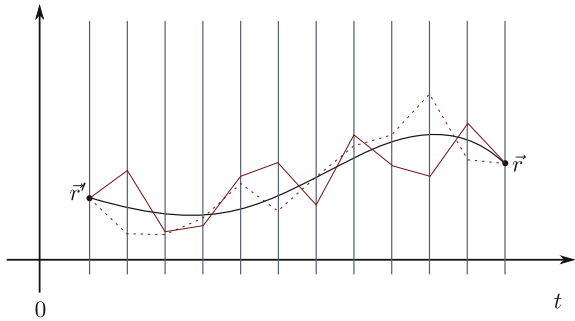
$$K(\mathbf{r}, \mathbf{r}', t) = \int D[\mathbf{q}] \exp \left[\frac{i}{\hbar} \int_0^t \mathcal{L}(\mathbf{q}(t'), \dot{\mathbf{q}}(t')) dt' \right]. \quad (4.3.35)$$

The latter is a functional integral, where $D[\mathbf{q}]$ formally denotes the integration over all paths. With classical paths we mean the trajectories the classical analogue system follows (these contributions are obtained by a stationary phase analysis as done in Sect. 4.3.3). Non-classical paths are all other possible connections as defined above which the classical system does not realize. The *Trotter product formula* [4] indeed guarantees that the terms of order δt^2 , which were neglected in (4.3.20), will not produce problems in the limit $N \rightarrow \infty$. To better digest what we have done in this section, we recommend the interested reader to have a glance at the original and very well written paper by Feynman [22] or at textbooks like [3, 23].

4.3.3 Method of Stationary Phase

We are going to see that in the limit $\hbar \rightarrow 0$, the path-integral Eq. (4.3.35) is dominated by the critical path of the phase where the derivative of $S[\mathbf{q}, \dot{\mathbf{q}}] \equiv$

Fig. 4.13 Trajectories starting at \vec{r}' and ending at \vec{r} moving in discrete Trotter steps $\delta t \rightarrow 0$ forward in time



$\int \mathcal{L}(\mathbf{q}(t'), \dot{\mathbf{q}}(t')) dt'$ vanishes. Hence, in the following section we will recover the contribution of just the classical paths upon use of a saddle-point approximation. It is also called the *method of stationary phase* or also *saddle-point method*. As a mathematical foundation we recall the *Riemann-Lebesgue lemma* which can be found in standard analysis textbooks [24].

Given a function whose absolute value is integrable $f \in \mathcal{L}^1$, i.e.

$$\int_{\mathbb{R}} |f| dx < \infty. \quad (4.3.36)$$

Then the Riemann-Lebesgue lemma states that

$$\int_{\mathbb{R}} f(x) e^{-izx} dx \rightarrow 0, \quad \text{as } |z| \rightarrow \infty, \text{ for } z \in \mathbb{C}. \quad (4.3.37)$$

Now we consider the following integral for a well behaved real valued function g

$$\int_a^b g(x) e^{\frac{i}{\hbar} f(x)} dx. \quad (4.3.38)$$

Maximal contributions to Eq. (4.3.38) are expected from points x_v where the function f is extremal. Taylor expanding the function around these points gives

$$f(x - x_v) \approx f(x_v) + \underbrace{f'(x_v)}_{=0}(x - x_v) + f''(x_v) \frac{(x - x_v)^2}{2}. \quad (4.3.39)$$

Here the primes denote derivatives with respect to the argument of f . We define $f, g : (a, b) \rightarrow \mathbb{R}$ and $x_v \in (a, b)$ to be an isolated root of f' together with $f''(x_v) \neq 0$ and $g(x_v) \neq 0$. Then we can approximate (4.3.38) in the classical limit

$$\int_a^b g(x) e^{\frac{i}{\hbar} f(x)} dx \underset{\hbar \rightarrow 0}{\sim} \sum_v g(x_v) e^{\frac{i}{\hbar} f(x_v)} \sqrt{\frac{2\pi\hbar}{|f''(x_v)|}} e^{i\frac{\pi}{4}\alpha_v} + O(\hbar). \quad (4.3.40)$$

Here we have used the complex Gaussian integral Eq. (4.3.25) and

$$\alpha_v = \text{sgn}(f''(x_v)) = \begin{cases} 1 & : f''(x_v) > 0 \\ -1 & : f''(x_v) < 0 \end{cases}. \quad (4.3.41)$$

The relation (4.3.40) can be generalized to integrals in n dimensions. Let therefore $f, g : C \subseteq \mathbb{R}^n \rightarrow \mathbb{R}$ with $\mathbf{x}_v \in C$ an isolated root of $\nabla f(\mathbf{x})$ with $\det\left(\frac{\partial^2 f}{\partial x_i \partial x_j}(\mathbf{x}_v)\right) \neq 0$ and $g(\mathbf{x}_v) \neq 0$. Then, it holds:

$$\int d^n x g(\mathbf{x}) e^{\frac{i}{\hbar} f(\mathbf{x})} d^n x \underset{\hbar \rightarrow 0}{\sim} \sum_v g(\mathbf{x}_v) e^{\frac{i}{\hbar} f(\mathbf{x}_v)} \frac{\sqrt{2\pi\hbar}}{\sqrt{\det\left(\frac{\partial^2 f}{\partial x_i \partial x_j}(\mathbf{x}_v)\right)}} e^{i\frac{\pi}{4}\alpha_v} + O(\hbar) \quad (4.3.42)$$

Here we have $\alpha_v = \sum_{j=1}^n \text{sgn}(\lambda^{(v)})$ where $\lambda^{(v)}$ denote the eigenvalues of the functional determinant matrix $\left\{ \det\left(\frac{\partial^2 f}{\partial x_i \partial x_j}(\mathbf{x}_v)\right) \right\}_{n \times n}$.

4.3.4 Van-Vleck Propagator

We will apply the method of stationary phase to the Feynman propagator given by Eq. (4.3.34):

$$K(\mathbf{r}, \mathbf{r}', t) = \left(\frac{m}{2\pi i\hbar\delta t}\right)^{N\frac{d}{2}} \int d\mathbf{r}_1 \dots \int d\mathbf{r}_{N-1} \exp\left[\frac{i}{\hbar}\delta t \sum_{j=1}^N \mathcal{L}\left(\mathbf{r}_{j-1}, \frac{\mathbf{r}_j - \mathbf{r}_{j-1}}{\delta t}\right)\right]. \quad (4.3.43)$$

Taking the limit $N \rightarrow \infty$, we can rewrite the discrete path $\mathbf{x} \equiv (\mathbf{r}_1, \dots, \mathbf{r}_{N-1}) \in \mathbb{R}^{(N-1)d}$ as a continuous function of time $\mathbf{q}(t)$. For the phase function we can thus use a continuous approximation of the sum

$$f(\mathbf{x}) \equiv \delta t \sum_{j=1}^N \mathcal{L}\left(\mathbf{r}_{j-1}, \frac{\mathbf{r}_j - \mathbf{r}_{j-1}}{\delta t}\right) \rightarrow \int_0^t \mathcal{L}(\mathbf{q}(t'), \dot{\mathbf{q}}(t')) dt'. \quad (4.3.44)$$

To apply the method of stationary phase we have to find the critical points of the function (4.3.44). Hence we look for solution of

$$0 = \frac{\partial}{\partial \mathbf{r}_j} f(\mathbf{r}_1, \dots, \mathbf{r}_{N-1}) \rightarrow 0 = \frac{\delta}{\delta \mathbf{q}(\tilde{t})} \int_0^t \mathcal{L}(\mathbf{q}, \dot{\mathbf{q}}) dt'. \quad (4.3.45)$$

The identity on the right hand side corresponds to the variation of the action integral leading to the *Euler-Lagrange equation* of classical mechanics [15, 21].

We have found the really important result that, in the semiclassical limit, the largest contribution to the propagator arises from the classical trajectory with boundary conditions $\mathbf{q}(0) = \mathbf{r}'$ and $\mathbf{q}(t) = \mathbf{r}$. This main contribution is just one of the paths sketched in Fig. 4.13.

Choosing for the exponent in Eq. (4.3.42)

$$f(x_v) \rightarrow R_v(\mathbf{r}', \mathbf{r}, t) \equiv \int_0^t \mathcal{L}(\mathbf{q}_v, \dot{\mathbf{q}}_v) dt', \quad (4.3.46)$$

with $R_v(\mathbf{r}', \mathbf{r}, t)$ as Hamilton's principal function along \mathbf{q}_v , we now derive the *Van-Vleck-Gutzwiller propagator*

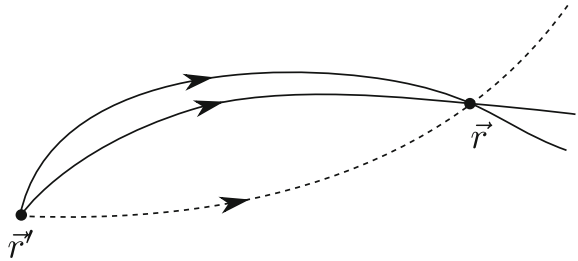
$$\begin{aligned} K(\mathbf{r}', \mathbf{r}, t) &\approx \sum_{v \in C} \frac{1}{(2\pi i \hbar)^{\frac{d}{2}}} \sqrt{\left| \det \left(-\frac{\partial^2 R_v}{\partial \mathbf{r} \partial \mathbf{r}'}(\mathbf{r}, \mathbf{r}', t) \right) \right|} e^{\frac{i}{\hbar} R_v(\mathbf{r}', \mathbf{r}, t)} e^{-i \frac{\pi}{2} \mu_v} \\ &\equiv K_{SC}(\mathbf{r}', \mathbf{r}, t), \end{aligned} \quad (4.3.47)$$

where $\mu_v = \frac{1}{2}[(N-1)d - \alpha_v]$ with $\alpha_v = \sum_{j=1}^{(N-1)d} \text{sgn}(\lambda_j^{(v)})$. μ_v corresponds to the number of negative eigenvalues of the matrix $\det \left(\frac{\partial^2 f}{\partial x_i \partial x_j}(\mathbf{x}_v) \right)$, which is exactly the number of conjugated points along the trajectory \mathbf{q}_v . As we know from Sect. 4.2.2 this number is called *Morse index* or *Maslov index* [12, 14].

In the following, we motivate the above expression for the *Van Vleck-Gutzwiller propagator* $K_{SC}(\mathbf{r}', \mathbf{r}, t)$. For a derivation in full detail we recommend Chap. 10.2 in [20] and the exhaustive book by Schulman [25, Chap. 13]. We consider the factor in Eq. (4.3.43) in front of the integral together with the determinant expression Eq. (4.3.42)⁵

⁵ A similar relation was actually shown in Sect. 4.2.4. Here one starts from the infinitesimal action $R(\mathbf{r}', \mathbf{r}) = \frac{m}{2\delta t}(\mathbf{r}' - \mathbf{r})^2 - \delta t V(\mathbf{r}')$ with momentum $p = \frac{\mathbf{r}' - \mathbf{r}}{\delta t}$, and shows that $\frac{\delta t}{m} \frac{\partial \mathbf{r}'}{\partial \mathbf{r}}|_{\mathbf{r}=\mathbf{r}'} = \frac{\partial \mathbf{r}'}{\partial p}|_{\mathbf{p}(\mathbf{r}=\mathbf{r}')}$, which in turn is the inverse of the matrix $-\frac{\partial R}{\partial \mathbf{r}' \partial \mathbf{r}}$.

Fig. 4.14 Several projections of trajectories in phase space into configuration space meet at focus points corresponding to the turning points in Fig. 4.12. Here the determinant matrix of the propagator becomes singular



$$\underbrace{\sqrt{\left| \det \left(\frac{\partial^2 f(\mathbf{x}_v)}{\partial x_i \partial x_j} \right) \right|}}_{\equiv A} \rightarrow \sqrt{\underbrace{\det \left(-\frac{\partial^2 R_v}{\partial \mathbf{r} \partial \mathbf{r}'}(\mathbf{r}', \mathbf{r}, t) \right)}_{\equiv B}} \quad \text{as } N \rightarrow \infty \text{ and } \delta t \rightarrow 0. \quad (4.3.48)$$

Now the factor in front of the integral in (4.3.43), together with the phase factor in Eq. (4.3.42)) becomes

$$\left(\frac{m}{2\pi i \hbar \delta t} \right)^{N \frac{d}{2}} \frac{(2\pi \hbar)^{(N-1) \frac{d}{2}}}{A} e^{i \frac{\pi}{4} \alpha_v} \rightarrow \frac{1}{(2\pi i \hbar)^{\frac{d}{2}}} B e^{-i \frac{\pi}{2} \mu_v}, \quad (4.3.49)$$

from which our result (4.3.47) follows.

As a final note, we consider the initial momentum of the trajectory which is divergent at the focus points (also known as conjugated points), i.e.

$$\frac{\partial R_v}{\partial \mathbf{r}'} = -\mathbf{p}' \Rightarrow \left(-\frac{\partial^2 R_v}{\partial \mathbf{r} \partial \mathbf{r}'} \right)_{d \times d} = \left(\frac{\partial \mathbf{p}'}{\partial \mathbf{r}}|_{\mathbf{r}'} \right)_{d \times d} = \left(\frac{\partial \mathbf{r}}{\partial \mathbf{p}'}|_{\mathbf{r}'} \right)_{d \times d}^{-1}. \quad (4.3.50)$$

As a consequence, we have that

$$(\mathbf{r}', \mathbf{p}' + \delta \mathbf{p}') \mapsto (\mathbf{r} + O(\delta \mathbf{p}'^2), \dots). \quad (4.3.51)$$

Thus, there do not exist simple isolated roots of ∇f here. This is illustrated in Fig. 4.14. The problem of conjugated points at which the determinate matrix changes sign (crosses a zero eigenvalue) is cured by the Morse index in Eq. (4.3.47).

4.3.5 Semiclassical Green's Function

Finally, we are able to construct the *semiclassical Green function* using the results for the retarded Green function Eq. (4.3.5) and the Van-Vleck-Gutzwiller propagator Eq. (4.3.47):

$$G(\mathbf{r}, \mathbf{r}'; E) = \langle \mathbf{r} | \hat{G}(E) | \mathbf{r}' \rangle = -\frac{i}{\hbar} \int_0^\infty K(\mathbf{r}, \mathbf{r}'; t) e^{\frac{i}{\hbar}(E+i\varepsilon)t} dt \quad (4.3.52)$$

$$\longrightarrow -\frac{i}{\hbar} \sum_v (2\pi\hbar)^{-\frac{d}{2}} \int_0^\infty \sqrt{\left| \det \left(-\frac{\partial^2 R_v}{\partial \mathbf{r} \partial \mathbf{r}'}(\mathbf{r}, \mathbf{r}', t) \right) \right|} e^{\frac{i}{\hbar}[R_v(\mathbf{r}', \mathbf{r}, t) + Et]} e^{-i\frac{\pi}{2}\mu_v} dt, \quad (4.3.53)$$

where the arrow stands for the semiclassical limit using the propagator $K_{SC}(\mathbf{r}', \mathbf{r}, t)$.

Now we use again the method of stationary phase at the propagation time t together with $\frac{\partial R_v}{\partial t} = -E$, which will give us the semiclassical Green function as the sum over all classical trajectories from \mathbf{r}' to \mathbf{r} at energy E . In the following, we calculate the terms and factors appearing in Eq. (4.3.53) in detailed.

- The exponent denotes the classical action integral along \mathbf{q}_v :

$$R_v + Et = S_v(\mathbf{r}', \mathbf{r}; E) \equiv \int_0^t \mathbf{p}_v(t') \dot{\mathbf{q}}_v(t') dt'. \quad (4.3.54)$$

- For the prefactor we have

$$\frac{\partial^2 R_v}{\partial t^2}(\mathbf{r}', \mathbf{r}, t) = -\frac{\partial E}{\partial t}|_{\mathbf{r}, \mathbf{r}'} \Rightarrow \frac{\det \left(-\frac{\partial^2 R_v}{\partial \mathbf{r} \partial \mathbf{r}'} \right)}{-\frac{\partial^2 R_v}{\partial t^2}} = \det \left(\frac{\partial \mathbf{p}'}{\partial \mathbf{r}}|_{\mathbf{r}', t} \right) \cdot \left(\frac{\partial E}{\partial t}|_{\mathbf{r}, \mathbf{r}'} \right)^{-1} \quad (4.3.55)$$

$$= \det \left(\frac{\partial (\mathbf{p}', \mathbf{r}', t)}{\partial (\mathbf{r}, \mathbf{r}', t)} \right) \det \left(\frac{\partial (\mathbf{r}, \mathbf{r}', t)}{\partial (\mathbf{r}, \mathbf{r}', E)} \right) \quad (4.3.56)$$

$$= \det \left(\frac{\partial (\mathbf{p}', \mathbf{r}', t)}{\partial (\mathbf{r}, \mathbf{r}', E)} \right) \quad (4.3.57)$$

$$= \det \left(\begin{array}{c|c} \left\{ \frac{\partial \mathbf{p}'}{\partial \mathbf{r}}|_{\mathbf{r}', E} \right\}_{d \times d} & \left\{ \frac{\partial \mathbf{p}'}{\partial E}|_{\mathbf{r}, \mathbf{r}'} \right\}_{d \times 1} \\ \hline \left\{ \frac{\partial t}{\partial \mathbf{r}}|_{\mathbf{r}', E} \right\}_{1 \times d} & \left\{ \frac{\partial t}{\partial E}|_{\mathbf{r}, \mathbf{r}'} \right\}_{1 \times 1} \end{array} \right) \quad (4.3.58)$$

$$= (-1)^d \det \begin{pmatrix} \frac{\partial^2 S_v}{\partial \mathbf{r} \partial \mathbf{r}'} & \frac{\partial^2 S_v}{\partial E \partial \mathbf{r}'} \\ \frac{\partial^2 S_v}{\partial \mathbf{r} \partial E} & \frac{\partial^2 S_v}{\partial E^2} \end{pmatrix} \quad (4.3.59)$$

$$\equiv (-1)^d D_v(\mathbf{r}', \mathbf{r}, E). \quad (4.3.60)$$

- We furthermore consider the phase factor⁶

$$e^{-i\frac{\pi}{2}\mu_v} e^{i\frac{\pi}{4}\operatorname{sgn}\left(\frac{\partial^2 R_v}{\partial t^2}\right)} = \sqrt{i} e^{-i\frac{\pi}{2}\beta_v}. \quad (4.3.61)$$

Here we defined

$$\beta_v := \mu_v + \begin{cases} 1 & : \frac{\partial^2 R_v}{\partial t^2} = \frac{-\partial E}{\partial t} < 0 \\ 0 & : \frac{\partial^2 R_v}{\partial t^2} = \frac{-\partial E}{\partial t} > 0. \end{cases} \quad (4.3.62)$$

Remembering Eq. (4.3.25) and using the results from the Eqs. (4.3.54), (4.3.60), and (4.3.61) we finally arrive at an appropriate expression for the *semiclassical Green function*

$$G_{\text{SC}}(\mathbf{r}, \mathbf{r}', E) = \sum_v \frac{2\pi}{(2\pi i \hbar)^{\frac{d+1}{2}}} \sqrt{|D_v(\mathbf{r}', \mathbf{r}, E)|} e^{\frac{i}{\hbar} S_v(\mathbf{r}', \mathbf{r}, E) - i\frac{\pi}{2}\beta_v}. \quad (4.3.63)$$

4.3.6 Gutzwiller's Trace Formula

Having at hand a semiclassical expression for the Green function, we come now to the central result of this Sect. 4.3. We recall Eq. (4.3.10) for the relation with the density of states

$$\rho(E) = -\frac{1}{\pi} \operatorname{Im} \left[\operatorname{tr} \left(\hat{G}^+(E) \right) \right] \quad (4.3.64)$$

$$= -\frac{1}{\pi} \operatorname{Im} \left[\operatorname{tr} \left(\int d\mathbf{r} |\mathbf{r}\rangle \langle \mathbf{r}| \hat{G}^+(E) \right) \right] \quad (4.3.65)$$

$$= -\frac{1}{\pi} \operatorname{Im} \int d\mathbf{r} G^+(\mathbf{r}, \mathbf{r}, E). \quad (4.3.66)$$

Let us split the density of states into two parts

$$\rho(E) = \bar{\rho}(E) + \rho_{\text{fl}}(E), \quad (4.3.67)$$

a smooth part $\bar{\rho}(E)$ and an oscillating part $\rho_{\text{fl}}(E)$, c.f. the sketch in Fig. 4.15.

We may approximate the smooth part by extending the argument reported at the end of Sect. 4.2.3.1. We imagine the available phase space for a fixed energy divided into the number of Planck cells. This gives

⁶Please remember the phase convention right after Eq. (4.3.25).

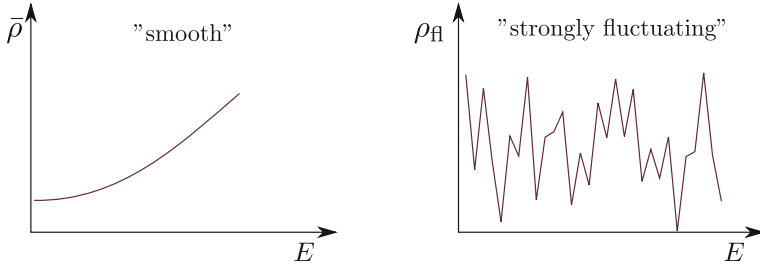


Fig. 4.15 The quantum mechanical density of states $\rho(E)$ can always be decomposed into smooth part (left) and a fluctuating part (right)

$$\bar{\rho}(E) \approx \frac{1}{(2\pi\hbar)^d} \int d\mathbf{p} \int d\mathbf{r} \delta(E - H_{\text{class}}(\mathbf{p}, \mathbf{r})) = \bar{\rho}_{\text{TF}}(E) \quad (4.3.68)$$

This is a kind of Thomas-Fermi (TF) approximation [26] also known under the name *Weyl's law* [17].

From the form of the semiclassical Green's function $G_{\text{SC}}(\mathbf{r}, \mathbf{r}', E)$, we see that the dominant contributions come from trajectories with constant phase. These correspond to infinitesimally short trajectories with $\mathbf{r}' = \mathbf{r}$. These contributions can be interpreted as the one leading to Weyl's law.

A second possibility for $\mathbf{r} = \mathbf{r}'$ is given by closed-loop trajectories, giving rise to the dominant contribution of the fluctuating part of the density of states

$$\rho_{\text{fl}}(E) \approx -\frac{1}{\pi} \text{Im} \sum_v \frac{2\pi}{\sqrt{2\pi i \hbar^{d+1}}} \int d\mathbf{r} \sqrt{|D_v(\mathbf{r}, \mathbf{r}, E)|} e^{\frac{i}{\hbar} S_v(\mathbf{r}, \mathbf{r}, E) - i \frac{\pi}{2} \beta_v}. \quad (4.3.69)$$

Applying again here the stationary phase argument for the phases $S_v(\mathbf{r}, \mathbf{r}', E)$ yields

$$\left. \frac{\partial S_v}{\partial \mathbf{r}} \right|_{\mathbf{r}=\mathbf{r}_0} = \left[\underbrace{\left. \frac{\partial S_v}{\partial \mathbf{r}'}(\mathbf{r}', \mathbf{r}, E) \right|_{\mathbf{r}'=\mathbf{r}=\mathbf{r}_0}}_{=-\mathbf{p}'} + \underbrace{\left. \frac{\partial S_v}{\partial \mathbf{r}}(\mathbf{r}', \mathbf{r}, E) \right|_{\mathbf{r}=\mathbf{r}'=\mathbf{r}_0}}_{=\mathbf{p}} \right] = 0. \quad (4.3.70)$$

Here, we vary both spatial arguments of $S_v(\mathbf{r}, \mathbf{r}', E)$ at the starting and ending point of the trajectory. Hence, $-\mathbf{p}'$ corresponds to the initial and \mathbf{p} to the final momentum, c.f. Sect. 3.2. Moreover it holds that $S_v = \int_{\mathbf{r}'}^{\mathbf{r}} p(\mathbf{r}'') d\mathbf{r}''$. Consequently, in Eq. (4.3.69), we have to sum over *periodic orbits* (PO) in phase space with $\mathbf{r}' = \mathbf{r}$ and $\mathbf{p}' = \mathbf{p}$. The prefactor $\sqrt{|D_v|}$ in (4.3.69) can be simplified by rewriting its expression. For this, we decompose the spatial vector \mathbf{r} into a parallel and a perpendicular part with respect to the classical orbit, i.e.

$$\mathbf{r} \mapsto (r_{||}, \mathbf{r}_{\perp}) \quad (4.3.71)$$

$$d^d \mathbf{r} = dr_{||} d^{d-1} \mathbf{r}_{\perp}. \quad (4.3.72)$$

Here $r_{||}$ denotes the component along and \mathbf{r}_{\perp} the one perpendicular to the orbit. Now, we apply the method of stationary phase only for the \mathbf{r}_{\perp} integration at the point $\mathbf{r}_{\perp} = 0$. Then the new prefactor in Eq. (4.3.69) becomes

$$\sqrt{\frac{|D_v|}{\left| \frac{\partial^2}{\partial \mathbf{r}_{\perp} \partial \mathbf{r}'_{\perp}} S_v(\mathbf{r}, \mathbf{r}, E) \right|}}. \quad (4.3.73)$$

Note that the deviation $\mathbf{r}' = (r_{||} + \delta r_{||}, \mathbf{r}_{\perp})$ along the trajectories corresponds to the same orbit. We therefore have, c.f. Sect. 3.2, the following relations

$$\frac{\partial^2 S_v}{\partial r_{||} \partial r'_{||}} = \frac{\partial p_{||}}{\partial r'_{||}} = 0 \quad (4.3.74)$$

$$\frac{\partial^2 S_v}{\partial \mathbf{r}_{\perp} \partial r'_{||}} = \frac{\partial p_{\perp}}{\partial r'_{||}} = 0 \quad (4.3.75)$$

$$\frac{\partial^2 S_v}{\partial r_{||} \partial \mathbf{r}'_{\perp}} = \frac{\partial p_{||}}{\partial \mathbf{r}'_{\perp}} = 0 \quad (4.3.76)$$

$$\frac{\partial^2 S_v}{\partial r_{||} \partial E} = \frac{\partial t}{\partial r_{||}} = \frac{1}{\dot{r}(r_{||})} \quad (4.3.77)$$

$$\frac{\partial^2 S_v}{\partial E \partial r'_{||}} = -\frac{1}{\dot{r}(r_{||})} = 0. \quad (4.3.78)$$

The expression $\dot{r}(r_{||})$ denotes the classical velocity along, i.e. parallel to the orbit. Putting these expressions into the definition of D_v , see Eq. (4.3.60), we arrive at

$$|D_v| = \left| \det \begin{pmatrix} 0 & 0 \dots 0 & -\frac{1}{\dot{r}} \\ \vdots & \frac{\partial^2 S_v}{\partial \mathbf{r}_{\perp} \partial \mathbf{r}'_{\perp}} & * \\ 0 & * & * \end{pmatrix} \right| = \frac{1}{\dot{r}^2} \left| \det \left(\frac{\partial^2 S_v}{\partial \mathbf{r}_{\perp} \partial \mathbf{r}'_{\perp}} \right) \right| = \frac{1}{\dot{r}^2} \left| \det \left(\frac{\partial \mathbf{p}'_{\perp}}{\partial \mathbf{r}_{\perp}} \right) \right|. \quad (4.3.79)$$

To compute the missing determinant of derivatives we have to consider both coordinates independently as above in Eq. (4.3.70):

$$\left| \det \left(\frac{\partial^2}{\partial \mathbf{r}_{\perp} \partial \mathbf{r}_{\perp}} S_v(\mathbf{r}, \mathbf{r}, E) \right) \right| = \left| \det \left(\frac{\partial^2 S_v}{\partial \mathbf{r}_{\perp} \partial \mathbf{r}_{\perp}} + \frac{\partial^2 S_v}{\partial \mathbf{r}_{\perp} \partial \mathbf{r}'_{\perp}} + \frac{\partial^2 S_v}{\partial \mathbf{r}'_{\perp} \partial \mathbf{r}_{\perp}} + \frac{\partial^2 S_v}{\partial \mathbf{r}'_{\perp} \partial \mathbf{r}'_{\perp}} \right) \right| \quad (4.3.80)$$

$$= \left| \det \left(\frac{\partial \mathbf{p}_{\perp}}{\partial \mathbf{r}_{\perp}} - \frac{\partial \mathbf{p}'_{\perp}}{\partial \mathbf{r}_{\perp}} + \frac{\partial \mathbf{p}_{\perp}}{\partial \mathbf{r}'_{\perp}} - \frac{\partial \mathbf{p}'_{\perp}}{\partial \mathbf{r}'_{\perp}} \right) \right| \quad (4.3.81)$$

$$= \left| \det \left(\frac{\partial(\mathbf{p}_\perp - \mathbf{p}'_\perp, \mathbf{r}_\perp - \mathbf{r}'_\perp)}{\partial(\mathbf{r}_\perp, \mathbf{r}'_\perp)} \right) \right|. \quad (4.3.82)$$

This leaves us with the following result for the prefactor in Eq. (4.3.73)

$$\sqrt{\frac{|D_v|}{\left| \frac{\partial^2}{\partial \mathbf{r}_\perp \partial \mathbf{r}_\perp} S_v(\mathbf{r}, \mathbf{r}, E) \right|}} = \sqrt{\frac{\frac{1}{\dot{r}^2(r_{||})} \left| \det \left(\frac{\partial \mathbf{p}'_\perp}{\partial \mathbf{r}_\perp} \right) \right|}{\left| \det \left(\frac{\partial(\mathbf{p}_\perp - \mathbf{p}'_\perp, \mathbf{r}_\perp - \mathbf{r}'_\perp)}{\partial(\mathbf{r}_\perp, \mathbf{r}'_\perp)} \right) \right|}} \quad (4.3.83)$$

$$= \frac{1}{|\dot{r}|} \frac{1}{\sqrt{\left| \det \left(\frac{\partial(\mathbf{r}_\perp, \mathbf{r}'_\perp)}{\partial(\mathbf{p}_\perp, \mathbf{r}'_\perp)} \frac{\partial(\mathbf{p}_\perp - \mathbf{p}'_\perp, \mathbf{r}_\perp - \mathbf{r}'_\perp)}{\partial(\mathbf{r}_\perp, \mathbf{r}'_\perp)} \right) \right|}} \quad (4.3.84)$$

$$= \frac{1}{|\dot{r}|} \frac{1}{\sqrt{\left| \det \left(\frac{\partial(\mathbf{p}_\perp - \mathbf{p}'_\perp, \mathbf{r}_\perp - \mathbf{r}'_\perp)}{\partial(\mathbf{p}'_\perp, \mathbf{r}'_\perp)} \right) \right|}} = \frac{1}{|\dot{r}|} \frac{1}{\sqrt{|\det(M - I)|}}. \quad (4.3.85)$$

Here I is the identity matrix of the same dimension as

$$M = \frac{\partial(\mathbf{p}_\perp, \mathbf{r}_\perp)}{\partial(\mathbf{p}'_\perp, \mathbf{r}'_\perp)} \in \mathbb{R}^{(2d-2) \times (2d-2)}. \quad (4.3.86)$$

M denotes the monodromy matrix or stability matrix of the PO with respect to the traversal degrees of freedom (\mathbf{r}_\perp), see Sect. 3.8.4. Note that the monodromy matrix can be interpreted now as the one for a Poincaré map of Sect. 3.8.1 taking points always at $r_{||} = r_{||}^{(0)}$. The corresponding Poincaré map lifts the dynamics from the local evolution to the full PO:

$$\begin{aligned} \mathbf{r}' &= (r_{||}, \mathbf{r}'_\perp) & \xrightarrow[1 \text{ period}]{} \mathbf{r} &= (r_{||}, \mathbf{r}_\perp) \\ \mathbf{p}' &= (p_{||}, \mathbf{p}'_\perp) & & \mathbf{p} = (p_{||}, \mathbf{p}_\perp). \end{aligned} \quad (4.3.87)$$

Intuitively, it is then clear that the determinant $|\det(M - I)|$ is independent of the parallel component $r_{||}$, i.e. at which point the trajectory starts along the perpendicular degree of freedom. This can be shown more rigorously as done, for instance, in [20].

The final result is a semiclassical approximation for the fluctuating part of the density of states:

$$\Rightarrow \rho_{\text{fl}}(E) \approx -\frac{1}{\pi} \text{Im} \sum_{\text{PO}} \frac{2\pi}{(2\pi i \hbar)^{\frac{d+1}{2}}} \frac{(2\pi i \hbar)^{d-\frac{1}{2}}}{\sqrt{|\det(M_{\text{PO}} - I)|}} \underbrace{\int dr_{||} \frac{1}{\dot{r}(r_{||})}}_{T_{\text{PPO}}} e^{\frac{i}{\hbar} S_{\text{PO}} - i \frac{\pi}{2} \sigma_{\text{PO}}}, \quad (4.3.88)$$

where T_{PPO} denotes the period of the primitive periodic orbit (PPO). This leads us to the very useful *Gutzwiller trace formula*, keeping in mind that the phase parts

depending on S_{PO} and σ_{PO} are independent of the starting point r_{\parallel} of the PO:

$$\rho_{\text{fl}}(E) = \frac{1}{\hbar\pi} \sum_{\text{PO}} \frac{T_{\text{PPO}}}{\sqrt{|\det(M_{\text{PO}} - I)|}} \cos\left(\frac{S_{\text{PO}}}{\hbar} - \frac{\pi}{2}\sigma_{\text{PO}}\right). \quad (4.3.89)$$

The symbol σ_{PO} denotes the Maslov index of the periodic orbit (PO), which is a canonically and topologically invariant natural number. Particularly, it does not depend on the choice of the coordinate system.

The sum over all periodic orbits can be decomposed formally in the following manner

$$\sum_{\text{PO}} = \sum_{\text{PPO}} \sum_{n=1}^{\infty}, \quad (4.3.90)$$

where PPO denotes the primitive periodic orbits of minimal length and n the number of cycles of each PPO giving the corresponding PO. Hence we have with

$$S_{\text{PO}} = n S_{\text{PPO}}, \quad \sigma_{\text{PO}} = n \sigma_{\text{PPO}}, \quad M_{\text{PO}} = M_{\text{PPO}}^n \quad (4.3.91)$$

the final expression for the fluctuating part

$$\Rightarrow \rho_{\text{fl}}(E) \approx \frac{1}{\hbar\pi} \sum_{\text{PPO}} T_{\text{PPO}} \sum_{n=1}^{\infty} \frac{1}{\sqrt{|\det(M_{\text{PPO}}^n - I)|}} \cos\left[n\left(\frac{S_{\text{PPO}}}{\hbar} - \frac{\pi}{2}\sigma_{\text{PPO}}\right)\right]. \quad (4.3.92)$$

Let us conclude this section with a simple example of a two-dimensional Poincaré map with either completely chaotic or fully regular dynamics. In the fully chaotic case, the eigenvalues of M_{PPO} are following Sect. 3.8.4

$$\text{EV}(M_{\text{PPO}}) = \{e^{\pm\lambda_{\text{PPO}}}, -e^{\pm\lambda_{\text{PPO}}}\}. \quad (4.3.93)$$

As a result, M_{PPO}^n has the eigenvalues

$$\text{EV}(M_{\text{PPO}}^n) = \{e^{\pm n\lambda_{\text{PPO}}}, (-1)^n e^{\pm n\lambda_{\text{PPO}}}\}. \quad (4.3.94)$$

Then the determinant is

$$\sqrt{|\det(M_{\text{PPO}}^n - I)|} = \sqrt{(e^{n\lambda_{\text{PPO}}} - 1)(e^{-n\lambda_{\text{PPO}}} - 1)} \quad (4.3.95)$$

$$= 2 \left| \sinh\left(\frac{n\lambda_{\text{PPO}}}{2}\right) \right|. \quad (4.3.96)$$

The maximal contribution to ρ_{fl} is thus expected to come from orbits with the smallest Lyapunov exponents $\lambda_{\text{PPO}} \equiv \sigma$ of the chaotic dynamics.⁷

⁷ In the notation of Sect. 3.8.4, the exponents are called σ , see Eq. (3.8.36).

Stable periodic orbits of regular systems have the eigenvalues $e^{\pm i\beta}$ of M_{PPO} , cf. Eq. (3.8.31):

$$\Rightarrow \sqrt{|\det(M_{\text{PPO}}^n - I)|} = 2 \left| \sin\left(\frac{n\beta}{2}\right) \right|. \quad (4.3.97)$$

For irrational $\beta/2\pi$ this gives a finite contribution to Eq. (4.3.91). For rational winding numbers we get, however, a divergent behavior, i.e. when

$$\frac{\beta}{2\pi} = \frac{s}{q}, \quad s, q \in \mathbb{N}. \quad (4.3.98)$$

Trace formulae for regular integrable systems are discussed in great detail in [27].

4.3.7 Applications of Semiclassical Theory

4.3.7.1 Spectral Analysis of Periodic Orbits

We started out with the quantum mechanical density of states

$$\rho(E) = \bar{\rho}(E) + \rho_{\text{fl}}(E), \quad (4.3.99)$$

in which we approximated the fluctuating part using Gutzwiller's trace formula

$$\text{where } \rho_{\text{fl}}(E) \approx \frac{1}{\pi\hbar} \sum_{\text{PO}} \frac{T_{\text{PPO}}}{\sqrt{|\det(M_{\text{PO}} - I)|}} \cos\left(\frac{S_{\text{PO}}}{\hbar} - \frac{\pi}{2}\sigma_{\text{PO}}\right), \quad (4.3.100)$$

with T_{PPO} as the period of the primitive periodic orbit (PPO) corresponding to each periodic orbit (PO). How can we apply this formula to a specific physical situation and why is it useful? First of all, there are some problems with Gutzwiller's trace formula. A priori we should know all classical POs which are extremely many in general. Their number increases exponentially with the period T_{PPO} at fixed energy in a chaotic system. The sum over them is therefore not necessarily converging. Actually, it is typical for a chaotic system that the sum is not absolutely convergent. The problem is essentially formulated in the following way:

$$\sum_{\text{PO}} \left| \frac{T_{\text{PPO}}}{\sqrt{|\det(M_{\text{PO}} - I)|}} \right| \xrightarrow{\text{typical}} \infty. \quad (4.3.101)$$

Moreover, we considered only isolated periodic orbits in the stationary phase expansion. Mixed regular-chaotic systems typically have non-isolated POs, in particular, close to bifurcations, see Sect. 3.8.7. In the case of non-isolated POs, one must go beyond the stationary phase approximation. More details on this problem are found in the textbooks [17, 27].

The divergence issue may be cured by a convolution of the spectrum with a smooth function, e.g., a Gaussian function, giving

$$\tilde{\rho}(E) = \frac{1}{\sqrt{\pi} \Delta E} \int_{\mathbb{R}} \rho(E') \exp \left\{ -\frac{(E - E')^2}{\Delta E^2} \right\} dE'. \quad (4.3.102)$$

This can be thought of as a finite “measurement” resolution of the spectrum, as it would, e.g., be observed in a real-life experiment. The implication for (4.3.99) is a stronger damping of the contributions with longer periodic orbits. This can be seen from the expansion

$$S_{\text{PO}}(E') \approx S_{\text{PO}}(E) + (E' - E) T_{\text{PO}}(E) \quad (4.3.103)$$

where the period of the PO is $T_{\text{PO}}(E) = \frac{\partial S_{\text{PO}}}{\partial E}$. This gives in Eq. (4.3.100)

$$\frac{1}{\sqrt{\pi} \Delta E} \int_{\mathbb{R}} dE' \cos \left[\frac{S_{\text{PO}}(E')}{\hbar} - \frac{\pi}{2} \sigma_{\text{PO}} \right] \exp \left\{ - \left(\frac{E - E'}{\Delta E} \right)^2 \right\} \quad (4.3.104)$$

$$\approx \cos \left[\frac{S_{\text{PO}}(E)}{\hbar} - \frac{\pi}{2} \sigma_{\text{PO}} \right] \underbrace{\exp \left\{ - \left(\frac{\Delta E \cdot T_{\text{PO}}}{2\hbar} \right)^2 \right\}}_{\rightarrow 0 \text{ for } (T_{\text{PO}} \rightarrow \infty)}. \quad (4.3.105)$$

The logic of applying Gutzwiller’s trace formula is simply the connection between classical POs and the quantum density of states

$$\text{“classical periodic orbits} \Rightarrow \rho_{\text{QM}} \text{”}. \quad (4.3.106)$$

Similarly, it is also possible to extract the dominant periodic orbits from a given quantum spectrum that was, e.g., measured in an experiment, or produced from numerical simulations. Hence, we may invert the logic in the following sense:

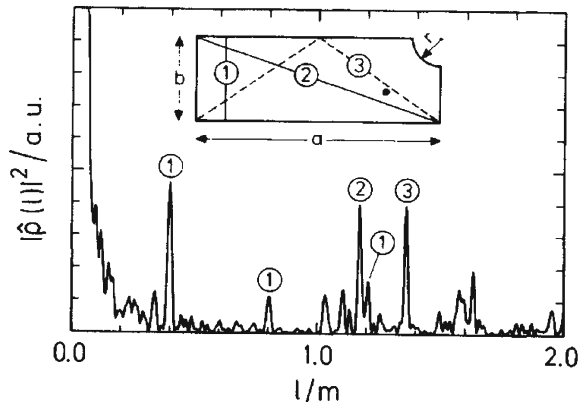
$$\text{“quantum spectrum} \Rightarrow \text{classical periodic orbits} \text{”}. \quad (4.3.107)$$

It is the latter direction which makes Gutzwiller’s trace formula very valuable for comparison between theory and experiments.

4.3.7.2 Examples for the Spectroscopy of Periodic Orbits

We discuss now two real experiments which measured quantum mechanical spectra of two different chaotic systems. The first one is a two-dimensional Sinai billiard, see Sect. 3.9.1, the second one is a hydrogen atom in a strong external magnetic field.

Fig. 4.16 Measured density of states as a function of length in a realization of a two-dimensional chaotic Sinai billiard. The numbers at the peaks correspond to the periodic orbits shown in the billiard. Reprinted with kind permission by H. J. Stöckmann, copyright 1990 by the American Physical Society [29]



Two-dimensional quantum billiards are most easily realized in a quasi two-dimensional setup for electromagnetic fields. In two-dimensions, the electromagnetic field equation, known as Helmholtz equation, is identical to a two-dimensional stationary Schrödinger equation [28]. The billiards are typically realized with microwaves with wavelength of the order of centimeters. The measured observable is the spectral density as a function of the frequency of the waves or, equivalently, of the wave numbers k . Fourier transforming into

$$\tilde{\rho}_{\text{fl}}(l) \propto \int \rho_{\text{fl}}(k) e^{ikl} dk, \quad (4.3.108)$$

gives a density with peaks at the PO contributions with actions $S_{\text{PO}} = \hbar k l_{\text{PO}}$. These POs correspond to the eigenmodes of the two-dimensional wave resonator. Fig. 4.16 shows $\tilde{\rho}_{\text{fl}}(l)$ with characteristic peaks arising from the shortest periodic orbits sketched in the billiard.

Spectral data for a hydrogen atom in a magnetic field are provided by astrophysical observations which show irregularities [30]. More recent laboratory experiments allow for very precise measurements of the spectrum even at high energies [31]. The Hamiltonian of the problem reads

$$H = \frac{p^2}{2m} - \frac{e^2}{4\pi\epsilon_0 r} + \omega L_z + \frac{1}{2}m\omega^2(x^2 + y^2) \quad (4.3.109)$$

$$\omega = \frac{eB}{2m}, \quad (4.3.110)$$

where B is the strength of the external magnetic field and L_z denotes the z component of the angular momentum. The problem has a planar symmetry as we immediately see from the Hamiltonian. Hence it is effectively two dimensional, just enough to allow for chaos, see Sect. 3.4. The classical dynamics is scale-invariant under the transformation for any $n \in \mathbb{R}^+$

$$\mathbf{r} \mapsto n^2 \mathbf{r} \quad (4.3.111)$$

$$\mathbf{p} \mapsto \frac{\mathbf{p}}{n} \quad (4.3.112)$$

$$E \mapsto n^{-2} E \quad (4.3.113)$$

$$\omega \mapsto n^{-3} \omega. \quad (4.3.114)$$

The natural choice for n is to interpret it as the principle quantum number of the hydrogen atom with $n \in \mathbb{N}$. For large n , the actions of periodic orbits are large compared to \hbar and we are effectively in the semiclassical limit. Since classical dynamics are invariant, the periodic orbits are then identical for all n . The action just has to be rescaled as

$$S_{\text{PO}}(E)|_n = n S_{\text{PO}}(E)|_{n=1}. \quad (4.3.115)$$

Then it follows that

$$\rho_{\text{fl}}(E)|_n \sim \sum_{\text{PO}} \frac{T_{\text{PPO}}|_{n=1}}{\sqrt{|\det(M_{\text{PO}} - I)|}} \cos \left[\frac{n}{\hbar} S_{\text{PO}}(E)|_{n=1} - \frac{\pi}{2} \sigma_{\text{PO}} \right]. \quad (4.3.116)$$

The spectrum is now measured as a function of the principal quantum number in the Rydberg regime, i.e. $n \gg 1$, while at the same time $B \sim |E|^{3/2}$ is varied according to the scaling above. Technically, this method is known as *scaled spectroscopy*. Fourier transforming with respect to n leads to the following density of states

$$\tilde{\rho}_{\text{fl}}(s) \propto \int \rho_{\text{fl}}(E)|_n e^{ins} dn. \quad (4.3.117)$$

This new density has its maxima exactly at the periodic orbits with action $S_{\text{PO}} = \hbar s$ by construction. Hence, the measured peaks in $\tilde{\rho}_{\text{fl}}(s)$ directly relate to periodic orbits of a certain length. A comprehensive description of hydrogen in strong magnetic fields and numerical computations were worked out by Dieter Wintgen in the 1980ties [32–34], see also [35]. A good general introduction into the occurrence of quantum chaos in hydrogen atoms in external fields is given in Delande’s contribution in [36].

4.3.7.3 Semiclassical Form Factor

Another important concept for the characterization of quantum spectra are spectral correlation functions [20]. To some extent we will come back to this issue in Sect. 4.6 when introducing concepts of random matrix theory. Please remember the decomposition of the density of states into

$$\rho(E) = \bar{\rho}(E) + \rho_{\text{fl}}(E), \quad (4.3.118)$$

see Eq. (4.3.67). We may now average the density over a finite window ΔE in energy such that

$$\frac{1}{\bar{\rho}} \ll \Delta E \ll \left(\frac{1}{\bar{\rho}} \frac{d\bar{\rho}}{dE} \right)^{-1}. \quad (4.3.119)$$

These conditions guarantee (i) a sufficient number of states for good statistics and (ii) that the averages are taken over ΔE much smaller than the typical variation of the density. Then we obtain

$$\langle \rho(E) \rangle \equiv \int_{E - \frac{1}{2}\Delta E}^{E + \frac{1}{2}\Delta E} \rho(E') dE' = \bar{\rho}(E), \quad (4.3.120)$$

and for the correlation function

$$\langle \rho(E)\rho(E') \rangle \equiv \int_{E - \frac{1}{2}\Delta E}^{E + \frac{1}{2}\Delta E} \rho(E'')\rho(E'' + (E' - E)) dE'' \quad (4.3.121)$$

$$\approx \bar{\rho}(E)\bar{\rho}(E') + \langle \rho_{fl}(E)\rho_{fl}(E') \rangle. \quad (4.3.122)$$

The spectral auto-correlation function is now defined as

$$C(E, E') = \frac{\langle \rho(E)\rho(E') \rangle - \langle \rho(E) \rangle \langle \rho(E') \rangle}{\bar{\rho}(E)\bar{\rho}(E')} \quad (4.3.123)$$

$$\approx \frac{\langle \rho_{fl}(E)\rho_{fl}(E') \rangle}{\bar{\rho}(E)\bar{\rho}(E')}. \quad (4.3.124)$$

Spectral correlation functions are very important for characterizing the fluctuations in the spectrum. They can be compared also with predictions from random matrix theory, see Sect. 4.6.8, in order to characterize if a given spectrum can be considered chaotic or regular. For the following discussion it is suitable to renormalize the local density of states by its smooth part, i.e. to set

$$E \mapsto \bar{\rho}(E)E. \quad (4.3.125)$$

This procedure gives dimensionless rescaled energies. It is known as unfolding of the spectrum and is necessary in order to compare with the universal prediction of random matrix theory. We will come back to it again in Sect. 4.6.4. From the correlation function we obtain the spectral form factor defined by

$$k(\tau) \equiv \int_{\mathbb{R}} C \left(E_0 + \frac{1}{2}E, E_0 - \frac{1}{2}E \right) e^{-2\pi i \bar{\rho}(E_0)E\tau} dE. \quad (4.3.126)$$

In the correlation function, using the semiclassical expression (4.3.89), a double sum over PO's enters which reads

$$\rho_{\text{fl}}(E)\rho_{\text{fl}}(E') \approx \sum_{\text{PO}, \text{PO}'} A_{\text{PO}} A_{\text{PO}'} \cos \left[\frac{S_{\text{PO}}}{\hbar} - \frac{\pi}{2} \sigma_{\text{PO}} \right] \cos \left[\frac{S_{\text{PO}'}}{\hbar} - \frac{\pi}{2} \sigma_{\text{PO}'} \right], \quad (4.3.127)$$

where

$$A_{\text{PO}} = \frac{1}{\pi \hbar} \frac{T_{\text{PO}}}{\sqrt{|\det(M_{\text{PO}} - I)|}}. \quad (4.3.128)$$

When averaging over the energy for systems without time-reversal symmetry, contributions with equal periodic orbits $\text{PO} = \text{PO}'$ dominate. We can therefore use the “diagonal approximation”

$$\cos \left[\frac{S_{\text{PO}}}{\hbar} - \frac{\pi}{2} \sigma_{\text{PO}} \right] \cos \left[\frac{S_{\text{PO}'}}{\hbar} - \frac{\pi}{2} \sigma_{\text{PO}'} \right] \quad (4.3.129)$$

$$\approx \frac{1}{2} \cos \left[\frac{S_{\text{PO}}(E) - S_{\text{PO}}(E')}{\hbar} \right] \delta_{\text{PO}, \text{PO}'} \quad (4.3.130)$$

$$\stackrel{E \approx E'}{\approx} \frac{1}{2} \cos \left[\frac{1}{\hbar} [E - E'] T_{\text{PO}} \left(E + \frac{E'}{2} \right) \right] \delta_{\text{PO}, \text{PO}'}, \quad (4.3.131)$$

where we have as usual $T_{\text{PO}} = \frac{\partial S_{\text{PO}}}{\partial E}$. Now we can approximate the correlation function

$$\langle \rho_{\text{fl}}(E_0 + \frac{1}{2}E) \rho_{\text{fl}}(E_0 - \frac{1}{2}E) \rangle \approx \sum_P \frac{1}{2} A_{\text{PO}}^2(E_0) \cos \left[\frac{1}{\hbar} T_{\text{PO}}(E_0) E \right]. \quad (4.3.132)$$

This leads with Eq. (4.3.126) to

$$k(\tau) \approx \frac{1}{\bar{\rho}^2(E_0)} \sum_{\text{PO}} \underbrace{\frac{1}{2} A_{\text{PO}}^2(E_0) \int_{\mathbb{R}} \cos \left[\frac{1}{\hbar} T_{\text{PO}}(E_0) E \right] e^{-2\pi i \bar{\rho}(E_0) E \tau} dE}_{\tau \geq 0 \frac{1}{2} 2\pi \delta \left(2\pi \bar{\rho}(E_0) \tau - \frac{1}{\hbar} T_{\text{PO}}(E_0) \right)} \quad (4.3.133)$$

$$= \sum_{\text{PO}} \frac{\left(\frac{T_{\text{PO}}}{T_H} \right)^2}{|\det(M_{\text{PO}} - I)|} \delta \left(\tau - \frac{T_{\text{PO}}}{T_H} \right) \quad (4.3.134)$$

$$\equiv k_{\text{diag}}(\tau). \quad (4.3.135)$$

$T_H = 2\pi \hbar / \bar{\rho}$ is the so-called Heisenberg time since it is inversely proportionally to the mean level spacing, following an energy-time uncertainty relation. For chaotic systems, it can be shown now, see [20], that

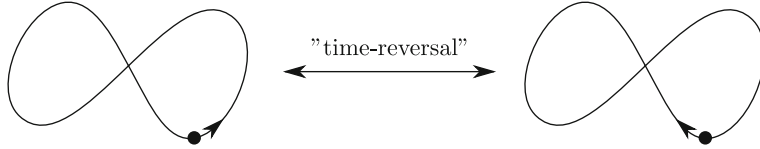
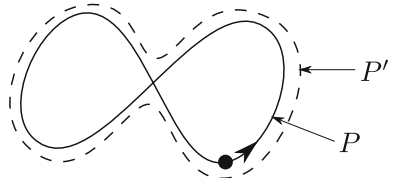


Fig. 4.17 In a time-reversal invariant system, every orbit has a time-reversed partner that shares its properties

Fig. 4.18 Sketch of the Sieber-Richter contributions to the form factor (dashed path). The two partner paths P and P' are known as Sieber-Richter pairs



$$k_{\text{diag}}(\tau) = \tau, \quad (4.3.136)$$

which corresponds to the prediction from random matrix theory, see Sect. 4.6, for short correlation times⁸ $\tau < 1$ [20]:

$$k_{\text{GUE}}(\tau) = \begin{cases} \tau : & 0 < \tau < 1 \\ 1 : & \tau > 1 \end{cases}. \quad (4.3.137)$$

For systems which are time-reversal invariant, we obtain

$$K_{\text{diag}}(\tau) = 2\tau, \quad (4.3.138)$$

since every orbit can run forward and backward in time as sketched in Fig. 4.17. In the diagonal approximation, we thus obtain two contributions to the sum

$$\sum_{\text{PO}, \text{PO}'} \dots \rightarrow \sum_{\text{PO}, \text{PO}' \neq \text{PO}} \dots + \sum_{\text{PO}, \text{PO}'=\text{reverse } (\text{PO})} \dots \quad (4.3.139)$$

Here reverse (PO) denotes the time reversed orbit of the periodic orbit (PO). Because of the time-reversal symmetry, reverse (PO) has the same values S_{PO} , T_{PO} , σ_{PO} , M_{PO} which characterize the periodic orbit.

As a final remark, we want to mention that modern semiclassical theory provides more subtle corrections to the form factor. One contribution is due to Sieber and Richter [37], who noted the importance of shadowing paths close to the POs, see the sketch in Fig. 4.18.

⁸ The unfolding from Eq.(4.3.125) makes the unit of time 1 corresponding to the inverse level spacing in dimensionless units. Hence only for energies larger than the inverse level spacing we can expect good correspondence.

Taking the Sieber-Richter pairs into account one can show for time-reversal invariant systems that

$$\Rightarrow k_{\text{diag+loops}}(\tau) = 2\tau - 2\tau^2 + \mathcal{O}(\tau^3) \quad (4.3.140)$$

as compared with the prediction from random matrix theory [20]

$$k_{\text{GOE}}(\tau) = \begin{cases} 2\tau - \tau \ln(1 + 2\tau) : \tau < 1 \\ 2 - \tau \ln\left(\frac{2\tau + 1}{2\tau - 1}\right) : \tau > 1 \end{cases} \stackrel{\tau \ll 1}{\approx} k_{\text{diag+loops}}(\tau). \quad (4.3.141)$$

Hence, also here we get good correspondence between both results provided that τ is small.

Higher order corrections to the form factor have recently been computed by Fritz Haake and collaborators, see the original Refs. [38, 39] and the latest edition of his book [20].

4.3.7.4 Alternative Form of the Trace Formula for Hyperbolic Systems

We may rewrite the trace formula of Eq. (4.3.91) in a compact form for fully chaotic, so-called hyperbolic systems, see Sect. 3.9. From the consideration in Eq. (4.3.96) we can start with the following form

$$\rho_{\text{fl}} \approx \frac{1}{\pi\hbar} \sum_{\text{PPO}} \sum_{n=1}^{\infty} \frac{T_{\text{PPO}}}{2 \sinh\left(\frac{n\lambda_{\text{PPO}}}{2}\right)} \underbrace{\cos\left[\frac{n}{\hbar} \left(S_{\text{PPO}} - \frac{\pi}{2} \sigma_{\text{PPO}}\right)\right]}_{=\text{Re } \exp\left(in\left[\frac{S_{\text{PPO}}}{\hbar} - \frac{\pi}{2} \sigma_{\text{PPO}}\right]\right)}, \quad (4.3.142)$$

where the sum runs over all primitive PO's and λ_{PPO} denote the Lyapunov exponent of these orbits. From

$$\frac{1}{2 \sinh\left(\frac{n\lambda_{\text{PPO}}}{2}\right)} = \frac{e^{-\frac{n}{2}\lambda_{\text{PPO}}}}{1 - e^{-n\lambda_{\text{PPO}}}} \stackrel{!}{=} \sum_{m=0}^{\infty} \exp\left\{-\left(m + \frac{1}{2}\right)n\lambda_{\text{PPO}}\right\} \quad (4.3.143)$$

we can define

$$t_{\text{PPO}}^{(m)} \equiv \exp\left[i\left(\frac{S_{\text{PPO}}}{\hbar} - \frac{\pi}{2} \sigma_{\text{PPO}}\right) - \left(m + \frac{1}{2}\right)\lambda_{\text{PPO}}\right]. \quad (4.3.144)$$

This definition can be used to compute the sum over phase terms

$$T_{\text{PPO}} \sum_{n=1}^{\infty} \left[t_{\text{PPO}}^{(m)}\right]^n = T_{\text{PPO}} \left(\frac{1}{1 - t_{\text{PPO}}^{(m)}} - 1\right) = T_{\text{PPO}} \frac{t_{\text{PPO}}^{(m)}}{1 - t_{\text{PPO}}^{(m)}}$$

$$= -i\hbar \frac{\partial}{\partial E} \ln \left(1 - t_{\text{PPO}}^{(m)} \right), \quad \text{with } T_{\text{PPO}} = \frac{\partial S_{\text{PPO}}}{\partial E}. \quad (4.3.145)$$

Thus we finally can identify

$$\rho_{\text{fl}}(E) \approx -\frac{1}{\pi} \text{Im} \left[\frac{\partial}{\partial E} \ln[Z(E)] \right], \quad (4.3.146)$$

with

$$Z(E) \equiv \prod_{\text{PPO}} \prod_{m=0}^{\infty} \left(1 - t_{\text{PPO}}^{(m)} \right). \quad (4.3.147)$$

The latter defines a partition function as it is known in statistical physics. Under certain circumstances, Z can be computed exactly, e.g. via a method known as “cycle expansion” [40]. This approach opens a whole new field of studying hyperbolic systems, based on techniques summarized under the name thermodynamic formalism. We refer to the online book [40] and the monograph [41], both written by experts of this field, for more details.

4.4 Wave Functions in Phase Space

In order to understand better the quantum mechanical evolution we have seen that we can use classical input to define approximate semiclassical wave functions, see Sects. 4.2.2.1, 4.2.4 and 4.3.4 in particular. The missing link between the classical and quantum description of the same physical problem is a comparison between densities evolving in phase space with wave packets chosen in one particular representation in quantum mechanics, e.g. in the spatial representation. To tackle the problem of projecting wave packets onto phase space we will introduce the useful concept of Weyl transforms in the following.

4.4.1 Phase Space Densities

For a classical Hamiltonian function of the form

$$H(\mathbf{q}, \mathbf{p}) = \frac{\mathbf{p}^2}{2m} + V(\mathbf{q}), \quad (4.4.1)$$

Liouville’s theorem from Sect. 3.3.3 for a density in phase space $\rho(\mathbf{q}, \mathbf{p}, t)$, see Eq. (3.4.7), can be formulated as

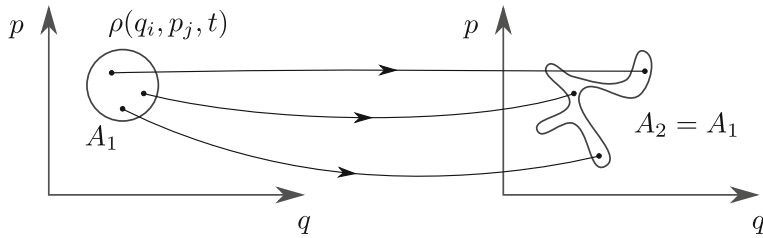


Fig. 4.19 According to Liouville’s theorem the shape of the classical phase-space volume can change but its area is conserved by the Hamiltonian evolution. $\rho(\mathbf{q}, \mathbf{p}, t)$ denotes a time-dependent phase-space density

$$\frac{\partial \rho(\mathbf{q}, \mathbf{p}, t)}{\partial t} = -\frac{\mathbf{p}}{m} \cdot \nabla_{\mathbf{q}} \rho - F(\mathbf{q}) \cdot \nabla_{\mathbf{p}} \rho = -\left(\frac{\dot{\mathbf{q}}}{\dot{\mathbf{p}}}\right) \cdot \nabla_{\mathbf{q}, \mathbf{p}} \rho(\mathbf{q}, \mathbf{p}, t), \quad (4.4.2)$$

where we used $\dot{\mathbf{q}} = \mathbf{p}/m$ and $\dot{\mathbf{p}} = F(\mathbf{q}) = -\nabla_{\mathbf{q}} V(\mathbf{q})$. The evolution of an initially spherical density is sketched in Fig. 4.19.

The question is what is a good analogue of the classical density $\rho(\mathbf{q}, \mathbf{p}, t)$ in quantum mechanics. For this let us have a look at the quantum mechanical density operator $\hat{\rho}$. $|\psi(t)\rangle$ shall denote a state of the Hilbert space of wave functions, and we restrict here to density operators representing pure states in the state space of density matrices. For mixed states, the reader may consult the literature on open quantum systems [42]. Then, we have

$$\hat{\rho} \equiv |\psi(t)\rangle \langle \psi(t)|. \quad (4.4.3)$$

For closed systems exclusively studied here in the following, the Schrödinger equation for the state $|\psi(t)\rangle$ is equivalent to the following von Neumann equation for the density operator

$$\frac{d\hat{\rho}}{dt} = -\frac{i}{\hbar} [\hat{H}, \hat{\rho}]. \quad (4.4.4)$$

How can we project the density operator onto phase space? This question is not at all trivial since Heisenberg’s uncertainty relation forbids us in quantum mechanics to specify the canonically conjugated phase space coordinates simultaneously. One way to do this will be described in the next subsection.

4.4.2 Weyl Transform and Wigner Function

A solution for the problem of specifying both coordinates (\mathbf{q}, \mathbf{p}) simultaneously is naturally given by the idea of smoothing the dependence on the coordinates such that Heisenberg’s uncertainty relation is not affected. To formalize this, we introduce the

Weyl symbol \hat{A}_W of a hermitian operator \hat{A} . Let $|\mathbf{q}\rangle$ be the spatial eigenmodes of a quantum system, then the Weyl symbol is defined by

$$A_W(\mathbf{q}, \mathbf{p}) \equiv \frac{1}{(2\pi\hbar)^d} \int d^d\mathbf{x} \langle \mathbf{q} + \frac{\mathbf{x}}{2} | \hat{A} | \mathbf{q} - \frac{\mathbf{x}}{2} \rangle e^{-\frac{i}{\hbar} \mathbf{p} \cdot \mathbf{x}}. \quad (4.4.5)$$

It is clear that the Weyl symbol is additive, i.e. the symbol for the operator $\hat{A} + \hat{B}$ it is just $A_W + B_W$. However, the symbols have a more complicated structure for products of operators. This is related to the usual ordering problem of the application of operators in quantum mechanics. We get, for instance, that $\hat{A}\hat{B}$ transforms into [43]

$$A_W \left(\mathbf{q} - \frac{\hbar}{2i} \frac{\partial}{\partial \mathbf{p}}, \mathbf{p} + \frac{\hbar}{2i} \frac{\partial}{\partial \mathbf{q}} \right) B_W(\mathbf{q}, \mathbf{p}). \quad (4.4.6)$$

Now the main operator of interest is the density operator $\hat{\rho}$ for which we may define the corresponding Weyl symbol

$$W_\rho(\mathbf{q}, \mathbf{p}) \equiv \frac{1}{(2\pi\hbar)^d} \int d^d\mathbf{x} \langle \mathbf{q} + \frac{\mathbf{x}}{2} | \hat{\rho} | \mathbf{q} - \frac{\mathbf{x}}{2} \rangle e^{-\frac{i}{\hbar} \mathbf{p} \cdot \mathbf{x}}. \quad (4.4.7)$$

W_ρ is also called Wigner function. It represents a generalized probability density in phase space of the quantum state characterized by $\hat{\rho}$. That W_ρ is not a real probability density will become clear from its properties summarized in the following.

4.4.2.1 Properties of the Wigner Function

Most of the properties of Wigner function are easily proven. Some of the following statements are given as problems for the reader, please see the problem section at the end of this chapter:

- (a) The Wigner function can be equally defined in the momentum representation which is identical to Eq. (4.4.7):

$$W_\rho(\mathbf{q}, \mathbf{p}) \equiv \frac{1}{(2\pi\hbar)^d} \int d^d\mathbf{p} \langle \mathbf{p} + \frac{\mathbf{s}}{2} | \hat{\rho} | \mathbf{p} - \frac{\mathbf{s}}{2} \rangle e^{\frac{i}{\hbar} \mathbf{q} \cdot \mathbf{s}}. \quad (4.4.8)$$

- (b) The two marginals of the Wigner function correspond to the quantum mechanical probabilities of finding the particle described by the wave function at the position \mathbf{q} or momentum \mathbf{p} , respectively:

$$\begin{aligned} \int d^d\mathbf{p} W_\rho(\mathbf{q}, \mathbf{p}) &= \langle \mathbf{q} | \hat{\rho} | \mathbf{q} \rangle = |\psi(\mathbf{q}, t)|^2 \geq 0 \\ \int d^d\mathbf{q} W_\rho(\mathbf{q}, \mathbf{p}) &= \langle \mathbf{p} | \hat{\rho} | \mathbf{p} \rangle = |\psi(\mathbf{p}, t)|^2 \geq 0. \end{aligned} \quad (4.4.9)$$

As stated in Sect. 4.4.1, we always assume that the quantum system is in a pure state.

(c) Normalization condition:

$$\int d^d \mathbf{p} W_\rho(\mathbf{q}, \mathbf{p}) = 1. \quad (4.4.10)$$

(d) Product rule for the trace:

$$\text{tr}(\hat{\rho}_1 \hat{\rho}_2) = \int d^d \mathbf{q} \int d^d \mathbf{p} W_{\rho_1}(\mathbf{q}, \mathbf{p}) W_{\rho_2}(\mathbf{q}, \mathbf{p}). \quad (4.4.11)$$

- (e) The Wigner function may assume negative values. This is the reason why we cannot consider it as a probability density in the strict sense. In order to see that the Wigner function can be negative we give the following argument. We may choose two quantum states which have no common support (or overlap in any representation), i.e. $\text{tr}(\hat{\rho}_1 \hat{\rho}_2) = 0$. Then, by property (d), at least one of the two Wigner functions must be identical to zero if negative values were forbidden. Only if negative values are allowed, the overlap integral (4.4.11) can become zero for both Wigner functions not identical to zero.
- (f) As a generalization of (d), we also have for the quantum mechanical expectation value of hermitian operators that

$$\langle \hat{A} \rangle \equiv \text{tr}(\hat{\rho} \hat{A}) = \int d^d \mathbf{q} \int d^d \mathbf{p} A_w(\mathbf{q}, \mathbf{p}) W_\rho(\mathbf{q}, \mathbf{p}). \quad (4.4.12)$$

- (g) The von Neumann equation (4.4.4) reduces in the Weyl representation approximately to the classical Liouville equation (4.4.2) for the Wigner function. This is most easily seen for a Hamiltonian of the form

$$\hat{H} = \hat{T} + \hat{V} \quad \text{with} \quad \hat{T} = \frac{\hat{\mathbf{p}}^2}{2m}, \quad \hat{V} = V(\mathbf{q}). \quad (4.4.13)$$

We then get for the two commutators in their Weyl representation

$$\begin{aligned} [\hat{T}, \hat{\rho}]_W &= \frac{1}{(2\pi\hbar)^d} \int d^d \mathbf{s} \frac{1}{2m} \left[\left(\mathbf{p} + \frac{\mathbf{s}}{2} \right)^2 - \left(\mathbf{p} - \frac{\mathbf{s}}{2} \right)^2 \right] \rho_p(\mathbf{p} + \frac{\mathbf{s}}{2}, \mathbf{p} - \frac{\mathbf{s}}{2}, t) e^{\frac{i}{\hbar} \mathbf{q} \cdot \mathbf{s}} \\ &= \frac{\hbar p}{im} \nabla_{\mathbf{q}} W_\rho(\mathbf{q}, \mathbf{p}, t), \\ [\hat{V}, \hat{\rho}]_W &= \frac{1}{(2\pi\hbar)^d} \int d^d \mathbf{p} \frac{1}{2m} \left[V\left(\mathbf{q} + \frac{\mathbf{x}}{2}\right) - V\left(\mathbf{q} - \frac{\mathbf{x}}{2}\right) \right] \rho_q(\mathbf{q} + \frac{\mathbf{x}}{2}, \mathbf{q} - \frac{\mathbf{x}}{2}, t) e^{-\frac{i}{\hbar} \mathbf{p} \cdot \mathbf{x}}. \end{aligned} \quad (4.4.14)$$

Taylor expanding the potential

$$V\left(q \pm \frac{\mathbf{x}}{2}\right) = V(\mathbf{q}) \pm \frac{\mathbf{x}}{2} \cdot \nabla_{\mathbf{q}} V(\mathbf{q}) + \dots, \quad (4.4.15)$$

and using (4.4.4)⁹ we arrive at the following equation for the Wigner function phase space pseudo-density

$$\frac{\partial W_\rho(\mathbf{q}, \mathbf{p}, t)}{\partial t} = -\frac{\mathbf{p}}{m} \nabla_{\mathbf{q}} W_\rho - F(\mathbf{p}) \cdot \nabla_{\mathbf{p}} W_\rho + \dots, \quad (4.4.16)$$

with $F = -\nabla_{\mathbf{q}} V(\mathbf{q})$. This relation is very similar to Eq. (4.4.2) above. E.g. for a one-dimensional harmonic oscillator with a potential $V(q) = a + bq + cq^2$, Eq. (4.4.16) is indeed exact since the even terms in the Taylor expansion cancel themselves in the commutator $[\hat{V}, \hat{\rho}]_W$. Hence, in the semiclassical limit (see also the next point (h)), when the effective quantum coarse graining by \mathbf{x} is small, we obtain the classical Liouville equation for the Wigner densities.

The above Eq. (4.4.16) tells us even more. It effectively means that the classical evolution for an initial density in phase space is already dispersive, see Fig. 4.19. Hence, the dispersion of a wave packet with time, contrary to the standard believe, see e.g. the textbook [1], does not originate in the particular properties of the quantum evolution, but it is simply a consequence of Heisenberg's uncertainty relation. The latter implies that a quantum state must be modeled by an ensemble of initial conditions on the classical level, and any non-sharp initial density will spread during its classical evolution in phase space! This property is the origin of an approximation method to describe the quantum evolution of quantum optical systems, the so-called truncated Wigner approximation, see e.g. [44, 45].

- (h) For classically integrable systems, we can show that the semiclassical density, and hence also the Wigner function, localizes around the corresponding integrable tori. To show this, we take the semiclassical wave function from Eq. (4.2.99) for the torus action $\mathbf{I}_n = \hbar(n_1 + 1/2, n_2 + 1/2, \dots, n_d + 1/2)$ and define $\mathbf{r} = \mathbf{x}/\hbar$ for a formal expansion in orders of \hbar . Then the Wigner function reads

$$\begin{aligned} W_\rho(\mathbf{q}, \mathbf{p}) &= \frac{1}{(2\pi)^d} \int d^d \mathbf{r} \psi_n^* \left(q - \hbar \frac{\mathbf{r}}{2} \right) \psi_n \left(q + \hbar \frac{\mathbf{r}}{2} \right) e^{-i\mathbf{p}\cdot\mathbf{r}} \\ &\approx \frac{1}{(2\pi)^d} \int d^d \mathbf{r} \sqrt{\left| \det \left(\frac{\partial^2 S}{\partial \mathbf{r} \partial \mathbf{I}} \left(\mathbf{q} - \hbar \frac{\mathbf{r}}{2}, \mathbf{I}_n \right) \right) \det \left(\frac{\partial^2 S}{\partial \mathbf{r} \partial \mathbf{I}} \left(\mathbf{q} + \hbar \frac{\mathbf{r}}{2}, \mathbf{I}_n \right) \right) \right|} \\ &\quad \exp \left(\frac{i}{\hbar} \left[S \left(\mathbf{q} + \hbar \frac{\mathbf{r}}{2}, \mathbf{I}_n \right) - S \left(\mathbf{q} - \hbar \frac{\mathbf{r}}{2}, \mathbf{I}_n \right) - \hbar \mathbf{p} \cdot \mathbf{r} \right] \right). \end{aligned} \quad (4.4.17)$$

Using the Taylor expansion of the phase

$$S(\mathbf{q} \pm \hbar \mathbf{r}/2, \mathbf{I}) \approx S(\mathbf{q}, \mathbf{I}) \pm \frac{\hbar}{2} \mathbf{r} \cdot \frac{\partial S}{\partial \mathbf{q}}(\mathbf{q}, \mathbf{I}) + O(\hbar^2 \mathbf{r}^2)$$

for $\hbar \rightarrow 0$ and the classical relations

⁹ We assume that the integral in the definition of the Weyl symbol and the time-derivative can be interchanged.

$$\begin{aligned}\frac{\partial S}{\partial \mathbf{r}} &= \mathbf{p}, \\ \frac{\partial^2 S}{\partial \mathbf{r} \partial \mathbf{I}} &= \frac{\partial \mathbf{p}}{\partial \mathbf{I}},\end{aligned}\quad (4.4.18)$$

see Eq. (3.3.12), we obtain

$$W_\rho(\mathbf{q}, \mathbf{p}) \approx \left| \det \left(\frac{\partial \mathbf{p}}{\partial \mathbf{I}_n} \right) \right| \frac{1}{(2\pi)^d} \int d^d \mathbf{r} e^{i \mathbf{r} \cdot [\mathbf{p}(\mathbf{q}, \mathbf{I}_n) - \mathbf{p}]} = \delta(\mathbf{I}(\mathbf{q}, \mathbf{p}) - \mathbf{I}_n). \quad (4.4.19)$$

In the last step we transformed from the momentum variable \mathbf{p} to the action variable \mathbf{I}_n . Hence, in the limit $\hbar \rightarrow 0$, the Wigner function localizes along the classical invariant orbit with action \mathbf{I}_n . We call this *localization* of the wave packet around classical regular tori in phase space.

4.4.2.2 Husimi Function

The problem of the Wigner function is that it can take negative values. An alternative probability density which is always positive is the Husimi distribution function, which in quantum optics is known as Q function [46]. One way to obtain it is by smoothing the Wigner function in the following manner:

$$H_{|\psi\rangle}(\mathbf{q}, \mathbf{p}) \equiv \int d\mathbf{q}' d\mathbf{p}' W_{|\psi\rangle}(\mathbf{q}', \mathbf{p}') f(\mathbf{q}, \mathbf{p}; \mathbf{q}', \mathbf{p}'), \quad (4.4.20)$$

with the coarse-graining function f . The usual choice for this function is a coherent state (an harmonic oscillator state) constructed in phase space, i.e.

$$f(\mathbf{q}, \mathbf{p}; \mathbf{q}', \mathbf{p}') = W_{|\psi\rangle_{\text{coherent}}} = \frac{1}{(\pi\hbar)^d} e^{-\left(\frac{(\mathbf{q}-\mathbf{q}')^2}{\sigma_q^2} + \frac{\sigma_q^2(\mathbf{p}-\mathbf{p}')^2}{\hbar^2}\right)} \geq 0. \quad (4.4.21)$$

σ_q is known as squeezing parameter which controls the relative resolution of the distribution (i.e. of the projection of the quantum state onto phase space) in the two variables \mathbf{q} and \mathbf{p} , respectively. In Problem 4.9 you may show that the above definition is equivalent to defining the Husimi function by projecting directly the wave packet $|\psi\rangle$ onto coherent states and taking the absolute value. From the latter definition it is then clear that the Husimi function cannot have negative values. Husimi functions will be shown in the following examples.

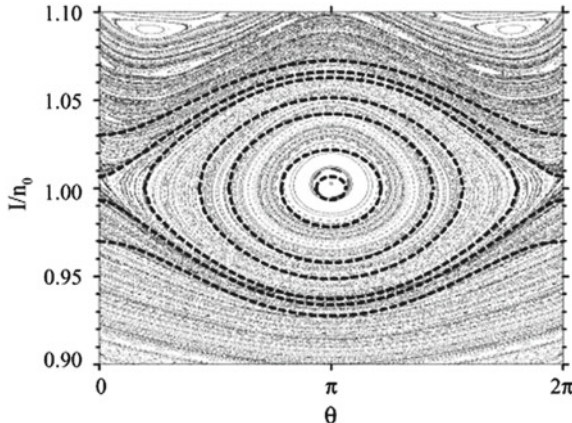


Fig. 4.20 Comparison between the resonance island of a one-dimensional pendulum (dashed lines) and a one-dimensional model of a driven hydrogen Rydberg atom with principle quantum number $n_0 \gg 1$. The electronic motion in the atom follows the periodic driving. This creates a resonance island in phase space resembling closely the one of the pendulum. The axes are given in terms of the action-angle variables of the unperturbed hydrogen problem, and the action is rescaled by $\hbar n_0$. Reprinted from [47], copyright 2002, with permission from the authors and Elsevier

4.4.3 Localization Around Classical Phase Space Structures

4.4.3.1 Localization Along Regular Phase Space Structures

As just shown in Sect. 4.4.2.1, see point (h), quantum mechanical wave packets can stick to regular classical invariant tori. Loosely speaking the necessary condition for this sticking effect is that the classical regular structure in phase space should have a size of the order of \hbar^d , where d is the dimension of the Hilbert space. This implies for areas $A_{\text{cl.}} \gtrsim \hbar$ in two-dimensional phase space plots (for which $d = 1$). In particular, we may find energy eigenstates of a quantum problem which have strong overlap with classical regular structures. In the limit of $\hbar \rightarrow 0$, the quantum wave packets are completely localized by this sticking process. They can then only escape by tunneling through the classically invariant tori. Since no static potential barrier is necessarily present here, one speaks about *dynamical tunneling* in this context. The latter subject is quite topical and a modern review is found in Ref. [48].

Arguably the most prominent example of classically localized and also dynamically stabilized wave packets are those anchored to regular islands in phase space. These *non-dispersive wave packets* are extremely stable in the long-time evolution but may breath periodically in time since they follow a periodic classical orbit motion. For an electron excited to a high lying Rydberg state, its quantum motion may resemble a classical planetary orbit. The non-dispersive wave packets can only decay via the mechanism of dynamical tunneling mentioned above which is very slow. In Sect. 3.7.6 we have seen that the motion close to the stable center of a resonance island

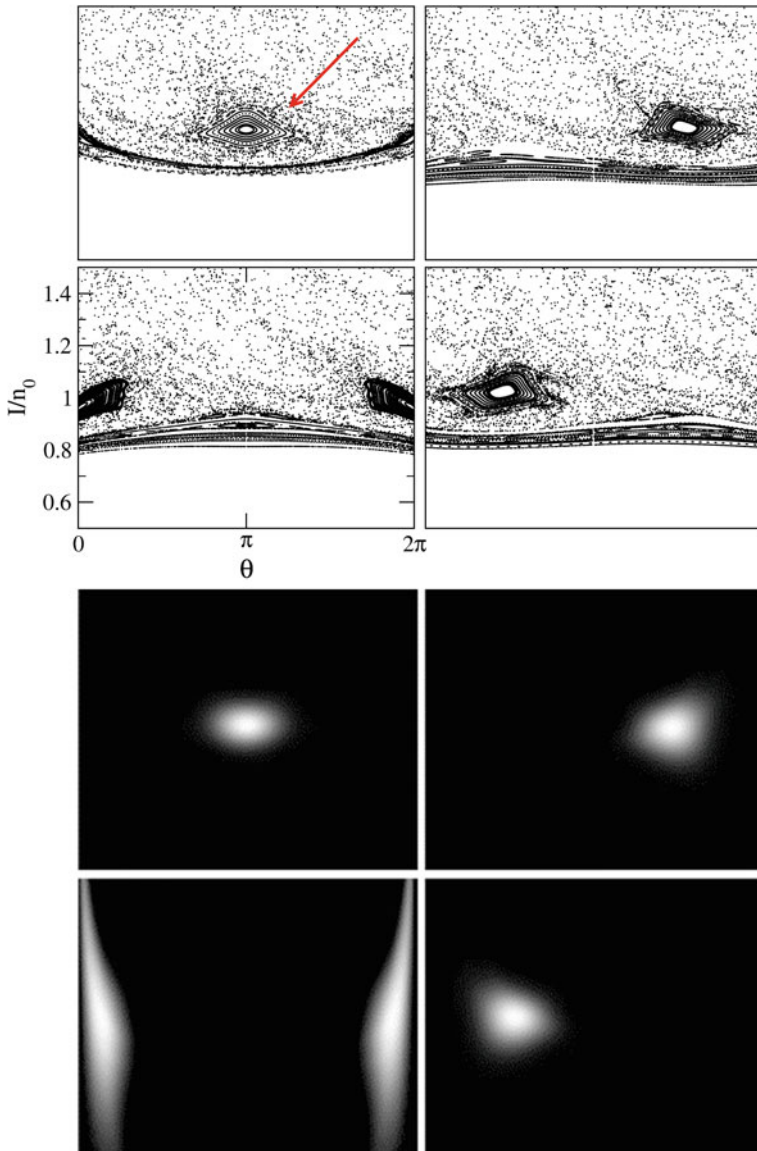


Fig. 4.21 Upper panels: Poincaré surface of sections for a driven one-dimensional hydrogen atom. The four plots are taken at different times within a period of the drive. The arrow marks the resonance island (moving with the phase of the drive). The (almost) continuous lines below the islands represent regions below which the motion is quasi-regular (here the driving is not perturbing much since the frequency times \hbar is typically much smaller than the level spacing, see also Fig. 4.27 in the next section). Lower panels: Husimi plots of a non-dispersive wave packet anchored to the 1:1 island seen in the upper panels. Reprinted from [47], copyright 2002, with permission from the authors and Elsevier

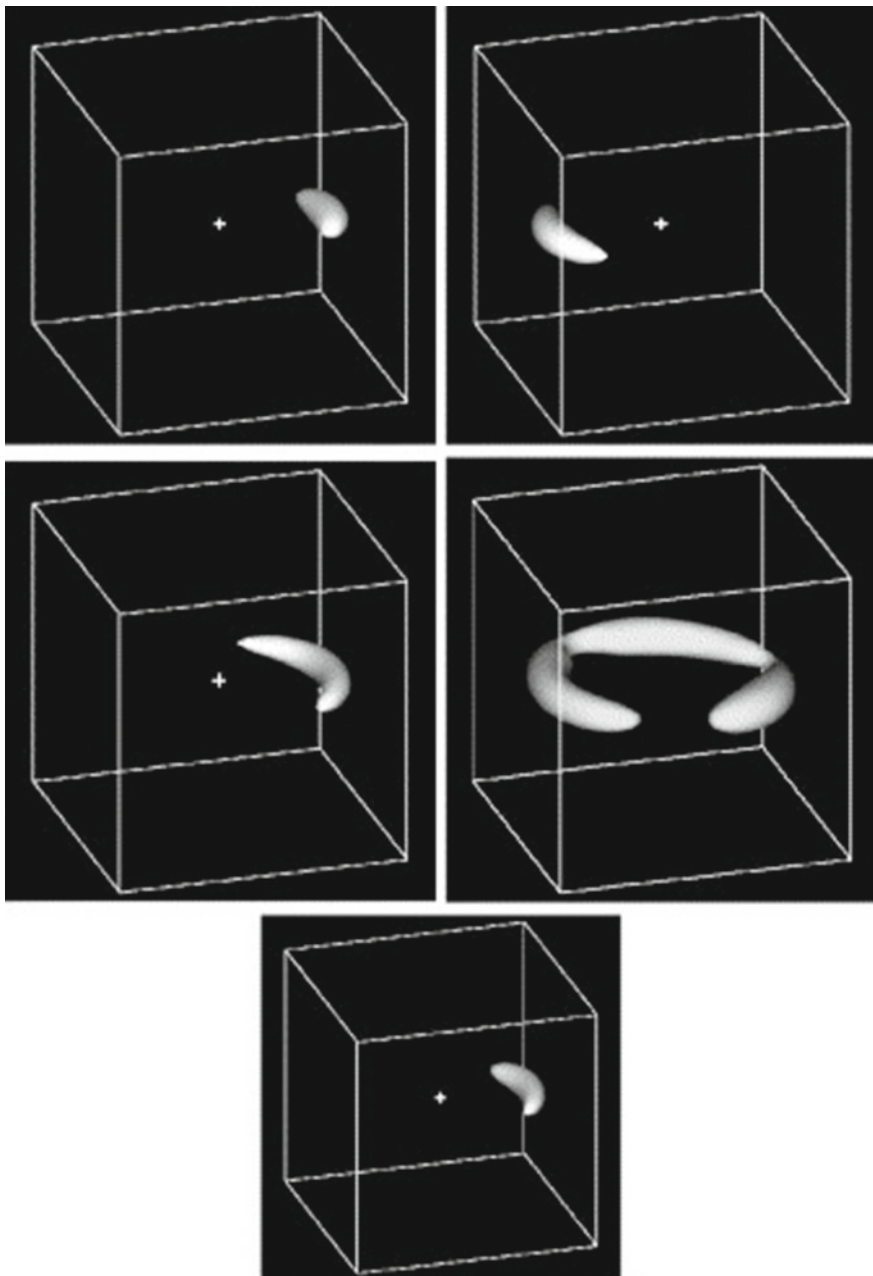


Fig. 4.22 Three-dimensional version of a non-dispersive wave packet (the system is a hydrogen atom in a periodic driving field, the nucleus is fixed and shown by the cross, the electronic wave packet is shown as a Husimi plot in white/grey). The wave packet moves around the nucleus dispersing partially but recombining after a period of the motion. Reprinted from [47], copyright 2002, with permission from the authors and Elsevier

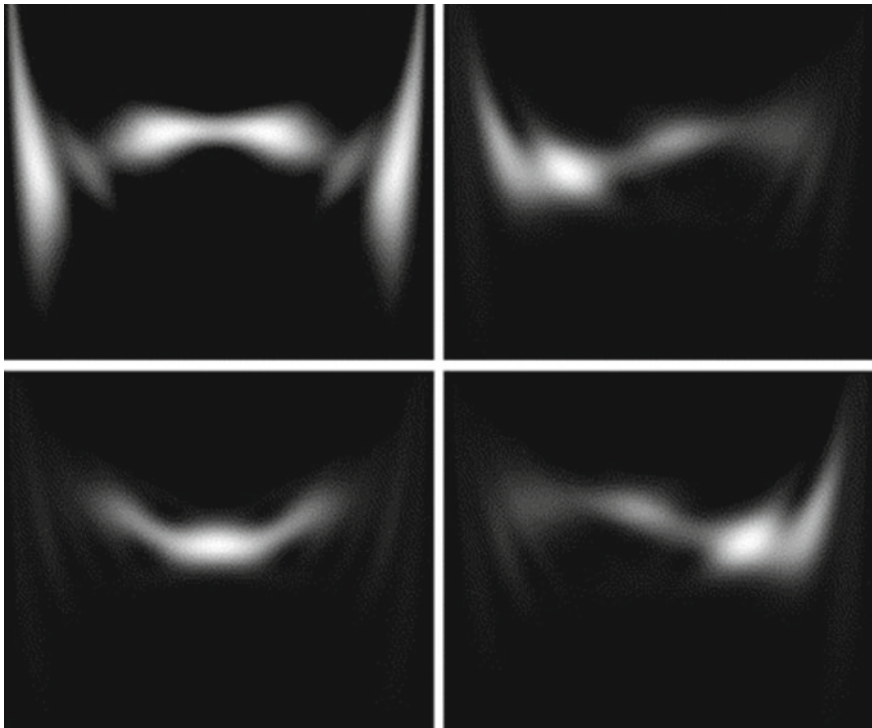


Fig. 4.23 For the same system as in Fig. 4.21 we see a Husimi plot of a quantum wave packet (white/grey) sticking to the separatrix region. The four Poincaré plots are taken at four different times (or phases) of the periodic motion. Reprinted from [47], copyright 2002, with permission from the authors and Elsevier

may be described by a pendulum in good approximation. The quantum mechanical wave packets are then very similar to quantized pendulum states. Figure 4.20 shows the good correspondence with a Poincaré surface of section of a driven Rydberg electron in hydrogen (for simplicity it is constructed for an electron moving in one-dimension and at one side of the nucleus only). Figures 4.21 and 4.22 show the evolution of the corresponding quantum wave packets for the one-dimensional model and a true three-dimensional description, respectively. Apart from the mentioned system of driven Rydberg states [49–51], nondispersive wave packets are experimentally realized, e.g. in (slightly amended) kicked rotor systems [52–54].

4.4.3.2 Localization Around Hyperbolic Fixed Points and Along Broken Separatrices

Around a hyperbolic or unstable fixed point in phase space the classical dynamics is highly unstable as we have seen, in Sects. 3.8.4 and 3.8.6. A quantum wave packet

prepared at the unstable point has a finite extension due to Heisenberg's uncertainty principle. Hence it may feel the impact of the classical stable manifold (which is of small measure in classical phase space and hence hard to hit classically). Such wave packets are then also relatively stable because the chaotic diffusion is counterbalanced by the finite extension of the wave packet. As seen in the example below, the tails of the Husimi function indeed are elongated along the unstable manifold (please c.f. Sects. 3.8.6 and 3.8.7). Nevertheless the wave packet remains concentrated around the classically stable region in its time evolution. Especially interesting are states which stick to the separatrix region of the pendulumlike classical motion. In a one-and-a-half-degree-of-freedom system the separatrix separates regular and unstable motion containing the unstable fixed point. Despite its high instability on the classical level, the corresponding quantum wave packet moves around the separatrix in one period of the drive but remains stuck to the separatrix without being destroyed. Figure 4.23 shows the evolution of such a wave packet for the one-dimensional model of driven hydrogen.

4.4.3.3 Localization Along Unstable Periodic Orbits: Scars

In 1984 Eric Heller published a theoretical paper predicting stable quantum wave packets that extend along the classical unstable periodic orbits [55], which have been discussed in Sect. 4.2.4. The quantum wave functions are said to *scar* these orbits. Figure 4.24 shows the original plot published by Heller. It represents quantum mechanical energy eigenstates of a two-dimensional stadium billiard which is classically chaotic. Three scarring states are shown corresponding to the periodic orbits highlighted on the right panels (b). Experimentally, traces of scarred states were observed, for instance, with electromagnetic billiards [56–58] and with light in optical fibers [59]. I refer to the short review on billiards [60] for nice comparisons between numerical and experimental data.

Again the quantum wave packets are much more robust than the corresponding classical unstable orbits, much in the same way as just discussed in the preceding subsection. Nevertheless, all the mechanisms for localization of quantum wave packets studied in this section can be understood by the classical phase space structure and Heisenberg's uncertainty relation.

4.5 Anderson and Dynamical Localization

In the previous section we discussed classical localization effects of wave packets caused by classical phase space properties. There are also quantum mechanical stabilization effects. In the following we report on quantum localization by disorder (a static problem) and by temporal evolution (in a dynamical setting). Both are very similar. Our aim is to give an intuitive picture of them. For this we restrict to one

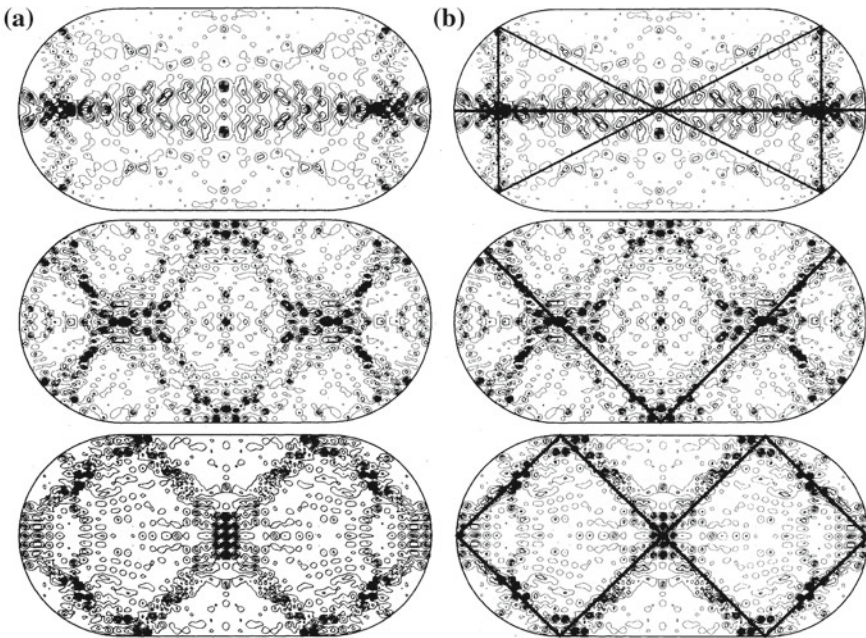


Fig. 4.24 **a** Eigenstates, represented by the contour plots, of the stadium billiard represented by the circumference. **b** Same as in (a) with the corresponding unstable periodic orbits of the classical motion: a bow-tie state (*upper panel*), a V-shaped state (*middle panel*) and an eight-like state (*lower panel*). Reprinted with kind permission by Eric Heller, copyright 1984 by the American Physical Society [55]

spatial dimension (plus temporal drive for the kicked rotor) and refer to the literature for exact derivations and further examples [20, 61–65].

4.5.1 Anderson Localization

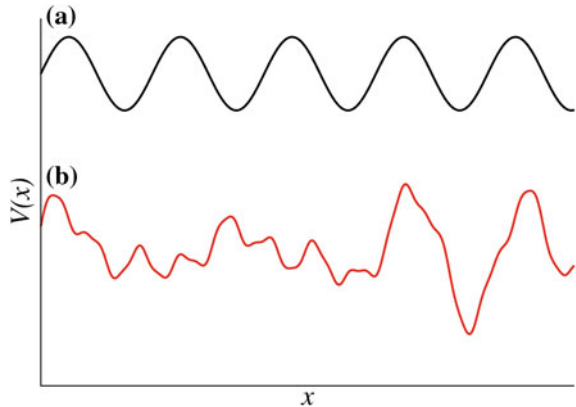
We start with a relatively simple model for a one-dimensional solid. The system is described by the Hamiltonian with a spatially dependent potential $V(x)$

$$\hat{H} = \frac{\hat{p}^2}{2m} + V(x). \quad (4.5.1)$$

If the potential is periodic with lattice constant d_L , i.e. $V(x + d_L) = V(x)$, the eigenfunctions are Bloch states, i.e. the following superpositions of plane waves [3]

$$\psi_\kappa(x) = e^{i\kappa x} u_\kappa(x). \quad (4.5.2)$$

Fig. 4.25 **a** Sinosoidally periodic potential. **b** Sketch of a disordered potential



Here κ is the quasi-momentum. It is a constant of the motion, induced by the translation invariance, which generates extended states. Spatially localized wave packets may be formed by appropriately superposing individual plane waves $\psi_\kappa(x)$. Such localized packets are typically not stable because they will generically disperse like most of quantum mechanical wave packets.

Stable and localized wave packets form, however, in a disordered potential. Hence, we look at what happens if the potential $V(x)$ is not translationally invariant but globally disordered, see Fig. 4.25b. To avoid discussions more complicated than necessary, we restrict to a lattice model in the following. Such a model may be obtained from the continuum model by using a basis of well-localized states $(|i\rangle)_i$, the so-called Wannier states [66–68], and expanding in this basis, i.e.

$$|\psi_n\rangle = \sum_i a_{i,n} |i\rangle. \quad (4.5.3)$$

With the matrix elements $\varepsilon_i \equiv \langle i | \hat{H} | i \rangle$ and $t_{ij} \equiv \langle i | \hat{H} | j \rangle$ for $i \neq j$, we can write down the following lattice Hamiltonian denoting nearest neighbor sites by $\langle j \rangle$

$$\hat{H}_{\text{lattice}} = \sum_{\langle j \rangle} t_{ij} |i\rangle \langle j| + \sum_i \varepsilon_i |i\rangle \langle i|. \quad (4.5.4)$$

A further simplified version of our model is obtained with the assumptions

$$t_{ij} = t = \text{const.} \quad \text{for } i = j \pm 1, \text{ and zero otherwise}$$

$$\langle \varepsilon_i \rangle = 0, \langle \varepsilon_i \varepsilon_j \rangle = \frac{W^2}{12} \delta_{i,j} \quad \text{for } \varepsilon_i \in \left[-\frac{W}{2}, \frac{W}{2} \right]. \quad (4.5.5)$$

Here W characterizes the strength of the disorder and the distribution of the random numbers ε_i is uniform in the given interval. We can then rescale the tight-binding

Hamiltonian (4.5.4) by dividing it by t , and the system depends only on the single parameter W/t , the dimensionless disorder strength. The stationary Schrödinger equation with energy eigenvalue E can be written in the form

$$t(a_{i-1} + a_{i+1}) + \varepsilon_i a_i = Ea_i, \quad (4.5.6)$$

from which we obtain the following matrix equation to solve for the eigenvalues E and the eigenvectors \mathbf{a}

$$\begin{pmatrix} \varepsilon_1 - E & t & 0 & 0 & 0 & 0 \\ t & \varepsilon_2 - E & t & 0 & 0 & 0 \\ 0 & . & . & 0 & 0 & 0 \\ \vdots & 0 & . & . & 0 & \vdots \\ 0 & 0 & 0 & 0 & t & \varepsilon_{L-1} - E \\ 0 & 0 & 0 & 0 & t & \varepsilon_L - E \end{pmatrix} \mathbf{a} = 0. \quad (4.5.7)$$

The matrix on the left hand side is of tridiagonal form. This property can be used to recast the problem in terms of transfer matrices:

$$\begin{pmatrix} a_{i+1} \\ a_i \end{pmatrix} = \begin{pmatrix} \frac{E-\varepsilon_i}{t} & -1 \\ 1 & 0 \end{pmatrix} \begin{pmatrix} a_i \\ a_{i-1} \end{pmatrix}. \quad (4.5.8)$$

With the transfer matrix we can start at one edge of the sample ($i = 1$) and move step by step to the second edge ($i = L$):

$$\begin{pmatrix} a_L \\ a_{L-1} \end{pmatrix} = T^{(L)} \begin{pmatrix} a_2 \\ a_1 \end{pmatrix} = T_L \circ T_{L-1} \circ \dots \circ T_2 \begin{pmatrix} a_2 \\ a_1 \end{pmatrix}. \quad (4.5.9)$$

Here $T^{(L)}$ is the total transfer matrix which is built by a concatenation of the single-step ones. Having cast the problem into the form of Eq. (4.5.9), the physical properties are hidden in the eigenvalues of the matrix $T^{(L)}$. As reviewed, for instance, in Chap. 7 of [20], there is a theorem by Fürstenberg on the growth of the elements of the vector \mathbf{a} with the sample length L . It states that the following limit exists

$$\lim_{L \rightarrow \infty} \frac{1}{L} \ln (\text{tr } T^{(L)}) = \frac{1}{\lambda}, \quad (4.5.10)$$

with $\lambda > 0$. This theorem implies, in practice for large L , that the matrix $T^{(L)}$ has two eigenvalues $e^{\pm \frac{L}{\lambda}}$ since its determinant must be one. $T^{(L)}$ is so to speak an area-preserving map similar to the ones studied in Sect. 3.8 and $1/\lambda$ corresponds to the Lyapunov exponent. We may collect all these insights in the following theorem:

Theorem (Anderson localization) *In our one dimensional lattice model described by \hat{H}_{lattice} , Eq. (4.5.4), all eigenstates $\psi_{\lambda(E)}$ are exponentially localized in coordinate space for any disorder strength $\frac{W}{t} > 0$, i.e. any eigenstate with eigenenergy E*

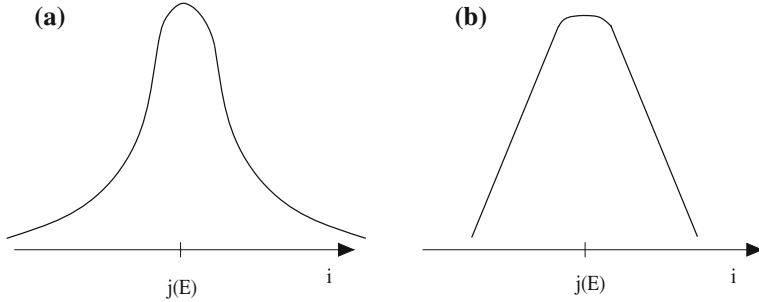


Fig. 4.26 Sketches of an exponentially decaying eigenfunction $|\psi_{\lambda(E)}(i)|$ centered around $j(E)$ on a linear (a) and a semilogarithmic (b) scale

behaves asymptotically for large $|i|$ as

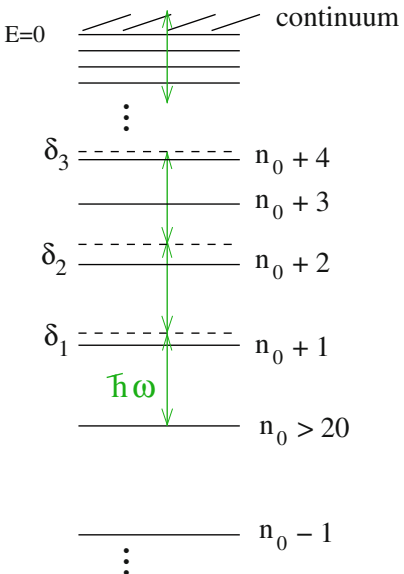
$$|\psi_{\lambda(E)}(i)| \sim e^{-\frac{|i-j(E)|}{\lambda(E)}}. \quad (4.5.11)$$

The truly exponential scaling with localization length $\lambda(E)$ is sometimes understood as a manifestation of *strong localization* implying Anderson localization, see our sketch in Fig. 4.26, in contrast to weak localization effects which manifest in a slower than exponential decay of the wave functions and other transport properties in solid-state samples [69]. In a sample of infinite length all eigenstates (for all eigenenergies, even much higher than the actual random potential peaks) are indeed localized in our model. For finite length L , some states may be practically extended if their localization length becomes comparable with L . This explains that diffusive transport may be possible in all finite-length disordered samples, provided that the energy-dependent localization length of the participating states is sufficiently large.

4.5.2 *Dynamical Localization in Periodically Driven Quantum Systems*

The above Anderson model describes a static disordered system. There exists a dynamical version of strong localization which we are going to present in the following. The dynamical systems are periodically driven ones, i.e. there is a well defined driving frequency (which can be the common frequency of several commensurate ones as well [70–72]). An example of such systems is the driven Rydberg problem of Eq. (3.7.58), which was presented in the previous section for initial conditions attached to regular phase space structures. In the present context of *dynamical localization* we assume that the initial wave packet starts in the chaotic part of phase space, i.e. typically at large energies or principal quantum numbers. Intuitively, the drive in the Rydberg atom couples the initial state with principal quantum number n_0

Fig. 4.27 The energy spectrum of a hydrogen Rydberg ladder with $E(n) = -\frac{1}{2n^2}$. The initial state with principal quantum number n_0 is coupled by the “photons” of the external drive with frequency ω to higher excited states. The detunings δ_i in the couplings of the states towards the electronic continuum (of free states) are essentially random. This forms a ladder of pseudorandomly coupled states, similarly to the situation of Anderson localization



to the next state with $n_0 + 1$ quasi-resonantly. This implies that there will always be a state within reach by a two-photon transition even closer to the continuum threshold and so forth, see the sketch in Fig. 4.27. Since the multiples of frequencies never hit exactly the electronic states there will always be essentially random detunings. Altogether, this semiclassical picture describes a ladder of quasi-resonantly coupled states in *energy space*, similar to the ladder of irregularly coupled lattice sites due to the disorder in our Anderson model. Further information on this analogy can be found in the original references [64, 73–77].

Another example for a periodically driven system is the quantized version of the standard map introduced in Sect. 3.8.3. In what follows we present this quantum kicked rotor model since it is reasonably simple and its classical version was extensively studied in Chap. 3.

The classical Hamiltonian of the kicked rotor from Eq. (3.8.13) can be recast for $L = I/T$ in a quantum Hamiltonian

$$\hat{H}(\hat{\theta}, \hat{L}, t) = \frac{\hat{L}^2}{2} T + k \cos(\hat{\theta}) \sum_{j=-\infty}^{\infty} \delta(t - j). \quad (4.5.12)$$

In this units the angular momentum eigenvalues are integers, which is rather convenient for practical purposes. Since

$$\delta(t) = \sum_{n=0}^{\infty} \cos\left(n \frac{2\pi}{T} t\right), \quad (4.5.13)$$

we get back in zeroth-order approximation a quantum pendulum Hamiltonian. The quantum kicked rotor has the great advantage that its evolution operator from right after one kick until right after the next one factorizes into a kick and a free rotation part:

$$\hat{U}(nT, (n+1)T) = \hat{U}(0, T) = e^{-ik \cos(\hat{\theta})} e^{-iT \frac{\hat{L}^2}{2}}. \quad (4.5.14)$$

This makes the analytical and numerical treatment of this model much simpler than for a system, like a driven Rydberg atom, for which the temporal dependence is continuous. The wave function after n kicks is then just given by applying n -times the kick-to-kick evolution operator:

$$\psi(t=n) = \hat{U}(0, nT)\psi(t=0) = \hat{U}(0, T)^n \psi(t=0). \quad (4.5.15)$$

From the form in which we have written \hat{H} and \hat{U} , we also see that the two parameters T and k are quantum mechanically independent, and we cannot just reduce them to a single parameter $K = kT$ as done in Eq. (3.8.13). The classical limit is obtained for $K = \text{const.}$ (constant classical phase space structure) while simultaneously $T \rightarrow 0$ and $k \rightarrow \infty$. In the scaling of variables used above, T is then the effective Planck constant, and we have for the commutator $[\hat{\theta}, \hat{L}] = iT$.

We can write the kick-to-kick evolution operator in matrix form expressing it in the basis of angular momenta $|m\rangle_{m \in \mathbb{Z}}$ in our units. Then the matrix elements are

$$\langle m' | \hat{U}(0, T) | m \rangle = e^{-i \frac{m'^2}{2} T} \frac{1}{2\pi} \int_0^{2\pi} d\theta e^{-ik \cos(\theta)} e^{i(m'-m)\theta} = e^{-i \frac{m'^2}{2} T} J_{m'-m}(k), \quad (4.5.16)$$

with the ordinary Bessel functions of order $m' - m$. For $k \rightarrow 0$, the matrix is essentially diagonal meaning that the kick couples hardly the different angular momentum states. For fixed kick strength, the off-diagonal elements sooner or later will decay quickly to zero since the Bessel functions are approaching zero rapidly for $(m' - m) \ll k$ [13]¹⁰

$$J_{m'-m}(k) \sim \frac{1}{\sqrt{2\pi|m'-m|}} \left(\frac{e}{2} \frac{k}{|m'-m|} \right)^{|m'-m|}. \quad (4.5.17)$$

Here $e = 2.71828\dots$ is Euler's number.

For periodically time-dependent Hamiltonians, we can still arrive at stationary equations from the Schrödinger equation, but not directly for the Hamiltonian, yet for the time-evolution operator. One can try to diagonalize the kick-to-kick operator

¹⁰Please see the asymptotic expansion with number [9.3.1] in Chap. 9 of [13].

and compute its eigenphases $\phi = -\varepsilon T$:

$$\hat{U}(0, T)|\psi_\phi\rangle = e^{i\phi}|\psi_\phi\rangle. \quad (4.5.18)$$

ε is the so-called quasi-energy corresponding to the eigenphase ϕ . This name indicates that the above ansatz is indeed the same as for a periodic dependence of the Hamiltonian in real space, for which we can use the Bloch ansatz from Eq. (4.5.2). Equation (4.5.18) describes translations in time induced by the so-called Floquet operator $\hat{U}(0, T)$, as similarly true for translations in space used to show that the solutions for transitional invariant problems are indeed of Bloch type, see e.g. [3].

Now the eigenvalue problem for the quantum kicked rotor can be cast into a form very similar to Eq. (4.5.7):

$$\left[\left(\langle m' | \hat{U}(0, T) | m \rangle \right)_{m', m} - e^{i\phi} I \right] (\langle m | \psi_\phi \rangle)_m = 0. \quad (4.5.19)$$

This system of equations is related to the Anderson model studied above. The only difference is that the disorder is not built in by random onsite energies but by the dynamics itself. The quantum kicked rotor can indeed be written in exactly the same form as Eq. (4.5.6) with diagonal elements which give, for typical choices of the parameter T , a *pseudo-random* sequence. This is explicitly shown by Fishman et al. in [63, 78], cf. also Chap. 7 in [20]. The result is that the eigenstates of the kick-to-kick operator $\hat{U}(0, T)$ are exponentially localized but now in angular-momentum space, c.f. Fig. 4.28. If the parameters of the kicked rotor are such that the classical phase space is chaotic, the quantum evolution nevertheless will localize after a finite number of kicks whose number is proportional to k (the effective bandwidths of the Floquet matrix in angular-momentum space, see Eq. (4.5.17)) [79, 80]. This type of localization is of pure quantum origin just like Anderson localization. It arises from many-path destructive interference in the semiclassical picture of the time evolution, see Sect. 4.3.2. Because of its dynamical origin this type of quantum localization is known as *dynamical localization*.¹¹

The effect of dynamical localization is visualized in Fig. 4.29. This figure shows the second moment of the angular-momentum distribution divided by two, i.e. the energy of the system, as a function of the number of applied kicks. While initially the energy grows just like in the classical kicked rotor system (dashed line), after about ten kicks the growth stops, and finally turns into a saturation. This is quite fascinating since the system is continuously kicked and, naively, one might expect that it would absorb more and more energy, yet it does not. The underlying classical model has completely chaotic phase space, imagine Fig. 3.27d for still larger kick strength $K = 7.5$, hence without any visible regular islands. For such a case the classical trajectories lose memory quickly, allowing to approximate the classical energy by

¹¹ The notion dynamic or dynamical localization is unfortunately also used in different contexts, one example being the suppression of tunneling by a periodic driving force [81], for experimental realizations of this latter effect see, e.g., [82, 83].

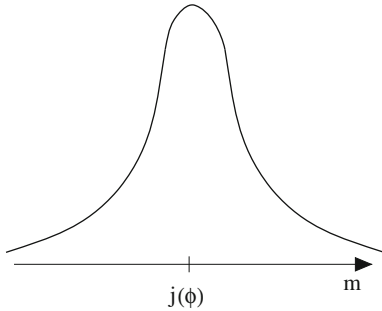


Fig. 4.28 Sketch of an exponentially localized eigenfunction $|\psi_\phi(m)| \sim e^{-|m-j(\phi)|/\lambda(\phi)}$ of the Floquet operator (4.5.18) centered around the angular momentum $j(\phi)$ with localization length $\lambda(\phi)$

the diagonal terms of the following sums obtained by iterations of the standard map

$$I_n = I_0 + K \sum_{j=1}^n \sin(\theta_j) \quad (4.5.20)$$

$$E_{\text{class}}(n) = \frac{I_n^2}{2} \approx \frac{I_0^2}{2} + \frac{K^2}{2} \sum_{j=1}^n \sin^2(\theta_j) \approx \frac{I_0^2}{2} + \frac{K^2}{4} n. \quad (4.5.21)$$

The classical diffusion in the chaotic phase space is hence drastically stopped in the quantum system as soon as it realizes its coarse-grained nature [84]. Hence the quantum system shows much more regular behavior than its classical version due to dynamical localization. This regularity of the quantum system is seen also in the spectral fluctuations in the quasi-energies [85]. These spectral properties of regular and chaotic quantum systems are studied in Sect. 4.6.

4.5.3 Experiments

Dynamical localization was experimentally observed in the two systems mentioned above. Independently, Bayfield [16, 87] and Koch [88, 89] and their respective collaborators measured the rise of the ionization threshold of driven alkali Rydberg states with increasing frequency. This counterintuitive effect had been predicted before as a direct consequence of dynamical localization [64, 90, 91]. The experimental implementation of the kicked rotor system was pioneered by Raizen's group using the center-of-mass degree-of-freedom of cold atoms. Dynamical localization and the exponential form of the momentum distribution of the atoms is largely discussed in the Ref. [92, 93]. It took about ten years more until *Anderson localization* could be measured *in situ* with light, see [94] and references therein, or dilute Bose-Einstein

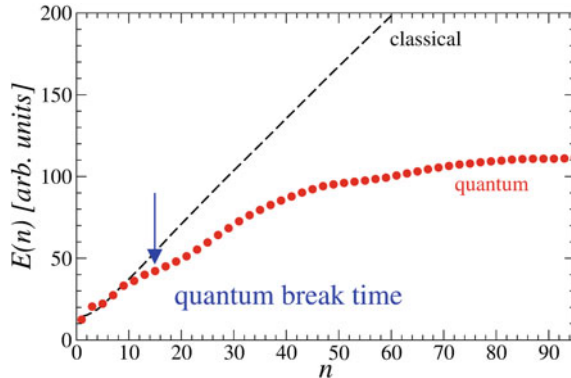


Fig. 4.29 The energy $E(n)$ as a function of the number of kicks n for the classical (black dashed line) and quantum (red symbols) kicked rotor problem. The blue arrow marks the *quantum break time* when both evolutions start to deviate from each other significantly. Both curves originate from averaging over different initial conditions to smooth the strong fluctuations characteristic of localized systems [65, 76, 86]

condensates [95] propagating or expanding in a disordered spatial potential, respectively.

4.6 Universal Level Statistics

Up to now we have not yet defined what chaos really means for a quantum system in general. We discussed the properties of quantum systems with a well-defined classical counterpart, which can be chaotic, regular or mixed, as we introduced in Chap. 3. In the previous section, we have seen that there may be a time for which the quantum system follows the classical motion, the so-called quantum break time, but after which the dynamics are different from the classical one. Chaos on the quantum level may, however, be introduced without a priori relation to any classical correspondence. This can be achieved by studying the properties of the very characteristics of quantum systems, their eigenspectra. The properties of the quantum mechanical spectrum are, of course, intimately related to the temporal evolution. This is a consequence of the spectral theorem [2, 4], which states that the time-evolution operator can always be expanded in the eigen(energy)basis of the Hamiltonian. Hence, irregular and complex dynamics go hand in hand with the quantum chaotic properties of the spectra.

This section gives a brief introduction to the theory of random matrices of finite size, modeling real physical systems with discrete spectra.¹² All of our sketches of proofs will be given for the simplest type of matrices, namely 2×2 ones. The

¹² A short overview over possible spectra of a quantum system is found in the appendix of this chapter.

shown ideas carry over to matrices of arbitrary but finite sizes, yet the proofs and computations are then rather difficult and call for more mathematical language. We refer to the specialized literature for further details, see e.g. Haake's book [20] or Mehta's standard reference for random matrices [96, 97].

4.6.1 Level Repulsion: Avoided Crossings

The essence in the study of the dynamical properties of quantum systems lies in the coupling of different states. The sensitivity of energy eigenlevels can be tested by varying, for instance, a control parameter in the Hamiltonian. If the states are coupled the levels will repel each other as predicted by perturbation theory [3]. Let us study the eigenvalues of an arbitrary hermitian 2×2 matrix $H = H^\dagger$:

$$\begin{pmatrix} H_{11} & H_{12} \\ H_{12}^* & H_{22} \end{pmatrix}. \quad (4.6.1)$$

The eigenvalues are easily computed

$$E_\pm = \frac{1}{2}(H_{11} + H_{22}) \pm \sqrt{\frac{1}{4}(H_{11} - H_{22})^2 + |H_{12}|^2} \equiv \frac{1}{2}(H_{11} + H_{22}) \pm \sqrt{\Delta}. \quad (4.6.2)$$

We can now distinguish the following possible cases:

- (a) No interaction between the levels, i.e. $H_{12} = 0$. Then the eigenvalues are simply $E_+ = H_{11}$ and $E_- = H_{22}$. Both eigenvalues can be forced into a crossing by a single parameter, let's say an appropriate parameter λ which enters the element H_{22} , such that $H_{11} - H_{22}(\lambda) = 0$.
- (b) More generally, $H_{12} \neq 0$, and we have a determinant $\Delta = \frac{1}{4}(H_{11} - H_{22})^2 + \text{Re}(H_{12})^2 + \text{Im}(H_{12})^2$. For real matrices, $\text{Im}(H_{12}) = 0$, implying that we need to change two matrix elements simultaneously to obtain a level crossing, i.e. a degeneracy of the two eigenvalues. This can be formalized as

$$\frac{1}{4}(H_{11} - H_{22}(\lambda_1))^2 + H_{12}(\lambda_2)^2 = 0 \quad (4.6.3)$$

$$\Leftrightarrow H_{11} - H_{22}(\lambda_1) = \pm 2iH_{12}(\lambda_2), \quad (4.6.4)$$

for an appropriate pair of parameters (λ_1, λ_2) . If also $\text{Im}(H_{12}) \neq 0$, we can easily see that three independent parameters are, in general, necessary to enforce a level crossing. The typical behavior of the energy levels while changing just one control parameter is sketched in Fig. 4.30. For randomly chosen parameters, the crossings will most likely be avoided ones!

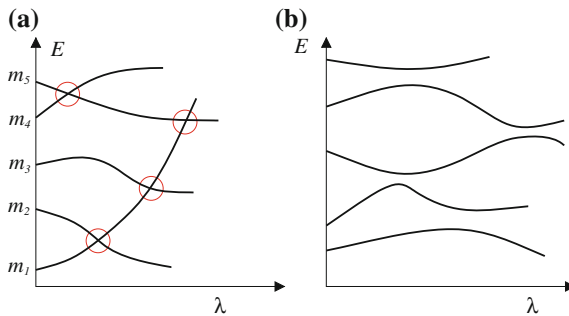


Fig. 4.30 Sketch of the energy levels for the same cases (a, b) as discussed in the text: an integrable systems (a) and of a typical system (b) versus a single control parameter λ . The good quantum numbers are labeled by m_i in (a). The avoided crossings in (b) make a global assignment of quantum numbers along the λ -axis impossible

For classically regular systems of arbitrary dimension, which can be quantized by the EBK method introduced in Sect. 4.2.3, we have a similar situation as in case (a) above. The quantum mechanical levels are approximated by the semiclassical EBK torus quantization as

$$E_{\mathbf{m}}(\lambda) \approx H \left[\mathbf{I} = \hbar \left(\mathbf{m} + \frac{\mu}{2} \right), \lambda \right], \quad (4.6.5)$$

where the dimension of the Hilbert space $\dim(\mathbf{m}) = N$. The levels are well characterized by their respective quantum numbers m_j . It is thus quite intuitive that locally one parameter, effecting just one level $E_{m_j}(\lambda)$, may suffice to enforce a level crossing between two of the eigenvalues. From this heuristic argument it is expected that a classically regular system does show level crossings with relatively large probability. We will come back to the case of regular classical systems more quantitatively in Sect. 4.6.5.

4.6.2 Level Statistics

For classically integrable systems we have a set of “good” quantum numbers, e.g. denoted \mathbf{m} in Eq. (4.6.5) for the semiclassical approximation of the levels. There is no such simple rule for classically non-integrable systems, whether mixed or chaotic. There may exist symmetries which allow to separate at least some degrees of freedom. Nevertheless, we typically lack a full set of good quantum numbers corresponding to the number of equations or to the size of the Hilbert space. How can we characterize the eigenspectra in these cases? Imagine that we were given spectra of a complex quantum system either from an experiment in the laboratory or from numerical computations. How can we decide that the spectra look “irregular”?

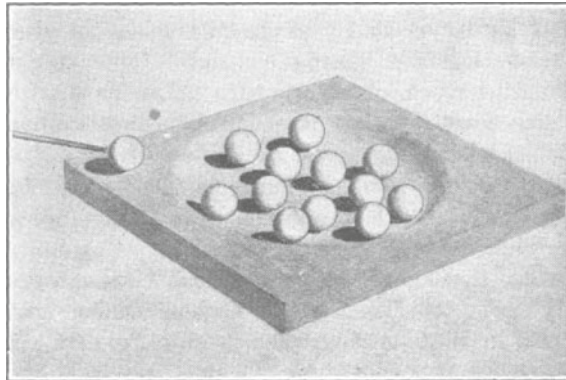


Fig. 4.31 A classical model for many-body scattering of a neutron on a heavy nucleus consisting of many constituents. Reprinted by permission from Macmillan Publishers Ltd. [99], copyright 1936

The idea is to study the statistics of the levels, in particular the fluctuations of the level distances, which tells us something about the probability of crossing or anti-crossing of levels.

On the other hand, they are systems much too complex for even knowing the precise form of the Hamiltonian. Heavy nuclei studied experimentally by scattering experiments are a good example. Assuming just minimal knowledge, like the existence of some symmetries, such systems can be modeled by matrices with essentially random entries. The random elements describe random couplings between the various degrees of freedom. This idea goes back to Wigner [98] and a simplified picture of Bohr who thought of the scattering process between a hadron and a heavy nucleus as a classical billiard-ball-like game, see Fig. 4.31.

Now it is the theory of random matrices which brings both aspects together in the question of how good the spectra of physical systems reflect the statistics of random matrix ensembles. Before we can introduce the two main hypotheses, which link both semiclassical and purely quantum aspects, we have to speak about symmetries, which must be considered as they can mix irregular spectra in an uncorrelated way such that they may look more regular than they actually are.

4.6.3 Symmetries and Constants of Motion

For practical purposes, an important step in analyzing complex quantum spectra is to separate them into subsystems which do not couple because of symmetries. Only after such a separation it makes sense to test the level statistics for each of the symmetry-reduced subsystems *independently*. The concept of symmetries is

well-known from quantum mechanics. We review it nevertheless since symmetries are essential for the spectral analysis.

4.6.3.1 Examples for Symmetries

- *Continuous symmetry*

The symmetry is described by a generating hermitian operator \hat{A} acting on the Hilbert space. Let λ be a real continuous parameter. If the Hamiltonian of the system commutes with \hat{A} , a symmetry may be given by translations of the form $\psi \rightarrow e^{i\lambda\hat{A}}\psi$, which follows from $\hat{H} = e^{-i\lambda\hat{A}}\hat{H}e^{i\lambda\hat{A}}$. An example for such a symmetry is a rotational invariance with respect to an axis, e.g. $\hat{A} = \hat{L}_z/\hbar$, corresponding to a rotation around the z axis by an angle λ .

- *Discrete symmetry*

The \mathbb{Z}_2 inversion symmetry defined by the parity operator \hat{A}_P with $\hat{A}_P\psi(x) = \psi(-x) = \lambda\psi(x)$ for $\lambda \in \{1, -1\}$.

4.6.3.2 Irreducible Representation of the Hamiltonian Matrix

If the operator \hat{A} defines a symmetry it commutes with the Hamiltonian. This means that we can find a common eigenbasis $|m, n\rangle$ for both operators, i.e.

$$[\hat{A}, \hat{H}] = 0 \Rightarrow \hat{A}|m, n\rangle = \alpha_m|m, n\rangle, \quad (4.6.6)$$

with $\alpha_m \in \mathbb{R}$. We can express the Hamiltonian in this basis representation

$$\langle m', n' | \hat{H} | m, n \rangle = \delta_{m,m'} H_{n,n'}^{(m)}, \quad (4.6.7)$$

which leads to the following block-diagonal form of the Hamiltonian matrix

$$\left(\begin{array}{c|c|c|c|c} \ddots & 0 & \dots & & 0 \\ \hline 0 & H_{n,n'}^{(m-1)} & \ddots & & \vdots \\ \hline \vdots & \ddots & H_{n,n'}^{(m)} & & \\ \hline & & & H_{n,n'}^{(m+1)} & 0 \\ \hline 0 & \dots & & 0 & \ddots \end{array} \right) \quad (4.6.8)$$

Here m is the index of the block while the second indices n, n' run from one to the size of the respective blocks, which is determined by the degeneracy of the eigenvalues α_m of \hat{A} .

If no further symmetries are present, the above form is said to be an *irreducible representation* of the Hamiltonian. The analysis of the spectrum must now be restricted to a single block of the full matrix. Of course, all of the blocks can be analyzed separately, which can be useful in order to improve the statistical value of such a spectral characterization.

If more than one symmetry is present, an eigenbasis can be found which commutes with all three operators, the Hamiltonian and the two corresponding to the symmetry. Then the Hamiltonian is represented in this common eigenbasis being of block-diagonal form within a cube. This procedure is extendable to any dimension if even more symmetries are simultaneously present. The important message is that the such obtained blocks should be analyzed independently. This is necessary to avoid the mixing of various blocks, which can induce degeneracies in the spectrum which may not be present *within* any of the single blocks. It is clear that any operator commuting with the Hamiltonian defines a constant of the motion. This means that an initially complex system can be reduced to a smaller space which turns out to be useful for practical computations. Hence, finding all symmetries helps to reduce the complexity, too.

4.6.4 Density of States and Unfolding of Spectra

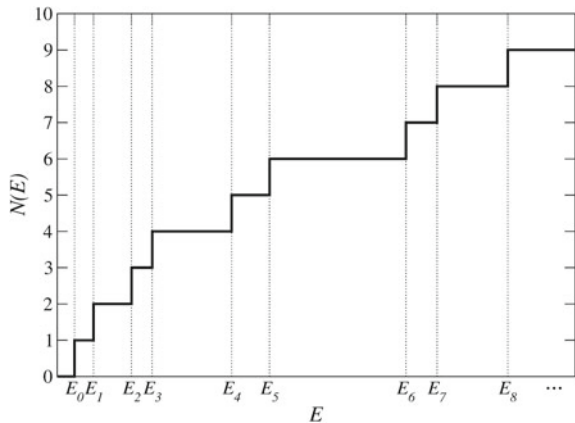
Yet another important step in the practical application of any spectral analysis has to do with the fact that we are interested in the statistics of local eigenvalue fluctuations and not in global trends which are system specific. The former corresponds to the fluctuating part of the level density, while the latter part is determined by the smooth part in Sect. 4.3.67.

In this section, we show how one can reduce the information contained in quantum spectra to the information relevant for us on *local fluctuations*. The aim is to renormalize the eigenenergies of one symmetry-reduced subspace, see the previous section, in such a way that the mean density of the levels is uniform over the entire spectrum of the subspace. This is known as *unfolding of the spectra*.

We assume a discrete quantum spectrum of finite size. The algorithm for spectral unfolding is as follows.

1. Sort the energies in increasing order, i.e. such that $E_0 \leq E_1 \leq E_2 \leq \dots \leq E_N$, where N is the dimension of the symmetry-reduced subspace.
2. Compute the integrated density of states, the so-called staircase function $N(E) = \Theta(E - E_n)$, giving all eigenvalues up to the energy E . Here Θ is the Heaviside step function. The construction of the level staircase function is sketched in Fig. 4.32. The level density is formally given by $\rho(E) = \frac{dN}{dE} = \sum_{n=0}^{\infty} \delta(E - E_n)$.

Fig. 4.32 Sketch of a level staircase $N(E)$ for the ordered spectrum of eigenenergies E_j . Each time a level pops up, the curve jumps by one. Differences in the local level density make the overall curve have a slope different from one



3. Approximate $N(E)$ by a smooth function $\bar{N}(E)$ interpolating between the jumps of the curve in Fig. 4.32.
4. With the help of the smooth function $\bar{N}(E)$ we finally can rescale the spectrum, such that the average level density is equal to one. Reading off the values of the points x_n in Fig. 4.33, which are defined by $x_n = \bar{N}(E_n)$, we arrive at the new density of states

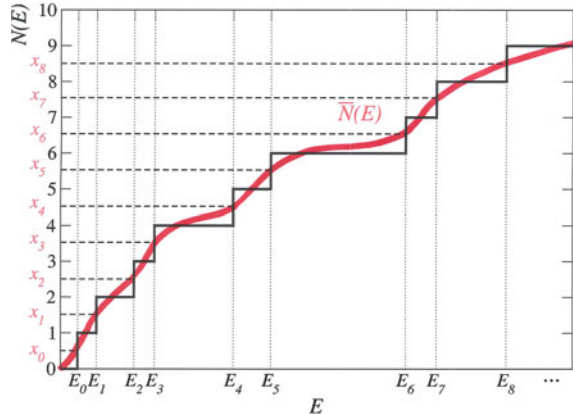
$$\bar{\rho}(x) = \sum_{n=0}^{\infty} \delta(x - x_n), \quad \text{with} \quad \langle \bar{\rho}(x) \rangle \equiv \frac{1}{\Delta x} \int_{x_0 - \Delta x/2}^{x_0 + \Delta x/2} dx \bar{\rho}(x) \approx 1. \quad (4.6.9)$$

The practical problem one faces is the question how to obtain a good estimate for the smoothed level density $\bar{N}(E)$. Sometimes a semiclassical estimate, e.g. based on Weyl's law, see Sect. 4.3.6, may be possible [100, 101]. In general, one will have to measure or to compute the spectrum and then to extract the local average of the level density numerically. With this average density we can finally rescale all energies to obtain approximately an average density of one. For the latter, there are many methods proposed in the literature [102], but most often a brute-force local averaging over an appropriate window of levels may suffice [103, 104]. This window must be small enough in order not to average too much the fluctuations in which we are interested, yet sufficiently wide in order to smooth the local density and to obtain a local mean of one in good approximation.

4.6.5 Nearest Neighbor Statistics for Integrable Systems

Let us focus on a subspace which is already symmetry reduced, in the sense as shown in Sect. 4.6.3. For an integrable system, we additionally have sufficient constants of

Fig. 4.33 $N(E)$ from the previous figure with a smoothed version $\bar{N}(E)$. The crossing points between the two functions determine the “new” levels, which are read off at the y axis. These values x_i have on average a level spacing of one by construction



motion, or quantum mechanically speaking, enough good quantum numbers. In this case, using EKB semiclassics, see Eq. (4.6.5), we can obtain corresponding estimates of the quantum levels at sufficiently high energies. Just varying a single parameter can then easily induce level crossings locally in the spectrum. This is possible since the individual levels do “not feel” each other and can be tampered individually.

Assuming a random distribution of ordered numbers on the real line, $-\infty \leq x_0 \leq x_1 \leq \dots \leq x_N < \infty$, the probability density of having a level within a certain distance s from another one, corresponds to the distribution of independent random numbers whose average “waiting time” of occurrence is constant. Such distances between numbers are Poisson distributed. In other words, we expect to obtain $P(s) = \sum_{i=0}^{N-1} \delta(s - (x_{i+1} - x_i)) \rightarrow e^{-s}$ in the limit of a level continuum. The most likely case is then $s = 0$, which corresponds to a level crossing. The unfolding, described in the previous section, is responsible for the average rate of occurrence (the mean waiting time) being exactly one, i.e. $\langle s \rangle = 1$. Another way of seeing this, is to ask for the probability $P(s)ds$ to have one level within the distance ds of a given one. This probability is proportional to the probability $g(s)ds$ of having exactly one level in the interval $[x + s, x + s + ds]$. $g(s)$ denotes the distribution of random numbers on the real positive line. It is also proportional to the probability of having no level in the interval $[x, x + s]$ of length s . The latter is identical to the complement of $\int_0^s ds' P(s')$, which is $\int_s^\infty ds' P(s')$. Hence we obtain

$$P(s)ds = g(s)ds \times \int_s^\infty ds' P(s'), \quad (4.6.10)$$

The solution of this relation is

$$P(s) = g(s)ds e^{-\int_0^s ds' g(s')} \quad (4.6.11)$$

Assuming a uniform distribution of random numbers with $g(s) = 1$, the conditions of normalization and average level spacing one,

$$\int_0^\infty ds P(s) = 1 \quad \text{and} \quad \int_0^\infty ds s P(s) = 1, \quad (4.6.12)$$

immediately imply $P(s) = e^{-s}$.

Generally, for classical integrable nonlinear systems, i.e. $\det(\frac{\partial^2 H}{\partial I_i \partial I_j}) \neq 0$, with respect to the action variables I_i , with at least two independent degrees of freedom, Berry and Tabor convincingly argued in favor of the following conjecture [105]:

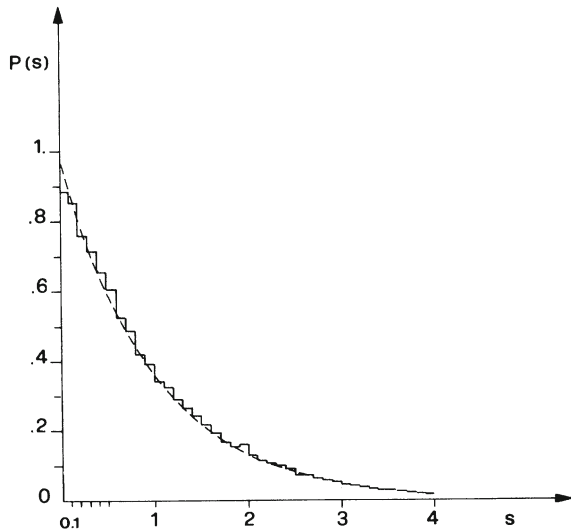
Berry-Tabor conjecture: In the limit of large energies (semiclassical limit), the statistical properties of the quantum spectra of classically integrable systems correspond to the prediction for *randomly* distributed energy levels.

We met an example for a quantum system with Poisson distributed level distances in Sect. 4.5.2, the quantum kicked rotor when showing dynamical localization. This is no contradiction to the above hypothesis for *integrable* systems. Anderson (or dynamical) localization give eigenstates which have exponentially small overlap in real (or momentum) space, and hence essentially independently distributed energy levels which do not “feel each” other. This implies regular behavior and Poisson distributed level spacings (despite the classical chaoticity of the kicked rotor) [85]. A better simple example, where we find Poisson spectral statistics, is the rectangular billiard, introduced in Sect. 4.2.3.1, if the two side-lengths of the billiard are incommensurate. Then the mixing of the levels, corresponding to the two different quantum numbers for each dimension, leads to randomly distributed level spacings. This case was analyzed also in the original paper by Berry and Tabor [105]. A similar result from [106] is shown in Fig. 4.34 and we invite the reader to test this for him/herself, see Problem 4.12. As usual for any real physical system, slight deviations are found and discussed in [106] from the exact predictions from random matrix theory (RMT), in particular when analysing spectral correlation functions, which we briefly introduce later in Sect. 4.6.8.

4.6.6 Nearest Neighbor Statistics for Chaotic Systems

We have seen in Sect. 4.6.1 that the more degrees of freedom we have, the harder it is to enforce a level crossing. For complex hermitian 2×2 matrices, we needed already three parameters for enforcing a degeneracy. For larger matrices the situation becomes even worse and level crossings are, in general, unlikely. Figure 4.30 sketches the spectra for an integrable system, for which we may follow the individual levels with the control parameter λ , and for a chaotic spectrum, for which many irregular avoided crossings occur. In the language of 2×2 matrices, the former case may be described by the following matrix

Fig. 4.34 Spectral analysis of a two-dimensional billiard with incommensurate side lengths (*histogram*) and Poisson distribution $P(s) = e^{-s}$ (*dotted line*). Adapted reprint with kind permission by Giulio Casati, copyright 1985 by the American Physical Society [106]



$$\begin{pmatrix} E_1(\lambda) & 0 \\ 0 & E_2(\lambda) \end{pmatrix} \quad (4.6.13)$$

The latter case may be represented by additional couplings V :

$$\begin{pmatrix} E_0 - \Delta & V \\ V^* & E_0 + \Delta \end{pmatrix}, \quad (4.6.14)$$

where we introduce the parameter Δ for convenience. The level splitting for (4.6.14) is given by $D = \sqrt{\Delta^2 + |V|^2}$, with $V = V_R + i V_I$, see Fig. 4.35 and Problem 4.13. We may then estimate the probability for small spacings, i.e. $\Delta E \rightarrow 0$, by

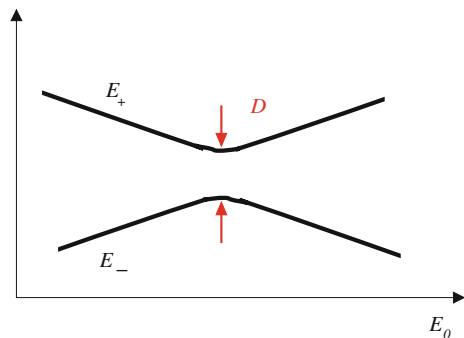
$$P(\Delta E) \sim \int dV_R \int dV_I \int d\Delta P(V_R, V_I, \Delta) \delta(\Delta E - D). \quad (4.6.15)$$

Here, $P(V_R, V_I, \Delta)$ is the probability distribution of the mentioned three independent parameters. We may assume that $P(V_R, V_I, \Delta) \approx \text{const.} > 0$ for $V_R, V_I, \Delta \rightarrow 0$. Then the three-dimensional volume integral over (V_R, V_I, Δ) can be computed as

$$P(\Delta E) \sim 4\pi \int dV V^2 \delta(\Delta E - V) \propto \Delta E^2. \quad (4.6.16)$$

Our much simplified argument shows that the levels repel each other when approaching small distances. For a real matrix with just two independent parameters (V, Δ) , both real, we obtain in a similar manner:

Fig. 4.35 Energy eigenvalues of a 2×2 matrix versus the control parameter E_0 . The splitting is determined by D defined in the text



$$P(\Delta E) \sim \int dV \int d\Delta P(V, \Delta) \delta(\Delta E - D) \sim 2\pi \int dV V \delta(\Delta E - V) \propto \Delta E, \quad (4.6.17)$$

for small $\Delta \rightarrow 0$ to allow for the approximation $D \approx |V|$ in the argument of the δ -function.

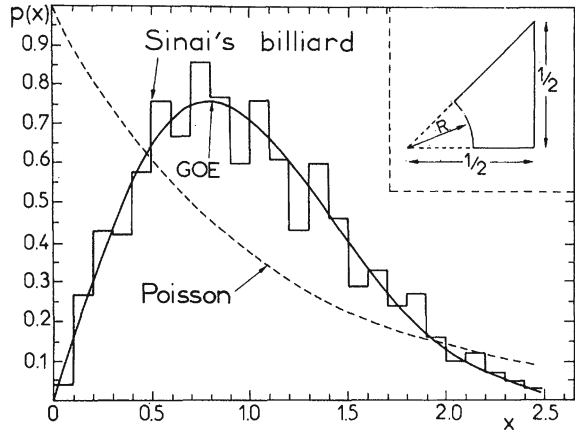
After a long experimental experience with spectral data from heavy nuclei, it was found that their excitation spectra correspond quite well to the predictions made for certain ensembles of random matrices [98, 107, 108]. It was Casati et al. [109], and later in more precise form Bohigas et al. [100], after some ideas by McDonald and Kaufman [110] and Michael Berry [111], who formulated the following hypothesis, and thus generalized the statement to arbitrary quantum systems:

Bohigas-Giannoni-Schmit conjecture: The eigenvalues of a quantum system, whose classical analogue is fully chaotic, obey the same universal statistics of level spacings as predicted for the eigenvalues of Gaussian random matrices.

The theory of random matrices (RMT) has a long history, going back to Wigner [98]. Dyson was studying independently unitary ensembles in the context of scattering problems (of unitary S matrices) [98]. The different symmetry conditions give different predictions for the level spacings, depending on whether the Hamiltonian is real, corresponding to the so-called Gaussian orthogonal ensemble (GOE), or complex, giving the Gaussian unitary ensemble (GUE). There is another case for spin systems, for instance, which implies Gaussian symplectic ensembles (GSE). We will come back to these ensembles in the next section in more detail. For now, let us just state the prediction for the level spacing distributions for the respective cases:

$$P(s) = \begin{cases} e^{-s} & \text{integrable} \\ s \frac{\pi}{2} e^{-s^2 \frac{\pi}{4}} & \text{GOE} \\ s^2 \frac{32}{\pi} e^{-s^2 \frac{4}{\pi}} & \text{GUE} \\ s^3 \frac{2^{18}}{3^6 \pi^3} e^{-s^2 \frac{64}{9\pi}} & \text{GSE} \end{cases}. \quad (4.6.18)$$

Fig. 4.36 Spectral analysis of a variant of the Sinai billiard (*histogram*) and GOE distribution (*solid line*). The billiard is shown in the *inset*, with a defocussing boundary in the *lower left corner*. Reproduced from [100], copyright 1984 by the American Physical Society



All cases obey the conditions of normalization and mean-level spacing one:

$$\int_0^\infty ds P(s) = 1 \text{ and } \int_0^\infty ds s P(s) = 1. \quad (4.6.19)$$

Unfolding automatically guarantees the latter condition. Then s is dimensionless such that all spectra can be directly compared without another scaling factor. The major difference in the distributions lies in (i) the slope at $s = 0$, which is negative for the Poissonian case, constant for the GOE case, and linear or cubic for the GUE and GSE cases, respectively. The second (ii) important difference between the Poisson and the other cases is the weight in the tail, which in the Poissonian case decays less fast. These most robust characteristics are usually checked first when analyzing data from an experiment or from a numerical diagonalisation. The predictions from Eq. (4.6.18) can be exactly derived for ensembles of random 2×2 matrices [20, 97]. This will be exemplified for the GOE case in the next section. In the general case of $N \times N$ matrices, one expects the results to hold as well, which is the content of the so-called *Wigner surmise*. Analytic closed-form expressions can then be rigorously proven only for $s \rightarrow 0$ and $s \rightarrow \infty$ because of complicated integrals over matrix ensembles appearing in the derivation [97]. Figure 4.36, from the original paper by Bohigas, Giannoni and Schmit, highlights the good correspondence of the spectra of a quantum Sinai billiard (see also Sect. 3.9.1) with the GOE prediction.

4.6.7 Gaussian Ensembles of Random Matrices

As mentioned above, random matrix ensembles were introduced as models for many-body quantum systems of heavy nuclei where the couplings are basically unknown.

The idea was to assume as little as possible about the specific systems and considering mainly their symmetries. We can build a statistical ensemble of matrices with reasonable conditions for their entries. The conditions used are

- Statistical independence of the matrix elements, i.e. the entries are independent random numbers. This means that the distribution of a whole matrix factorizes into its independent parts:

$$P\left(H = \{H_{i,j}\}_{i,j}\right) = \prod_{i,j} p_{i,j}(H_{i,j}). \quad (4.6.20)$$

- The statistical properties should not depend on the representation (or basis) chosen to built the matrix. This implies that the result is stable with respect to basis transformations obeying the following symmetries:

1. The system is invariant under time-reversal, i.e. the Hamiltonian commutes with the time reversal operator \hat{T} . In this case, H can, without loss of generality, chosen real with $H = H^\dagger = H^t$, hence H is a symmetric matrix with real entries. Our probability distribution should be independent of the basis choice, implying that it is invariant with respect to any arbitrary orthogonal transformation $O^{-1} = O^t \in {}^N\mathbb{R}^N$. In formulae:

$$[\hat{H}, \hat{T}] = 0, \text{ with } \hat{T}^2 = 1, \text{ and } P(H) = P(OHO^t). \quad (4.6.21)$$

Now it becomes clear why the ensemble is called orthogonal ensemble (GOE) in this case.

2. The system is not time-reversal invariant, and H is, in general, hermitian with complex entries. The requirement is then invariance under any unitary basis transformation with a unitary matrix $U^{-1} = U^\dagger \in {}^N\mathbb{C}^N$. This gives the Gaussian unitary ensemble (GUE), characterized by

$$[\hat{H}, \hat{T}] \neq 0 \text{ and } P(H) = P(UHU^\dagger). \quad (4.6.22)$$

3. If the system is time-reversal invariant, yet with $\hat{T}^2 = -1$ (\hat{T} being then a so-called antiunitary operator [112]), any level is twofold degenerate (the so-called Kramers degeneracy). In this case the basis transformations are given by unitary symplectic matrices S , c.f. also Sect. 3.2:

$$[\hat{H}, \hat{T}] = 0, \text{ with } \hat{T}^2 = -1, \text{ and } P(H) = P(SHS^\dagger). \quad (4.6.23)$$

This defines the Gaussian symplectic ensemble (GSE). Such a situation occurs naturally, for instance, for systems with spin one half that are time-reversal invariant. More information on this more exotic ensemble can be found in [20].

For all the three universality classes, we obtain under the the above conditions of independence and invariance

$$P(H) = C e^{-A \text{tr}[H^2]} \quad (4.6.24)$$

with positive constants A and C chosen to fulfill (4.6.19). Whilst the latter result is valid for all ensembles (GOE, GUE, GSE), the following equalities follow from explicitly evaluating the trace of the product of the two identical GOE matrices H :

$$P(H) = C e^{-A \text{tr}[H^2]} = C e^{-A \sum_{i,j=1}^N H_{i,j}^2} \equiv \prod_{i,j=1}^N p(H_{i,j}). \quad (4.6.25)$$

Similar relations hold also for the other two ensembles, where one must introduce the real and imaginary parts of the matrices separately [20]. Finally, we can appreciate why the random matrix ensembles are called Gaussian ensembles. The distributions of the single matrix elements must be Gaussian in order to fulfill the above criteria. It should not come as a surprise to find the matrix trace in the universal distributions (4.6.24) since the trace is naturally invariant with respect to the required transformations.

We conclude this section by proving for 2×2 matrix ensembles that (i) $P(H)$ is indeed as given in (4.6.24), and that (ii) we obtain $P(s)$ as stated in (4.6.18). For simplicity, we restrict to the GOE case in what follows.

- (i) Let us start with a real symmetric matrix with the three independent entries H_{11}, H_{22}, H_{12} :

$$\begin{pmatrix} H_{11} & H_{12} \\ H_{12} & H_{22} \end{pmatrix}. \quad (4.6.26)$$

The condition of independence of the random variables immediately gives for the probability distribution of the matrix:

$$P(H) = p_{11}(H_{11})p_{22}(H_{22})p_{12}(H_{12}). \quad (4.6.27)$$

Additionally, we have a normalization condition and the requested invariance with respect to orthogonal transformations:

$$\int dH_{11} dH_{22} dH_{12} P(H) = 1, \quad (4.6.28)$$

$$P(H) = P(OHO^t) \equiv P(H'). \quad (4.6.29)$$

The general form of an orthogonal transformation in two dimensions is

$$O(\theta) = \begin{pmatrix} \cos(\theta) & -\sin(\theta) \\ \sin(\theta) & \cos(\theta) \end{pmatrix} \rightarrow \begin{pmatrix} 1 & -\theta \\ \theta & 1 \end{pmatrix}, \quad (4.6.30)$$

where the latter step is valid for small $\theta \rightarrow 0$. In this limit, we obtain for the transformed matrix

$$H'_{11} = H_{11} - 2\theta H_{12} \quad (4.6.31)$$

$$H'_{22} = H_{22} + 2\theta H_{12} \quad (4.6.32)$$

$$H'_{12} = H_{12} + \theta (H_{11} - H_{22}). \quad (4.6.33)$$

Using the independent property (4.6.27) and (4.6.29), we get

$$\Delta P = \frac{dp_{11}}{dH_{11}} \Delta H_{11} p_{22} p_{12} + \frac{dp_{22}}{dH_{22}} \Delta H_{22} p_{11} p_{12} + \frac{dp_{12}}{dH_{12}} \Delta H_{12} p_{11} p_{22}. \quad (4.6.34)$$

Remembering

$$\frac{d \ln p_{11}}{dH_{11}} = \frac{1}{p_{11}} \frac{dp_{11}}{dH_{11}}, \quad (4.6.35)$$

and similarly for the other two variables, we arrive at the condition

$$P(H) = P(H) \left[1 - \theta \left(2H_{12} \frac{d \ln p_{11}}{dH_{11}} - 2H_{12} \frac{d \ln p_{22}}{dH_{22}} - (H_{11} - H_{22}) \frac{d \ln p_{12}}{dH_{12}} \right) \right]. \quad (4.6.36)$$

This implies that the correction term, the second term in the brackets, must vanish for all θ , i.e.

$$\frac{1}{2(H_{11} - H_{22})} \left(\frac{d \ln p_{11}}{dH_{11}} - \frac{d \ln p_{22}}{dH_{22}} \right) - \frac{1}{H_{12}} \frac{d \ln p_{12}}{dH_{12}} = 0. \quad (4.6.37)$$

One may easily check that the following uncoupled functions solve this differential equation

$$p_{11}(H_{11}) = e^{-AH_{11}^2 - BH_{11}} \quad (4.6.38)$$

$$p_{22}(H_{22}) = e^{-AH_{22}^2 - BH_{22}} \quad (4.6.39)$$

$$p_{12}(H_{12}) = e^{-2AH_{12}^2}. \quad (4.6.40)$$

Here A and B are two positive constants. With Eq. (4.6.27), we finally arrive at

$$P(H) = Ce^{-A \text{tr}(H^2)}, \quad (4.6.41)$$

after an appropriate shift of the energy offset such that $H_{11} + H_{22} = 0$. This is exactly what was predicted in Eq. (4.6.24) for the general case. Hence any individual distribution does not depend on its index (i,j) . All of them are indeed identical. For the GOE case, as shown here, we must only be careful at counting the contributions from the off-diagonal elements, i.e.¹³ $p_{12}(H_{12}) \equiv p(H_{12})^2 = p(H_{12})p(H_{21})$, which implies the correspondence with Eq. (4.6.25).

¹³To make the statement as clear as possible we abuse the notation here a bit.

- (ii) Secondly, we want to show that the actual distribution of level spacings is given by the GOE prediction from Eq. (4.6.18). Hence we need the eigenvalues of our 2×2 matrix, which are

$$E_{\pm} = \frac{1}{2}(H_{11} + H_{22}) \pm \frac{1}{2}\sqrt{(H_{11} - H_{22})^2 + 4H_{12}^2}. \quad (4.6.42)$$

The matrix is diagonalized by an appropriate orthogonal transformation which we call $O(\phi)$ to give the diagonal matrix $D_{\pm} = OHO^t$. The entries of both matrices are then connected by the following equations

$$H_{11} = E_+ \cos^2(\phi) + E_- \sin^2(\phi) \quad (4.6.43)$$

$$H_{22} = E_+ \sin^2(\phi) + E_- \cos^2(\phi) \quad (4.6.44)$$

$$H_{12} = (E_+ - E_-) \cos(\phi) \sin(\phi). \quad (4.6.45)$$

The corresponding probability densities in the old and new variables are connected by

$$P(H)dH = p(E_+, E_-, \phi)dE_+dE_-d\phi, \quad (4.6.46)$$

or

$$p(E_+, E_-, \phi) = P(H) \left| \det \left(\frac{\partial(H_{11}, H_{22}, H_{12})}{\partial(E_+, E_-, \phi)} \right) \right| = P(H) |E_+ - E_-|, \quad (4.6.47)$$

which is independent of the transformation angle ϕ . With Eq. (4.6.41) and $\text{tr}[H^2] = E_+^2 + E_-^2$, we finally obtain

$$p(E_+, E_-, \phi) = p(E_+, E_-) = C |E_+ - E_-| e^{-A(E_+^2 + E_-^2)}. \quad (4.6.48)$$

Changing variables to introduce the level spacing $s = E_+ - E_-$ and $z = (E_+ + E_-)/2$, this gives

$$p(s, z) = C s e^{-A\left(\frac{s^2}{2} + 2z^2\right)}. \quad (4.6.49)$$

The Gaussian integral over z can be performed:

$$\int_{-\infty}^{\infty} dz e^{-2Az^2} = \sqrt{\frac{\pi}{2A}}. \quad (4.6.50)$$

Since we fixed the energy scale $H_{11} + H_{22} = 0$, we may as well have directly set $z = 0$ in our simple example of 2×2 matrices. This leads to the wanted result after computing the constants $A = C = \pi/2$, which are fixed by the conditions from Eq. (4.6.19). In conclusion, we have indeed proven that the

level spacing distribution is the one of Eq. (4.6.18) for GOE. As shown above, the level distance comes into the game because of the change of variables and the corresponding functional determinant, see Eq. (4.6.47). The same mechanism carries over to the case of larger matrices, see e.g. the detailed presentation of random matrix theory in [97].

4.6.8 More Sophisticated Methods

Up to now we have discussed just one property of the predictions for the universal random matrix ensembles, the level spacing distributions. The latter characterize *local* correlations in the spectrum, dealing with the nearest neighbor distances of levels. Much more is known from the theory of random matrices. For instance, there are predictions for two-point spectral correlation functions, which include products of spectral functions, see Eq. (4.3.124) for an example. Here we present two of such functions characterizing also the spectral correlations more globally in the spectrum. In the practical analysis of quantum spectra, the computation of these functions gives an additional test of whether and how well the analyzed quantum system follows the predictions of random matrix theory. We state the definition of the spectral functions and the random matrix results, while details on the derivations are found in the literature [97].

4.6.8.1 Number Variance

The number variance compares the spectral cumulative density to a straight line of given length. It is defined as

$$\Sigma^2(L) \equiv \left\langle \left(\int_{\tilde{E}-L/2}^{\tilde{E}+L/2} dE \rho(E) - L \right)^2 \right\rangle_{\tilde{E}}. \quad (4.6.51)$$

The densities $\rho(E)$ must be unfolded and L is then a dimensionless positive real number. The average is taken over all spectral positions \tilde{E} . The number variance is a correlation function, of order two because of the square. For random matrix ensembles in the sense of the previous two subsections, we have the following predictions [97, 108]

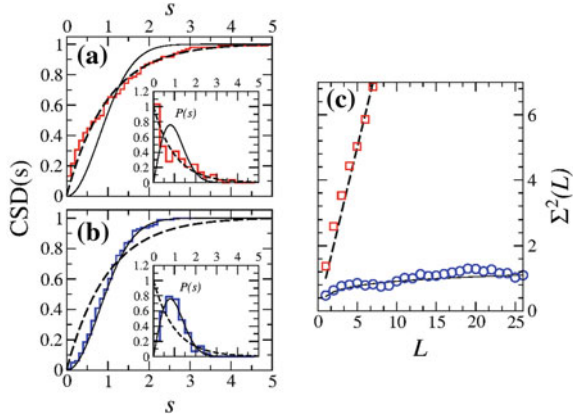


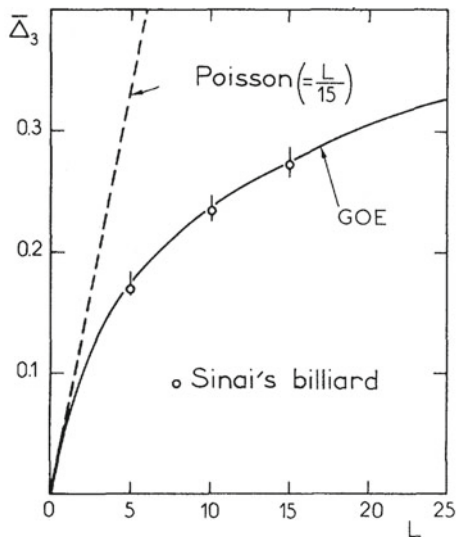
Fig. 4.37 Analysis of the quantum spectra of a many-body system whose spectral properties can be controlled by one parameter. For a regular limit: **(a)** and *red squares* in **(b)**; and for a chaotic limit: **(b)** and *blue circles* in **(c)**. **(a–b)** show the cumulative level spacing distributions $CSD(s) = \int_0^s ds' P(s')$ in the main panels, and $P(s)$ in the insets. The solid line represents the GOE prediction, while the dashed line shows the Poisson distribution. In **(c)** the number variance is shown for the two cases of **(a)** and **(b)**, respectively. The many-body quantum systems obeys nicely the predictions of RMT in the two limiting cases. Adapted from [114]

$$\Sigma^2(L) = \begin{cases} L & \text{Poisson (integrable)} \\ \frac{2}{\pi^2} \left[\ln(2\pi L) + \gamma + 1 - \frac{\pi^2}{8} \right] + O\left(\frac{1}{L}\right) & \text{GOE} \\ \frac{1}{\pi^2} \left[\ln(2\pi L) + \gamma + 1 \right] + O\left(\frac{1}{L}\right) & \text{GUE} \\ \frac{1}{2\pi^2} \left[\ln(4\pi L) + \gamma + 1 + \frac{\pi^2}{8} \right] + O\left(\frac{1}{L}\right) & \text{GSE} \end{cases} \quad (4.6.52)$$

The Poissonian case is fairly easy to understand, when thinking about the relative fluctuations around the “mean” L in a Poissonian random process scaling with \sqrt{L} [108]. The parameter $\gamma \approx 0.57722$ is the Euler constant. The results for the Gaussian ensembles are valid asymptotically for not too small L . If the analyzed physical system has a typical maximal energy scale (like for the shortest periodic orbit in a billiard, for instance), its number variance will follow the above predictions maximally up to this scale. Beyond this scale, non-universal (system specific) properties will typically induce a different scaling.

As an example, we show the number variance and the level spacing distributions for a quantum many-body system in Fig. 4.37. The system is a tight-binding model for interacting bosons in a one-dimensional lattice, described by the so-called Bose-Hubbard Hamiltonian [113], with a parameter controlling the spectral properties [114].

Fig. 4.38 Spectral analysis of the Sinai billiard from Fig. 4.36 (symbols) and GOE prediction for the spectral rigidity $\Delta(L)$ (solid line) as compared with the Poissonian case (dashed line). Copyright 1984 by the American Physical Society [100]



4.6.8.2 Spectral Rigidity

A quantity very similar to the number variance is the so-called spectral rigidity function. It allows for an additional optimization in the comparison with a straight line with respect to (4.6.51). The spectral rigidity is defined as

$$\Delta_3(L) \equiv \frac{1}{L} \left\langle \min_{\{a,b\}} \int_{\tilde{E}-L/2}^{\tilde{E}+L/2} dE \left[\int_0^E dE' \rho(E') - (a + bE) \right]^2 \right\rangle_{\tilde{E}}, \quad (4.6.53)$$

with appropriate constants a and b . The random matrix predictions for it are [97, 108]

$$\Delta_3(L) = \begin{cases} \frac{L}{15} & \text{Poisson (integrable)} \\ \frac{1}{\pi^2} \left[\ln(2\pi L) + \gamma - \frac{5}{4} - \frac{\pi^2}{8} \right] + O\left(\frac{1}{L}\right) & \text{GOE} \\ \frac{1}{2\pi^2} \left[\ln(2\pi L) + \gamma - \frac{5}{4} \right] + O\left(\frac{1}{L}\right) & \text{GUE} \\ \frac{1}{4\pi^2} \left[\ln(4\pi L) + \gamma - \frac{5}{4} + \frac{\pi^2}{8} \right] + O\left(\frac{1}{L}\right) & \text{GSE} \end{cases}. \quad (4.6.54)$$

Figure 4.38 presents the spectral rigidity for the same Sinai billiard as shown in Fig. 4.36, nicely supporting the conjecture of Bohigas, Giannoni and Schmit.

4.6.8.3 More Random Matrix Theory

Having analyzed the nearest neighbor level spacings and the spectral correlation functions introduced in the previous sections, one can well characterize the properties of a given quantum system. At least in the two limits of being integrable or fully chaotic in the sense of the two conjectures by Berry-Tabor and Bohigas-Giannoni-Schmit, respectively. For mixed classical systems, the quantum spectra will typically not follow the predictions of random matrix theory for these two limits. For such cases, it is argued that they follow distributions which interpolate in some way or another between the two limits, see e.g. [107, 108, 115]. While very plausible these arguments lack mathematical rigor up to now, and we do not discuss them here.

Random matrix theory offers predictions not only for the eigenvalues but also for the eigenvectors of the corresponding matrix ensembles. Properties of the eigenvectors are relevant if one wants to make statements about the behavior of eigenfunctions of chaotic systems. Choosing a typical basis for the problem (the eigenbasis is very untypical in this sense!), the coefficients of the eigenstates of random matrices in this basis obey certain distributions. Since for a chaotic system, all coefficients can be expected to behave equally on average, one can choose one of the coefficients c_i , for fixed i , and define $\eta \equiv |c_i|^2 N$, where N is the number of eigenvectors (the system dimension). If the coefficients are correctly normalized, i.e. $\sum_{i=1}^N |c_i|^2 = 1$, random matrix theory predicts for the distribution of η values [20]:

$$P(\eta) = \begin{cases} \frac{1}{2\pi\eta} e^{-\frac{\eta}{2}} & \text{GOE} \\ e^{-\eta} & \text{GUE} \\ \eta e^{-\eta} & \text{GSE} \end{cases} \quad (4.6.55)$$

Hence also eigenfunctions of a given system can be checked with respect to the expectations of random matrix theory. The practical access to eigenfunction is, however, much harder than measuring the eigenvalues. The same is true for numerical diagonalizations. This is the reason why, most of the time, the eigenvalues are preferably analyzed.

Practically, it may turn out to be better to study the integrated or cumulative level spacing distribution $CSD(s) \equiv \int_0^s ds' P(s')$ since this quantity is statistically more robust if not too many eigenvalues are available. Integrated distributions are shown in the main panels of Fig. 4.37a, b for instance.

The predictions for Gaussian ensembles, which were presented here, carry over to ensembles of unitary random matrices with the corresponding symmetry properties. The ensembles are then called circular orthogonal, unitary, and symplectic ensembles (COE, CUE, CSE), respectively. Unitary matrices occur naturally in scattering processes (the S matrix is unitary), and for periodically time-dependent systems. In the latter case, the evolution over one period is given by the Floquet operator $\hat{U}(nT, (n+1)T)$, just like in Sect. 4.5.2, where T is the period and n an integer. Unitary operators have real *eigenphases* ϕ_j

$$\hat{U}(0, T)|\phi_j\rangle = e^{i\phi_j}|\phi_j\rangle, \quad (4.6.56)$$

whose spectral statistics are the same as given in Eq. (4.6.18) for instance. Since these phases are understood modulo 2π , often one finds the statement that unfolding was not necessary for Floquet spectra [20]. This is true if the quasi-energies $\varepsilon_j = -\frac{\phi_j}{T}$ uniformly fill the so-called Floquet zone of eigenvalues, i.e. if $\varepsilon_j \in [-\frac{\pi}{T}, \frac{\pi}{T}]$ is uniformly distributed. Sometimes this may not be the case, as, for instance, for the many-body system similar as the one shown in Fig. 4.37 and analyzed in [116]. In other words, unfolding cannot hurt, if it is done carefully (see Sect. 4.6.4).

4.7 Concluding Remarks

Let us end this chapter with the important statement that random matrix theory and the comparison of the spectral properties of physical systems with its predictions offers a way to define quantum chaos. This approach goes back to Wigner, who analyzed data of nuclear spectra, and it is obviously independent of any connection with its classical analogue and semiclassics. The conjectures by Berry-Tabor and Bohigas-Giannoni-Schmit connect then such predictions with the classical analogues, which reconciles both “definitions” of quantum chaoticity as mentioned in Sect. 1.3. Semiclassics has the advantage that we gain quite a lot of intuition for the evolution of a quantum system, simply because we are intuitively more used to classical motion. Yet, constructing semiclassical propagators for a specific problem in full detail is at least as hard as directly solving the Schrödinger equation (e.g. by numerical diagonalization).

Modern research on quantum chaos is concerned with many aspects which are not covered in this book. Random matrix theory, for instance, is applied in many different fields of physics like solid-state theory [117, 118], but also in econophysics [119]. In particular, people try to understand whether (not full random matrices but) sparse matrices with many zero entries and special structures can model physical systems more realistically, see e.g. [117, 118, 120, 121].

Higher dimensional problems, for which phase space methods like Poincaré sections are not very useful, are also in the focus of current research projects. Classically, even the presence of KAM tori does not preclude transport in phase space since the tori do not necessarily divide the phase space into unconnected parts (as they do in a three dimensional phase space). This transport mechanism is however extremely slow, and known as Arnold diffusion [122]. Semiclassics in higher-dimensional systems is therefore quite challenging. One branch of investigation is, for instance, connected with tunneling phenomena out of classically bound regions (like stable resonance islands) [123, 124]. A recent review on this topic of dynamical tunneling is found in [48], with discussions also on higher-dimensional tunneling. Experimentally, Arnold diffusion and dynamical tunneling are notoriously hard to test, but signatures of tunneling across phase space barriers have been found recently in different experimental setups [53, 125–130].

One of the paradigms of quantum chaos are driven Rydberg atoms, which we discussed in Sects. 3.7.6, 4.4.3 and 4.5.2 in various contexts. Most of the experiments were performed with hydrogen or alkali Rydberg atoms showing in good approximation only single electron motion [16, 49–51, 87–89, 131]. Today well controlled experiments with singly or doubly excited electronic states of helium are in reach, see e.g. [132, 133]. Even if helium represents a system of very few bodies (three!) the excitation spectra are hard to compute numerically. This is true even more if an additional drive is added, see e.g. [133–135]. Classical helium bears similarities to the three-body Kepler problem, see Sects. 3.5 and 4.2.1, and it shows interesting classical stability properties [136]. In reality it is a quantum problem, nicely connecting Poincaré’s classical studies and classical chaos with aspects of quantum chaos [134–136].

Appendix

Quantum Mechanical Spectra

Spectra of quantum mechanical Hamiltonians can be categorized as follows [4]:

- *Point spectrum*: The spectrum of the Hamiltonian is discrete.
- *Absolutely continuous spectrum*: In physics it is usually known just as the continuous spectrum, i.e. the spectrum of a hydrogen atom above the ionisation threshold $E \geq 0$.
- *Singular-continuous spectrum*: A singular-continuous spectrum is not a point spectrum and not a continuous spectrum (it has a fractal structure, for the Hausdorff dimension D_H of the spectrum one finds $0 < D_H < 1$, see [137]). Structures like this occur as well in power spectra of classical observables in the chaotic regime [138]. Additionally, a singular continuous spectrum leads to dynamics [139] which can be brought in relation to chaos. Examples of Hamiltonian operators with such exotic spectra can be found in [140]. The special structure of singular spectra makes them, in principle, a candidate to define true chaos in a quantum system with such a spectrum.

In the case of a discrete quantum spectrum, the correspondence between the classical and the quantum mechanical system is certainly less good than for an *absolutely continuous spectrum*, simply because classically also a continuum of energies is allowed. For a quantum mechanical point spectrum the correspondence can be better if the energy levels lie closer (higher density of states), which naturally happens in the semiclassical limit. There are indeed intriguing similarities in the rigorous treatment of spectra of classical and quantum systems when discussing e.g. the spectra of classical evolution operators (known as Perron-Frobenius operators) [138].

Problems

4.1. WKB approximation—energy levels. Given the one-dimensional potentials for a particle of mass m

$$V_1(x) = \begin{cases} \frac{1}{2}m\omega^2x^2, & x > 0 \\ \infty, & x < 0 \end{cases} \quad (4.7.1)$$

$$V_2(x) = \begin{cases} mgx, & x > 0(g > 0) \\ \infty, & x < 0 \end{cases} . \quad (4.7.2)$$

- (a) Show that for the outer turning point a

$$\int_0^a p(x)d(x) = \pi\hbar(n + \frac{3}{4}) \quad (n \in \mathbb{N}_0) \quad (4.7.3)$$

implicitly defines the WKB-quantized energy levels.

- (b) Compute the two series of WKB energy levels $E(n)$ and extract the scaling of the density of states (the inverse level distance) with energy E .
- (c) Imagine a point mass with $m = 1 \text{ kg}$ (with g being the gravity constant on earth). In which quantum state n would it be if you let it fall from a height of $h = 1 \text{ m}$ above the floor? How large would h be in the quantum mechanical ground state with $n = 0$?

4.2. WKB approximation II—Tunneling. A particle is trapped in the 1D potential

$$V_1(x) = \begin{cases} -U_0, & |x| < a \\ A/|x|, & |x| > a, \end{cases} \quad (4.7.4)$$

with $A > 0$. What is the maximal value of E such that the particle is still trapped?

- (a) Calculate the probability of the particle escaping if it bounces on a wall once after starting at $x = 0$ with momentum p .
- (b) Using the above result, calculate the half-life of the particle escaping from the potential as a function of its energy E . (Hint: Compute the number of bounces for which the particle has the chance of 1/2 for being still inside).

4.3. EKB quantization. For $V(r) = -e^2/r$ we get in spherical coordinates (r, θ, ϕ) , with $r \in [0, \infty)$, $\theta \in [0, \pi]$, $\phi \in [0, 2\pi]$ the following Hamiltonian

$$H = \frac{\mathbf{p}^2}{2m} - \frac{e^2}{r} = \frac{1}{2m} \left(p_r^2 + \frac{p_\theta^2}{r^2} + \frac{p_\phi^2}{r^2 \sin^2 \theta} \right) - \frac{e^2}{r}. \quad (4.7.5)$$

- (a) Show that

$$p_r = m\dot{r}, \quad p_\theta = mr^2\dot{\theta}, \quad p_\phi = mr^2 \sin(\theta)\dot{\phi} (= L_z) \quad (4.7.6)$$

- (b) Show the the system is integrable by finding three constants of the motion.
(c) Using the integrals

$$\begin{aligned} I_r &= \frac{1}{2\pi} \oint p_r dr = \frac{me^2}{\sqrt{-2mE}} - L \\ I_\theta &= \frac{1}{2\pi} \oint p_\theta d\theta = L - |L_z| \\ I_\phi &= \frac{1}{2\pi} \oint p_\phi d\phi = |L_z|, \end{aligned} \quad (4.7.7)$$

show that one can obtain the quantized energies in the form

$$E = -\frac{me^4}{2} \frac{1}{(I_r + I_\theta + I_\phi)^2}. \quad (4.7.8)$$

Use now the quantization conditions of EKB to arrive at the usual well-known quantum mechanical eigenenergies of the Coulomb problem.

- (d) Show that the above formulae for the integrals are correct.

Hint 1: Use the identities

$$\mathbf{L}^2 = L^2 = p_\theta^2 + \frac{p_\phi^2}{\sin^2 \theta} = p_\theta^2 + \frac{L_z^2}{\sin^2 \theta} \quad (L \leq 0, -L \leq L_z \leq L) \quad (4.7.9)$$

Hint 2: Determine first the turning points for the motion corresponding to the tori actions $I_{r,\theta,\phi}$, i.e. for

$$V_{\text{eff}}(r) = -\frac{e^2}{r} + \frac{\mathbf{L}^2}{2mr^2} \quad (4.7.10)$$

from $\sin^2 \theta_{1,2} = (L_z/L)^2 \leq 1$, and for the cyclic coordinate ϕ . Then show that one can write the integrals as an integral on the complex plane such that one uses a contour which encircles the real axis between the endpoints, for I_r

$$I_r = \frac{\sqrt{2m}}{2\pi} \frac{1}{i} \oint \sqrt{-Er^2 - e^2 r + \frac{L^2}{2m}} \frac{dr}{r} \quad (4.7.11)$$

and for I_θ

$$I_\theta = \frac{1}{2\pi} \oint \sqrt{L^2 - \frac{L_z^2}{\sin^2 \theta}} d\theta = -\frac{L}{2\pi i} \oint \frac{\sqrt{a^2 - x^2}}{\sqrt{1-x^2}} \frac{dx}{x}. \quad (4.7.12)$$

Study the singularities of the integrand and use Cauchy's theorem to calculate this integral.

- (e) Compare the semi-classical and quantum mechanical quantization of L and L_z .
- (f) What are the multiplicites of the energy levels, i.e. how many different orbits are possible for some energy level satisfying the EKB quantization conditions?

4.4. Poisson summation formula

- (a) Show for $x \in \mathbb{R}$

$$\sum_{m=-\infty}^{\infty} e^{2\pi imx} = \sum_{n=-\infty}^{\infty} \delta(x - n). \quad (4.7.13)$$

- (b) Show that for $\alpha \in \mathbb{R}$

$$\sum_{n=-\infty}^{\infty} f(\alpha n) = \frac{\sqrt{2\pi}}{\alpha} \sum_{m=-\infty}^{\infty} F\left(\frac{2\pi m}{\alpha}\right), \quad (4.7.14)$$

for a periodic function $f(x)$ and its Fourier transformation

$$F(k) = \frac{1}{\sqrt{2\pi}} \int_{-\infty}^{\infty} f(x) e^{ikx} dx. \quad (4.7.15)$$

4.5. Mean Density of States—the Weyl formula. A semiclassical expression for the mean density of states in a system with n degrees of freedom is given by the Thomas-Fermi formula of Eq. (4.3.68)

$$\bar{\rho} = \frac{1}{(2\pi\hbar)^n} \int d^n p \int d^n r \delta(E - H(\mathbf{p}, \mathbf{r})), \quad (4.7.16)$$

where $\mathbf{r} = (r_1, \dots, r_n)$ are the space coordinates, $\mathbf{p} = (p_1, \dots, p_n)$ are the corresponding momenta and $H(\mathbf{p}, \mathbf{r})$ is the classical Hamiltonian of the system. The formula is based on the consideration that there is, on average, exactly one quantum state per Planck cell within the phase space volume $(2\pi\hbar)^n$.

- (1) Show for $n = 3$ and $H = \mathbf{p}^2/2m + V(\mathbf{r})$:

$$\bar{\rho} = \frac{m}{2\pi^2\hbar^3} \int d^3 r \sqrt{2m(E - V(\mathbf{r}))} \Theta(E - V(r)), \quad (4.7.17)$$

where $\Theta(x) = \begin{cases} 1, & x > 0 \\ 0, & x < 1 \end{cases}$ is the Heaviside step function.

- (2) Calculate the mean density of states for:

- (a) the three dimensional infinite box potential with edge lengths a, b and c ,
- (b) the three dimensional isotrop harmonic oscillator with the frequency ω ,

(c) the hydrogen atom.

Compare each case with the exact density of states in the quantum mechanical system.

Hint:

$$\int_0^1 x^2 \sqrt{1-x^2} dx = \int_0^1 x^2 \sqrt{\frac{1}{x} - 1} dx = \frac{\pi}{16} \quad (4.7.18)$$

4.6. Propagator I. From Eq. (4.3.26), we deduce the propagator of a free particle:

$$K_f(x, t|x_0, 0) = \left(\frac{m}{2\pi i \hbar t} \right)^{\frac{1}{2}} e^{\frac{i m (x-x_0)^2}{2\hbar t}}. \quad (4.7.19)$$

Consider now the potentials

$$V_1(x) = \begin{cases} 0 & \text{for } x > 0, \\ \infty & \text{for } x < 0, \end{cases} \quad (4.7.20)$$

and

$$V_2(x) = \begin{cases} 0 & \text{for } 0 < x < a, \\ \infty & \text{for } x < 0 \text{ or } x > a. \end{cases} \quad (4.7.21)$$

(a) Show that the free propagator satisfies the rule

$$K_f(x, t|y, 0) = \int_{-\infty}^{\infty} dz K_f(x, t|z, t') K_f(z, t'|y, 0) \quad (4.7.22)$$

with $0 < t' < t$. Which property of the paths in the path integral does this correspond to?

(b) Show that the propagator $K_1(x, t|x_0, 0)$ of a particle moving in the potential $V_1(x)$ is

$$K_1(x, t|x_0) = K_f(x, t|x_0, 0) - K_f(x, t|-x_0, 0) \quad (4.7.23)$$

by noticing that each non allowed path (i.e. which crosses the wall) is equivalent to a path of a free particle from $-x_0$ to x . Show that K_1 also satisfies the rule given in (a).

(c) Consider a particle moving in the potential $V_2(x)$. Show that its propagator is

$$K_2(x, t|x_0) = \sum_{j=-\infty}^{\infty} K_f(x, t|2ja + x_0, 0) - K_f(x, t|2ja - x_0, 0) \quad (4.7.24)$$

- (d) Show that both $K_1(x, t|x_0, 0)$ and $K_2(x, t|x_0, 0)$ satisfy

$$\begin{aligned} K_1(0, t|x_0, 0) &= 0 \\ K_2(0, t|x_0, 0) &= K_2(a, t|x_0, 0) = 0, \end{aligned} \quad (4.7.25)$$

i.e. the propagator is zero if the endpoint is on the wall.

- (e) *Particle on a ring.* Consider a free particle moving on a ring with radius R . Its position can be described using an angle θ . Calculate the propagator of the particle as a sum of all the free paths which go around the ring $n \in \mathbb{Z}$ times. Using Poisson's summation formula from Problem 4.4, show that we have

$$K_{\text{ring}}(\theta, t|\theta_0, 0) = \frac{1}{2\pi R} \sum_k e^{ik(\theta-\theta_0)} e^{\frac{-i\hbar k^2 t}{2mR^2}}. \quad (4.7.26)$$

- 4.7. Propagator II—the harmonic oscillator.** The propagator of a particle in a harmonic potential is given by the path integral formula

$$K(x, T|x_0, 0) = \int_{x_0}^x D[x] e^{\frac{i}{\hbar} S[x(t)]}, \quad (4.7.27)$$

where the action of the particle is given by

$$S[x(t)] = \int_0^T \left(\frac{1}{2} m \dot{x}^2 - \frac{1}{2} m \omega^2 x^2 \right) dt. \quad (4.7.28)$$

- (a) Show that the propagator can be written as

$$K(x, T|x_0, 0) = e^{\frac{i}{\hbar} S_{\text{cl}}(x_0, x, t)} K(0, T|0, 0), \quad (4.7.29)$$

where $S_{\text{cl}}(x_0, x, T)$ is the action of the classical path between x_0 at the $t = 0$

and x at $t = T$. Hint: Write $x(t) = x_{\text{cl}}(t) + y(t)$ where x_{cl} is the classical path.

- (b) Show that the classical action defined above satisfies:

$$S_{\text{cl}}(x_0, x, T) = \frac{m\omega}{2 \sin \omega T} \left((x^2 + x_0^2) \cos \omega T - 2x x_0 \right) \quad (4.7.30)$$

and argue that this means

$$K(x, T|x_0, 0) = F(T) e^{\frac{im\omega}{2\hbar \sin \omega T} ((x^2 + x_0^2) \cos(\omega T) - 2x x_0)}. \quad (4.7.31)$$

- (c) To calculate $F(T)$ consider the path integral

$$K(0, T | 0, 0) = \int_0^0 D[y] \int_0^T \left(\frac{1}{2} m \dot{y}^2 - \frac{1}{2} m \omega^2 y^2 \right) dt, \quad (4.7.32)$$

write $y(t)$ as a Fourier series $y(t) = \sum_{n=1}^{\infty} a_n \sin \frac{n\pi t}{T}$. Replace the integral over $y(t)$ with an integral over the Fourier coefficients. After performing the integral show that

$$K(0, T | 0, 0) = C \left(\frac{\omega T}{\sin \omega T} \right)^{1/2} \quad (4.7.33)$$

with some ω -independent factor C . By requiring that the $\omega \rightarrow 0$ limit gives the known result for the free particle, show that the propagator of a particle in a harmonic potential is given by

$$K(x, T | x_0, 0) = \left(\frac{m\omega}{2\pi i \hbar \sin(\omega T)} \right)^{1/2} e^{\frac{i m \omega ((x^2 + x_0^2) \cos(\omega T) - 2 x x_0)}{2 \hbar \sin(\omega T)}}. \quad (4.7.34)$$

Hint: use the following formula due to Euler:

$$\sin(\pi z) = \pi z \prod_{n=1}^{\infty} \left(1 - \frac{z^2}{n^2} \right) \quad (4.7.35)$$

4.8. Density operator. Given the density operator of a quantum system

$$\hat{\rho} = \sum_n c_n |\psi_n\rangle \langle \psi_n| \text{ with } c_n \in [0, 1], \quad \sum_n c_n = 1, \quad (4.7.36)$$

answer the following question:

Have the states $|\psi_n\rangle$ to be orthogonal in general?

and prove the following statements:

(a) the eigenvalues λ_i of $\hat{\rho}$ are real; (b) $\lambda_i \in [0, 1]$; (c) $\sum_i \lambda_i = 1$; (d) $\sum_i \lambda_i^2 \leq 1$.

4.9. Wigner and Husimi functions.

(a) Prove for a 1D system that both of the following definitions give the same Wigner function $W_{|\psi\rangle}(x, p)$:

$$\frac{1}{2\pi\hbar} \int ds \hat{\psi}^*(p + \frac{s}{2}) \hat{\psi}(p - \frac{s}{2}) e^{isx/\hbar} \quad (4.7.37)$$

$$\frac{1}{2\pi\hbar} \int ds \psi^*(x + \frac{s}{2}) \psi(x - \frac{s}{2}) e^{-ips/\hbar}. \quad (4.7.38)$$

(b) Prove the trace product rule for two density matrices $\hat{\rho}_1$ and $\hat{\rho}_2$:

$$\text{tr}(\hat{\rho}_1 \hat{\rho}_2) = 2\pi\hbar \int dx \int dp W_{\hat{\rho}_1}(x, p) W_{\hat{\rho}_2}(x, p). \quad (4.7.39)$$

- (c) A quantum state $|\psi\rangle$ may be projected onto phase space by the following definition:

$$Q_{|\psi\rangle}(x, p) \equiv \frac{1}{\pi} |\langle \Phi_{p,q} | \psi \rangle|^2, \quad (4.7.40)$$

with

$$\Phi_{p,q}(x) \equiv N e^{-\frac{(x-q)^2}{2\sigma_q^2} - \frac{i}{\hbar} px}, \quad (4.7.41)$$

with appropriate normalization constant $N = (\pi^{1/4} \sigma_q^{1/2})^{-1}$. Prove that $Q_{|\psi\rangle}(x, p)$ coincides with the definition of the Husimi function $H_{|\psi\rangle}(x, p)$ defined in Eq. (4.4.20).

- 4.10. Quantum kicked rotor.** The QKR is described by the following kick-to-kick time evolution operator

$$\hat{U} = \hat{K} \hat{F}, \text{ with } \hat{K} = e^{-ik \cos(\hat{\theta})} \text{ and } \hat{F} = e^{-iT\hat{n}^2/2}. \quad (4.7.42)$$

k and T are two independent parameters characterizing the kick strength and period, respectively. For a rotor, periodic boundary conditions are assumed, i.e. in angle representation we have for all times $\psi(\theta = 0) = \psi(\theta = 2\pi)$.

- (a) Compute the matrix elements of \hat{K} in the angle representation for a finite basis of length N and a grid $\theta_i = \frac{2\pi}{N}i$, for $i = 1, 2, \dots, N$.
- (b) Compute the matrix elements of \hat{K} in the angular momentum representation for a finite basis of length N and a grid $n = -N/2, -N/2 + 1, \dots, N/2$.
- (c) For $k = 5$ and $T = 1$ and an initial state in momentum representation of the form $\psi(n) = \delta_{0,n}$, compute numerically the temporal evolution induced by \hat{U} , i.e. compute

$$\psi(t) = \hat{U}^t \psi(0), \quad (4.7.43)$$

for $t = 1, 2, \dots, 200$.

- (d) Plot the angular momentum distribution $|\psi(n, t)|^2$ for $t = 1, 5, 10, 50, 100, 200$ kicks, making sure that your wavefunction is properly normalized, i.e. that $\sum_n |\psi(n, t)|^2 = 1$ for all times t .
- (e) Compute the second moment of the angular momentum distribution, i.e. the expectation value of the energy $E(t) = \langle \psi(n, t) | \frac{n^2}{2} | \psi(n, t) \rangle$ for all $t = 1, 2, \dots, 200$, and plot it versus t .
- (f) For a better interpretation of your results, plot also the time-averaged quantities corresponding to (d) and (e), i.e. the quantities $X(t) = \sum_{t'=1}^t Y(t')/t$, for $Y(t) = |\psi(n, t)|^2$ or $Y(t) = E(t)$, again as a function of t .

Hints for the time evolution in (c):

- (1) First compute $\hat{F}\psi(0)$ in (angular) momentum representation, then use a Fast Fourier Transform (FFT), see e.g. [141], into angle representation before computing $\hat{K}\hat{F}\psi(0)$. Then use the inverse FFT to get back to momentum representation to compute $\hat{F}\hat{K}\hat{F}\psi(0)$, and continue now this procedure iteratively. Choose a grid which is adequate for applying FFT, i.e. $N = 2^x$ for some integer x .
- (2) Make sure that the matrix dimension N is large enough to guarantee a numerically exact evolution. You can directly check this by looking at $|\psi(n, t)|^2$ versus n for various values of $N = 2^x$ and $x = 7, 8, 9, 10, 11, \dots$

4.11. Poisson distribution. Given n real random numbers x_1, \dots, x_n , uniformly distributed in the interval $x_i \in [0, n]$. Compute numerically for $n = 10^5$ the probability density $P(s)$ such that the distance on the x -axis of a given x_i to its nearest (larger) neighbour x_j equals s .

Hints:

- Compute 10^5 real random numbers in $[0, 10^5]$ using a standard random number generator (cf., e.g., [141])
- Sort the x_j in such a way that $x_i < x_j \forall i < j$ with $i, j \in \{1, 2, \dots, 10^5\}$.
- Count how many distances $s = x_{j+1} - x_j$ are in the intervals $[0, 0.1], [0.1, 0.2], \dots, [9.9, 10]$, and plot the normalized numbers (relative frequencies) in a histogram.
- What is the functional form of the obtained normalized distribution $P(s)$ (obeying the conditions from Eq. (4.6.19))?

4.12. Rectangular billard.

- (a) Show that for

$$V(x, y) = \begin{cases} 0, & 0 < x < a \quad 0 < y < b \\ \infty, & \text{otherwise} \end{cases} \quad (4.7.44)$$

the exact quantum mechanical spectrum coincides with the EKB solution from Sect. 4.2.3.1:

$$E_{n,k} = \frac{\hbar^2\pi^2}{2m} \left(\frac{n^2}{a^2} + \frac{k^2}{b^2} \right).$$

- (b) Fix $a = 1, b = \frac{1}{2}(\sqrt{5} - 1)$, $\frac{\hbar^2\pi^2}{2m} = 1$, and compute the probability distribution $P(s)$.

Hint:

Use the 10^5 lowest eigenvalues and count how many distances are in the intervals $[0, 0.1], [0.1, 0.2], \dots, [9.9, 10]$, respectively.

4.13. Level repulsion I.

A spin-1/2 system may be described by the following Hamiltonian in matrix form

$$H = \begin{pmatrix} E_0 + \Delta & V \\ V^* & E_0 - \Delta \end{pmatrix} \quad (4.7.45)$$

with E_0, Δ real and V complex parameters.

- (a) Compute the eigenvalues of H .
- (b) Imagine that $E_0(\lambda), \Delta(\lambda), V(\lambda)$ depend on the real parameter λ . Argue that in general there is no such value λ_0 that gives a degenerate spectrum.

Hint: How many real equations must λ satisfy to realise degenerate eigenenergies?

How does the situation change for real V ?

- (c) Sketch the eigenlevels of H as a function of λ for $\Delta(\lambda) = \lambda\Delta_0$ and fixed values of E_0 and V (both assumed to be independent on λ). What happens to the eigenstate of the lower level (and of the higher level, respectively) when λ is adiabatically varied between $\lambda = -100V/\Delta_0$ and $\lambda = 100V/\Delta_0$?

4.14. Level repulsion II.

A two-level system with time-dependent energy levels is swept through an (almost) degeneracy linearly in time, i.e., the time-dependent Hamiltonian is given by

$$H = \begin{pmatrix} E_0 + \Delta t & V \\ V^* & E_0 - \Delta t \end{pmatrix}. \quad (4.7.46)$$

This realizes the famous Landau-Zener-Majorana-Stückelberg problem [142–145]. In the following you may solve for the transition probability following the relatively simple method reported in [146, 147].

- (a) First consider $V = 0$. Give the solution of the time-dependent Schrödinger equation for the two cases where the system starts at one of the levels at the initial time $t = -T$.
- (b) Generalize the wave functions of exercise (a) to a general ansatz by adding the two wave functions with time-dependent coefficients,

$$\Psi = A(t)\Psi_1(x, t) + B(t)\Psi_2(x, t), \quad (4.7.47)$$

and calculate the differential equations which $A(t)$ and $B(t)$ satisfy. What can you say about the large time behaviour of the transition amplitude? Hint: Use the assumption that the amplitudes vary slowly for large times.

- (c) In terms of the generalized ansatz

$$\Psi = A(t)\Psi_1(x, t) + B(t)\Psi_2(x, t) \quad (4.7.48)$$

using the eigenfunctions of the $V = 0$ Hamiltonian, give an expression for the probability of a nonadiabatic level jump, provided the system was in one of the eigenstates of the unperturbed Hamiltonian in the far past (i.e. for $t \rightarrow -\infty$).

(d) Using the equation of motion of $B(t)$ and $A(t)$ show that

$$\ln \frac{B(t \rightarrow \infty)}{B(t \rightarrow -\infty)} = -\frac{1}{i2\Delta} \int_{-\infty}^{\infty} \frac{|V|^2 + \ddot{B}(t)/B(t)}{t} dt. \quad (4.7.49)$$

(e) Use now a complex contour integration to evaluate the integral.

Hint: Close the contour with a large semicircle going on the upper or lower half plane, and show that there is no pole at $t = 0$.

(f) Using the result above, argue that the probability of jump, the so-called Landau-Zener formula, is

$$P = e^{-\pi|V|^2/|\Delta|}. \quad (4.7.50)$$

References

1. Schwabl, F.: Quantum Mechanics. Springer, Berlin (2005)
2. Landau, L.D., Lifschitz, E.M.: Course in Theoretical Physics III, Quantum Mechanics: Non-Relativistic Theory. Pergamon Press, Oxford (1994)
3. Sakurai, J.J.: Modern Quantum Mechanics. Addison-Wesley Publishing Company, Reading (1994)
4. Reed, M.C., Simon, B.: Methods of Modern Mathematical Physics I: Functional analysis. Academic Press, San Diego (1972)
5. Peres, A.: Phys. Rev. A **30**, 1610 (1984)
6. Gorin, T., Prosen, T., Seligman, T.H., Žnidaric, M.: Phys. Rep. **435**, 33 (2006)
7. Jacquod, P., Petitjean, C.: Adv. Phys. **58**(2), 67 (2009)
8. Berry, M.V.: Proc. R. Soc. Lond. A: Math. Phys. Sci. **413**(1844), 183 (1987)
9. Berry, M.V.: Phys. Scr. **40**(3), 335 (1989)
10. Einstein, A.: Verh. Dt. Phys. Ges. **19**, 82 (1917)
11. Poincaré, H.: Les Méthodes nouvelles de la mécanique céleste. Gauthier-Villars, Paris (1899)
12. Arnold, V.I.: Mathematical Methods of Classical Mechanics. Springer, New York (1989)
13. Abramowitz, M., Stegun, I.A.: Handbook of Mathematical Functions. Dover, New York (1972)
14. Maslov, V., Fedoriuk, M.: Semi-Classical Approximations in Quantum Mechanics. Reidel, Dordrecht (1981)
15. Landau, L.D., Lifschitz, E.M.: Course in Theoretical Physics I, Mechanics. Pergamon Press, Oxford (1960)
16. Bayfield, J.E.: Quantum Evolution: An Introduction to Time-Dependent Quantum Mechanics. Wiley, New York (1999)
17. Ozorio de Almeida, A.M.: Hamiltonian Systems: Chaos and Quantization. Cambridge University Press, Cambridge (1988)
18. Vleck, J.H.V.: Proc. Natl. Acad. Sci. USA **14**, 178 (1928)
19. Peskin, M.E., Schroeder, D.V.: An Introduction to Quantum Field Theory. Addison-Wesley, Reading (1995)
20. Haake, F.: Quantum Signatures of Chaos (Springer Series in Synergetics). Springer, Berlin (2010)
21. Rebhan, E.: Theoretische Physik: Mechanik. Spektrum Akademischer Verlag, Heidelberg (2006)
22. Feynman, R.P.: Rev. Mod. Phys. **20**, 367 (1948)

23. Feynman, R.P., Hibbs, A.R.: *Quantum Mechanics and Path Integrals*. McGraw-Hill, New York (1965)
24. Lieb, E.H., Loss, M.: *Analysis*. American Mathematical Society, Providence (2001)
25. Schulman, L.S.: *Techniques and Applications of Path Integration*. Wiley, New York (1981)
26. Bransden, B.H., Joachain, C.J.: *Physics of Atoms and Molecules*. Prentiss Hall, New York (2003)
27. Brack, M., Bhaduri, R.K.: *Semiclassical Physics*. Westview Press, Oxford (2003)
28. Stöckmann, H.J.: *Quantum Chaos, An Introduction*, 1st edn. Cambridge University Press, Cambridge (1999)
29. Stöckmann, H.J., Stein, J.: *Phys. Rev. Lett.* **64**, 2215 (1990)
30. Garton, W.R.S., Tomkins, F.S.: *Astrophys. J.* **158**, 839 (1969)
31. Holle, A., Main, J., Wiebusch, G., Rottke, H., Welge, K.H.: *Phys. Rev. Lett.* **61**(2), 161 (1988)
32. Wintgen, D.: *Phys. Rev. Lett.* **58**, 1589 (1987)
33. Wintgen, D.: *Phys. Rev. Lett.* **61**, 1803 (1988)
34. Friedrich, H., Wintgen, D.: *Phys. Rep.* **183**, 37 (1989)
35. Delande, D., Gay, J.C.: *Phys. Rev. Lett.* **57**(16), 2006 (1986)
36. Delande, D.: *Les Houches lectures*, 1989. In: Giannoni, M.J., Voros, A., Zinn-Justin, J. (eds.) *Chaos and Quantum physics*, vol. 52, pp. 665. North-Holland, Amsterdam (1991)
37. Sieber, M., Richter, K.: *Phys. Scr.* **2001**(T90), 128 (2001)
38. Heusler, S., Müller, S., Altland, A., Braun, P., Haake, F.: *Phys. Rev. Lett.* **98**, 044103 (2007)
39. Müller, S., Heusler, S., Altland, A., Braun, P., Haake, F.: *New J. Phys.* **11**(10), 103025 (2009)
40. Cvitanović, P., Artuso, R., Mainieri, R., Tanner, G., Vattay, G.: *Chaos: Classical and Quantum*. Niels Bohr Institute, Copenhagen (2012). <http://ChaosBook.org>
41. Ruelle, D.: *The Thermodynamic Formalism*. Cambridge University Press, Cambridge (2004)
42. Breuer, P., Petruccione, F.: *The Theory of Open Quantum Systems*. Oxford University Press, Oxford (2007)
43. Wong, M.W.: *Weyl Transforms*. Springer, Heidelberg (1997)
44. Gardiner, C.: *Quantum Noise. Phase Space Methods* (Chap. 4). Springer, Berlin, (1998)
45. Kordas, G., Wimberger, S., Witthaut, D.: *Phys. Rev. A* **87**, 043618 (2013) (See Appendix B)
46. Walls, D.F., Milburn, G.J.: *Quantum Optics*. Springer, Berlin (2008)
47. Buchleitner, A., Delande, D., Zakrzewski, J.: *Phys. Rep.* **368**(5), 409 (2002)
48. Keshavamurthy, S., Schlagheck, P. (eds.): *Dynamical Tunneling: Theory and Experiment*. CRC Press, Taylor and Francis Group, Boca Raton (2011)
49. Maeda, H., Gallagher, T.F.: *Phys. Rev. Lett.* **92**, 133004 (2004)
50. Maeda, H., Gurian, J.H., Gallagher, T.F.: *Phys. Rev. Lett.* **102**, 103001 (2009)
51. Mestayer, J.J., Wyker, B., Lancaster, J.C., Dunning, F.B., Reinhold, C.O., Yoshida, S., Burgdörfer, J.: *Phys. Rev. Lett.* **100**, 243004 (2008)
52. Behinaini, G., Ramareddy, V., Ahmadi, P., Summy, G.S.: *Phys. Rev. Lett.* **97**, 244101 (2006)
53. Shrestha, R.K., Ni, J., Lam, W.K., Summy, G.S., Wimberger, S.: *Phys. Rev. E* **88**, 034901 (2013)
54. Sadgrove, M., Wimberger, S.: Chapter 7—a pseudoclassical method for the atom-optics kicked rotor: from theory to experiment and back. In: Berman, P.R., Arimondo, E., Lin, C.C. (eds.) *Advances in Atomic, Molecular, and Optical Physics*, *Advances In Atomic, Molecular, and Optical Physics*, vol. 60, pp. 315–369. Academic Press, New York (2011)
55. Heller, E.J.: *Phys. Rev. Lett.* **53**, 1515 (1984)
56. Sridhar, S.: *Phys. Rev. Lett.* **67**, 785 (1991)
57. Stein, J., Stöckmann, H.J.: *Phys. Rev. Lett.* **68**, 2867 (1992)
58. Sridhar, S., Heller, E.J.: *Phys. Rev. A* **46**, R1728 (1992)
59. Doya, V., Legrand, O., Mortessagne, F., Miniatura, C.: *Phys. Rev. Lett.* **88**, 014102 (2001)
60. de Menezes, D.D., Jar e Silva, M., de Aguiar, F.M.: *Chaos* **17**(2), 023116 (2007)
61. Anderson, P.W.: *Phys. Rev.* **109**, 1492 (1958)
62. Anderson, P.W.: *Rev. Mod. Phys.* **50**, 191 (1978)
63. Fishman, S., Grempel, D.R., Prange, R.E.: *Phys. Rev. Lett.* **49**, 509 (1982)
64. Casati, G., Chirikov, V., Shepelyansky, D.L., Guarneri, I.: *Phys. Rep.* **154**(2), 77 (1987)

65. Kramers, B., MacKinnon, A.: Rep. Prog. Phys. **56**, 1469 (1993)
66. Kohn, W.: Phys. Rev. B **7**, 4388 (1973)
67. Wannier, G.H.: Phys. Rev. **117**, 432 (1960)
68. Nolting, W.: Grundkurs Theoretische Physik 7: Vielteilchentheorie. Springer, Berlin (2005)
69. Datta, S.: Electronic Transport in Mesoscopic Systems. Cambridge University Press, Cambridge (1995)
70. Casati, G., Guarneri, I., Shepelyansky, D.L.: Phys. Rev. Lett. **62**, 345 (1989)
71. Ho, T.S., Chu, S.I.: Phys. Rev. A **31**, 659 (1985)
72. Ringot, J., Szcifgiser, P., Garreau, J.C., Delande, D.: Phys. Rev. Lett. **85**, 2741 (2000)
73. Brenner, N., Fishman, S.: J. Phys. A: Math. Gen. **28**(21), 5973 (1995)
74. Buchleitner, A., Guarneri, I., Zakrzewski, J.: Europhys. Lett. **44**(2), 162 (1998)
75. Jensen, R., Susskind, S., Sanders, M.: Phys. Rep. **201**(1), 1 (1991)
76. Wimberger, S., Buchleitner, A.: J. Phys. A: Math. Gen. **34**(36), 7181 (2001)
77. Krug, A., Wimberger, S., Buchleitner, A.: Eur. Phys. J. D **26**(1), 21 (2003)
78. Fishman, S., Prange, R.E., Griniasty, M.: Phys. Rev. A **39**(4), 1628 (1989)
79. Izrailev, F.M.: Phys. Rep. **196**(56), 299–392 (1990)
80. Shepelyansky, D.: Physica D **28**, 103 (1987)
81. Dunlap, D.H., Kenkre, V.M.: Phys. Rev. B **34**, 3625 (1986)
82. Lignier, H., Sias, C., Ciampini, D., Singh, Y., Zenesini, A., Morsch, O., Arimondo, E.: Phys. Rev. Lett. **99**, 220403 (2007)
83. Kierig, E., Schnorrberger, U., Schietinger, A., Tomkovic, J., Oberthaler, M.K.: Phys. Rev. Lett. **100**, 190405 (2008)
84. Casati, G., Chirikov, B.V., Ford, J., Izrailev, F.M.: Stochastic behavior in classical and quantum hamiltonian systems. In: Casati, G., Ford, J. (eds.) Lecture Notes in Physics, vol. 93, p. 334. Springer, Berlin (1979)
85. Feingold, M., Fishman, S., Grempel, D.R., Prange, R.E.: Phys. Rev. B **31**, 6852 (1985)
86. Pichard, J.L., Zanon, N., Imry, Y., Douglas Stone, A.: J. Phys. France **51**(7), 587–609 (1990)
87. Bayfield, J.E., Casati, G., Guarneri, I., Sokol, D.W.: Phys. Rev. Lett. **63**, 364 (1989)
88. Galvez, E.J., Sauer, J.E., Moorman, L., Koch, P.M., Richards, D.: Phys. Rev. Lett. **61**, 2011 (1988)
89. Koch, P., van Leeuwen, K.: Phys. Rep. **255**, 289 (1995)
90. Casati, G., Chirikov, B.V., Shepelyansky, D.L.: Phys. Rev. Lett. **53**, 2525 (1984)
91. Casati, G., Guarneri, I., Shepelyansky, D.L.: IEEE J. Quantum Electron. **24**, 1420 (1988)
92. Raizen, M.G.: Adv. At. Mol. Phys. **41**, 43 (1999)
93. Bharucha, C.F., Robinson, J.C., Moore, F.L., Sundaram, B., Niu, Q., Raizen, M.G.: Phys. Rev. E **60**, 3881 (1999)
94. Schwartz, T., Bartal, G., Fishman, S., Segev, M.: Nature **446**, 52 (2007)
95. Billy, J., Josse, V., Zuo, Z., Bernard, A., Hambrecht, B., Lugan, P., Clement, D., Sanchez-Palencia, L., Bouyer, P., Aspect, A.: Nature (London) **453**, 891 (2008)
96. Mehta, M.L.: Random Matrices. Academic Press, New York (1991)
97. Mehta, M.L.: Random Matrices. Elsevier, Amsterdam (2004)
98. Porter, C.E. (ed.): Statistical Theories of Spectra: Fluctuations. Academic, New York (1965)
99. Bohr, N.: Nature (London) **137**, 351 (1936)
100. Bohigas, O., Giannoni, M.J., Schmit, C.: Phys. Rev. Lett. **52**, 1 (1984)
101. Aurich, R., Scheffler, F., Steiner, F.: Phys. Rev. E **51**, 4173 (1995)
102. Gómez, J.M.G., Molina, R.A., Relaño, A., Retamosa, J.: Phys. Rev. E **66**, 036209 (2002)
103. Haller, E., Köppel, H., Cederbaum, L.: Chem. Phys. Lett. **101**(3), 215–220 (1983)
104. Venkataraman, R.: J. Phys. B: At. Mol. Phys. **15**(23), 4293 (1982)
105. Berry, M.V., Tabor, M.: Proc. R. Soc. Lond. A **356**, 375 (1977)
106. Casati, G., Chirikov, B.V., Guarneri, I.: Phys. Rev. Lett. **54**, 1350 (1985)
107. Brody, T.A., Flores, J., French, J.B., Mello, P.A., Pandey, A., Wong, S.S.M.: Rev. Mod. Phys. **53**, 385 (1981)
108. Guhr, T., Müller-Gröling, A.: Phys. Rep. **299**(4–6), 189 (1998)
109. Casati, G., Valz-Gris, F., Guarneri, I.: Lett. Nuovo Cimento **28**, 279 (1980)

110. McDonald, S.W., Kaufman, A.N.: Phys. Rev. Lett. **42**, 1189 (1979)
111. Berry, M.: Ann. Phys. **131**(1), 163–216 (1981)
112. Schwabl, F.: Advanced Quantum Mechanics. Springer, Berlin (2008)
113. Bloch, I., Dalibard, J., Zwerger, W.: Rev. Mod. Phys. **80**, 885 (2008)
114. Tomadin, A., Mannella, R., Wimberger, S.: Phys. Rev. Lett. **98**, 130402 (2007)
115. Berry, M.V., Robnik, M.: J. Phys. A **17**, 2413 (1984)
116. Parra-Murillo, C.A., Madroñero, J., Wimberger, S.: Phys. Rev. A **88**, 032119 (2013)
117. Beenakker, C.W.J.: Rev. Mod. Phys. **69**, 731 (1997)
118. Evers, F., Mirlin, A.D.: Rev. Mod. Phys. **80**, 1355 (2008)
119. Plerou, V., Gopikrishnan, P., Rosenow, B., Amaral, L.A.N., Guhr, T., Stanley, H.E.: Phys. Rev. E **65**, 066126 (2002)
120. Weidenmüller, H.A., Mitchell, G.E.: Rev. Mod. Phys. **81**, 539 (2009)
121. Mitchell, G.E., Richter, A., Weidenmüller, H.A.: Rev. Mod. Phys. **82**, 2845 (2010)
122. Lichtenberg, A.J., Lieberman, M.A.: Regular and Chaotic Dynamics. Springer, Berlin (1992)
123. Bohigas, O., Tomsovic, S., Ullmo, D.: Phys. Rep. **223**, 43 (1993)
124. Tomsovic, S., Ullmo, D.: Phys. Rev. E **50**, 145 (1994)
125. Steck, D.A., Oskay, W.H., Raizen, M.G.: Science **293**, 274 (2001)
126. Hensinger, W.K., et al.: Nature (London) **412**, 52 (2001)
127. Hofferbert, R., Alt, H., Dembowksi, C., Gräf, H.D., Harney, H.L., Heine, A., Rehfeld, H., Richter, A.: Phys. Rev. E **71**, 046201 (2005)
128. Bäcker, A., Ketzmerick, R., Löck, S., Robnik, M., Vidmar, G., Höhmann, R., Kuhl, U., Stöckmann, H.J.: Phys. Rev. Lett. **100**, 174103 (2008)
129. Chaudhury, S., Smith, A., Anderson, B.E., Ghose, S., Jessen, P.S.: Nature (London) **461**, 768 (2009)
130. Shinohara, S., Harayama, T., Fukushima, T., Hentschel, M., Sasaki, T., Narimanov, E.E.: Phys. Rev. Lett. **104**, 163902 (2010)
131. Bayfield, J.E., Koch, P.M.: Phys. Rev. Lett. **33**, 258 (1974)
132. Domke, M., Schulz, K., Remmers, G., Kaindl, G., Wintgen, D.: Phys. Rev. A **53**, 1424 (1996)
133. Jiang, Y.H., Püttnner, R., Delande, D., Martins, M., Kaindl, G.: Phys. Rev. A **78**, 021401 (2008)
134. Eglspurger, J., Madroñero, J.: Phys. Rev. A **82**, 033422 (2010)
135. Jörder, F., Zimmermann, K., Rodriguez, A., Buchleitner, A.: ArXiv e-prints (2013)
136. Tanner, G., Richter, K., Rost, J.M.: Rev. Mod. Phys. **72**, 497 (2000)
137. Ott, E.: Chaos in Dynamical Systems. Cambridge University Press, Cambridge (2002)
138. Gaspard, P.: Chaos, Scattering and Statistical Mechanics. Cambridge University Press, Cambridge (1998)
139. Guarneri, I., Mantica, G.: Phys. Rev. Lett. **73**, 3379 (1994)
140. Jitomirskaya, S.Y., Last, Y.: Phys. Rev. Lett. **76**, 1765 (1996)
141. Press, W.H., Teukolsky, S.A., Vetterling, W.T., Flannery, B.P.: Numerical Recipes: The Art of Scientific Computing, 3rd edn. Cambridge University Press, New York (2007)
142. Landau, L.D.: Phys. Z. Sowjetunion **2**, 46 (1932)
143. Zener, C.: Proc. R. Soc. Lond. A **137**(833), 696 (1932)
144. Majorana, E.: Il Nuovo Cimento **9**(2), 43 (1932)
145. Stückelberg, E.C.G.: Helv. Phys. Acta **5**, 369 (1932)
146. Wittig, C.: J. Phys. Chem. B **109**, 8428 (2005)
147. Chichinin, A.I.: J. Phys. Chem. B **117**, 6018 (2013)

Index

A

Abramov's theorem, 90
Absolutely continuous spectrum, 189
Action-angle variables, 35
Adiabatic invariant, 41
Airy equation, 110
Airy functions, 110
Anderson, P. W., 4, 160
Area preserving, 65
Arnold diffusion, 188
Arnold's cat map, 86
Arnold, V. I., 40, 86
Attractive/repulsive fixed point, 12
Autocorrelation function, 83
Autonomous system, 27
Avoided crossing, 169

B

Baker–Campbell–Hausdorff formula, 128
Bernoulli shift, 15
Berry, M. V., 6, 176, 178
Bifurcation, 13, 14, 80, 96
Birkhoff, G. D., 60
Block-diagonal form, 172
Bohigas, O., 178
Bohr's model for nucleus, 171
Bohr, N., 105, 171
Bohr–Sommerfeld quantization, 106
Brillouin, L. N., 106, 119

C

Canonical perturbation theory, 47
Canonical transformation, 29
Canonically conjugated variables, 30

Casati, G., 178
Chirikov, B., 66, 95
Chirikov–Taylor map, 66
Circular ensembles, 187
Classical localization of wave packets, 154
Classical path, 130
Classical scale invariance, 144
Classically allowed region, 109
Classically forbidden region, 109
Completely hyperbolic system, 87
Complex nuclei, 5
Complex system, 3
Computer simulations, 4
Conjugated points, 134
Conservative system, 3
Constant of motion, 21
Continued fraction expansion, 56
Continuous dynamical system, 9
Continuous spectrum, 189
Continuous symmetry, 172
Contour integral, 199
Correspondence principle, 5
Cumulative level spacing distribution (CSD), 187
Cycle expansion, 149

D

De Broglie wave length, 107
De Broglie, L., 104
Decoherence, 5
Degree of freedom, 2
Density of states, 127
Density operator, 150
Deterministic chaos, 1

Diagonal approximation, 146
 Diophantine condition, 54, 55
 Discrete dynamical system, 9
 Discrete symmetry, 172
 Driven Rydberg atoms, 189
 Dyadic map, 15
 Dynamical localization, 166
 Dynamical tunneling, 155, 188
 Dyson, F. J., 178

E

Effective Planck constant, 165
 Eigenvector statistics, 187
 Einstein, A., 106, 119
 Einstein–Keller–Brillouin (EKB) quantization, 119
 Elementary loop, 119
 Elliptic fixed point, 74
 Elliptic integral, 23
 Energy–time uncertainty relation, 146
 Ergodicity, 84
 Euler constant, 185
 Euler–Lagrange equation, 133
 Extended phase space, 27

F

Fast Fourier transform, 197
 Feigenbaum constant, 14
 Feigenbaum, M., 14
 Feynman propagator, 130
 Feynman, R. P., 130
 Fidelity, 105
 Finite system, 4
 Fixed point, 12, 67
 Floquet operator, 165, 166, 187
 Floquet spectra, 188
 Form factor, 146
 Frequency pulling, 50

G

Gauß averaging, 46, 50
 Gaussian ensembles, 181
 Gaussian orthogonal ensemble (GOE), 178, 180
 Gaussian symplectic ensemble (GSE), 178, 180
 Gaussian unitary ensemble (GUE), 178, 180
 Generating function, 29
 Giannoni, M. J., 178
 Golden mean, 56
 Good quantum numbers, 170

Green’s function, 126
 Guarneri, I., 178
 Gutzwiller trace formula, 139
 Gutzwiller, M., 125, 139

H

Hénon and Heiles model, 80
 Haake, F., 148, 169
 Hamilton operator, 104
 Hamilton, W. R., 25
 Hamilton–Jacobi equation, 33
 Hamiltonian system, 11, 21
 Harmonic oscillator, 22
 Heavy nuclei, 171
 Heisenberg time, 146
 Helium atom, 106, 189
 Heller, E. J., 159
 Heteroclinic point, 76
 Homoclinic point, 76
 Husimi function, 154, 195, 196
 Hydrogen atom, 59, 158, 189
 Hydrogen in external magnetic field, 142
 Hydrogen Rydberg states, 144
 Hyperbolic fixed point, 70

I

Integrable system, 36
 Invariant curves, 73
 Invertible dynamical system, 10
 Invertible map, 10
 Irreducible representation, 173

K

K system, 95
 KAM theorem, 52, 55
 Keller, J. B., 119
 Kepler problem, 4, 40
 Kick-to-kick evolution operator, 165
 Kicked rotor, 66, 95
 Kolmogorov, A. N., 40
 Kolmogorov–Sinai entropy, 83, 94
 Kramers degeneracy, 180

L

Landau–Zener formula, 199
 Landau–Zener–Majorana–Stückelberg problem, 198
 Level crossing, 169
 Level density, 127
 Level repulsion, 197
 Level staircase, 173

- Lifetime, 116
 Liouville's theorem, 31
 Liouville, J., 31
 Logistic map, 11
 Lorentz gas model, 95
 Lyapunov exponent, 70, 83, 87, 140
 Lyapunov spectrum, 92
- M**
 Maslov index, 133
 Mehta, M. L., 169
 Metastable state, 115
 Method of stationary phase, 131
 Mixed phase space, 78
 Mixing, 84, 86
 Monodromy matrix, 67, 68, 88, 139
 Morse index, 118, 133, 134
 Moser, J. K., 40
- N**
 Newton's algorithm, 52
 Non-classical path, 130
 Non-dispersive wave packets, 155
 Non-integrable system, 40
 Nondegeneracy condition, 54
 Nonlinear resonance, 66, 67
 Nonlinear resonance island, 66
 Nonlinear system, 23, 54
 Number variance, 184
- O**
 One-and-a-half-degree-of-freedom system, 28
 One-parameter flow, 9
 One-parameter map, 9
 Orbit, 10
 Orthogonal transformation, 180
- P**
 Parabolic fixed point, 70
 Particle in a box, 116
 Partition function, 149
 Pendulum, 24, 75
 Pendulum approximation, 59
 Period doubling, 14
 Periodic orbit (PO), 12, 137, 140
 Periodically driven hydrogen atom, 59, 158
 Perturbation theory, 47
 Phase space, 9, 25, 27, 60
 Planck cell, 121, 136
 Poincaré map, 61, 67
- Poincaré recurrence, 85
 Poincaré recurrence theorem, 85
 Poincaré surface of section, 60
 Poincaré, J. H., 40, 60
 Poincaré–Birkhoff theorem, 73
 Poincaré–Cartan integral invariant, 63
 Poincaré–Cartan theorem, 63
 Point spectrum, 189
 Poisson bracket, 30
 Poisson distribution, 175
 Power spectrum, 84
 Primitive periodic orbit (PPO), 139, 141
 Principle of averaging, 43
 Principle of extremal action, 29
 Problem of small divisors, 52
 Propagator, 126
 Pure state, 150
- Q**
 Q function, 154
 Quantum break time, 168
 Quantum chaology, 6, 105
 Quantum chaos, 105
 Quantum Hamiltonian, 104
 Quantum kicked rotor, 164, 196
 Quantum localization, 166
 Quantum pendulum, 165
 Quasi-energy, 166
- R**
 Radioactive alpha decay, 115
 Random matrix, 5, 169
 Random matrix theory (RMT), 144, 176, 178
 Random number generator, 17
 Rectangular billiard, 119, 197
 Rectangular billiard, 176
 Resonance overlap criterion, 83, 95
 Resonant perturbation theory, 56
 Retarded Green's function, 126
 Riemann–Lebesgue lemma, 131
 Rydberg atom, 5, 59, 144, 158
- S**
 Saddle-point method, 131
 Scaled spectroscopy, 144
 Schmit, C., 178
 Schrödinger equation, 104
 Schrödinger, E., 104
 Secular perturbation theory, 56
 Self similarity, 79
 Semiclassical Green's function, 134, 136

Semiclassical limit, 5
 Separable quantum problem, 5
 Separable system, 35
 Separatrix, 25, 27, 75, 97
 Sieber–Richter pairs, 147
 Sinai billiard, 87, 95, 142, 186
 Sinai, Y., 87, 142, 179
 Smooth level staircase, 174
 Sommerfeld, A., 105
 Spectral analysis, 141
 Spectral auto-correlation function, 145
 Spectral correlation function, 144, 184
 Spectral form factor, 146
 Spectral rigidity, 186
 Stability matrix, 139
 Stable fixed points, 73
 Stable manifold, 74
 Standard map, 66, 87, 95
 Stationary Schrödinger equation, 107
 Stroboscopic map, 62
 Strong localization, 163
 Surface of section (SOS), 60, 61
 Symmetry, 171
 Symmetry-reduced subspace, 171
 Symplectic, 25, 28
 Symplectic matrix, 180
 Symplectic transformation, 180

T

Tabor, M., 176
 Tendril, 78
 Theorem of Stone, 104
 Theorem on Anderson localization, 162
 Thermodynamic formalism, 149
 Thomas-Fermi approximation, 137
 Three-body problem, 4, 40, 189
 Time-reversal symmetry, 180
 Torus, 37, 54, 60
 Trajectory, 10

Trotter product formula, 130
 Tunneling rate, 115
 Turning point, 109
 Twist map, 65

U

Unfolding of spectra, 173
 Unitary transformation, 180
 Universality, 2
 Unstable fixed points, 73
 Unstable manifold, 74

V

Van Vleck, J. H., 125
 Van-Vleck propagator, 132
 Van-Vleck–Gutzwiller propagator, 133
 Verhulst, P. F., 11
 Von Neumann equation, 150

W

Wentzel–Kramer–Brillouin–Jeffreys approximation, 106
 Weyl symbol, 151
 Weyl’s law, 137, 174
 Weyl, H., 137, 149
 Whorl, 77
 Wigner function, 151, 195
 Wigner surmise, 179
 Wigner, E. P., 171, 178
 Winding number, 65
 Wintgen, D., 144
 WKB approximation, 106
 WKBJ ansatz, 107

Z

Zero point energy, 115